Hydrogen Production from Methane Using Oxygen-permeable Ceramic Membranes

By

Sedigheh Faraji

Submitted to the graduate degree program in Chemical and Petroleum Engineering and the Graduate Faculty of the University of Kansas in partial fulfillment of the requirements for the degree of Doctor of Philosophy.

_____
Dr. Susan Williams (Chair)

_____
Dr. Karen Nordheden (Co-Chair)

_____
Dr. Aaron Scurto

_____
Dr. Kyle Camarda

_____
Dr. Judy Wu

Date defended: _____

The Dissertation Committee for Sedigheh Faraji certifies that this is the approved Version of the following dissertation:

Hydrogen Production from Methane Using Oxygen-permeable Ceramic Membranes

_____
Dr. Susan Williams (Chair)

_____
Dr. Karen Nordheden (Co-Chair)

_____
Dr. Aaron Scurto

_____
Dr. Kyle Camarda

_____
Dr. Judy Wu

Date defended: _____

Table of Content

List of Figures

List of Tables

Abstract

Non-porous ceramic membranes with mixed ionic and electronic conductivity have received significant interest in membrane reactor systems for the conversion of methane and higher hydrocarbons to higher value products like hydrogen. However, hydrogen generation by this method has not yet been commercialized and suffers from low membrane stability, low membrane oxygen flux, high membrane fabrication costs, and high reaction temperature requirements.

In this dissertation, hydrogen production from methane on two different types of ceramic membranes (dense SFC and BSCF) has been investigated. The focus of this research was on the effects of different parameters to improve hydrogen production in a membrane reactor. These parameters included operating temperature, type of catalyst, membrane material, membrane thickness, membrane preparation pH, and feed ratio.

The role of the membrane in the conversion of methane and the interaction with a $Pt/CeZrO_2$ catalyst has been studied. Pulse studies of reactants and products over physical mixtures of crushed membrane material and catalyst have clearly demonstrated that a synergy exists between the membrane and the catalyst under reaction conditions. The degree of catalyst/membrane interaction strongly impacts the conversion of methane and the catalyst performance.

During thermogravimetric analysis, the onset temperature of oxygen release for BSCF was observed to be lower than that for SFC while the amount of oxygen release was significantly greater. Pulse injections of CO_2 over crushed membranes at

800°C have shown more CO_2 dissociation on the BSCF membrane than the SFC membrane, resulting in higher CO formation on the BSCF membrane. Similar to the CO_2 pulses, when CO was injected on the samples at 800°C, CO_2 production was higher on BSCF than SFC. It was found that hydrogen consumption on BSCF particles is 24 times higher than that on SFC particles. Furthermore, Raman spectroscopy and temperature programmed desorption studies of CO and CO_2 showed a higher CO and CO_2 adsorption (for temperatures ranging from room temperature to 600°C) on BSCF compared to the SFC membrane.

CO_2 reforming reactions on BSCF and SFC dense membranes in a membrane reactor showed higher methane conversion and H_2/CO ratio on BSCF than SFC in the presence of the Pt/$CeZrO_2$ catalyst. This high conversion and H_2/CO ratio could be ascribed to higher CO, CO_2, and H_2 adsorption on BSCF than SFC, resulting in higher steam and CO_2 reforming on the BSCF.

The Pt-Ni/$CeZrO_2$ catalyst exhibits promising performance for hydrogen production. Platinum enhances the reducibility of Ni/Al_2O_3 and Ni/$CeZrO_2$ catalysts resulting in improved catalysts for H_2 production at moderate temperatures. TPR and Raman studies show an alloy formation in the Pt-Ni/Al_2O_3 catalyst. Further work is required to study the interaction between Pt and Ni in the bimetallic Pt-Ni/$CeZrO_2$ and Pt-Ni/Al_2O_3 catalysts.

Although the Pt-Ni/Al_2O_3 catalyst shows high methane conversion in the presence of the BSCF membrane at 800°C, the activity of this catalyst is low at 600°C. Pt-Ni/$CeZrO_2$ bimetallic catalyst demonstrates superior performance

compared to Pt-Ni/Al_2O_3 catalyst at 600°C. The thinner BSCF membrane (2.2 mm) demonstrates a higher methane conversion and H_2:CO ratio than the thicker BSCF membrane (2.6 mm) because membrane oxygen flux is inversely proportional to thickness. Varying the pH of the precursor solution during membrane preparation has no significant effect on the oxygen flux or the reaction. The CH_4:CO_2 feed ratio significantly affects the hydrogen production over the BSCF membrane. Altering the CH_4:CO_2 ratio has a direct impact on the oxygen flux, which in turn can influence the reaction pathway. These studies suggest that the Pt-Ni/$CeZrO_2$ catalyst might be suitable for low-temperature hydrocarbon conversion reactions over thin BSCF ceramic membranes. Most importantly, the BSCF membrane can reduce the apparent activation energy of the CO_2 reforming reaction by changing the reaction pathway to include more steam reforming.

Acknowledgements

First, I would like to thank Dr. Susan Williams and Dr. Karen Nordheden for their guidance, ideas, and support while working on this research project. The graduate and undergraduate members of the research group also provided valuable support and help in finishing up lab work. I would like to thank my wonderful husband, Hameed, who helped me through all these years with his never-ending patience, tremendous support, and unconditional love. Without him, I could not have completed my Ph.D. studies.

Finally, I appreciate the financial support for this project, which was provided by the Office of Naval Research (N00014-03-1-0601), the US Department of Transportation Research Innovative Technology Administration (DTOS59-06-G-0047), and KU Transportation Research Institute. I also thank MEL chemicals for providing the catalyst supports.

Chapter 1: Introduction

1.1 Overview

Hydrogen is one of the most important intermediate products in a refinery, and is largely used in the oil and petrochemical industries. One of the main usages of hydrogen in refineries is to treat heavier oil feedstock (hydrotreating) [1]. For example, sulfur is removed from natural gas and refined petroleum products by using hydrogen [2]. Another main usage of hydrogen in refineries is to break long-chain hydrocarbons into shorter ones (hydrocracking) [1]. Hydrogen has several other important uses such as a reactant in ammonia production for the fertilizer market [3], and also as a hydrogenating agent, particularly in increasing the level of saturation of unsaturated fats and oils [4]. In addition, hydrogen is an alternative source of clean energy for use in fuel cells [5]. For these reasons, H_2 is an important industrial gas with many existing and future applications.

Mixtures of hydrogen and carbon monoxide, known as synthesis gas (or syngas), are critical intermediates in the production of both fuel-cell quality hydrogen and ultra-clean liquid fuels (Fischer-Tropsch Synthesis), which are easier to transport and store than natural gas [6, 7]. The Fischer-Tropsch process has received significant attention in the quest to produce low-sulfur diesel fuel in order to minimize environmental degradation from the use of diesel engines. Also, another application of syngas is in the synthesis of methanol, which is a reactant used in the biodiesel generation process [8]. At present, nearly more than 96% of the syngas being produced comes from oil, gas, and coal feedstocks [5, 9].

Hydrogen production is an industry with an approximate 10% growth rate per year [10]. With increasing demand for hydrogen and syngas in the global energy market, attention is being paid to new methods of hydrogen or syngas production. One of the promising methods for hydrogen production in the literature is using ceramic membranes (metal oxides) as an oxygen supplier and oxygen distributor [11]. These ceramic membranes are 100% selective to oxygen and oxygen produced from them is cheap, green, safe, and distributed. These membranes, which can be integrated into the syngas generator, eliminate the need for a large expensive air separation plant. The cost of hydrogen production in a membrane reactor was estimated to be $6-$8 /million BTU in 2002 and this cost was 10-12 times less than that for conventional hydrogen production process [12].

High oxygen fluxes through ceramic membranes are required in order to apply this method for industrial H_2 production. Although many materials have been introduced with oxygen transport ability [13, 14], a ceramic membrane with both high oxygen permeability and stability for industrial applications has not been found to date [15]. It is believed that cobalt-based membranes have high oxygen flux but low stability which leads to membrane failure during long-term operation (cracks in membrane or a drop in oxygen flux), while the opposite is true about cobalt-free membranes [16]. Thus, current research efforts are focused on developing new higher oxygen flux materials.

Ceramic membranes have high oxygen permeability at high temperatures (higher than 800ºC); so, prior reaction studies on these membranes have been limited

to temperatures higher than 800ºC. Low and medium temperature reaction studies on these membranes are of interest for reducing heating costs. In addition to the operating temperature, there are other improvements (such as catalyst) in operating conditions and process requirements that need to be explored.

1.2 Research Objectives

It is necessary to develop and improve ceramic membrane technology for hydrogen production during CO_2 reforming reaction in order to introduce it as an industrial process. For this improvement, a deep understanding of the interaction between catalyst and membrane under reaction conditions is necessary. Also, it is important to know what controlling factors might affect hydrogen production via this process. The aim of this study is first to investigate the hydrogen production via CO_2 reforming of methane on $SrFeCo_{0.5}O_x$ (SFC) and $Ba_{0.5}Sr_{0.5}Co_{0.8}Fe_{0.2}O_x$ (BSCF) dense membranes in conjunction with Pt-based and Ni-based catalysts and then to explore the role of catalyst, membrane, and other parameters to enhance the reaction.

The following research objectives and activities will be accomplished in this dissertation:

- investigate the interaction between ceramic membrane and catalyst
- compare the dry reforming reaction on SFC with that on BSCF
- develop new catalysts for dry reforming of methane on BSCF

- determine the role of different factors like: pH, membrane thickness, feed concentration, catalyst, and reaction temperature on dry reforming of methane on BSCF

1.3 Structure of Dissertation

Chapter 2 describes both commercial methods and new technologies for hydrogen (or syngas) production. It also includes an introduction to membrane materials and membrane reactors. Chapter 3 outlines the materials preparation methods and all experimental techniques used in this research work. Chapter 4 discusses the interaction between ceramic membrane and catalysts inside the membrane reactor and how this interaction affects the overall reaction scheme. Chapter 5 compares the performance of dense SFC with that of dense BSCF for hydrogen production reaction. It will be shown how important the role of membrane material is for enhancing the dry reforming reaction of methane. New catalysts for the dry reforming reaction will be developed in Chapter 6. The promotion of catalyst metallic phase and the effects of catalyst support will be discussed in this chapter. The new catalysts developed in Chapter 6 will be studied more in Chapter 7 under real reaction conditions. The possibility of using theses catalysts for medium and low temperature hydrogen production will be investigated. Finally, Chapter 8 gives a summary of the dissertation and outlines the future directions of this work.

1.4 References

[1] A. M. Aitani and S. A. Ali, "Hydrogen Management in Modern Refineries," *Erdol & Kohle Erdgas Petrochemie*, vol. 48, pp. 19-24, 1995.

[2] H. Cui, S. Q. Turn, and M. A. Reese, "Removal of sulfur compounds from utility pipelined synthetic natural gas using modified activated carbons," *Catalysis Today*, vol. 139, pp. 274-279, 2009.

[3] M. Bowker, "Modeling of Ammonia-Synthesis Kinetics," *Catalysis Today*, vol. 12, pp. 153-163, 1992.

[4] J. W. Veldsink, M. J. Bouma, N. H. Schoon, and A. Beenackers, "Heterogeneous hydrogenation of vegetable oils: A literature review," *Catalysis Reviews-Science and Engineering*, vol. 39, pp. 253-318, 1997.

[5] http://www.hydrogenassociation.org/general/faqs.asp#howmuchproduced.

[6] M. Ikeguchi, T. Mimura, Y. Sekine, E. Kikuchi, and M. Matsukata, "Reaction and oxygen permeation studies in $Sm_{0.4}Ba_{0.6}Fe_{0.8}Co_{0.2}O_{3-\delta}$ membrane reactor for partial oxidation of methane to syngas," *Applied Catalysis A-General*, vol. 290, pp. 212-220, 2005.

[7] O. L. Eliseev, "Gas-to-Liquid Technologies," *Russian Journal of General Chemistry*, vol. 79, pp. 2509-2519, 2009.

[8] P. Chand, V. R. Chintareddy, J. G. Verkade, and D. Grewell, "Enhancing Biodiesel Production from Soybean Oil Using Ultrasonics," *Energy & Fuels*, vol. 24, pp. 2010-2015, 2010.

[9] M. Balat, "Possible Methods for Hydrogen Production," *Energy Sources Part a-Recovery Utilization and Environmental Effects*, vol. 31, pp. 39-50, 2009.

[10] http://en.wikipedia.org/wiki/Hydrogen_economy.

[11] U. Balachandran, J. T. Dusek, P. S. Maiya, B. Ma, R. L. Mieville, M. S. Kleefisch, and C. A. Udovich, "Ceramic membrane reactor for converting methane to syngas," *Catalysis Today*, vol. 36, pp. 265-272, 1997.

[12] S. Gopalan, "Using ceramic mixed ionic and electronic conductors for gas separation," *Jom-Journal of the Minerals Metals & Materials Society*, vol. 54, pp. 26-29, 2002.

[13] H. Wang, C. Tablet, W. Yang, and J. Caro, "In situ high temperature X-ray diffraction of mixed ionic and electronic conducting perovskite-type membranes," *Materials Letters*, vol. 59, pp. 3750-3755, 2005.

[14] G. Etchegoyen, E. Chartier, and P. Del-Gallo, "Oxygen Permeation in $La_{0.6}Sr_{0.4}Fe_{0.9}Ga_{0.1}O_{3-\delta}$ Dense Membrane: Effects of Surface Microstructure " *J Solid State Electrochem*, pp. 597-603, 2006.

[15] H. J. Bouwmeester, "Dense ceramic membranes for methane conversion," *Catalysis Today*, vol. 82, pp. 141-150, 2003.

[16] P. Zeng, Z. Chen, W. Zhou, H. Gu, Z. Shao, and S. Liu, "Re-evaluation of $Ba_{0.5}Sr_{0.5}Co_{0.8}Fe_{0.2}O_{3-\delta}$ Perovskite as Oxygen Semi-permeable Membrane," *J.Membrane Science*, vol. 291, pp. 148-156, 2007.

Chapter 2: Background

The significance of H_2 production is increasing because fossil fuels are being depleted. For this reason, new methods of H_2 production need to be developed. In this chapter, current methods for hydrogen production are investigated and a new method for producing hydrogen using ceramic membranes is introduced.

2.1 Current Technologies for Hydrogen Production

Hydrogen can be generated from two different resources: hydrocarbons and water. Currently, most of hydrogen is produced from hydrocarbons (natural gas, gasoline, and coal) in the world.

2.1.1 Hydrogen from Hydrocarbons

The commercial process for hydrogen production is steam reforming of natural gas at high temperatures (700-1100ºC) [1]. In this process, steam reacts with methane (the most abundant component in natural gas) to yield syngas via the following reaction [2]:

$$CH_4 + H_2O \leftrightarrow CO + 3\ H_2 \qquad (\Delta H^o = +206\ kJ/mol) \qquad (1)$$

A great amount of heat is required for this reaction which is not desirable. For preventing carbon deposition, the steam to carbon ratio should be high. The high steam to carbon ratio as well as high heat requirement cause the cost of plant to increase (2-5 $/ Kg of H_2 [2]). In order to eliminate the CO produced by this reaction, CO is usually converted to CO_2 via another reaction which is called low-

temperature water gas shift, performed at about 200-300ºC [2, 3]:

$$CO + H_2O \leftrightarrow CO_2 + H_2 \qquad (\Delta H^o = -41.1 \text{ kJ/mol}) \qquad (2)$$

Another method for hydrogen production from hydrocarbons is the partial oxidation of methane (or natural gas). This reaction provides a 2:1 ratio of H_2:CO which is beneficial to Fischer–Tropsch process and methanol synthesis [4]. Also, this reaction is exothermic which can reduce the overall hydrogen production plant cost [5].

$$CH_4 + \tfrac{1}{2} O_2 \leftrightarrow CO + 2 H_2 \qquad (\Delta H^o = -71 \text{ kJ/mol}) \qquad (3)$$

Oxygen used in this reaction is obtained from air separation plant which is expensive. Thus, one of the main drawbacks of this reaction is the high cost of oxygen separation from air [1]. Another drawback of this process is the existence of hot spots in the catalyst bed due to the reaction exothermicity [1]. This hydrogen production process could be cost-effective if oxygen is provided by sources other than air separation plant.

CO_2 reforming (or dry reforming) of methane is another process for hydrocarbon-based hydrogen production. This process has gained increasing attention over the past few decades commercially and environmentally. The main idea of this process is to utilize CO_2 and CH_4, which are two of the most abundant greenhouse gases, resulting in a cleaner environment [1, 6].

$$CH_4 + CO_2 \leftrightarrow 2 CO + 2 H_2 \qquad (\Delta H^o = 247 \text{ kJ/mol}) \qquad (4)$$

Although this reaction is highly endothermic, the CO_2 utilization provides a source of clean oxygen, which eliminates the need for a costly air separation plant.

Furthermore, a 1:1 ratio of H_2:CO is produced in dry reforming, which is a good ratio for the production of oxygenated compounds [7].

It should be noted that reactions 1-4 are reversible. Detailed information about equilibrium product compositions and equilibrium constants at different temperatures were provided by one of the former students in Dr Susan Williams' research group [8].

Syngas can also be produced by coal gasification. The syngas generated from coal is also known as town gas or coal gas. During gasification, coal reacts with oxygen and steam under heat and pressure [2].

$$\text{Coal} + O_2 + H_2O \rightarrow H_2 + CO \quad (5)$$

This reaction could be economical where coal is abundant. However, this method requires a great amount of heat, construction of a large gasifier, and coal storage facilities which results in high plant investment and operating costs [9].

The hydrogen production methods explained so far are methods using non-renewable resources (fossil fuels). Currently, a great deal of research is devoted to the development of a process to produce hydrogen from renewable resources like waste glycerol from the biodiesel industry [10]. Ethanol is another renewable feedstock that can be used for hydrogen production [11]. These renewable-based methods are outside the scope of this dissertation but should be considered for future research.

2.1.2 Hydrogen from Water

One of the cheapest methods for hydrogen generation is by water decomposition into hydrogen and oxygen due to an electric current (electrolysis). However, the direct decompsition of water is very difficult under normal conditions.

$$H_2O \rightarrow H_2 + 0.5\ O_2 \quad (6)$$

This process will be cost-effective if cheap water resources are available. The cost of electricity for this method needs to be low. If solar-driven electricity is used in this process, the environmental impacts would be minimized [12].

The selection of one of the methods, described in this section, for hydrogen production depends on several factors such as: the desired H_2:CO ratio, the capital and operating costs, and the plant location. Sometimes, the selection of catalyst can also impact the whole production process. Therefore, it is important to know what kinds of catalysts are currently used for hydrogen production and how they impact the reaction.

2.2 Supported Metal Catalysts

2.2.1 The Problem of Carbon Deposition

Since the majority of hydrogen production processes are performed at high temperatures, carbon deposition can easily occur at such high temperatures via the following reactions [1]:

$$2CO \rightarrow C + CO_2 \qquad (\Delta H^o = -171\ kJ/mol) \quad (7)$$

$$CH_4 \rightarrow C + 2H_2 \qquad (\Delta H^o = 75\ kJ/mol) \quad (8)$$

$CO + H_2 \rightarrow C + H_2O$ ($\Delta H^o = -131$ kJ/mol) (9)

Carbon, which is formed via the above-mentioned reactions, covers the catalyst active sites and reduces the activity of catalyst significantly [13]. Carbon or coke formation is one of the main problems of the dry reforming reaction of methane (reaction 4) and one of the reasons why this reaction has not yet been commercialized [14]. The type of catalyst can affect the carbon deposition rate, so current research efforts have focused on developing highly active catalysts which are less susceptible to carbon deposition over a long period of reaction [15]. A fully deactivated catalyst which is covered by a layer of carbon has a black color and most of the time can be distinguished from fresh catalyst.

2.2.2 The Role of Metal

Choosing an efficient catalyst plays an important role in increasing the reaction conversion as well as product selectivity. The amount of metal content in a catalyst is very important and the catalyst performance is strongly dependent on the metal percentage [16, 17]. Transition metals (group VIII metals) like Pt, Ni, Ru, and Rh on a variety of supports have been studied in the literature for catalyzing hydrogen production reactions [5, 17-19]. These kinds of catalysts are divided into two groups: catalysts that contain one type of metal (monometallic) and catalysts that generally contain two types of metals (bimetallic). Among these transition metals, Ni has received a great deal of attention and has been used commercially due to its low price and also its high availability. However, commercial Ni supported on Al_2O_3 suffers

from severe deactivation due to carbon deposition [13, 17, 20], leading to blockage of the reactor bed, large pressure drops, and crushing the catalyst pellets. This catalyst can also be poisoned by small amounts of sulfur present in the feed [13]. Several groups have focused on the promotion of the Ni catalyst in order to reduce the coke formation and improve the catalyst stability and they have proved that adding noble metals can enhance the reactivity of the catalyst [20-22]. Although both Pt and Rh metals have shown very good performances with less carbon deposition for hydrogen production reaction [23, 24], they are more expensive and less abundant than Ni-based catalysts. Thus, if the process of hydrogen production is improved so that no carbon deposition occurred, the Ni-based catalyst would be the most commercially feasible metal for this process.

2.2.3 The Role of Catalyst Support

It has been shown that the support can increase the activity of catalyst for H_2 production reaction. In fact, support can affect the metal dispersion, coke resistance, and the metal-support interactions [1, 17]. Different acidic and basic supports with different surface areas have been studied for H_2 production: Al_2O_3, ZrO_2, CeO_2, $CeZrO_2$, SiO_2, CaO, zeolite, and MgO [1, 16, 25]. Among these materials, alumina is the most commonly used support. Some studies have reported that modification of Al_2O_3 support with other metal oxides such as ZrO_2 can improve the coking resistance of Ni/Al_2O_3 catalyst due to oxygen release capability of ZrO_2 [17].

Therefore, if a coke-resistant support is found, the Ni-based catalyst would be the most commercially feasible metal for the hydrogen production reaction.

2.3 Oxygen Permeable Ceramic Membrane Materials

Mixed ionic and electronic conductive (MIEC) ceramic membranes have received substantial interest in recent decades for various applications requiring gas separations [26-28]. MIEC ceramic membranes, which are metal oxides, are made of dense conductive materials that only allow electrons and certain ions to pass through. Oxygen permeable ceramic membranes, which are used for oxygen separation, can conduct oxygen ions at elevated temperatures.

The ideal amount of oxygen separation could be achieved by ceramic membranes with high oxygen permeability. Although all ceramic membranes are metal oxides, the composition of ceramic membranes can vary significantly. Composition is one of the dominant factors for that determines the oxygen flux. According to the literature, several types of ceramic membranes like $SrFeCo_{0.5}O_x$, $SrFe_{0.2}Co_{0.5}O_x$, $Ba_{0.5}Sr_{0.5}Co_{0.8}Fe_{0.2}O_x$, $BaCo_{0.4}Fe_{0.4}Zr_{0.2}O_x$, $La_{0.6}Sr_{0.4}CoO_x$, and $Sr_{0.5}La_{0.5}Fe_{0.8}Ga_{0.2}O_x$ have been used [29-33]; however, most of the researchers who have used $SrFeCo_{0.5}O_{x,}$ have reported the problem of low oxygen flux through this ceramic membrane [34, 35]. Some ceramic materials have a perovskite-type structure. The perovskite materials have the general chemical formula of ABO_3 [36], which is shown in Figure 2.1. A is the larger cation with a 12-fold oxygen ion coordination

and B is the smaller cation with a 6-fold coordination. A-site choices in the literature include La, Sr, and Ba, while B-site choices include Fe, Co, Cr, Cu, Mn, and Ga [37].

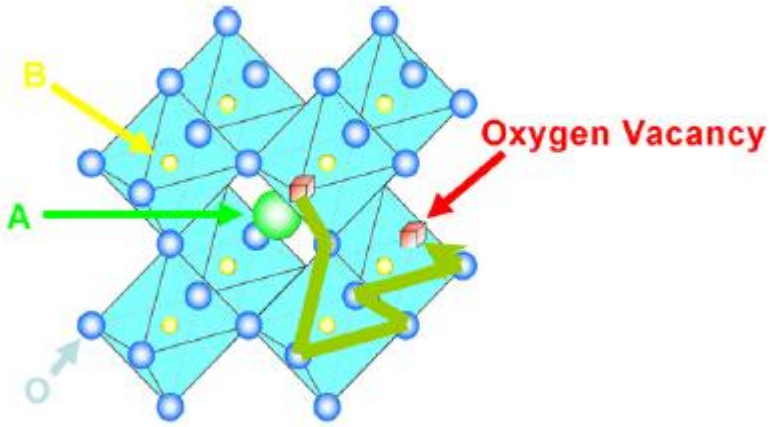

Figure 2.1. Perovskite structure [38].

MIEC materials have ionic conduction properties due to the presence of oxygen vacancies in the lattice structure [37, 39]. The number of oxygen vacancies is a function of material composition and structure, temperature, pressure, and ambient atmospheric condition. At sufficiently high temperatures, these oxygen vacancies become mobile and migrate through the lattice. In fact, oxygen vacancy mobility is the main reason for the oxygen transport [37].

The oxygen transport mechanism is shown in Figure 2.2. First, an oxygen molecule from gas phase is adsorbed to the surface of ceramic material and then this molecule dissociates into two oxygen ions by receiving electrons from the membrane surface. Oxygen ions are transferred across the membrane through oxygen vacancies and eventually these ions reach the other side of membrane, where these two ions

recombine and produce one oxygen molecule by releasing electrons. Finally, the produced oxygen molecule desorbs back to the gas phase.

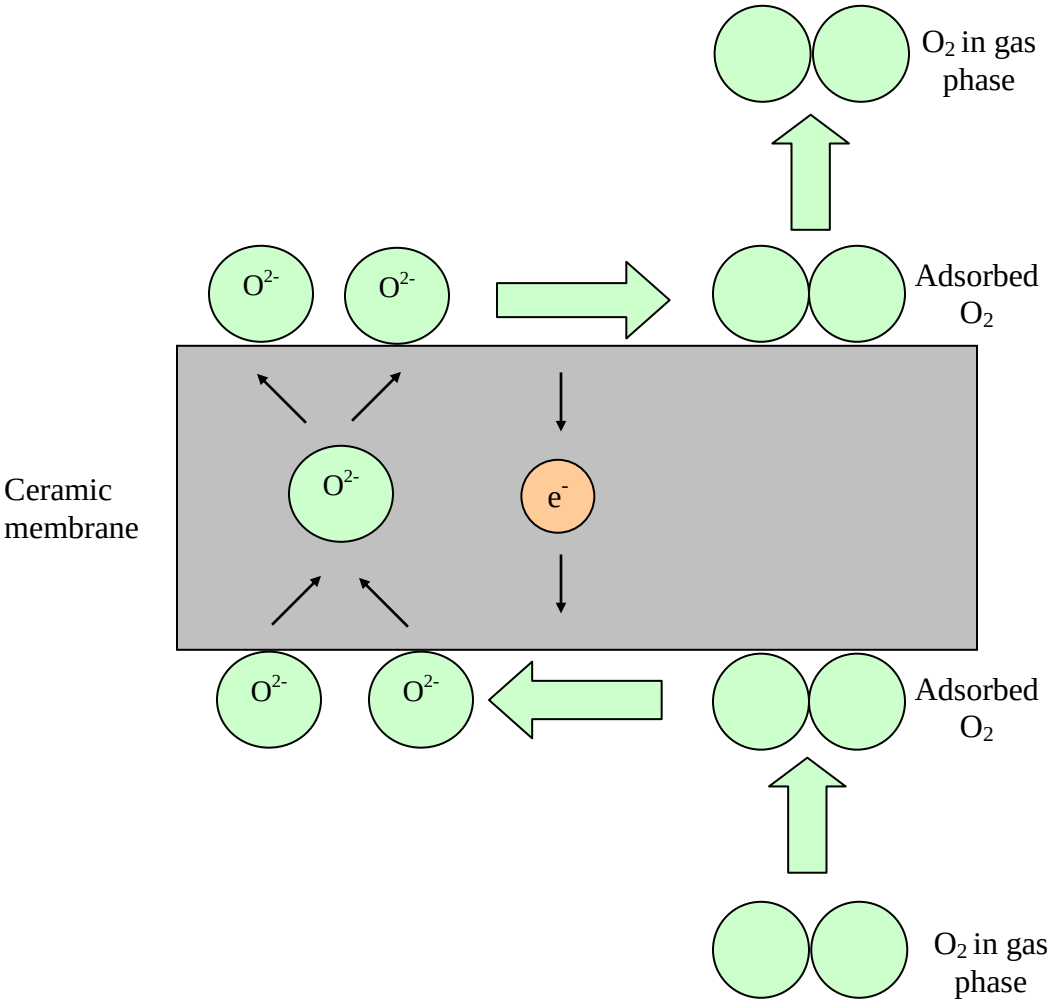

Figure 2.2. O_2 transport mechanism.

The permeation of oxygen ions through ceramic membranes is affected by driving forces, which are the operating temperature and oxygen partial pressure on both sides of the selected membrane [33, 40]. The oxygen permeation increases with

an increase in the operating temperature and an increase in the differential pressure of oxygen between the two sides of the membrane.

The geometry of the membrane systems is also another factor for increasing oxygen permeation as it can affect the surface area of the membranes [40]. The larger the surface area of the ceramic membranes, the more easily the oxygen ions can penetrate the ceramic membranes. For instance, the surface area per unit volume of a hollow fiber membrane is much greater than that of a disk-shaped membrane. Thus, the hollow fiber membrane exhibits more oxygen flux compared to the disk-shaped membrane [41]. A study in the literature has suggested that hollow fiber ceramic membranes can successfully separate oxygen from air at flux rates that could be considered commercially worthwhile and, thus, have potential application for improving the economy for methane conversion processes [42]. According to the published article, by using these types of ceramic membranes, methane conversions around 80% have been observed [42].

One of the mechanical requirements of a membrane is long-term stability. The membrane thickness can influence the oxygen permeation. The resistivity of membranes against oxygen penetration becomes more considerable as membrane thickness increases; for this reason, the membranes are usually chosen to be as thin as possible to display a satisfying oxygen flux [43, 44]. However, it is not possible to decrease the thickness of a dense membrane as much as is desired because the membrane has reduced mechanical stability and might crack. For this reason, asymmetric ceramic membranes have been developed with a very thin dense layer

supported on a thick porous layer [45]. These membranes have shown superior performance compared to planar membranes [46].

2.4 Membrane Reactors

If oxygen permeable ceramic membranes are used in conjunction with a catalyst to enhance a reaction, these systems are called membrane reactors. In other words, in membrane reactors (shown in Figure 2.3) separation and reaction will occur simultaneously. To express it in simple terms, oxygen from the air penetrates the dense ceramic membrane and reacts over a selective catalyst with methane, which exists on the other side of the membrane, and, consequently, hydrogen will be synthesized (typically at temperatures higher than 800ºC) via the chemical reactions previously mentioned in this dissertation (reactions 1-4).

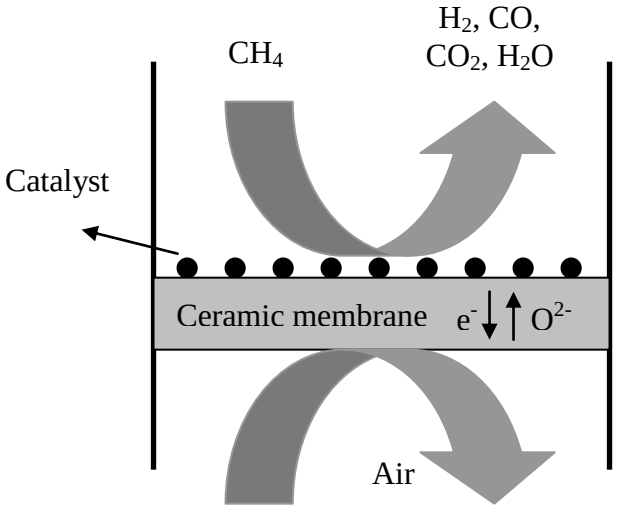

Figure 2.3. Membrane reactor scheme for the methane conversion to syngas using an electron/ion conductive ceramic membrane.

Oxygen permeable membrane reactors offer a promising alternative oxygen supply technology for synthesis gas production, while they control the distribution of oxygen supply along the reactor. Therefore, these membranes, which can be integrated into the syngas generator, eliminate the need for a large expensive air separation plant. Several groups have applied these reactors for hydrogen and syngas production from different hydrocarbons and it was shown that membrane materials with higher oxygen flux are promising candidates for hydrogen production [4, 47-52].

In order to have industrially feasible membrane reactors, there are several requirements that need to be met [51]:

- The membrane material must have a very high oxygen flux during the reaction period.
- The membrane material must exhibit considerable long-term mechanical and thermal stability under reaction reducing environment.
- The membrane material and its preparation method must be inexpensive.

The type of catalyst that is used in the membrane reactor is one of the controlling factors affecting the reaction part of this hydrogen production process, and it obviously has a significant impact on the reaction rate and the conversion of hydrocarbons. For achieving high efficiency in the membrane reactor systems, the catalyst must be chosen accurately. According to the literature, the nickel-based catalyst has been developed for partial oxidation of methane in membrane reactors [35, 53]. As mentioned before, the main problem with employing this kind of catalyst

is the deactivation of the catalyst by carbon deposition on the surface of the catalyst at high temperatures [17]. In other words, the deactivation of catalyst leads to the undesirable reduction of the reaction rate with time. Ni-based catalysts have not been used for dry reforming of methane in a ceramic membrane reactor so the performances of these catalysts need to be studied on the surface of the ceramic membrane. Oxygen from the ceramic membrane might be able to remove carbon deposited on the surface of this catalyst and improve its long-term stability for dry reforming of methane.

2.5 References

[1] M. S. Fan, A. Z. Abdullah, and S. Bhatia, "Catalytic Technology for Carbon Dioxide Reforming of Methane to Synthesis Gas," *Chemcatchem*, vol. 1, pp. 192-208, 2009.

[2] M. Balat, "Possible Methods for Hydrogen Production," *Energy Sources Part a-Recovery Utilization and Environmental Effects*, vol. 31, pp. 39-50, 2009.

[3] J. D. Holladay, J. Hu, D. L. King, and Y. Wang, "An overview of hydrogen production technologies," *Catalysis Today*, vol. 139, pp. 244-260, 2009.

[4] M. Ikeguchi, T. Mimura, Y. Sekine, E. Kikuchi, and M. Matsukata, "Reaction and oxygen permeation studies in $Sm_{0.4}Ba_{0.6}Fe_{0.8}Co_{0.2}O_{3-\delta}$ membrane reactor for partial oxidation of methane to syngas," *Applied Catalysis A-General*, vol. 290, pp. 212-220, 2005.

[5] S. B. Wang, G. Q. M. Lu, and G. J. Millar, "Carbon dioxide reforming of methane to produce synthesis gas over metal-supported catalysts: State of the art," *Energy & Fuels*, vol. 10, pp. 896-904, 1996.

[6] J. Ma, N. N. Sun, X. L. Zhang, N. Zhao, F. K. Mao, W. Wei, and Y. H. Sun, "A short review of catalysis for CO_2 conversion," *Catalysis Today*, vol. 148, pp. 221-231, 2009.

[7] K. W. Jun, H. S. Roh, and K. V. R. Chary, "Structure and catalytic properties of ceria-based nickel catalysts for CO_2 reforming of methane," *Catalysis Surveys from Asia*, vol. 11, pp. 97-113, 2007.

[8] D. A. Slade, "Mixed Ionic/Electronic Conducting Ceramic Membranes for Oxygen-Assisted CO_2 Reforming," in *Chemical Engineering*, Ph.D. Lawrence: The University of Kansas, 2010, pp. 212.

[9] E. Shafirovich and A. Varma, "Underground Coal Gasification: A Brief Review of Current Status," *Industrial & Engineering Chemistry Research*, vol. 48, pp. 7865-7875, 2009.

[10] B. L. Dou, G. L. Rickett, V. Dupont, P. T. Williams, H. S. Chen, Y. L. Ding, and M. Ghadiri, "Steam reforming of crude glycerol with in situ CO_2 sorption," *Bioresource Technology*, vol. 101, pp. 2436-2442.

[11] J. Sun, Y. G. Wang, J. G. Li, G. L. Xiao, L. G. Zhang, H. Li, Y. L. Cheng, C. W. Sun, Z. X. Cheng, Z. C. Dong, and L. Q. Chen, "H-2 production from stable ethanol steam reforming over catalyst of NiO based on flowerlike CeO_2 microspheres," *International Journal of Hydrogen Energy*, vol. 35, pp. 3087-3091.

[12] "eere.energy.gov/hydrogenandfuelcells/mypp/.../production.pdf."

[13] J. Sehested, "Four challenges for nickel steam-reforming catalysts," *Catalysis Today*, vol. 111, pp. 103-110, 2006.

[14] S. Ozkara-Aydinoglu, E. Ozensoy, and A. E. Aksoylu, "The effect of impregnation strategy on methane dry reforming activity of Ce promoted Pt/ZrO_2," *International Journal of Hydrogen Energy*, vol. 34, pp. 9711-9722, 2009.

[15] J. A. C. Dias and J. M. Assaf, "Autoreduction of promoted $Ni/\gamma\text{-}Al_2O_3$ during autothermal reforming of methane," *Journal of Power Sources*, vol. 139, pp. 176-181, 2005.

[16] B. Pawelec, S. Damyanova, K. Arishtirova, J. L. G. Fierro, and L. Petrov, "Structural and surface features of PtNi catalysts for reforming of methane with
CO_2," *Applied Catalysis A-General*, vol. 323, pp. 188-201, 2007.

[17] S. Therdthianwong, C. Siangchin, and A. Therdthianwong, "Improvement of coke resistance of Ni/Al_2O_3 catalyst in CH_4/CO_2 reforming by ZrO_2 addition," *Fuel Processing Technology*, vol. 89, pp. 160-168, 2008.

[18] R. Lanza, P. Canu, and S. G. Jaras, "Partial oxidation of methane over Pt-Ru bimetallic catalyst for syngas production," *Applied Catalysis A-General*, vol. 348, pp. 221-228, 2008.

[19] A. Takano, T. Tagawa, and S. Goto, "Carbon-Dioxide Reforming of Methane on Supported Nickel-Catalysts," *Journal of Chemical Engineering of Japan*, vol. 27, pp. 727-731, 1994.

[20] Z. Y. Hou and T. Yashima, "Small amounts of Rh-promoted Ni catalysts for methane reforming with CO_2," *Catalysis Letters*, vol. 89, pp. 193-197, 2003.

[21] L. Ma and D. L. Trimm, "Alternative catalyst bed configurations for the autothermic conversion of methane to hydrogen," *Applied Catalysis A-General*, vol. 138, pp. 265-273, 1996.

[22] B. C. Enger, R. Lodeng, and A. Holmen, "Evaluation of reactor and catalyst performance in methane partial oxidation over modified nickel catalysts," *Applied Catalysis A-General*, vol. 364, pp. 15-26, 2009.

[23] S. Damyanova, B. Pawelec, K. Arishtirova, M. V. M. Huerta, and J. L. G. Fierro, "The effect of CeO_2 on the surface and catalytic properties of Pt/CeO_2-

ZrO_2 catalysts for methane dry reforming," *Applied Catalysis B-Environmental*, vol. 89, pp. 149-159, 2009.

[24] C. Carrara, A. Roa, L. Comaglia, E. A. Lornbardo, C. Mateos-Pedrero, and P. Ruiz, "Hydrogen production in membrane reactors using Rh catalysts on binary supports," *Catalysis Today*, vol. 133, pp. 344-350, 2008.

[25] J. A. C. Ruiz, F. B. Passos, J. M. C. Bueno, E. F. Souza-Aguiar, L. V. Mattos, and F. B. Noronha, "Syngas production by autothermal reforming of methane on supported platinum catalysts," *Applied Catalysis A-General*, vol. 334, pp. 259-267, 2008.

[26] M. Freemantle, "Membranes For Gas Separation," in *Chemical & Engineering News*, 2005.

[27] S. Gopalan, "Using ceramic mixed ionic and electronic conductors for gas separation," *Jom-Journal of the Minerals Metals & Materials Society*, vol. 54, pp. 26-29, 2002.

[28] A. J. Jacobson, S. Kim, A. Medina, Y. L. Yang, and B. Abeles, "Dense oxide membranes for oxygen separation and methane conversion," *Mat Res Soc Symp Proc*, vol. 497, pp. 29-34, 1998.

[29] Z. P. Shao, H. Dong, G. X. Xiong, Y. Gong, and W. S. Yang, "Performance of a mixed-conducting ceramic membrane reactor with high oxygen permeability for methane conversion," *Journal of Membrane Science*, vol. 183, pp. 181-192, 2001.

[30] J. T. Ritchie, J. T. Richardson, and D. Luss, "Ceramic membrane reactor for synthesis gas production," *Aiche Journal*, vol. 47, pp. 2092-2101, 2001.

[31] E. V. Kondratenko, H. H. Wang, V. A. Kondratenko, and J. Caro, "Selective oxidation of CH_4 and C_2H_6 over a mixed oxygen ion and electron conducting perovskite-A TAP and membrane reactors study," *Journal of Molecular Catalysis A-Chemical*, vol. 297, pp. 142-149, 2009.

[32] J. M. Kim, G. J. Hwang, S. H. Lee, C. S. Park, J. W. Kim, and Y. H. Kim, "Properties of oxygen permeation and partial oxidation of methane in $La_{0.6}Sr_{0.4}CoO_{3-\delta}$ (LSC) - $La_{0.7}Sr_{0.3}Ga_{0.6}Fe_{0.4}O_{3-\delta}$ (LSGF) membrane," *Journal of Membrane Science*, vol. 250, pp. 11-16, 2005.

[33] J. Tong, W. Yang, R. Cai, B. Zhu, and L. C. L.-. Lin, "Novel and ideal zirconium-based dense membrane reactors for partial oxidation of methane to syngas," *Catal Lett*, vol. 78, pp. 129-137, 2002.

[34] U. Balachandran, J. T. Dusek, P. S. Maiya, B. Ma, R. L. Mieville, M. S. Kleefisch, and C. A. Udovich, "Ceramic membrane reactor for converting methane to syngas," *Catalysis Today*, vol. 36, pp. 265-272, 1997.

[35] S. J. Feng, S. Ran, D. C. Zhu, W. Liu, and C. S. Chen, "Synthesis gas production from methane with $SrFeCo_{0.5}O_y$ membrane reactor," *Energy & Fuels*, vol. 18, pp. 385-389, 2004.

[36] A. S. Bhalla, R. Y. Guo, and R. Roy, "The perovskite structure - a review of its role in ceramic science and technology," *Materials Research Innovations*, vol. 4, pp. 3-26, 2000.

[37] W. Zhou, R. Ran, and Z. P. Shao, "Progress in understanding and development of $Ba_{0.5}Sr_{0.5}Co_{0.8}Fe_{0.2}O_{3-\delta}$-based cathodes for intermediate-temperature solid-oxide fuel cells: A review," *Journal of Power Sources*, vol. 192, pp. 231-246, 2009.

[38] P. Y. Zeng, Z. H. Chen, W. Zhou, H. X. Gu, Z. P. Shao, and S. M. Liu, "Re-evaluation of $Ba_{0.5}Sr_{0.5}Co_{0.8}Fe_{0.2}O_{3-\delta}$ perovskite as oxygen semi-permeable membrane," *Journal of Membrane Science*, vol. 291, pp. 148-156, 2007.

[39] P. Zeng, Z. Chen, W. Zhou, H. Gu, Z. Shao, and S. Liu, "Re-evaluation of $Ba_{0.5}Sr_{0.5}Co_{0.8}Fe_{0.2}O_{3-\delta}$ Perovskite as Oxygen Semi-permeable Membrane," *J.Membrane Science*, vol. 291, pp. 148-156, 2007.

[40] H. H. Wang, Y. Cong, and W. S. Yang, "Investigation on the partial oxidation of methane to syngas in a tubular $Ba_{0.5}Sr_{0.5}Co_{0.8}Fe_{0.2}O_{3-\delta}$ membrane reactor," *Catalysis Today*, vol. 82, pp. 157-166, 2003.

[41] F. T. Akin, Y. S. Lin, and Y. Zeng, "Comparative study on oxygen permeation and oxidative coupling of methane on disk-shaped and tubular dense ceramic membrane reactors," *Ind Eng Chem Res*, vol. 40, pp. 5908-5916, 2001.

[42] J. Caro, H. H. Wang, C. Tablet, A. Kleinert, A. Feldhoff, T. Schiestel, M. Kilgus, P. Kolsch, and S. Werth, "Evaluation of perovskites in hollow fibre and disk geometry in catalytic membrane reactors and in oxygen separators," *Catalysis Today*, vol. 118, pp. 128-135, 2006.

[43] Z. H. Chen, R. Ran, Z. P. Shao, H. Yu, J. C. D. da Costa, and S. M. Liu, "Further performance improvement of $Ba_{0.5}Sr_{0.5}Co_{0.8}Fe_{0.2}O_{3-\delta}$ perovskite membranes for air separation," *Ceramics International*, vol. 35, pp. 2455-2461, 2009.

[44] W. K. Hong and G. M. Choi, "Oxygen permeation of BSCF membrane with varying thickness and surface coating," *Journal of Membrane Science*, vol. 346, pp. 353-360.

[45] X. Yin, L. Hong, and Z. L. Liu, "Asymmetric tubular oxygen-permeable ceramic membrane reactor for partial oxidation of methane," *Journal of Physical Chemistry C*, vol. 111, pp. 9194-9202, 2007.

[46] D. A. Slade, Q. Y. Jiang, K. J. Nordheden, and S. M. Stagg-Williams, "A comparison of mixed-conducting oxygen-permeable membranes for CO_2 reforming," *Catalysis Today*, vol. 148, pp. 290-297, 2009.

[47] Y. W. Zhang, Q. Li, P. J. Shen, Y. Liu, Z. B. Yang, W. Z. Ding, and X. G. Lu, "Hydrogen amplification of coke oven gas by reforming of methane in a ceramic membrane reactor," *International Journal of Hydrogen Energy*, vol. 33, pp. 3311-3319, 2008.

[48] W. L. Zhu, W. Han, G. X. Xiong, and W. S. Yang, "Performance study of heptane reforming in the dense ceramic membrane reactors," *Aiche Journal*, vol. 54, pp. 242-248, 2008.

[49] H. H. Wang, Y. Cong, and W. S. Yang, "Partial oxidation of ethane to syngas in an oxygen-permeable membrane reactor," *Journal of Membrane Science*, vol. 209, pp. 143-152, 2002.

[50] W. L. Zhu, W. Han, G. X. Xiong, and W. S. Yang, "Mixed reforming of simulated gasoline to hydrogen in a BSCFO membrane reactor," *Catalysis Today*, vol. 118, pp. 39-43, 2006.

[51] W. S. Yang, H. H. Wang, X. F. Zhu, and L. W. Lin, "Development and application of oxygen permeable membrane in selective oxidation of light alkanes," *Topics in Catalysis*, vol. 35, pp. 155-167, 2005.

[52] W. L. Zhu, W. Han, G. X. Xiong, and W. S. Yang, "Mixed reforming of heptane to syngas in the $Ba_{0.5}Sr_{0.5}Co_{0.8}Fe_{0.2}O_3$ membrane reactor," *Catalysis Today*, vol. 104, pp. 149-153, 2005.

[53] C.-Y. Tsai, A. G. Dixon, W. R. Moser, and Y. H. Ma, "Dense perovskite membrane reactors for partial oxidation of methane to syngas," *AIChE Jnl*, vol. 43, pp. 2741-2750, 1997.

Chapter 3: Experimental

3.1 Materials

3.1.1 Gases

The gases used for this study were obtained from Linweld Company. These gases include but are not limited to 5% oxygen in helium (research grade), 5% hydrogen in argon (research grade), 1% CO in helium (research grade), 1% CO_2 in helium (research grade), zero grade air, ultra high purity argon, high purity hydrogen, CP grade methane, CP grade CO_2, calibration mixture gas (contains 25% CO, 25% H_2, 25% CH_4, and 25% CO_2), instrument grade nitrogen, and instrument grade helium. The flow rate of gases used in each experiment will be provided in each section describing that experiment.

3.1.2 Catalyst Preparation

Pt-based and Ni-based catalysts are studied in this work: Pt/ZrO_2, $Pt/CeZrO_2$, $Ni/CeZrO_2$, $Pt\text{-}Ni/CeZrO_2$, Ni/Al_2O_3, and $Pt\text{-}Ni/Al_2O_3$. These catalysts were chosen to compare the performance of commercial Ni/Al_2O_3 catalyst with that of expensive Pt-based catalysts in order to decide which catalyst performs better for hydrogen production at different temperatures. Table 3.1 lists the characteristics of the catalysts investigated. No catalyst reduction procedure was performed prior to reaction testing in both the plug flow reactor and the membrane reactor.

Table 3.1. The characteristics of the catalysts investigated.

Catalyst	Metal loading	Preparation Method	Precursor
Pt/ZrO_2	0.5 wt%	Impregnation	$H_2PtCl_6.6H_2O$
$Pt/CeZrO_2$	0.404 wt%	Impregnation	$H_2PtCl_6.6H_2O$
$Ni/CeZrO_2$	15 wt%	Impregnation	$Ni(NO_3)_2.6H_2O$
$Pt\text{-}Ni/CeZrO_2$	Ni:15wt%, Pt:0.2 wt%	Sequential Impregnation	$Pt(NH_3)_4(NO_3)_2$
Ni/Al_2O_3	15 wt%	Impregnation	$Ni(NO_3)_2.6H_2O$
$Pt\text{-}Ni/Al_2O_3$	Ni:15wt%, Pt:0.2 wt%	Sequential Impregnation	$Pt(NH_3)_4(NO_3)_2$

Both Pt/ZrO_2 and $Pt/CeZrO_2$ catalysts were prepared by depositing Pt on commercially available ZrO_2 and $CeZrO_2$ support materials (MEI CHEM, with 18 wt% of Ce) using the incipient wetness impregnation technique with an aqueous solution of $H_2PtCl_6.6H_2O$ (Alfa Aesar, 99.9%). Prior to deposition, the substrate was calcined at 800°C; after deposition it was dried overnight at 120°C and then calcined at 400°C for 2 hr in flowing air.

The commercial Ni/Al_2O_3 catalyst (15 wt% Ni supported on Al_2O_3) was also prepared by incipient wetness impregnation method. First, the $\delta\text{-}Al_2O_3$ support was prepared by heating the commercial $\gamma\text{-}Al_2O_3$ support (Alfa Aesar, 99.7%) at 200°C for 2 hours followed by calcining at 900°C for 4 hours [1]. This transformation from a $\gamma\text{-}Al_2O_3$ to $\delta\text{-}Al_2O_3$ support causes an improvement in thermal stability. The $Ni(NO_3)_2.6H_2O$ precursor (Alfa Aesar, 99.9%) was dissolved in distilled water and then this solution was impregnated on the $\delta\text{-}Al_2O_3$ support. After impregnation, the catalyst was dried overnight at 120°C and calcined for 4hr at 600°C under pure air

flow [1]. The preparation method for the $Ni/CeZrO_2$ catalyst (15 wt% Ni supported on $CeZrO_2$) was similar to the Ni/Al_2O_3 catalyst.

The bimetallic $Pt\text{-}Ni/Al_2O_3$ catalyst was prepared by a sequential impregnation technique. The dissolved $Pt(NH_3)_4(NO_3)_2$ precursor (Alfa Aesar, 99.9%) in distilled water was impregnated on Ni/Al_2O_3 catalyst. Then, the powder was dried overnight at 120°C and calcined for 4hr at 500°C under pure air flow [1]. The preparation method for bimetallic $Pt\text{-}Ni/CeZrO_2$ catalyst (15 wt% Ni & 0.2 wt% Pt supported on $CeZrO_2$) was similar to that of the $Pt\text{-}Ni/Al_2O_3$ catalyst.

3.1.3 Membrane Preparation

Two mixed oxide membrane materials are compared in this work: the non-perovskite $SrFeCo_{0.5}O_x$ and the perovskite $Ba_{0.5}Sr_{0.5}Co_{0.8}Fe_{0.2}O_x$ referred to hereafter as SFC and BSCF, respectively. SFC falls into the low oxygen flux category and BSCF falls into the category of high oxygen flux membrane candidates.

The BSCF powder was prepared by Citrate-EDTA (ethylene diamine tetra acetic acid) method [2]. Stoichiometric quantities of the nitrate salts of barium, strontium, cobalt, and iron were added to EDTA-$NH_3 \cdot H_2O$ solution followed by citric acid. The molar ratio of total metal ion (Ba, Sr, Co, and Fe) to EDTA to citric-acid was 1:1:1.5. The pH of the solution was adjusted to 6 by adding $NH_3 \cdot H_2O$. With heating and stirring, a dark purple gel was formed. The gel was heated and dried in air at 110-120°C to yield the preliminary powder. The powder was calcined at 950°C for 5.5 hours in a muffle furnace to obtain BSCF powder. The BSCF powder was

then pressed in a stainless steel die (2 cm diameter) under 250 MPa for 5 minutes. Finally, the membrane was sintered at 1100°C for 5 hours with ramping and cooling rate of 1°C·min^{-1} in a muffle furnace.

The SFC powder, which was obtained from Praxair Specialty Ceramics, was passed through a 60-mesh sieve and coated with 1 wt% ethylcellulose binder prior to pressing. SFC powder was then pressed at a pressure of 60 MPa for 3 minutes and finally was sintered at 1180 ºC in flowing air for 10 hours (heating rate: 1.2 °C/min). During the sintering procedure, the binder burns off between 350°C and 450°C. The presence of the binder did not significantly affect the density of the finished SFC membranes, which is approximately 94% of the theoretical density.

The surface of the final disk-shaped membranes (Figure 3.1) required substantial polishing with a combination of sandpaper and a lathe to ensure adequate sealing in the membrane reactor. The thickness of both membranes was approximately 2 mm after polishing. The fluxes of the SFC and BSCF membranes in an air:Ar gradient were measured at 0.05 sccm/cm^2 and 0.57 sccm/cm^2, respectively.

Figure 3.1. Unpolished BSCF membrane.

For pulse studies in a plug flow reactor and also thermogravimetric analysis (TGA) and Raman studies, the prepared disk-shaped SFC and BSCF membranes were subsequently crushed and then passed through a sieve to obtain a particle size smaller than 250 μm. This procedure ensures that the SFC and BSCF pieces used for the above studies have the same composition and state as the disc-shaped membranes.

3.2 Reaction Tests

Two different types of reactors have been used for reaction studies: a plug flow reactor (PFR) and a membrane reactor.

3.2.1 Plug Flow Reactor (PFR)

A couple of reaction experiments were performed in a 6 mm i.d. quartz tube flow reactor at atmospheric pressure. This reactor was equipped with a tubular and well-insulated furnace that could reach high temperatures. A K-type thermocouple (Omega) was attached to the outside of the reactor to measure temperature, which was controlled with a temperature controller (Omega; CN 3000). For studies where the ratio of catalyst and SFC were varied, a total of 20 mg of physical mixture of material was loaded into the reactor (the ratio varied from 0 to 20). This material was packed in the middle of the reactor using a small amount of quartz wool. The reactor was heated to 800°C with an argon-only feed (15 ml/min) and then held at this temperature. Fifty micro liter pulses of methane or a 1:1 CH_4/CO_2 volumetric ratio (10 ml/min of each gas) were injected into the reactor until no changes were

observed. The reactor effluent composition was quantified using a Balzers OmniStar mass spectrometer. In addition, the inlet flow rate was monitored continuously using an Agilent ADM2000 flowmeter. Quantification of the species in the effluent was performed using calibration injections of known mixtures. This reactor has also been used for Temperature Programmed Oxidation, Temperature Programmed Reduction, and Temperature Programmed Desorption studies. A schematic of this PFR is shown in Figure 3.2.

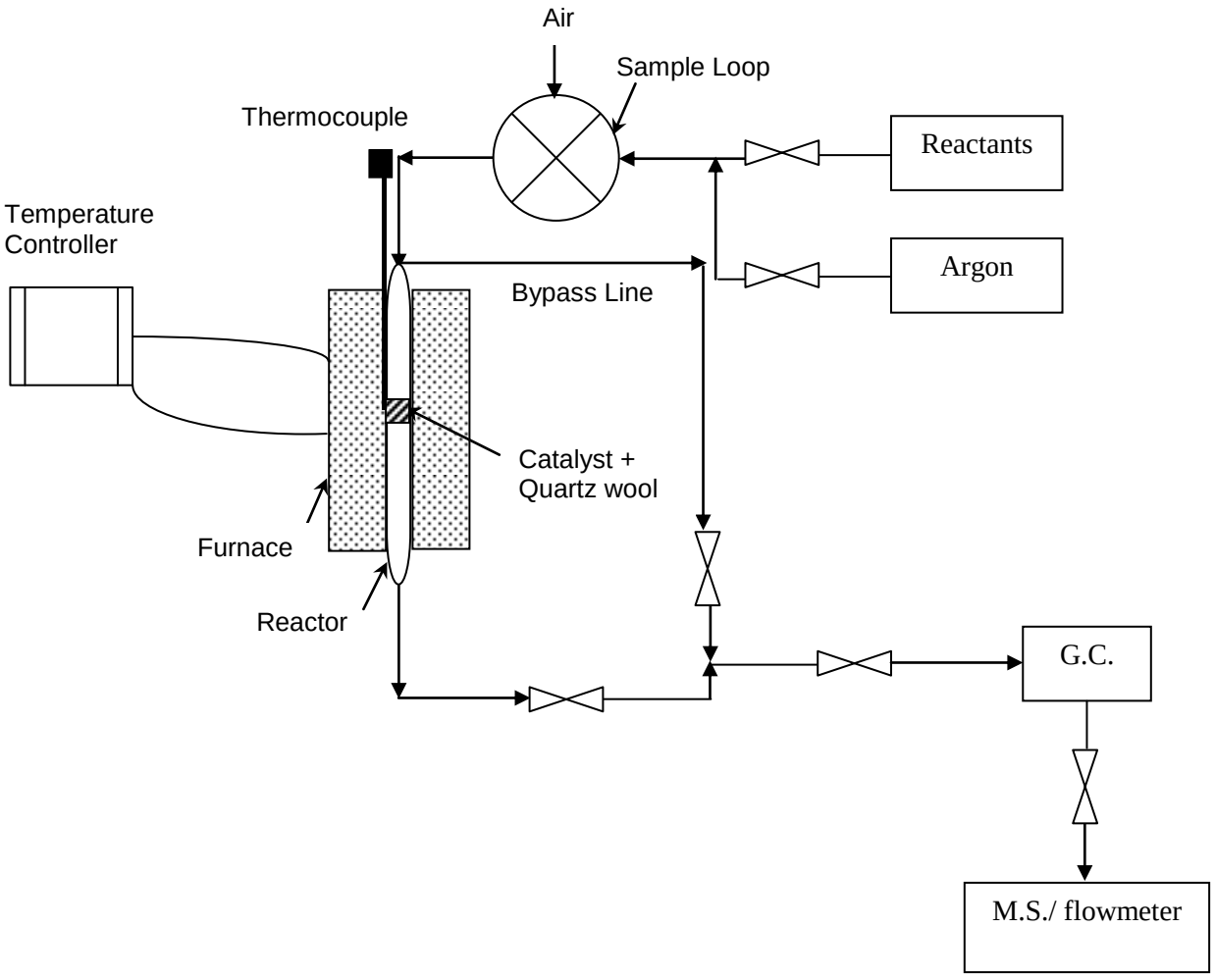

Figure 3.2. PFR schematic.

3.2.2 Membrane Reactor

All reaction tests over dense disk-shaped ceramic membranes were performed in a two-sided concentric quartz tube membrane reactor shown in Figure 3.3. Our experiment setup is shown in Figures 3.4 and 3.5. Two gold ring gaskets (Scientific Instrument Services Inc.) were used between the outer quartz tubes and the membrane surfaces (both on the top and the bottom surfaces). An external pneumatic press maintained pressure against the gold seals. Prior to reaction test, the amount of air leakage was monitored by mass spectrometer (by monitoring the nitrogen signal in the reactor effluent). The gold gaskets became soft and flat as the reactor system approached the 800°C temperature and the seal was completely formed within 30 minutes at 800°C. Temperatures higher than 850°C did not improve the seal.

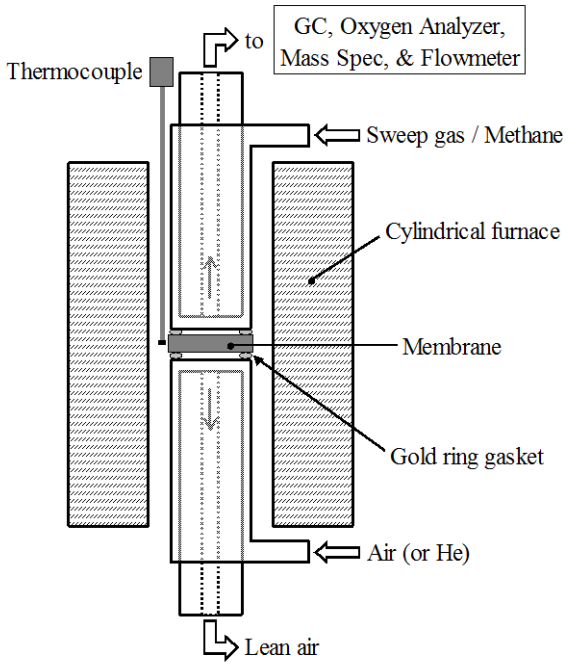

Figure 3.3. Membrane reactor schematic.

Figure 3.4. Midsection of membrane reactor.

Figure 3.5. Membrane reactor setup.

A great amount of leakage at room temperature and also during reactor heat-up was observed before the gold gaskets softened sufficiently at high temperatures (around 800 °C). The leak around the gold gaskets during operation was estimated to be less than 0.3% of the reactor feed flow rate for all reaction tests. In addition to the ceramic membranes, a stainless steel "blank" membrane painted with an inert BN_3 paint, to prevent reaction on the steel surface, was used as an inert control to provide baseline data for the ceramic membrane experiments. This painted blank membrane had been heated to 500°C for 3 hours prior to the reaction test.

All membrane reaction tests were conducted with similar operating conditions. A small amount (10 mg) of supported metal catalyst was spread in a thin layer (~1 mm) across the top side of the membrane or stainless steel blank surface using a spatula. It is important to mention that it was hard to get an even layer of catalyst on top of membrane in each test. This small quantity of catalyst reduces mass and heat transport limitations within the catalyst layer and ensures that the membrane material and the catalyst bed are in close contact. It also helps to observe the catalyst deactivation trends immediately.

During heating from room temperature to 800°C, 130 ml/min air was introduced into the bottom side of reactor (oxygen supply side of the membrane), and 20 ml/min argon was used to sweep the top side of reactor (oxygen permeate side of the membrane). The effluent of the oxygen-lean side of the membrane was monitored during heating in argon with the Balzers Omnistar mass spectrometer. After reaching 800°C, the argon flow rate through the reaction chamber of reactor was measured

using an Agilent ADM2000 flowmeter and this flow rate was compared with the argon flow rate at room temperature to ensure that there was no leakage. After sealing the reactor at 800°C but prior to reaction testing, all membranes were tested for possible cracks by flowing helium through the air side of the membrane reactor for 5 minutes while the reactor effluent was monitoring by the mass spectrometer (any changes in the helium signal could be due to a crack in membrane). Fortunately, no helium leakage was detected at 800°C in any of the tests.

A CH_4:CO_2 ratio of 1:1 was used in most of cases with 40 mol% CH_4, 40 mol% CO_2, and 20 mol% Ar in feed stream. For studying the effect of feed concentration on reaction, CH_4:CO_2 ratio was varied from 0.5 to 1. The total feed flowrate was 25 ml/min for all cases, which corresponds to a modified space velocity of 150 l/hr/$g_{catalyst}$. The 130 ml/min air at atmospheric pressure was used as the oxygen supply across the bottom side of membrane. The reactor effluent was analyzed with a SRI 8610C gas chromatograph. The gas chromatograph (GC) was equipped with a Supelco Carboxen 1010 PLOT column. For all reaction tests, effluent water was calculated from a hydrogen atom balance and the resulting trends were confirmed with mass spectrometer data. For each run, the material balance closed within approximately 2%.

3.3 Membrane and Catalyst Characterization

3.3.1 Transmission Electron Microscopy (TEM)

This analysis was performed at the Microscopy Laboratory at the University of Kansas on a FEI High Resolution Transmission electron microscope (TECNAI F20 X-Twin). This TEM equipment is also equipped with an Energy Dispersive X-ray Analysis (EDAX) detector for the compositional mapping of the catalysts. The fresh catalysts were ground into fine powders and then suspended in isopropyl alcohol [3]. One drop of the solution was placed on a 0.3 mm diameter Lacey carbon grid and allowed to dry. TEM images were taken to observe the dispersion of the metals on the supports.

3.3.2 Inductively Coupled Plasma (ICP)

ICP-OES is a type of emission spectroscopy that uses inductively coupled plasma to produce excited atoms and ions that emit electromagnetic radiation at wavelengths characteristic of a particular element. The chemical composition of the fresh catalysts was determined by conducting ICP analysis (Galbraith Laboratories).

3.3.3 Raman Spectroscopy

A Raman spectrometer was used to provide molecular-level information about adsorbed CO and CO_2 species on the fresh catalysts and ceramic membranes under different reaction conditions. A SENTERRA Dispersive Raman Spectrometer

(BRUKER), which is equipped with a CCD camera and located at the University of Kansas, was employed to collect the Raman spectra for each sample in the spectral range of 80-2630 cm^{-1}. The Raman spectra using a 785 nm excitation laser (10 mW power) were recorded at a resolution of 3-5 cm^{-1}. A 50X objective was used to focus on the sample surface. Helium, CO, and CO_2 gases were introduced to the samples, which were placed into the sample stage (Linkam, FTIR 600) at different temperatures. The sample stage was capable of raising the temperature up to 600°C. The desired flow rate of each gas was maintained within an FMA-5876A OMEGA flow controller.

3.3.4 Thermogravimetric Analysis (TGA)

TGA is a type of testing that is performed on samples to determine changes in mass and heat flow in relation to change in temperature. This method is useful for studying the carbon deposition on different catalysts and also the oxygen release of ceramic membranes. The change in mass is related to the changes taking place in the ceramic material during oxygen release in flowing nitrogen or air. This analysis was performed on a DSC-TGA (TA Q600) (capable of reaching 1500°C) at the University of Kansas. Ninety mg of a crushed SFC or BSCF ceramic material was placed into a clean alumina pan and heated to 800°C in nitrogen (100 ml/min) and also in air (20 ml/min) at a heating rate of 3 ºC/min.

3.3.5 Temperature Programmed Oxidation (TPO) of Carbon

A TPO spectrum is a plot of the oxygen consumption of a catalyst as a function of temperature and the area under a TPO curve represents the total oxygen consumption [4]. Carbon or carbonates, which might exist on the surface of catalyst, burns off in the presence of oxygen and CO_2 is produced. This experiment is useful if surface contaminants or deposited carbon on the catalyst surface is of interest. Ten mg of each fresh or used catalyst was placed inside the plug flow reactor. Then, a mixture of O_2 and He (5% O_2 in He) was introduced into the reactor at room temperature. The sample was heated at a rate of 10 ºC/min in the mixture of O_2 and He up to 800ºC. The exit gases were analyzed using a Balzers Omnistar mass spectrometer. The amount of coke formed on the catalysts or the amount of surface contaminants under the various conditions was determined using the calculated area for the known moles of CO_2 as a calibration.

3.3.6 Temperature Programmed Desorption (TPD)

TPD can be used on catalysts or ceramic materials, where one studies the desorption of gases from the sample into a flowing inert gas [4]. TPD is an excellent technique for determining surface coverage as well as the strength of the bond between adsorbate and the sample surface [4]. TPD for samples (crushed membranes and catalysts) was performed in the plug flow reactor. Samples were exposed to a continuous flow of CO (1% in helium) or CO_2 (1% in helium) at room temperature.

After flushing in argon at room temperature for 30 minutes, the samples were then heated in argon to 800ºC. The exit gases were analyzed using a Balzers Omnistar mass spectrometer. The amount of CO or CO_2 desorbed was calculated using the known moles of CO and CO_2 injected and the area of the CO and CO_2 injections.

3.3.7 Temperature Programmed Reduction (TPR)

A TPR spectrum shows the hydrogen consumption of a catalyst as a function of temperature [4]. The area under a TPR curve represents the total hydrogen consumption and TPR of supported bimetallic catalysts often reveals whether the two metals are in contact [4]. By performing TPR, the reduction temperatures of the catalysts were determined. TPR profiles of fresh catalysts with hydrogen (5% in argon) were performed in the plug flow reactor, which is equipped with a furnace and temperature controller, using a Balzers Omnistar mass spectrometer. Ten to thirty mg of each catalyst were loaded into the reactor and heated from room temperature to 800ºC at 3 ºC/min. Calibration of the hydrogen consumption were performed using 50 μl injections of hydrogen.

3.4 References

[1] A. K. Avci, D. L. Trimm, A. E. Aksoylu, and Z. I. Onsan, "Hydrogen production by steam reforming of n-butane over supported Ni and Pt-Ni catalysts," *Applied Catalysis A-General*, vol. 258, pp. 235-240, 2004.

[2] Z. P. Shao, W. S. Yang, Y. Cong, H. Dong, J. H. Tong, and G. X. Xiong, "Investigation of the permeation behavior and stability of a $Ba_{0.5}Sr_{0.5}Co_{0.8}Fe_{0.2}O_{3-\delta}$ oxygen membrane," *Journal of Membrane Science*, vol. 172, pp. 177-188, 2000.

[3] S. M. Stagg-Williams, "Novel catalytic materials for carbon dioxide reforming of methane under severely deactivating conditions," in *Chemical Engineering*, PhD. Norman, Oklahoma: University of Oklahoma, 1999, pp. 182.
[4] J. W. Niemantsverdriet, *Spectroscopy in Catalysis*. Weinheim: VCH, 1993.

Chapter 4: The Interaction Between the Ceramic Membrane and the Catalyst

4.1. Introduction

As mentioned in Chapter 1, several groups have investigated non-perovskite $SrFeCo_{0.5}O_x$ (SFC) as a type of cobalt-based ceramic membrane for methane conversion to syngas [1-3]. However, the roles of the ceramic membrane in the enhancement of this reaction and the interaction between SFC and the catalyst have not yet been investigated. The disadvantage of this ceramic material is that oxygen flux is low compared to other cobalt-based membranes [4]. However, because the membrane has been well characterized, it makes SFC a good choice for studying the interaction between the catalyst and the membrane.

Other students have fabricated dense SFC membranes successfully in Dr. Susan Stagg-Williams' group and this membrane has been studied for CO_2 reforming of methane over $Pt/CeZrO_2$ and Pt/ZrO_2 catalysts. In previous studies, the methane conversion using a $Pt/CeZrO_2$ (18 wt% Ce) catalyst loosely packed on the surface of an SFC membrane was shown to be much higher than the methane conversion for the same system with a Pt/ZrO_2 catalyst [5]; however, the benefit of using the SFC membrane was not observed until after 7 hours of reaction. So our motivation for this research is to understand the reasons why there is a lag time in observing the beneficial effects of SFC.

Previous studies with a Pt catalyst deposited directly on the surface of a $La_{0.6}Sr_{0.4}Co_{0.2}Fe_{0.8}O_{3-\alpha}$ (LSCF) membrane have suggested that catalyst activity is modified by the reverse spillover of oxygen species from the ceramic membrane onto

the catalyst surface [6]. While it is possible to envision the spillover occurring when the catalyst is supported directly on the membrane surface, it is unclear how likely the spillover would be when the catalyst is loosely packed on the surface of the membrane. However, it is possible that the presence of the Ce and its oxygen uptake ability is responsible for the changes in the behavior compared to the Pt/ZrO_2 catalyst on the SFC membrane. If oxygen spillover from the membrane to the catalyst were occurring, it is likely that the oxygen from the membrane would be scavenged by the Ce and would not be available for reaction. The delay time for observing a beneficial effect of the membrane could be the time for the oxygen in the Ce to reach an equilibrium state, after which oxygen from the SFC could be used in the reaction.

In this chapter, we investigate the role of the SFC membrane and the effect of the degree of membrane/catalyst contact on methane conversion to better understand the catalyst/membrane interaction. A series of pulse studies was conducted on SFC alone, $Pt/CeZrO_2$ and Pt/ZrO_2 alone, and physical mixtures of SFC and the catalysts, in order to better understand the surface reactions happening during both partial oxidation and CO_2 reforming of methane to syngas at 800 °C.

4.2. Experimental

All pulse studies were performed in a PFR, which was described in detail in Chapter 3. Detailed information about crushed SFC and catalysts preparation methods and characterization techniques can be found in Chapter 3. Crushing the SFC

membrane ensures that the SFC pieces used for the physical mixture study have the same composition and state as the disc-shaped membranes.

4.3. Results and Discussion

The reactions that might participate in the syngas production from methane are as follows [7-9]:

Steam reforming of methane: $CH_4 + H_2O \longrightarrow CO + 3H_2$ (1)

Partial oxidation of methane: $CH_4 + 0.5\ O_2 \longrightarrow CO + 2H_2$ (2)

Dry reforming of methane: $CH_4 + CO_2 \longrightarrow 2CO + 2H_2$ (3)

Water-gas shift reaction: $CO + H_2O \longleftrightarrow CO_2 + H_2$ (4)

Methanation reaction: $CO + 3\ H_2 \longrightarrow CH_4 + H_2O$ (5)

Water production: $H_2 + 0.5\ O_2 \longrightarrow H_2O$ (6)

Carbon dioxide production: $CO + 0.5\ O_2 \longrightarrow CO_2$ (7)

The primary products formed from the decomposition of methane in the presence of CO_2 (dry reforming) or O_2 (partial oxidation) are H_2 and CO. Previous studies have suggested that the hydrogen formed during the reaction can interact with oxygen species on the membrane surface to form water [10]. In addition, it has been suggested that CO_2 and CO can form carbonate species on the membrane surface [11, 12]. The formation of H_2O and the adsorption and potential reaction of CO and CO_2 on the membrane surface can significantly change the product composition and the overall reaction scheme. Thus, it is important to understand the interaction of the

product species with the SFC membrane material and any effects of having the catalyst and membrane material in contact.

4.3.1. H_2 and CO Interaction with SFC and $Pt/CeZrO_2$

Three samples were heated to 800°C in argon and then exposed to pulses of hydrogen while monitoring the effluent using a mass spectrometer. The first sample contained a fully sintered SFC membrane that was crushed into small particles. The second sample contained an unreduced $Pt/CeZrO_2$ catalyst. The final sample was a physical mixture of the crushed SFC and the $Pt/CeZrO_2$ catalyst with a mass ratio = 1. The physical mixture was not reduced prior to reaction.

Figure 4.1 compares the relative amount of total hydrogen consumption for the three samples. The amount of hydrogen consumed for the SFC alone was the smallest, thus, the hydrogen consumption values have been normalized to the case of the SFC alone. While hydrogen consumption was observed in all cases, it is clear from Figure 4.1 that the amount of hydrogen consumption for the physical mixture is greater than the summation of the SFC and catalyst independently. These results suggest that there is a synergistic relationship between the catalyst and the membrane material.

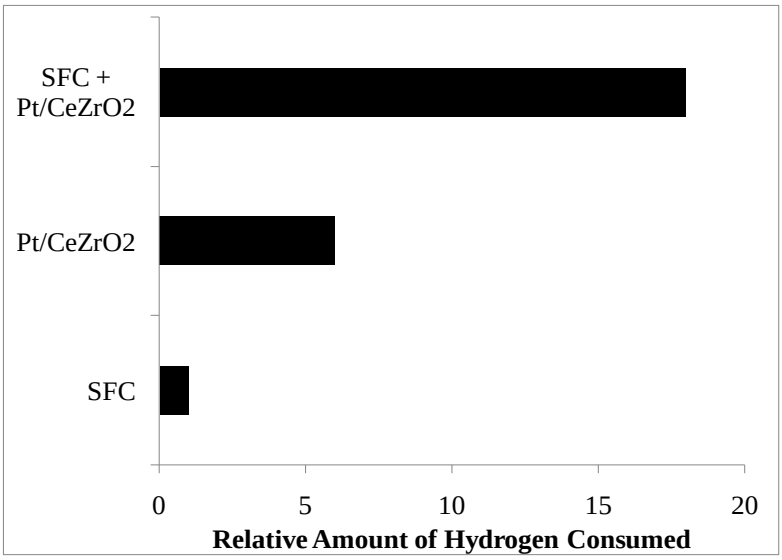

Figure 4.1. The relative amount of total hydrogen consumption at 800°C and atmospheric pressure for 1) SFC, 2) $Pt/CeZrO_2$, and 3) physical mixture of SFC and $Pt/CeZrO_2$ with mass ratio = 1.

When the SFC is exposed to hydrogen pulses in the absence of the catalyst, some hydrogen is consumed by reacting with oxygen in the SFC material to form water. The water production could not be quantified; however, water production was clearly visible at the outlet of the reactor and the water signal in the mass spectrometer increased during exposure to hydrogen. The consumption of hydrogen and the appearance of water, clearly demonstrates that the SFC membrane material has the ability to react with gas phase hydrogen. However, in the absence of an oxygen supply, the crushed membrane material is not able to replenish the oxygen in the lattice, and the hydrogen consumption quickly ceases.

Similarly, for the case with the catalyst alone, the hydrogen consumption is higher than that for the SFC sample. It is likely that some of the hydrogen consumption is due to reduction of the Pt. Additionally, due to the reducibility of Ce,

one would expect to have some spillover of hydrogen to the support. The presence of the Pt metal facilitates the reduction of the support, which, in turn, increases the total hydrogen consumption. Eventually, the oxygen in the support becomes depleted and the hydrogen consumption stops.

When the SFC and catalyst are present in the physical mixture, reduction of the Pt metal is again expected. However, when the catalyst and SFC are physically mixed, the presence of the metallic Pt appears to not only facilitate the reduction of the $CeZrO_2$ support, but also extract more oxygen from the SFC membrane as well. One possible explanation is that once the hydrogen has dissociated on the Pt, it is spilling over to the SFC even though the Pt is not directly supported on the membrane material. An alternative explanation is that the oxygen species on the surface of the SFC membrane material is spilling over to the $CeZrO_2$ and acting like an oxygen sink for the support. While it is not possible to identify the role of each species with the hydrogen pulse studies, it is clear that a strong synergy exists between the catalyst and membrane material.

Similar to the hydrogen pulses, when CO was injected on the samples (50 μl CO in each pulse), CO_2 production was seen in all three cases. However, the amount of CO consumed was greater than the amount of CO_2 produced for each sample, which is most likely due to the adsorption of CO on the surface. As can be seen in Figure 4.2, the amount of CO consumption for the physical mixture of SFC and catalyst was higher than the consumption for the experiments with only SFC and only

catalyst. In fact, the consumption for the physical mixture was greater than the summation of the individual SFC and catalyst experiments.

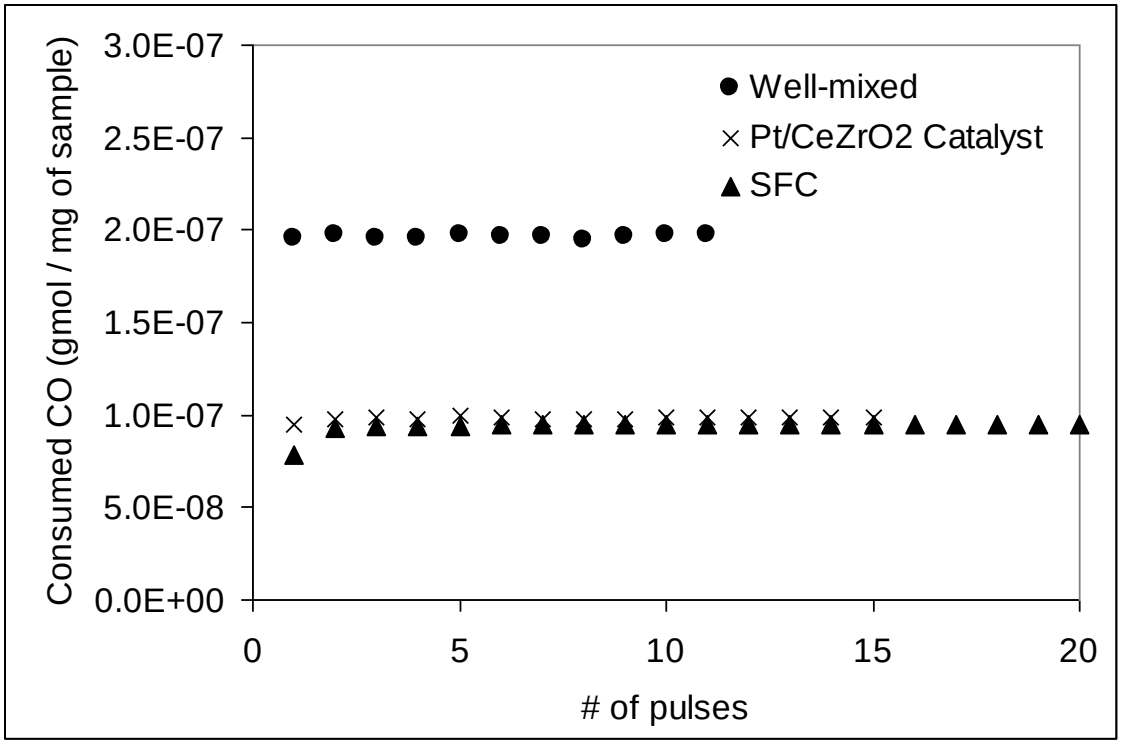

Figure 4.2. The relative amount of total CO consumption at 800°C.

The significantly higher CO consumption again demonstrates the existence of a synergistic relationship between the catalyst and SFC. It should be noted that compared to the hydrogen pulses, the CO consumption for the physical mixture was less than the hydrogen consumption. These results could indicate that the hydrogen may be a more likely candidate for spillover to the SFC. However, it cannot be ruled out that both CO and hydrogen species are capable of migrating to the SFC and acting as reducing species.

Temperature Programmed Desorption (TPD) of CO was performed on each of the three samples described above. Each sample was exposed to a continuous flow of CO at room temperature for 30 minutes and then heated to 800°C in argon (15 cc/min). The effluent was monitored using a mass spectrometer. Figure 4.3A shows the CO_2 desorption profile for the three samples. In all three cases, significant amounts of CO_2 were formed while no CO desorption was observed. Since the only source of oxygen in the reactor is from either the SFC or the catalyst support, it is believed that CO adsorbs to the surface in the form of a carbonate and then reduces the SFC, support, or both, to form CO_2. As in the case of the hydrogen, the amount of CO_2 formed for the physical mixture is greater than the two individual samples.

Figure 4.3B shows the O_2 profile observed for each sample during the CO-TPD. As would be expected, no significant O_2 release is observed for the $Pt/CeZrO_2$ catalyst while significant amounts of O_2 are observed for the SFC sample. The onset temperature of O_2 release is consistent with what has been observed for the onset temperature of oxygen flux for SFC membranes [13], with a larger amount of oxygen being released at higher temperatures. The CO_2 production for the physical mixture of SFC and catalyst was again higher than the CO_2 production for the individual samples. It should be noted that no O_2 was observed for the case of the physical mixture. Instead, two peaks of CO_2 were observed at the temperatures where oxygen release occurs for the SFC (500-800°C). These data again suggest that the oxygen species are reacting prior to forming gas phase oxygen. While it is still unclear as to

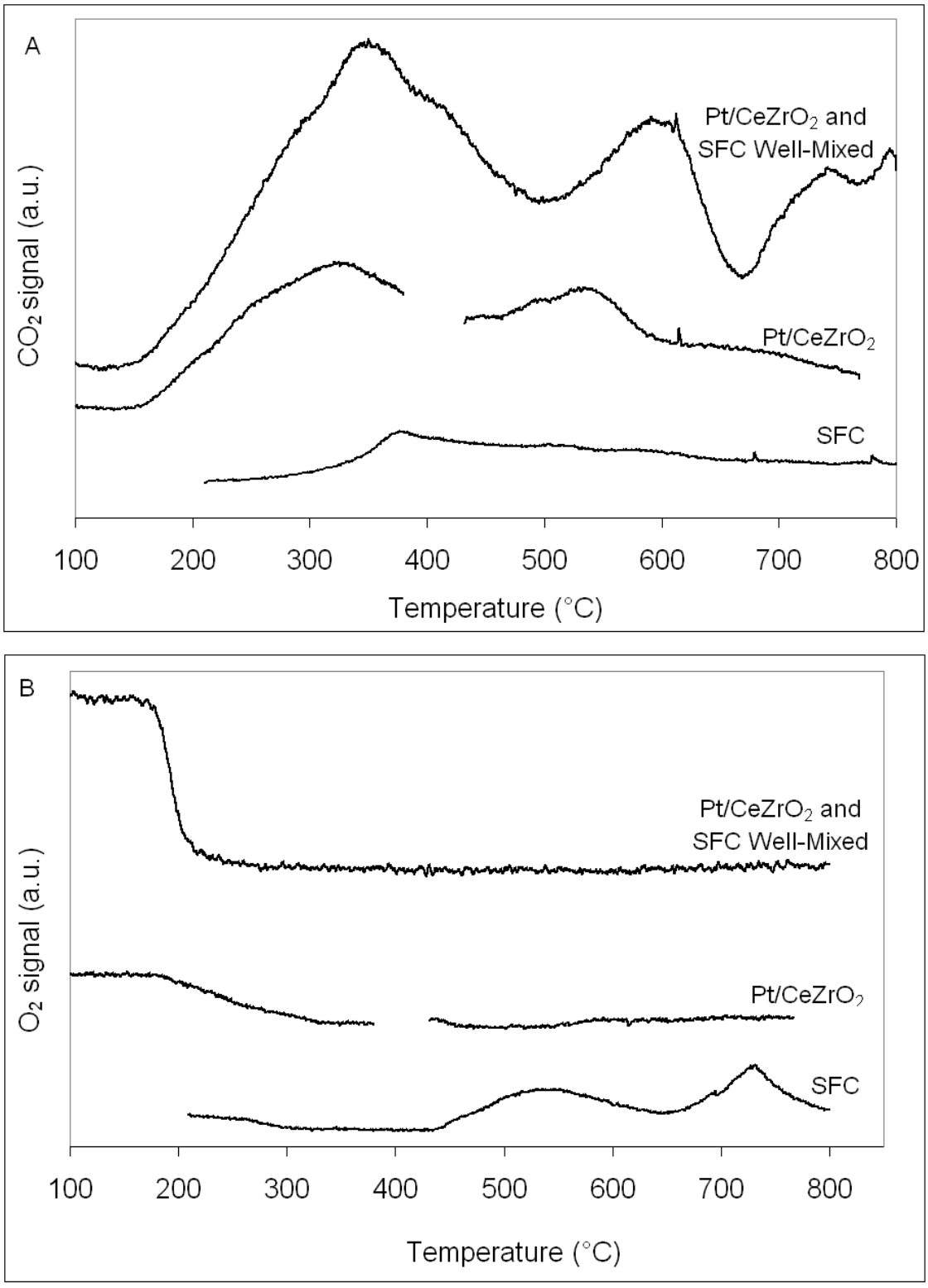

Figure 4.3. Mass spectrometer profiles for A) CO_2 and B) O_2, during temperature programmed desorption of CO after exposure to a continuous flow of CO at room temperature.

the mechanism of interaction between the catalyst and the SFC in the physical mixture, it is clear that the combination of the SFC and catalyst results in a synergy, which can significantly alter the interaction of H_2 and CO under reaction conditions.

4.3.2. Reaction of CH_4 over SFC and $Pt/CeZrO_2$

In order to determine the role of the SFC and the catalyst in the conversion of methane, samples were heated to 800°C in Ar and then exposed to pulses of methane (50 μl) while the effluent was monitored using the mass spectrometer. Four samples were studied: 1) a crushed SFC membrane, 2) a $Pt/CeZrO_2$ catalyst, 3) a Pt/ZrO_2 catalyst, and 4) a physical mixture of the SFC and $Pt/CeZrO_2$ catalyst with mass ratio = 1. These samples were chosen so that the effect of each individual component on the methane conversion and the possible synergistic effect of the combination of membrane and catalyst could be explored.

Figure 4.4 shows the methane conversion profile for all four cases. The methane conversion for the SFC was less than 5% for all of the pulses, which is similar to what is observed for methane conversion with SFC membranes in the absence of a catalyst [14]. Likewise, the methane conversion for the Pt/ZrO_2 catalyst alone was slightly higher for the first 3 pulses but then quickly decreased. The $Pt/CeZrO_2$ catalyst initially had high conversion but the conversion started to decline after 4 pulses and continued to decline with each subsequent pulse (average CH_4 fractional conversion = 49%). It is not unexpected that the methane conversion would quickly decrease, as the only species being fed into the reactor is methane and, in the

absence of an oxygen source, deactivation of the catalyst would be expected to rapidly occur. The delay in the onset of deactivation with the addition of Ce to the support can be explained by the ability of the Ce to provide a small amount of oxygen to the reaction. However, without an oxygen source in the gas phase to replenish the oxygen, the support lattice oxygen is quickly depleted and deactivation due to carbon deposition on the Pt occurs.

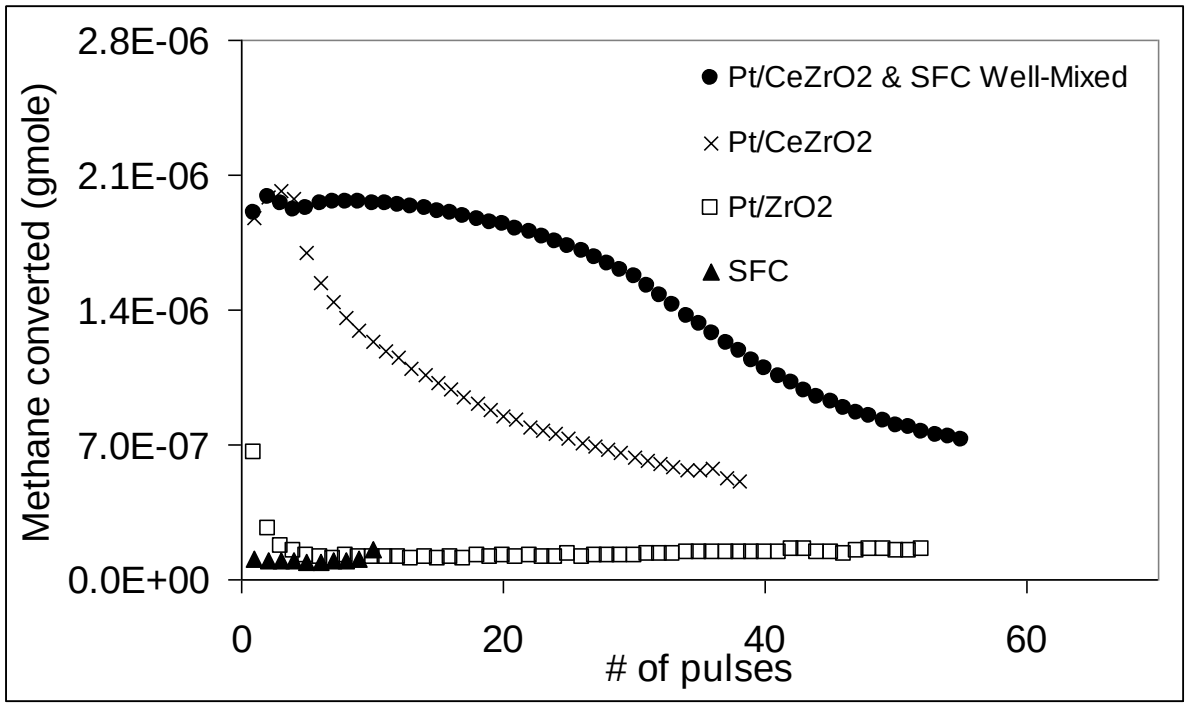

Figure 4.4. Methane conversion profiles for four samples during pulses of methane at 800°C and atmospheric pressure in a plug flow reactor. The four samples are: 1) crushed SFC, 2) $Pt/CeZrO_2$ catalyst, 3) Pt/ZrO_2 catalyst, and 4) physical mixture of SFC and $Pt/CeZrO_2$ catalyst (mass ratio = 1).

In contrast to the methane conversion for the membrane and catalyst alone, the methane conversion on the physical mixture of $Pt/CeZrO_2$ and SFC was maintained at a high level for approximately 20 pulses with significant decline in

conversion observed only after 30 pulses (average CH_4 fractional conversion = 72%). It is interesting to note that the methane conversion for the $Pt/CeZrO_2$ catalyst alone and the physical mixture are nearly the same for the first four pulses. These results are similar to the results obtained previously where the beneficial effects of the SFC membrane on a $Pt/CeZrO_2$ catalyst for CO_2 reforming of CH_4 in a membrane reactor were not observed until after 7 hours of reaction [5]. It is believed that the period, for which the conversions are the same, is the same time in which the ceria support is capable of providing oxygen to the reaction and thus, the membrane is not necessary. However, in the pulse studies, when the ceria lattice oxygen is depleted, the oxygen from the SFC is now available for reaction, resulting in a high methane conversion for a longer period of time. The conversion of methane begins to decline when the oxygen in the SFC is depleted.

For a better comparison to the membrane reactor system, an experiment was performed with the physical mixture of $Pt/CeZrO_2$ and SFC with exposure to pulses containing a 1:1 mixture of CH_4 and CO_2. Figure 4.5 shows the methane conversion profile for the physical mixtures with and without CO_2 in the pulses. Figure 4.5 also contains the methane conversion profile for the $Pt/CeZrO_2$ catalyst during exposure to pulses containing a 1:1 mixture of CH_4 and CO_2. It is clear that the presence of CO_2 increases the methane conversion and the ability of the catalyst to maintain conversion for longer periods of time. The CO_2 provides an oxygen source to replenish the oxygen in the catalyst support and SFC lattice, which assists in preventing carbon deposition. The results in Figure 4.5 also demonstrate the

beneficial effect of the SFC membrane on the methane conversion even when the catalyst and SFC are only physically mixed. Clearly the membrane material and the catalyst have a synergistic relationship, which significantly increases the methane conversion and helps to maintain catalyst performance.

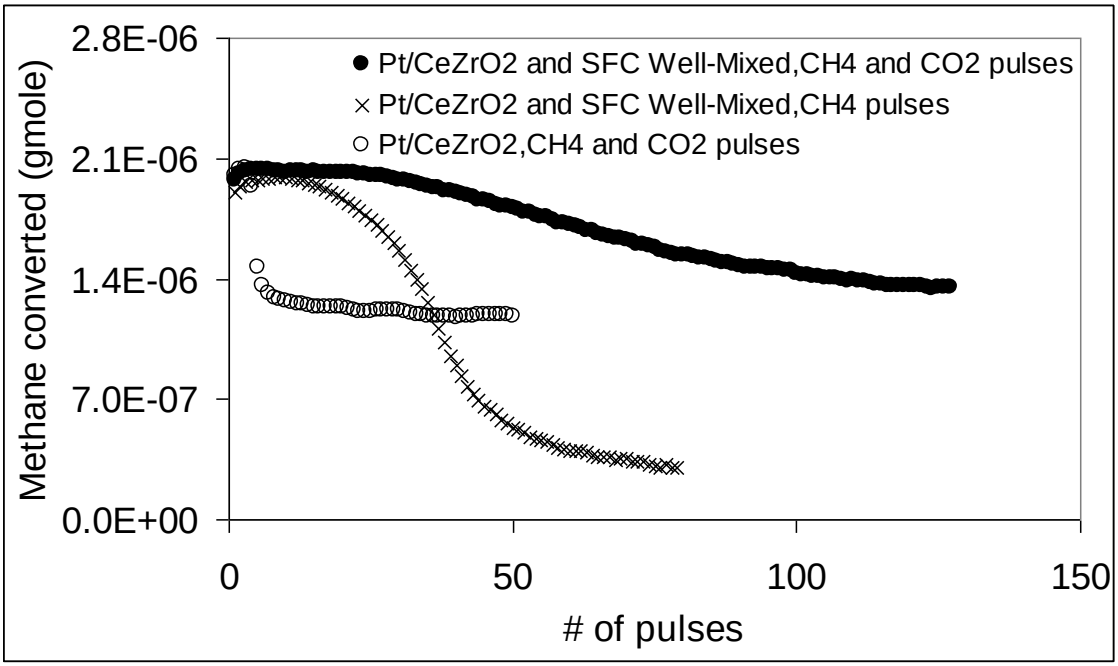

Figure 4.5. Methane conversion profiles for a physical mixture of SFC and $Pt/CeZrO_2$ (mass ratio = 1) and $Pt/CeZrO_2$ catalyst alone during pulses of CO_2 and CH_4 at 800°C. For comparison the methane conversion for the $Pt/CeZrO_2$ sample for pure CH_4 is also shown.

In an attempt to determine if there is an optimal ratio of catalyst and SFC membrane material in the physical mixture, physical mixtures of SFC and $Pt/CeZrO_2$ in mass ratios of 1, 4, and 0.25 were studied. In all cases the SFC and $Pt/CeZrO_2$ were mixed prior to adding to the quartz tube reactor. Figure 4.6 shows the methane conversion profiles for different mass ratios of SFC and catalyst exposed to methane

pulses at 800°C. When the SFC to catalyst ratio was low, the conversion profile looked very similar to the profile for the catalyst without SFC. The methane conversion for the low mass ratio showed a rapid decline within the first 5 pulses of methane. The rapid decline in CH_4 conversion can be ascribed to the low amount of SFC and thus, low amount of oxygen available for reaction.

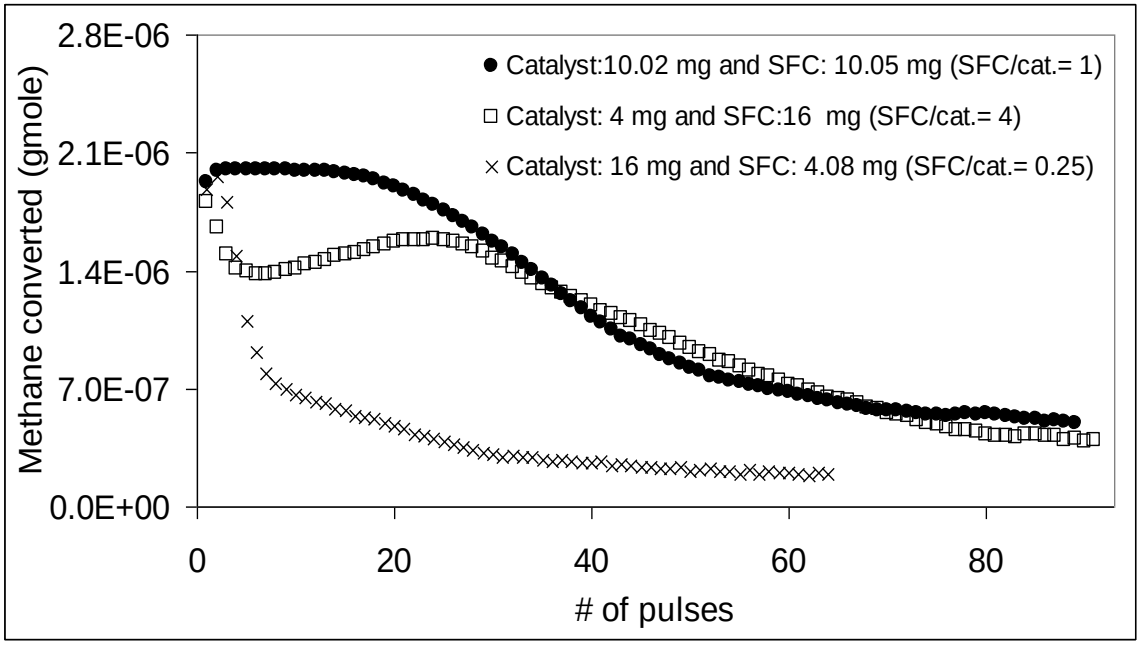

Figure 4.6. Methane conversion during pulses of CH_4 at 800°C. Three mass ratios of the physical mixture of the SFC and $Pt/CeZrO_2$ were studied: 0.25, 1, and 4.

As described previously, the mass ratio of 1 exhibited high conversion for 20 pulses, ascribed to the ability of the SFC to provide additional oxygen for the reaction and maintain a clean Pt surface for the methane conversion. In addition to the high methane conversion, large amounts of H_2, CO, and H_2O were also observed. The previously described pulse and TPD studies have shown that when the physical mixture with a mass ratio of 1 is exposed to H_2 and CO, H_2O and CO_2 formation

occurs. However, during the studies with the pulses of methane, only a small amount of CO_2 production was observed for the physical mixture with a mass ratio of 1. In fact, the CO_2 production was lower than the CO_2 produced for the case with the SFC alone. The production of CO_2 and H_2O and the lack of CO_2 observed in the effluent suggest that the CO_2 and H_2O are being consumed in the reaction, probably via the CO_2 and steam reforming reactions. The occurrence of both of the reactions would explain the high amounts of H_2 and CO produced and the prolonged methane conversion profile for the physical mixture with a mass ratio of 1.

Surprisingly, when the mass ratio of SFC to catalyst was increased to 4, the methane conversion during the first four pulses was very similar to the methane conversion observed for the mass ratio of 0.25. However, after 7 pulses, the methane conversion began to increase and eventually matched with the conversion profile for the study in which the mass ratio equaled 1. This behavior was also observed with a mass ratio of 2, with the only significant difference being the pulse number at which the maximum in conversion occurred.

4.3.3. The Effect of SFC and $Pt/CeZrO_2$ Interaction

Due to the large differences in the amount of SFC and catalyst in the physical mixture when the mass ratio was 4, it is hypothesized that the delay in the beneficial effect of the membrane could be due to segregation of the catalyst and the SFC in the reactor bed, limiting catalyst and SFC interaction. If segregation occurs when the bed is largely comprised of the denser SFC, the catalyst will be expected to be on the top

of the bed with the SFC on the bottom. In order to probe the effect of mixing, studies were performed in which the catalyst and SFC were intentionally segregated in the reactor with the only contact being at the interface of the two beds. Three cases were investigated for the mixing studies: a) well mixed with maximum catalyst and SFC contact, b) SFC on top and $Pt/CeZrO_2$ on bottom, c) $Pt/CeZrO_2$ on top and SFC on bottom. Figure 4.7 shows a schematic of the three cases investigated.

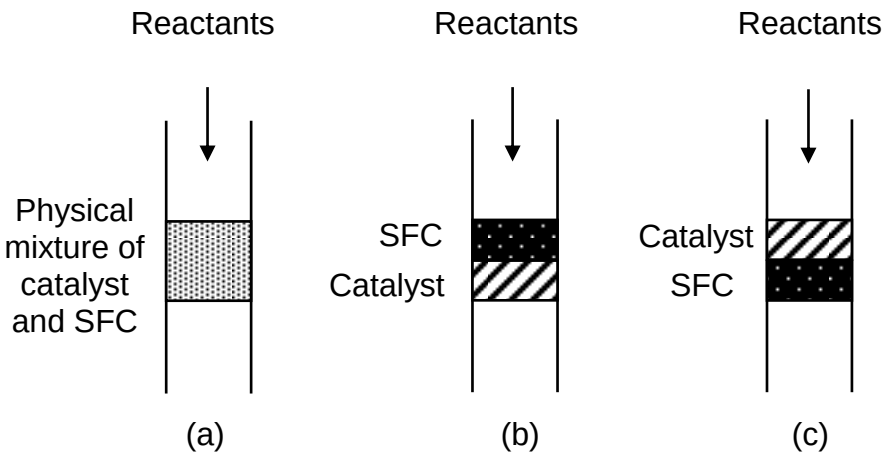

Figure 4.7. Schematic of different mixing patterns used in this study.

The methane conversion profiles for the three mixing patterns are shown in Figure 4.8. Also, Figure 4.9 shows the H_2/CO molar ratio for these different patterns. As was previously stated, the case of the well mixed SFC and catalyst sample resulted in significant methane conversion and the highest H_2:CO molar ratio in the effluent. The hydrogen formed from the decomposition of methane can react with oxygen on the surface of the membrane to form water. The water can then participate in steam reforming which increases the H_2:CO molar ratio. Likewise the CO formed can react

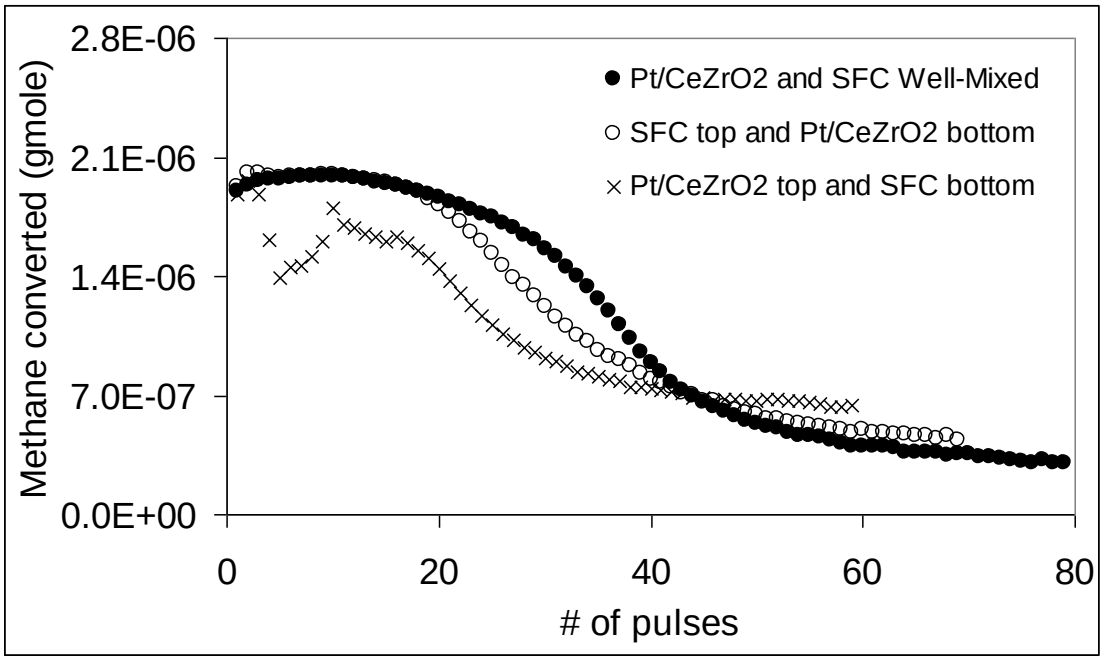

Figure 4.8. Methane conversion profiles for pulses of methane at 800°C over the $Pt/CeZrO_2$ and SFC in different mixing patterns.

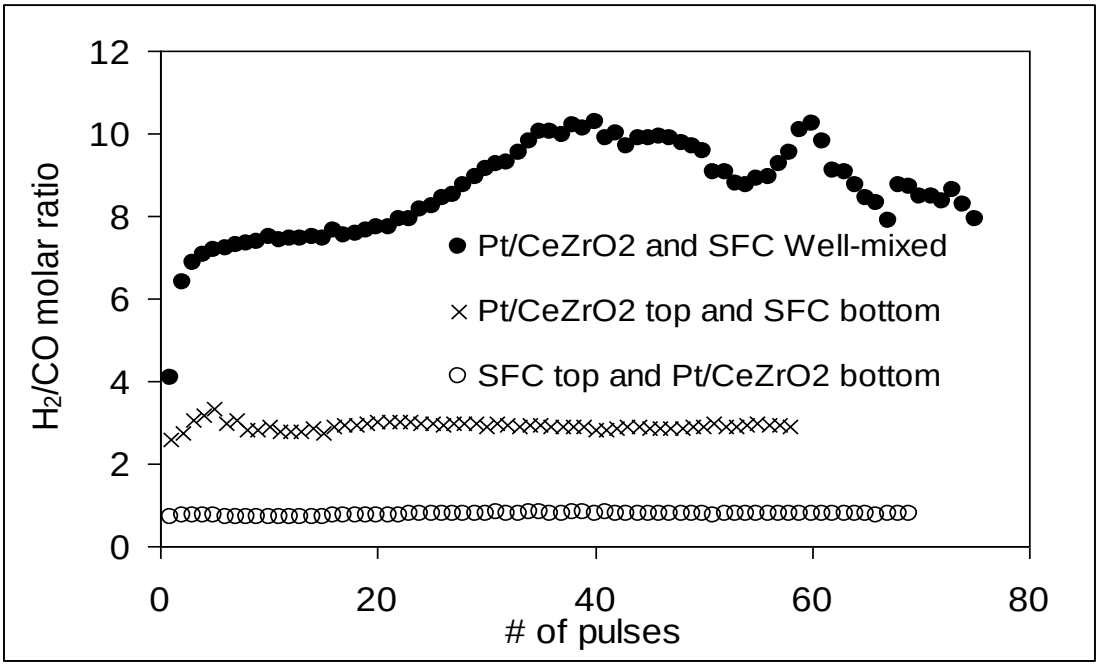

Figure 4.9. The H_2/CO molar ratio resulted from pulse injections of CH_4 at 800°C over the $Pt/CeZrO_2$ and SFC in different mixing patterns.

with oxygen in the SFC to form CO_2, which can subsequently react with CH_4 to form additional H_2 and CO.

When the SFC is positioned in the bed above the catalyst, the only contact between the SFC and catalyst is at the interface of the two layers. However, any oxygen released by the SFC would travel through the catalyst bed before being released from the reactor. This, in essence, behaves as if oxygen is co-fed to the catalyst bed with the methane. While the presence of oxygen would provide the ability to remove carbon from the metal and maintain methane conversion for a greater number of pulses, the interaction of the products with the SFC surface is minimal because of the placement of the SFC in the bed and the direction of flow in the reactor. In fact, the mass spectrometer profiles show an increase in the production of CO compared to the well-mixed case. The decreased interaction of the products with the SFC results in less H_2O and CO_2 formed in the reactor and a subsequent decrease in the H_2:CO ratio.

When the catalyst is located above the SFC, again the interaction is limited to the interface. In this configuration, the majority of the methane conversion happens at the top of the bed in the catalyst zone. The conversion of methane is high for the first two pulses, but begins to decline rapidly, behaving as if the SFC was not present in the bed. The interesting result is that after 5 pulses, the methane conversion begins to increase, showing the same behavior as was observed in the studies with the SFC:catalyst mass ratio of 4. Several factors could be contributing to the observed delay in the beneficial effects of the membrane. It is possible that the observed

behavior could be due to a delay in the buildup of water and CO_2 in the system and a subsequent delay in the onset of steam and CO_2 reforming. It is also possible that the segregation of the catalyst and the SFC hinders the ability of oxygen to spillover from the SFC to the catalyst. Again, it is unclear that spillover is occurring because the catalyst is not directly supported on the SFC material but rather only in contact through a physical mixture. However, it is possible that the presence of the Ce and its ability to take up oxygen could be assisting in the transfer of oxygen species from the SFC lattice to the catalyst surface facilitating the oxygen spillover.

Studies of the same mixing patterns were also performed with pulses of CH_4 and CO_2 to look at the impact of the SFC and catalyst interaction when an oxygen source is present in the gas phase. Figure 4.10 shows the methane conversion profiles for the three mixing patterns. The behavior for the well-mixed case and the case where SFC is located below the catalyst are very similar to the profiles for the pulses of methane alone (Figure 4.8). The only significant difference is that the extent of deactivation is smaller in the presence of CO_2, which is to be expected. However, unlike when the pulses contained only methane, when the SFC is located above the catalyst, the profile looks very similar to the profile for the SFC positioned below the catalyst. That is to say, the SFC appears to not be a factor in the reaction. It is likely that while minimal conversion (< 5%) of the methane occurs on the SFC, the CO_2 in the pulses adsorbs to the surface of the SFC and prevents oxygen from being released by the SFC and participating in the reaction. The ineffectiveness of the SFC and the removal of CO_2 from the reactant stream result in an initial methane conversion

profile similar to the case of the methane pulses alone (Figure 4.8). It is then possible that when the surface of the SFC is saturated, the CO_2 in the gas phase becomes available for reaction on the catalyst and the methane conversion increases.

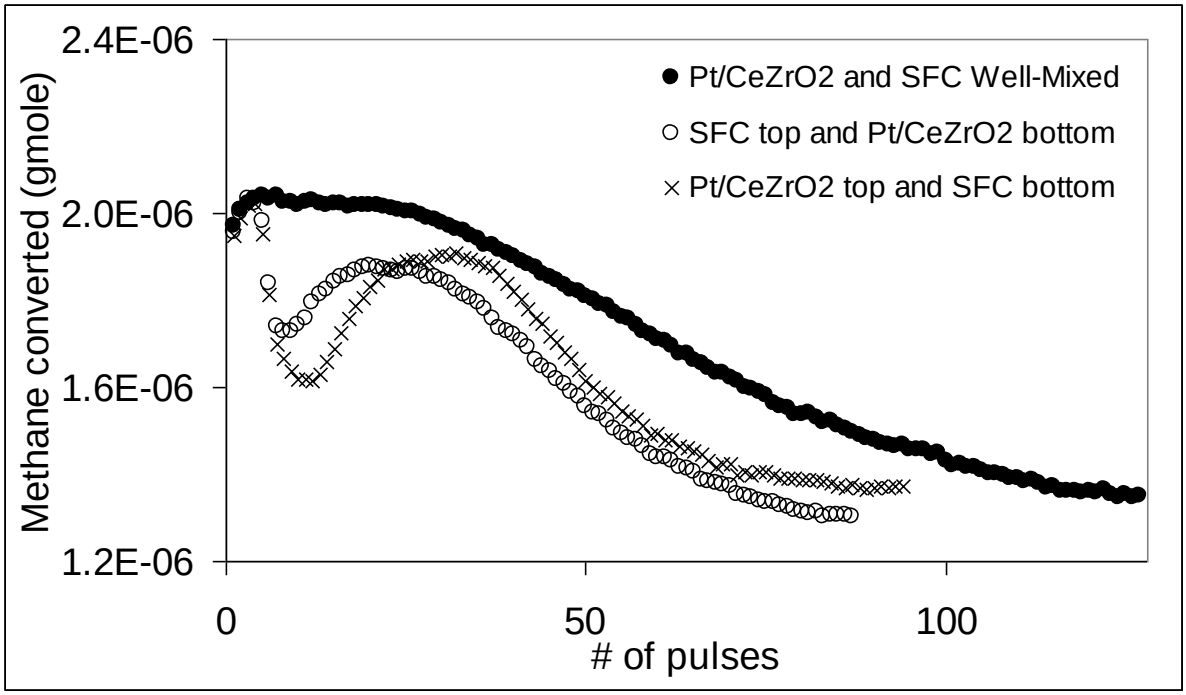

Figure 4.10. Methane conversion profiles for pulses of methane and carbon dioxide (1:1 ratio) at 800°C over the $Pt/CeZrO_2$ and SFC in different mixing patterns.

While it is still unknown what specifically causes the oscillatory behavior observed in the methane conversion, it is clear that the degree of interaction between the membrane material and the catalyst has a significant impact on the methane conversion and the product profiles. That is, when the oxygen from the SFC cannot be utilized, or the products of the reaction are unable to interact with the SFC surface, the methane conversion is lower. These results suggest that membrane reactors should be designed to maximize the interaction between the catalyst and the

membrane surface. Ideally, the catalyst would be directly deposited on the membrane surface to maximize the interaction; however, the stability of the catalyst on the membrane surface under reaction conditions would need to be explored. In addition, further studies to look at oxygen species on the membrane surface and the potential migration of those species between the membrane and the catalyst are needed to understand the surface chemistry and the reaction kinetics for hydrocarbon conversion reactions.

The advantages of addition of SFC to $Pt/CeZrO_2$ can also be seen for two different cases in Figure 4.11. According to this figure, the addition of a small amount of SFC to a physical mixture of SFC and catalyst with ratio of 1 can shift the methane conversion curve up considerably. The difference between curve 1 and curve 2

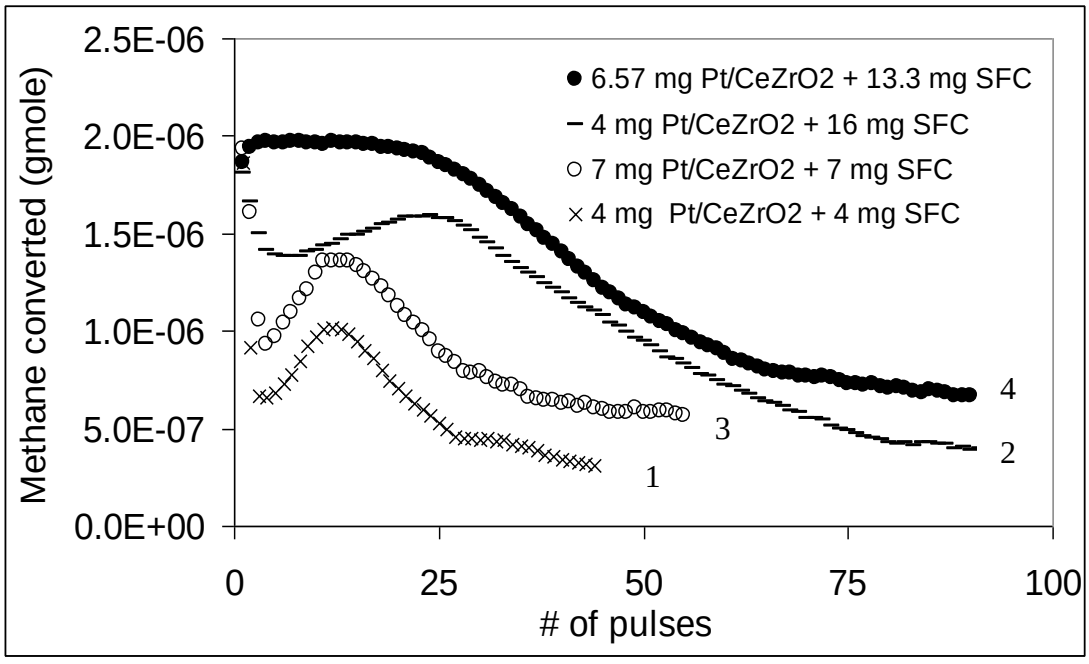

Figure 4.11. The advantageous effect of adding SFC to physical mixtures of SFC and $Pt/CeZrO_2$ catalyst with mass ratio=1 during methane injections at 800°C.

in Figure 4.11 is ascribed to the beneficial effect of 12 mg SFC and the change between curve 3 and 4 is attributed to advantageous impact of 7 mg SFC on conversion.

4.3.4 Raman Spectroscopy Study

4.3.4.1. Raman Spectroscopy at Room Temperature

In order to determine the interaction between catalyst and ceramic membrane during CO and CO_2 adsorption, the samples were scanned by a Raman spectroscope in different flowing gases (He, CO, and CO_2) at room temperature. Three different samples were used in this study: 1) a physical mixture of $Pt/CeZrO_2$ catalyst and SFC ceramic membrane with a mass ratio = 1, 2) SFC, and 3) $Pt/CeZrO_2$. The physical mixture and catalyst were not reduced prior to the gas exposure.

The spectra of samples after 30-minute exposure to CO and CO_2 at room temperature (Figures 4.12 and 4.13) showed adsorption of these chemicals on the surfaces of samples. For all samples, carbonate formation was observed at wavenumber 787 cm^{-1} during both exposure to CO and CO_2 [15]. In addition, the band previously assigned to linear CO bonded to the surface was detected at 2057 (cm^{-1}) in all three cases [16, 17]. The intensity of the band at 641cm^{-1}, which shows the metal oxides in lattice structure, is assumed to be unchanged during CO and CO_2 introduction to the surface. Thus, the intensity of the bands at 787 and 2057 cm^{-1} were normalized to the intensity of the band at 641 cm^{-1}.

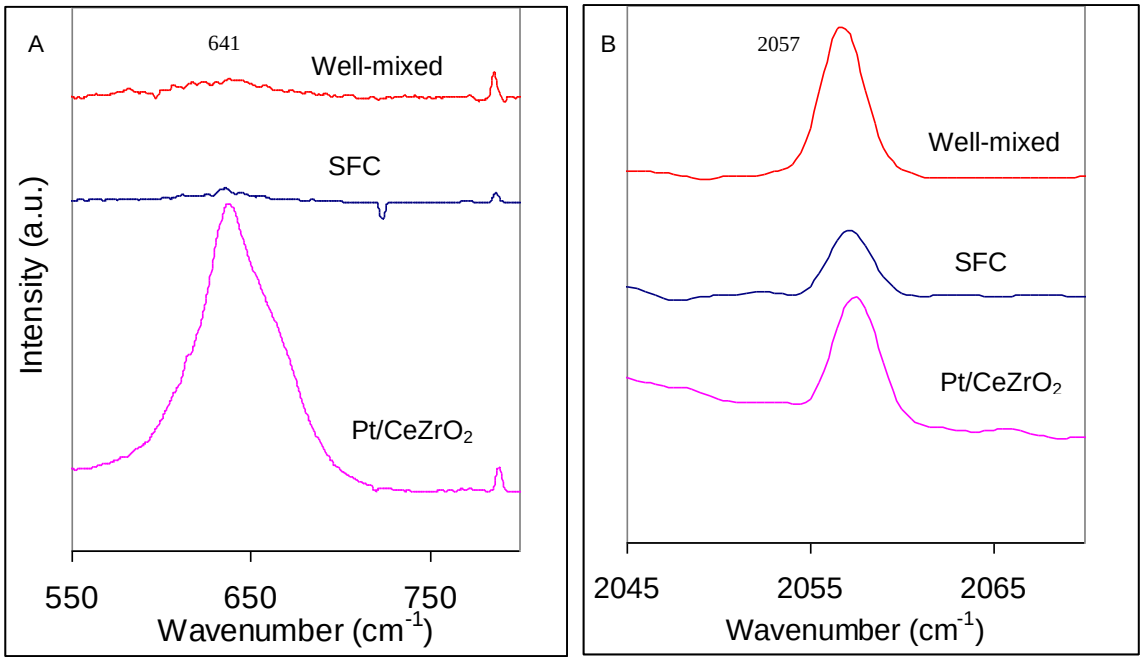

Figure 4.12. The Raman spectra for three different samples during exposure to CO at room temperature.

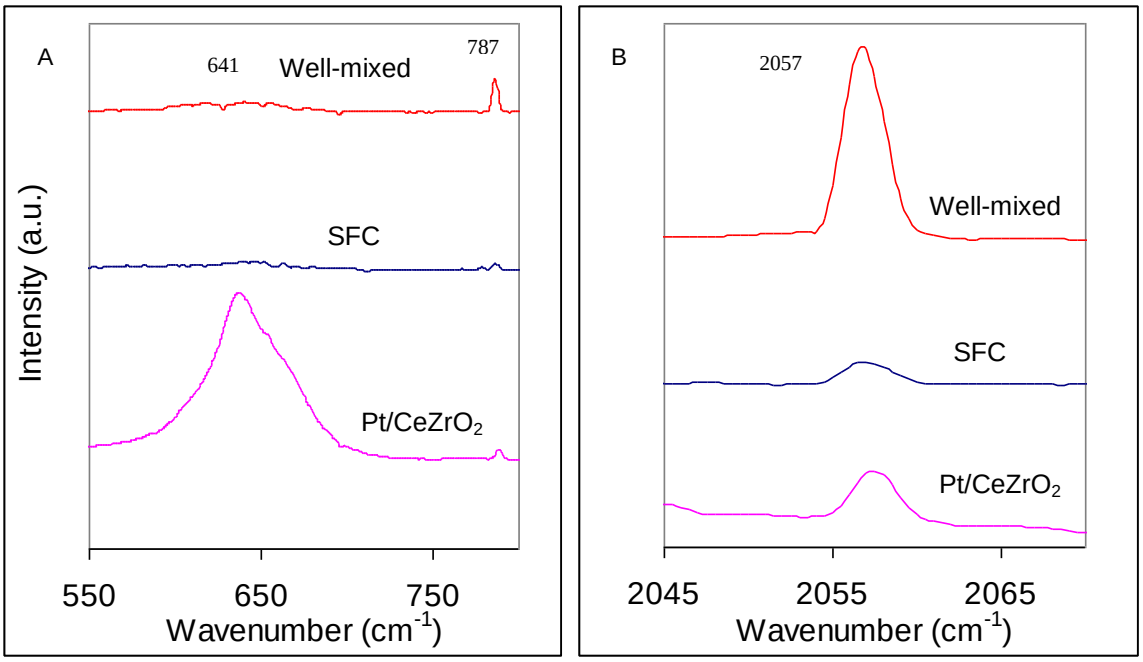

Figure 4.13. The Raman spectra for three different samples during exposure to CO_2 at room temperature.

After the normalization, the intensity of the carbonate band and linear CO band were significantly higher for well-mixed sample compared to the similar bands in SFC and $Pt/CeZrO_2$ samples. This observation is consistent with our previous observation in which more CO_2 production was observed for well-mixed sample during TPD of CO (Figure 4.3). These results suggest that there is an interaction between $Pt/CeZrO_2$ and SFC.

When CO passes over the sample, it can take oxygen from surface and form carbonate, which leads to the increase in the band intensity at $787cm^{-1}$. It is also possible for CO to attach linearly to the metal atoms on the surface (the band at $2057cm^{-1}$). With exposure to CO_2, dissociation of CO_2 occurs which results in CO production. Then, this CO can adsorb linearly to the metals on the surface of sample and causes an increase in the intensity of the band at $2057\ cm^{-1}$.

It should be noted that no significant changes in the Raman spectra of samples were observed when the samples were flushed in helium after CO and CO_2 exposure. This indicates that CO and CO_2 are not weakly adsorbed to the catalyst surface.

4.3.4.2. Raman Spectroscopy at Elevated Temperatures

High temperature Raman spectra of the three samples described above were studied at 200, 400, and 600°C in order to understand the interaction between the catalyst surface and SFC at these temperatures. The results are displayed in Figures 4.14, 4.15, 4.16, 4.17, 4.18 and 4.19.

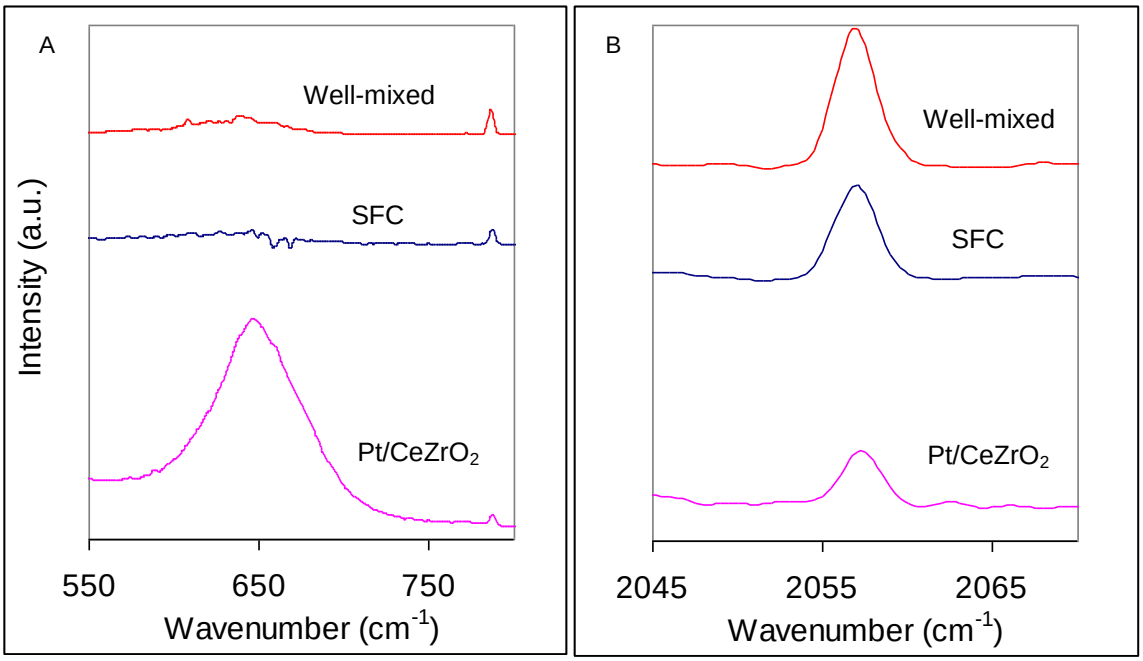

Figure 4.14. The Raman spectra for three different samples during exposure to CO at 200°C.

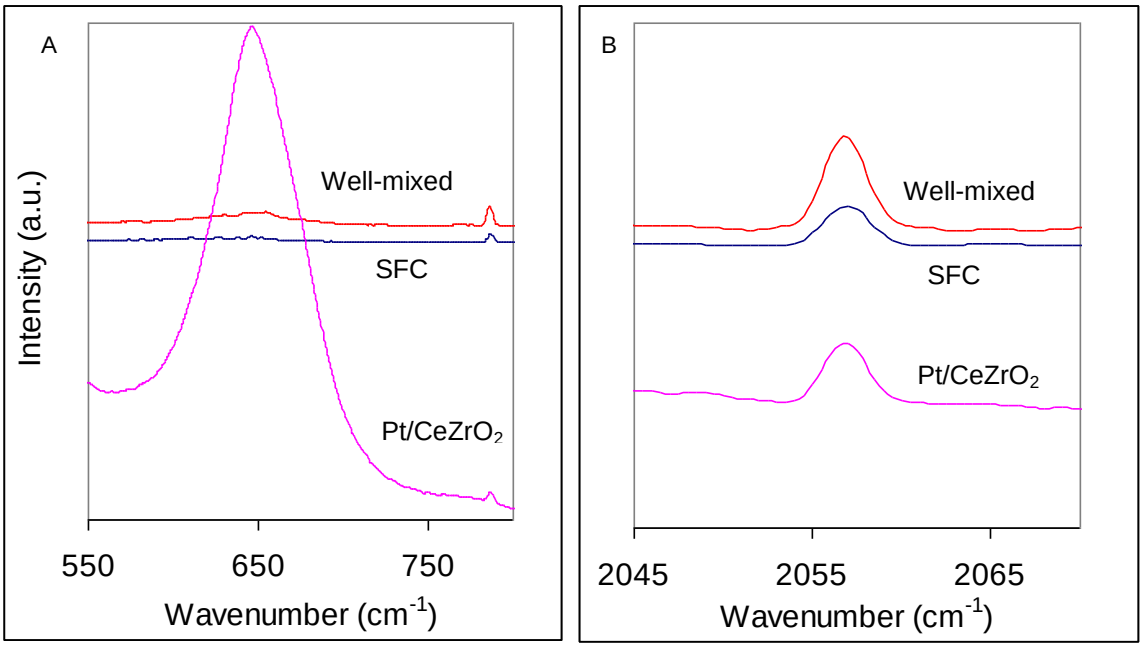

Figure 4.15. The Raman spectra for three different samples during exposure to CO_2 at 200°C.

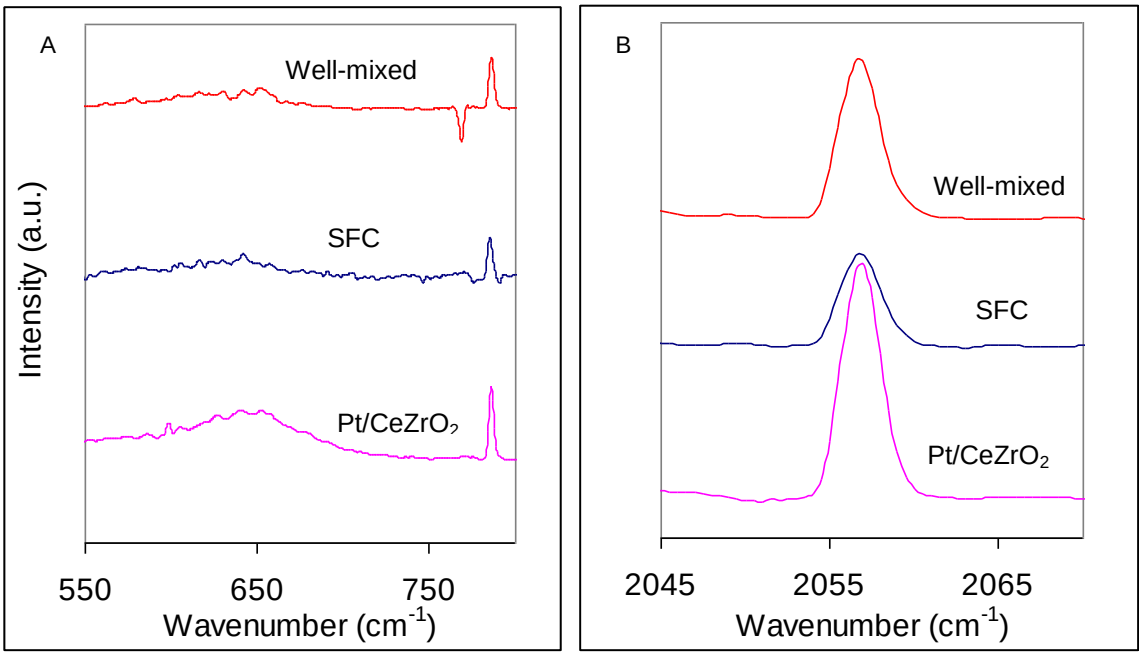

Figure 4.16. The Raman spectra for three different samples during exposure to CO at 400°C.

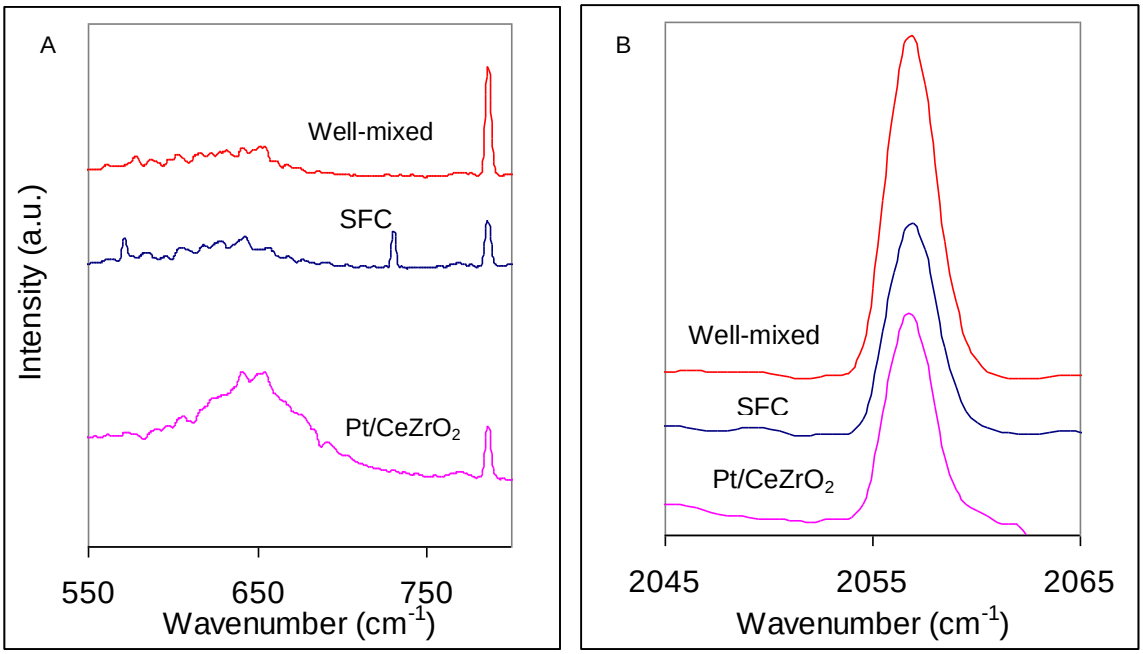

Figure 4.17. The Raman spectra for three different samples during exposure to CO_2 at 400°C.

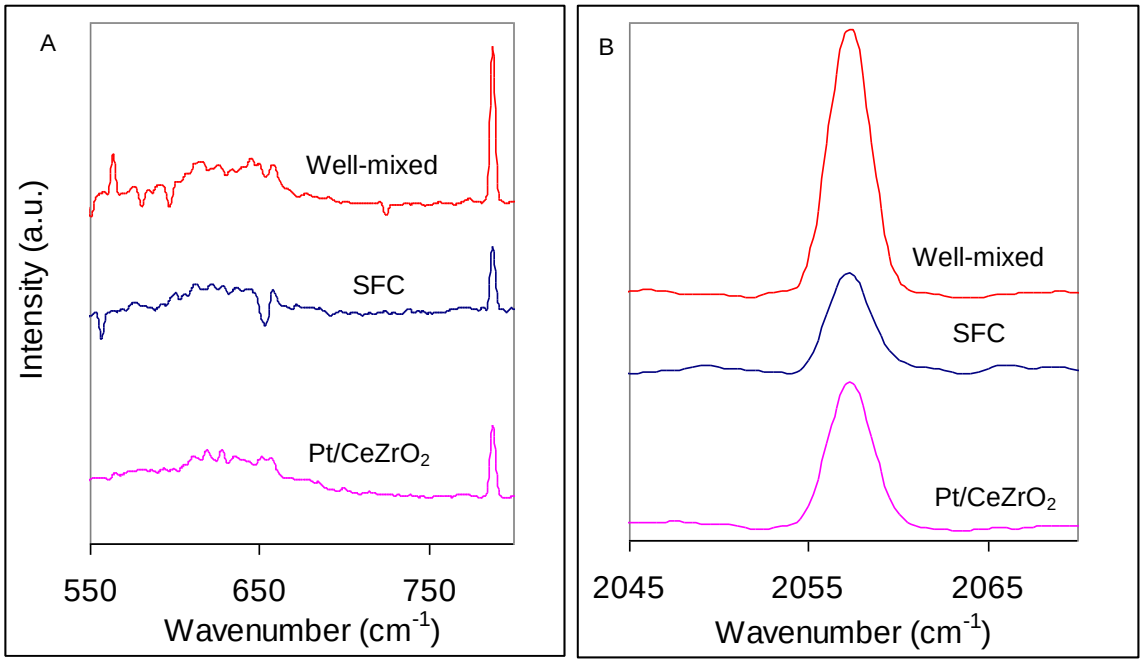

Figure 4.18. The Raman spectra for three different samples during exposure to CO at 600°C.

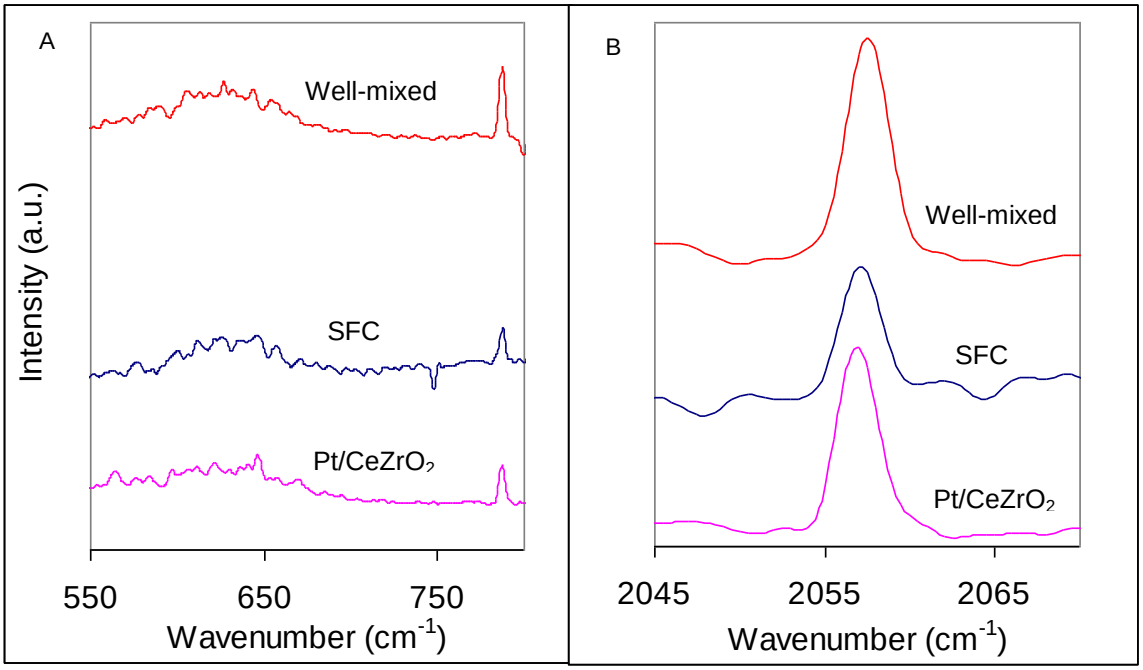

Figure 4.19. The Raman spectra for three different samples during exposure to CO_2 at 600°C.

The results obtained from CO and CO_2 adsorption studies at higher temperatures are similar to the results obtained at room temperature. For the well-mixed sample, Raman spectra during CO and CO_2 exposure at temperatures higher than room temperature showed higher intensity of the bands at 787 and 2057 cm^{-1} compared to SFC sample and $Pt/CeZrO_2$ sample. The higher CO and CO_2 adsorption on the well-mixed sample again demonstrates the existence of a synergistic relationship between the catalyst and SFC at higher temperatures. Although our Raman spectrometer was not capable of holding temperatures higher than 600°C, it is believed that a well-mixed sample adsorbs more CO and CO_2 than SFC alone and $Pt/CeZrO_2$ alone at 800°C, which is the temperature used for syngas production from methane in some membrane reactors.

4.4. Conclusions

The results of this study clearly demonstrate that there is a synergistic relationship between the catalyst and the SFC membrane. Physical mixtures of a $Pt/CeZrO_2$ catalyst and powdered SFC membrane material demonstrate significantly higher degrees of water and CO_2 production in the presence of H_2 and CO than the catalyst and SFC alone. Under reaction conditions, the increased formation of H_2O and CO_2 and subsequent occurrence of steam and carbon dioxide reforming of methane will lead to higher methane conversions. The degree of SFC and catalyst interaction has a significant impact on the ability of the membrane to provide beneficial effects to the reaction. Specifically, the utilization of membrane oxygen

either by a spillover to the catalyst or by direct reaction with the products of the reaction is maximized with intimate membrane catalyst contact. More importantly, the results of these studies have demonstrated that even though the plug flow reactor configuration is significantly different from the membrane reactor because oxygen is not continually supplied to the membrane, pulse studies can provide valuable information about the interaction between the catalyst and membrane under reaction conditions. Finally, Raman spectroscopy of physical mixtures of a $Pt/CeZrO_2$ catalyst and powdered SFC membrane material demonstrated higher CO and CO_2 adsorption than the catalyst and SFC alone at the temperatures ranging from room temperature to 600°C.

4.5. References

[1] P. S. Maiya, U. Balachandran, J. T. Dusek, R. L. Mieville, M. S. Kleefisch, and C. A. Udovich, "Oxygen transport by oxygen potential gradient in dense ceramic oxide membranes," *Solid State Ionics*, vol. 99, pp. 1-7, 1997.

[2] B. Ma, N. I. Victory, U. Balachandran, B. J. Mitchell, and J. W. Richardson, "Study of the mixed-conducting $SrFeCo_{0.5}O_y$ system," *J Am Ceram Soc*, vol. 85, pp. 2641-2645, 2002.

[3] B. Ma and U. Balachandran, "Phase stability of $SrFeCo_{0.5}O_x$ in reducing environments," *Mat Res Bull*, vol. 33, pp. 223-236, 1998.

[4] W. S. Yang, H. H. Wang, X. F. Zhu, and L. W. Lin, "Development and application of oxygen permeable membrane in selective oxidation of light alkanes," *Topics in Catalysis*, vol. 35, pp. 155-167, 2005.

[5] Q. Jiang, S. Faraji, D. A. Slade, K. J. Nordheden, and S. M. Stagg-Williams, "Performance analysis of mixed-conducting ceramic membranes for membrane reactor applications," presented at AIChE Annual Meeting, Salt Lake City, 2007.

[6] D. Poulidi, A. Craig, and I. S. Metcalfe, "Remote Control of the Activity of a Pt Catalyst Supported on a Mixed Ionic Electronic Conducting Membrane," *Solid State Ionics*, vol. 179, pp. 1347-1350, 2008.

[7] A. P. E. York, T. Xiao, and M. L. H. Green, "Brief Overview of the Partial Oxidation of Methane to Syngas," *Topics in Catalysis*, vol. 22, pp. 345-358, 2003.

[8] Y. H. Hu and E. Ruckenstein, "Catalytic Conversion of Methane to Synthesis Gas by Partial Oxidation and CO_2 Reforming," *Adv. Catal.*, vol. 48, pp. 297-345, 2004.

[9] X. Zhang, C. S. M. Lee, and D. O. Hayward, "Oscillatory Behaviour Observed in the Rate of Oxidation of Methane Over Metal Catalysts," *Catalysis Today*, vol. 105, pp. 283-294, 2005.

[10] M. Ikeguchi, T. Mimura, Y. Sekine, E. Kikuchi, and M. Matsukata, "Reaction and oxygen permeation studies in $Sm_{0.4}Ba_{0.6}Fe_{0.8}Co_{0.2}O_{3-\delta}$ membrane reactor for partial oxidation of methane to syngas," *Applied Catalysis A : General*, vol. 290, pp. 212-220, 2005.

[11] V. Galvita, L. K. Rihko-Struckmann, and K. Sundmacher, "The CO Adsorption on a Fe_2O_3-$Ce_{0.5}Zr_{0.5}O_2$ Catalyst Studied by TPD, Isotope Exchange and FTIR Spectroscopy," *Journal of Molecular Catalysis A: Chemical*, vol. 283, pp. 43-51, 2008.

[12] I. Kaus and K. Wiik, "Stability of $SrFeO_3$-Based Materials in H_2O/CO_2-Containing Atmospheres at High Temperatures and Pressures," *J. Am. Ceram. Soc.*, vol. 90, pp. 2226-2230, 2007.

[13] S. M. Murphy, D. A. Slade, K. J. Nordheden, and S. M. Stagg-Williams, "Increasing oxygen flux through a dense oxygen permeable membrane by photolithographic patterning of platinum," *Journal of Membrane Science*, vol. 277, pp. 94-98, 2006.

[14] D. A. Slade, A. M. Duncan, K. J. Nordheden, and S. M. Stagg-Williams, "Mixed-conducting oxygen permeable ceramic membranes for the carbon dioxide reforming of methane," *Green Chemistry*, vol. 9, pp. 577-581, 2007.

[15] C. Li, Y. Sakata, T. Arai, K. Domen, K. Maruya, and T. Onishi, "Carbon-Monoxide and Carbon-Dioxide Adsorption on Cerium Oxide Studied by Fourier-Transform Infrared-Spectroscopy .1. Formation of Carbonate Species on Dehydroxylated CeO_2 at Room-Temperature," *Journal of the Chemical Society-Faraday Transactions I*, vol. 85, pp. 929-943, 1989.

[16] L. S. F. Feio, C. E. Hori, S. Damyanova, F. B. Noronha, W. H. Cassinelli, C. M. P. Marques, and J. M. C. Bueno, "The effect of ceria content on the properties of $Pd/CeO_2/Al_2O_3$ catalysts for steam reforming of methane," *Applied Catalysis A : General*, vol. 316, pp. 107-116, 2007.

[17] A. Davydov, *Molecular Spectroscopy of Oxide Catalyst Surfaces*. Chichester: John Wiley & Sons Ltd., 2003.

Chapter 5: A Comparative Study of $Ba_{0.5}Sr_{0.5}Co_{0.8}Fe_{0.2}O_x$ (BSCF) and $SrFeCo_{0.5}O_x$ (SFC) Ceramic Membranes Used for Syngas Production

5.1. Introduction

We have shown in Chapter 4 that there is a synergistic relationship between a $Pt/CeZrO_2$ catalyst and a SFC ceramic membrane. The synergistic relationship results in the production of water and the subsequent occurrence of steam and CO_2 reforming of methane leads to higher methane formation when the catalyst and the ceramic membrane are in close contact under reaction condition. In our previous flux studies on ceramic membranes, dense BSCF membranes, which have a higher mechanical stability than SFC, demonstrated 10 times higher oxygen permeation flux than dense SFC membrane at 800°C [1]. These dense BSCF membranes maintain long-term mechanical integrity and stability in an air:Ar gradient at 800°C and the membrane oxygen flux (0.57 sccm/cm^2) at this condition is consistent with other literature studies [2, 3].

The goal of this study is to compare the performance of dense BSCF membranes with that of dense SFC ceramic membranes for converting CH_4 to syngas in the presence of $Pt/CeZrO_2$ and Pt/ZrO_2 catalysts. Specific emphasis will be placed on the surface reactions and reaction mechanisms. The role of the membrane material in the enhancement of methane conversion is investigated by studying the adsorption and desorption of reactant and product species. We explore how the partial substitution of Sr with Ba affects the interaction of ceramic material with O_2, H_2, CO,

and CO_2, and how it influences the product distribution and the H_2/CO ratio during CO_2 reforming of methane.

5.2. Experimental

All pulse studies and continuous reaction studies were performed in a PFR (Figure 3.2) and membrane reactor (Figure 3.3) respectively. Detailed information about membranes and catalysts preparation methods, TPD, TGA, and Raman techniques can be found in Chapter 3.

5.3. Results and Discussion

5.3.1. O_2 Uptake and Release Capability of SFC and BSCF

Ceramic materials can reduce or oxidize reaction species because of their oxygen uptake and release capabilities, leading to a change in the overall reaction mechanism. Thus, it is important to understand the interaction of oxygen with the BSCF and SFC membrane materials. For this purpose, each crushed ceramic material was loaded into a plug flow reactor and was heated to 800°C in argon. Figure 5.1A shows the mass spectrometer oxygen signal for both materials while heating in argon. The onset temperature of oxygen release for BSCF (~ 450°C) was observed to be lower than that for SFC, while the total amount of oxygen release was greater for BSCF (1.87×10^{-6} moles for BSCF vs. 4×10^{-7} moles for SFC). The SFC started to release oxygen at 550°C and it did not show a significant O_2 release before this temperature.

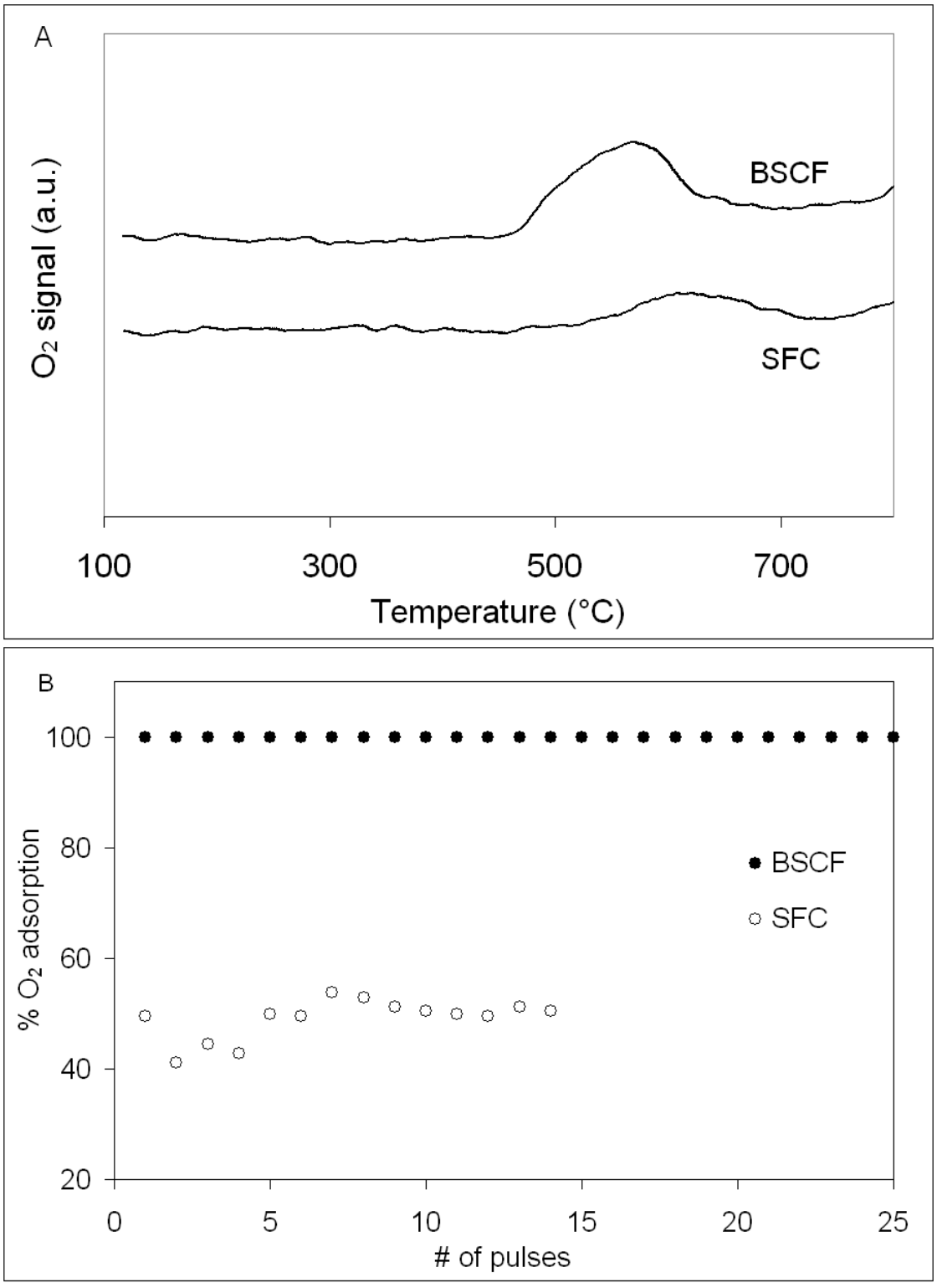

Figure 5.1. Oxygen interaction with crushed SFC and BSCF in plug flow reactor: A) thermal O_2 release in Ar and B) O_2 uptake during pulses of oxygen at 800°C and atmospheric pressure.

Figure 5.1A suggests that BSCF might be suitable for hydrocarbon conversion at much lower temperatures than conventional dense ceramic membranes. It is worth mentioning that a similar oxygen release experiment was performed in membrane reactor for disk-shaped BSCF and SFC membranes. The dense ceramic membranes were heated to 800°C in flowing argon, while the effluent oxygen signal was monitoring by mass spectrometer. The results in membrane reactor were similar to those in plug flow reactor (i.e., low-temperature oxygen release was greater for BSCF).

At 800°C, the crushed SFC and BSCF samples were exposed to 50 μl O_2 injections and both samples showed oxygen adsorption capability. However, according to Figure 5.1B, the amount of oxygen uptake on BSCF was significantly higher than that on SFC. For the crushed BSCF membrane, no oxygen peak was observed in mass spectrometer even 3 hours after the first oxygen injection, indicating that all of the oxygen was adsorbed by the BSCF. These results clearly show the higher adsorption capacity of the BSCF membranes compared to SFC.

TGA studies were used to clarify the mass changes of crushed ceramic materials in different atmospheres (air and nitrogen) from room temperature to 800°C. The results of the TGA studies are shown in Figure 5.2. During the heating process in N_2, both SFC and BSCF undergo weight loss due to their oxygen release capabilities. However, the amount of weight loss in the BSCF specimen is higher than that in the SFC specimen. This observation is consistent with Figure 5.1A in which the total amount of oxygen release in argon was greater for BSCF. The calculated

amount of weight loss for BSCF in N_2 is almost 0.0064 mg/mg BSCF. Based on Figure 5.1A, 92% of this weight loss is due to oxygen release and the remainder is probably due to water and other surface contaminants. It is interesting to note that the samples behave differently in air, where oxygen is available to replenish oxygen lost. According to Figure 5.2, at temperatures ranging from 400°C to 500°C in flowing air, BSCF shows a large weight loss while SFC gains weight. This means that in this temperature range, BSCF can release oxygen even in an oxygen-rich atmosphere, but SFC tends to adsorb oxygen in such an atmosphere. Over this temperature range, the drop in weight for BSCF in flowing air is smaller than that in nitrogen, which is to be expected due to the differences in the equilibrium oxygen content of the membrane in

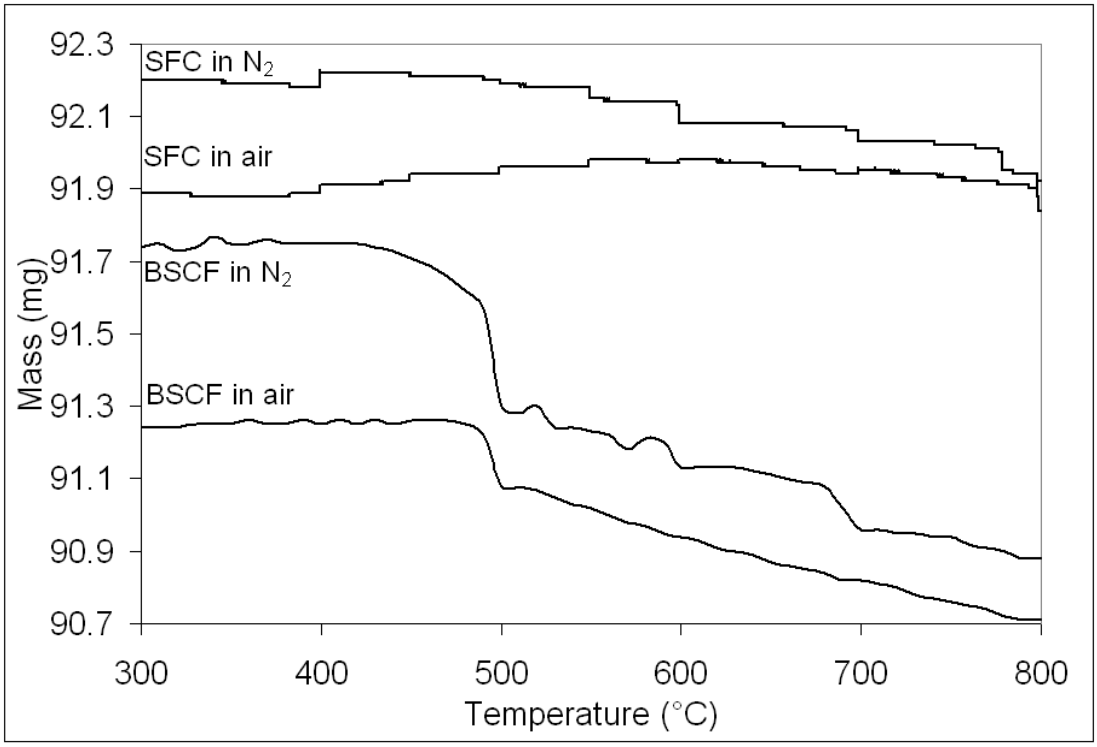

Figure 5.2. TGA profiles for crushed SFC and BSCF in flowing nitrogen and air.

the different environments. At temperatures above 600°C, SFC shows a weight loss similar to BSCF. These TGA studies again suggest that BSCF may be a suitable material for reactions occurring at low temperatures specifically between 400 and 500°C. During another TGA test (Figure 5.3) a continuous flow of air was introduced to crushed BSCF and SFC samples at 800°C, after being heated in flowing nitrogen to 800°C. The results show that samples gain weight upon exposure to air. However, the amount of mass increase, which represents the amount of oxygen uptake, for BSCF particles is 1.8 times higher than that for SFC particles. This observation is in agreement with what was observed in plug flow reactor during 50 μl O_2 injections at 800°C (Figure 5.1B). It should be noted that the mass increase observed at time = 200 min in Figure 5.3 is artificial because no mass increase was seen when samples were heating in nitrogen in Figure 5.2.

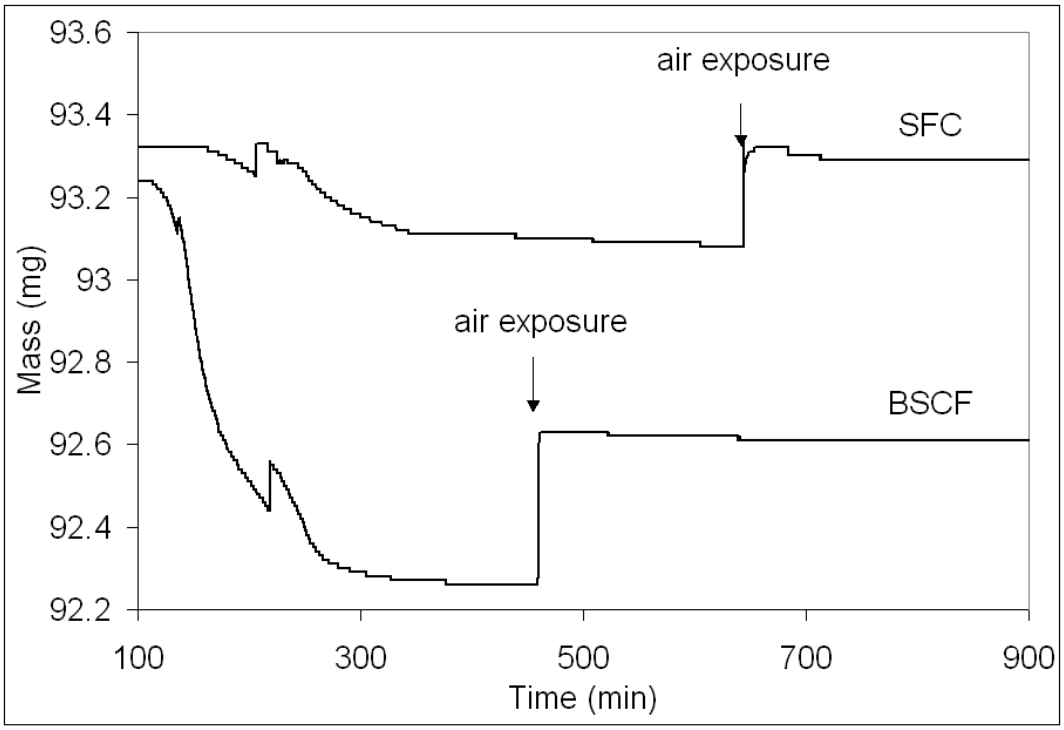

Figure 5.3. The effect of air exposure at 800°C on TGA profiles for crushed samples.

5.3.2. H_2, CO, and CO_2 Interaction with SFC and BSCF

The primary products formed from the decomposition of methane in the presence of CO_2 (dry reforming) or O_2 (partial oxidation) are H_2 and CO. Previous studies have suggested that the hydrogen formed during the reaction can interact with oxygen species on the membrane surface to form water [4]. In addition, it has been suggested that CO_2 and CO can form carbonate species on the membrane surface [5-9]. For BSCF, $Sr_{0.6}Ba_{0.4}CO_3$ carbonate has been observed after CO_2 adsorption [8]. The formation of H_2O, and the adsorption and potential reaction of CO and CO_2 on the membrane surface, can significantly change the product composition and the overall reaction scheme. Thus, it is important to understand the interaction of the reactant and product species with the membrane material.

To understand the interaction of ceramic membranes with H_2, CO, and CO_2 at 800°C, the crushed SFC and BSCF samples were heated to 800°C in argon in the plug flow reactor. Then, each sample was exposed to 50 μl pulses of H_2, CO, or CO_2 while monitoring the effluent using a mass spectrometer.

During H_2 injections at 800°C, hydrogen consumption and water production were observed for both the BSCF and SFC crushed samples. Figure 5.4 compares the relative amounts of total hydrogen consumption for BSCF and SFC. It is clear from Figure 5.4 that the amount of hydrogen consumed for the BSCF was more than 24 times higher than that for SFC. This increased hydrogen consumption resulted in a significant increase in the amount of water produced for BSCF compared to SFC. The consumption of hydrogen and the appearance of water, clearly demonstrates that

the both membrane materials have the ability to react with gaseous hydrogen. However, in the absence of an oxygen supply, the crushed SFC membrane material is not able to replenish the oxygen in the lattice, and the hydrogen consumption quickly ceases. For BSCF, lattice oxygen is available for water production even 4 hours after first hydrogen injection, again indicating that BSCF is a better oxygen supplier than SFC.

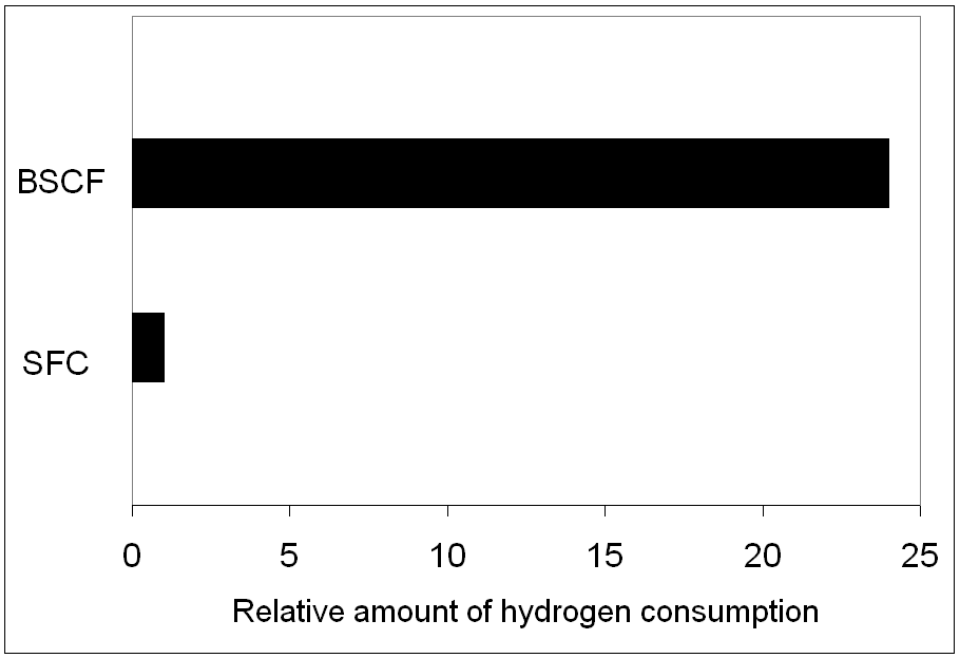

Figure 5.4. The relative amount of total hydrogen consumption at 800°C and atmospheric pressure for crushed BSCF and SFC.

When CO was injected on the BSCF and SFC samples at 800°C, CO_2 production was seen for both samples. Figures 5.5A and 5.5B show the CO consumption and CO_2 production per one mg of ceramic material. The amount of CO consumption and CO_2 production for BSCF were higher than for SFC. Since the only source of O_2 in the reactor is the oxygen in the membrane lattice, the CO_2 production

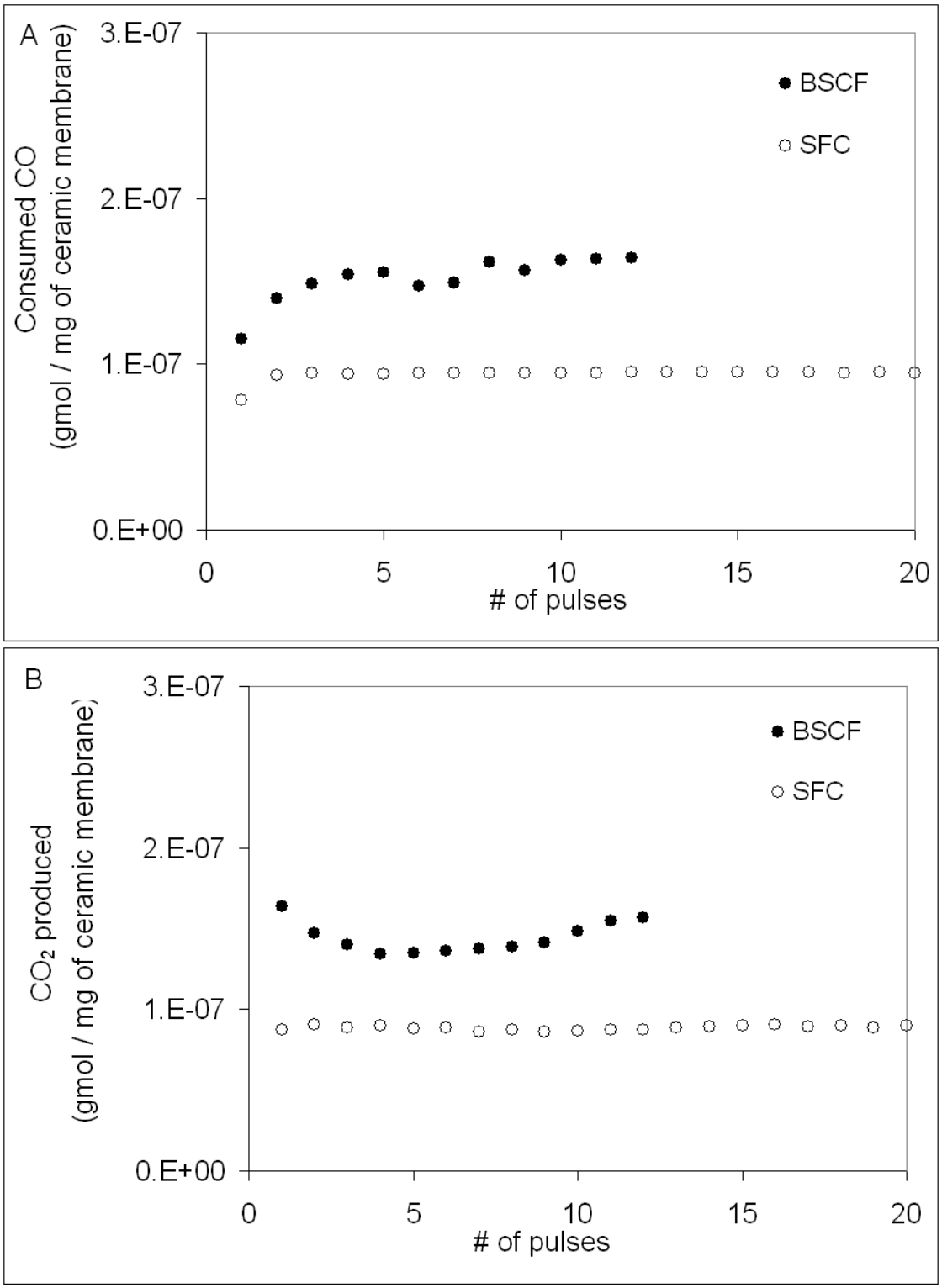

Figure 5.5. CO interaction with crushed SFC and BSCF in plug flow reactor at 800°C and atmospheric pressure: A) CO consumption profile and B) CO_2 production profile.

is ascribed to CO reduction of the membrane (CO fractional conversion:7.5% for BSCF vs. 4.5% for SFC). The increased production of CO_2 on the BSCF membrane compared to SFC clearly shows that the BSCF has the ability to provide higher amounts of oxygen under similar reducing environments than the SFC membrane material. When CO_2 was pulsed into reactor over the BSCF and SFC samples at 800°C, a small amount of CO production was observed for both membranes. However, there was no significant difference between the interaction of CO_2 with BSCF and that with SFC.

Another set of pulse studies was performed at 800°C in which the samples were exposed to three sets of pulses. The first set of pulses contained H_2. The second set had CO, followed by the third set, which again contained H_2. Figure 5.6 shows the results of this pulse study for the crushed BSCF membrane. Similar to the individual pulse studies, during the first set of H_2 pulses, hydrogen consumption was observed. Likewise, CO_2 was produced during the pulses of CO. It should be noted that the amount of CO_2 produced during the CO pulses is less than the amount of CO consumed. These results suggest that some of the CO does not reduce the membrane surface, but instead remains adsorbed on the membrane surface, possibly in the form of carbonates. During the last set of H_2 pulses, less hydrogen consumption was observed compared to the first set of hydrogen pulses.

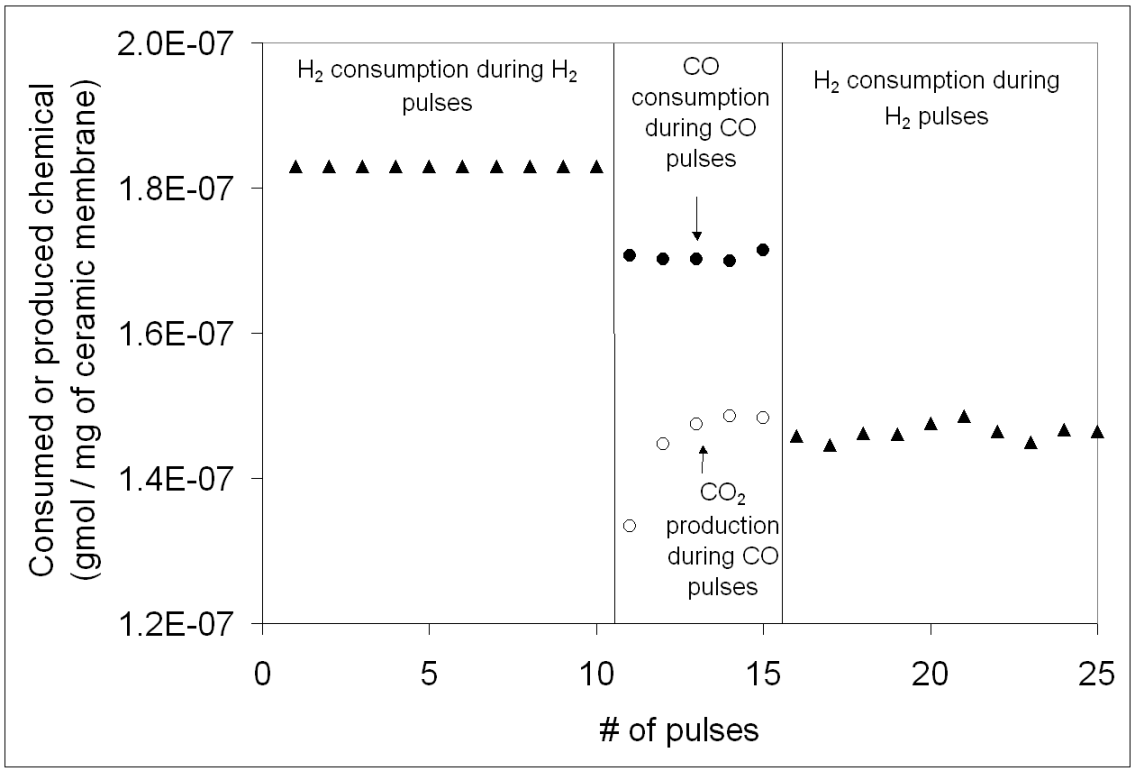

Figure 5.6. H_2 and CO interaction with crushed BSCF in plug flow reactor at 800°C and atmospheric pressure. The order of pulses was H_2/CO/ H_2.

The decrease in hydrogen consumption during the second set of hydrogen pulses is most likely due to the presence of the adsorbed CO species remaining from the CO pulses. While Figure 5.6 shows the results for the BSCF, similar results were observed for the SFC membrane material, indicating that CO adsorption, albeit to a lesser extent, can also occur on the SFC.

Another experiment was performed at 800°C except the order of the pulses was switched. In this experiment, the order of the pulses was CO/H_2/CO. Again, CO injections resulted in CO consumption and CO_2 production. However, the CO consumption after hydrogen exposure was higher than that before hydrogen exposure.

It is possible that the increase in CO adsorption is due to a hydrogen-assisted adsorption that occurs on the surface of the membrane.

Temperature Programmed Desorption (TPD) of CO and CO_2 were performed on each of the samples described above. Each sample was exposed to a continuous flow of CO or CO_2 at room temperature for 30 minutes and then heated to 800°C in argon (15 cc/min). The effluent was monitored using a mass spectrometer. Figures 5.7 and 5.8 show the CO_2 desorption profiles for the BSCF sample after CO and CO_2 exposure, respectively. Also shown in Figures 5.7 and 5.8 for comparison purposes are the profiles for SFC, under the same conditions, which have been previously reported [10]. In both cases, significant amounts of CO_2 were observed, and no CO was detected. As in the case of the CO pulses at 800°C, the total amount of CO_2 formed for the BSCF during the TPD of CO and CO_2 is higher than the SFC. It is believed that CO adsorbs to the surface of the ceramic material in the form of carbonates at room temperature but then forms CO_2 at higher temperatures by reducing the material.

The onset temperature of CO_2 desorption profile for BSCF sample is 200°C in Figure 5.7 and 250°C in Figure 5.8. Unlike the BSCF, SFC showed a slightly higher onset temperature of CO_2 release. The decreased temperature for CO_2 formation on the BSCF compared to the SFC demonstrates the ability of BSCF to release oxygen more readily than the SFC, and again suggests that BSCF might be a good material for low temperature reactions

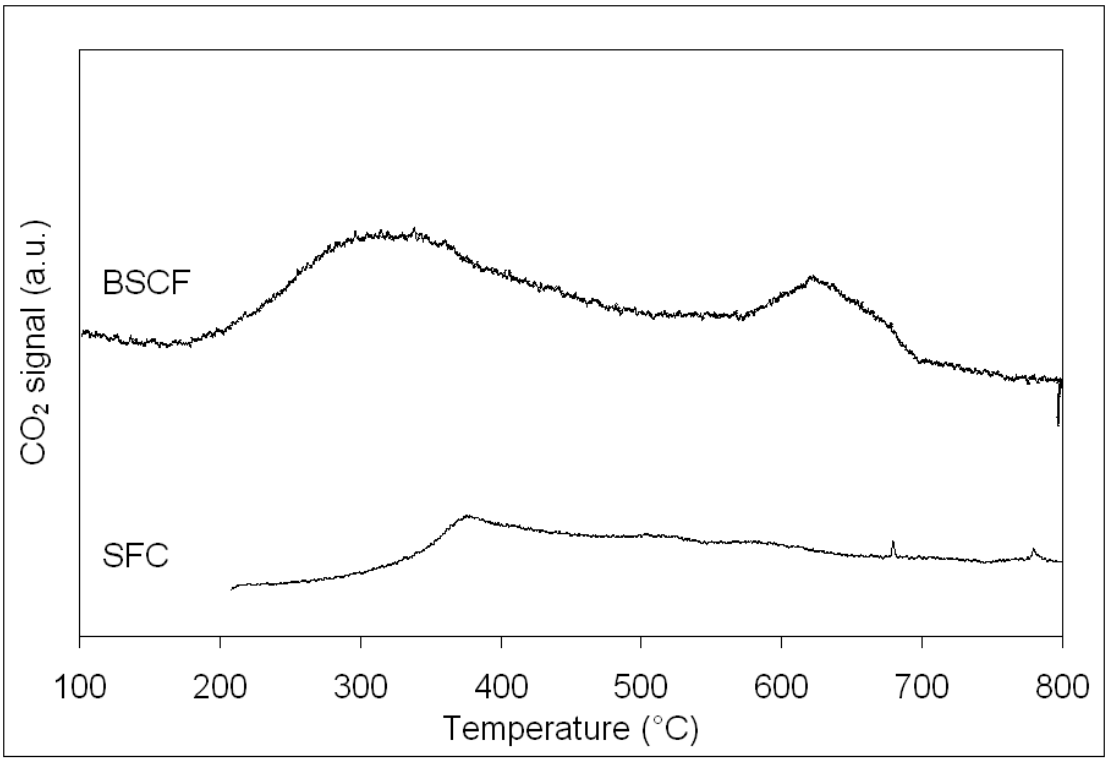

Figure 5.7. CO_2 desorption profiles during temperature programmed desorption of CO after exposure to a continuous flow of CO at room temperature.

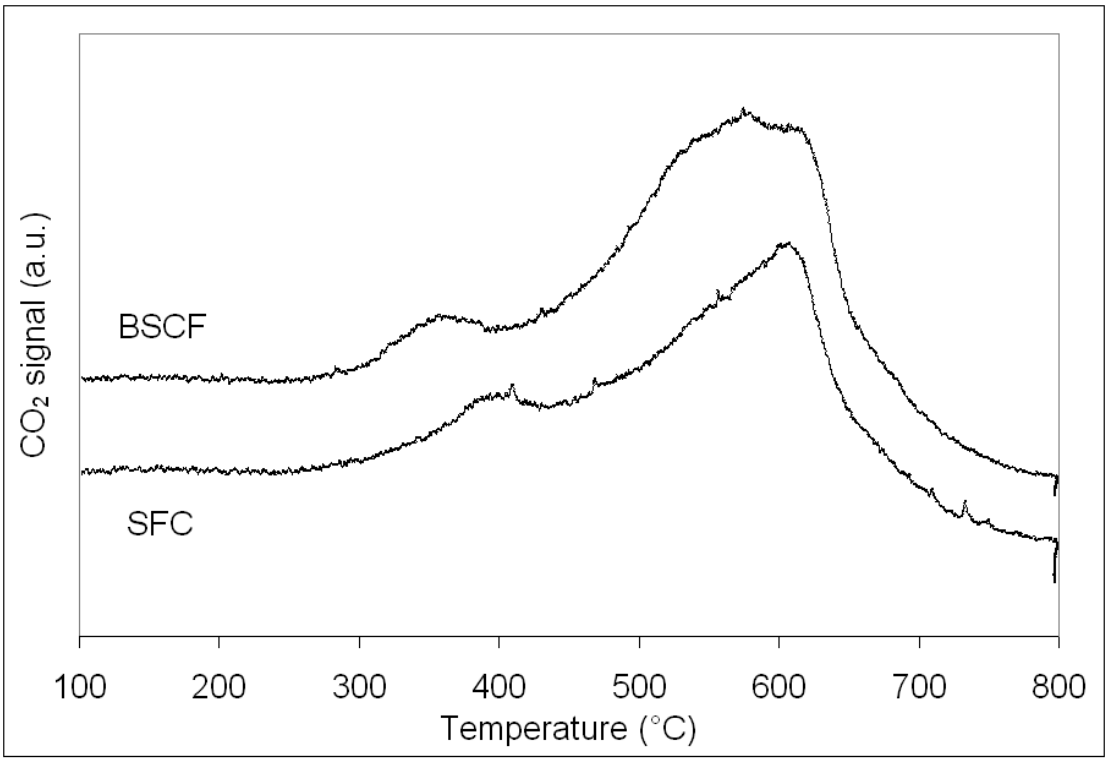

Figure 5.8. CO_2 desorption profiles during temperature programmed desorption of CO_2 after exposure to a continuous flow of CO_2 at room temperature.

According to Figures 5.7 and 5.8, two CO_2 desorption peaks were observed for BSCF during heating to 800°C. It is possible that the two peaks correspond to CO_2 that has been formed from different carbonate species adsorbed on the membrane surface. It is also possible that multiple peaks appear due to different oxygen species (surface versus bulk) contributing to the formation of CO_2. Further studies are needed to differentiate between these possible scenarios.

In order to determine the surface species formed during the ceramic material exposure to CO or CO_2 at different temperatures, samples were scanned by a Raman spectroscope in different flowing gases (He, CO, and CO_2). The results are shown in Figures 5.9, 5.10, 5.11, and 5.12.

The Raman spectra of BSCF and SFC at room temperature in helium are similar; however, the peaks in the spectra of BSCF are slightly shifted to lower wavenumbers. These changes are believed to be due to the presence of Ba in the BSCF sample. The Raman spectra of samples after 30-minute exposure to CO and CO_2 at room temperature (Figures 5.9 and 5.10) showed adsorption of these chemicals on the surfaces of BSCF and SFC. Carbonate formation was observed at wavenumber 786 cm^{-1} for BSCF and 787 cm^{-1} for SFC during both exposure to CO and CO_2 [11]. In addition, the band previously assigned to linear CO bonded to the surface was detected at 2056 and 2057 cm^{-1} for BSCF and SFC respectively [12, 13]. When CO passes over the sample, it can take oxygen from the surface and form carbonate, which leads to the increase in the band intensity at 786 and 787cm^{-1}. CO can also attach linearly to the metal atoms on the surface (the band near 2057cm^{-1}).

With exposure to CO_2, dissociation of CO_2 occurs, which results in CO production. Then, this CO can adsorb linearly to the metals on the surface of sample and cause an increase in the intensity of the band at 2057 cm^{-1}. Similarly, the Raman spectra of samples after CO and CO_2 exposure at 400°C (Figures 5.11 and 5.12) showed CO and CO_2 adsorption on the surfaces of BSCF and SFC. Although it is not possible to obtain the Raman spectra of samples at 800°C with our current setup, it is believed that surface species after CO and CO_2 exposure at this temperature are similar to those at room temperature and 400°C. It should be noted that no significant changes in the Raman spectra of the samples were observed when the samples were flushed in helium after CO and CO_2 exposure. This indicates that CO and CO_2 are not weakly adsorbed to the ceramic material surfaces.

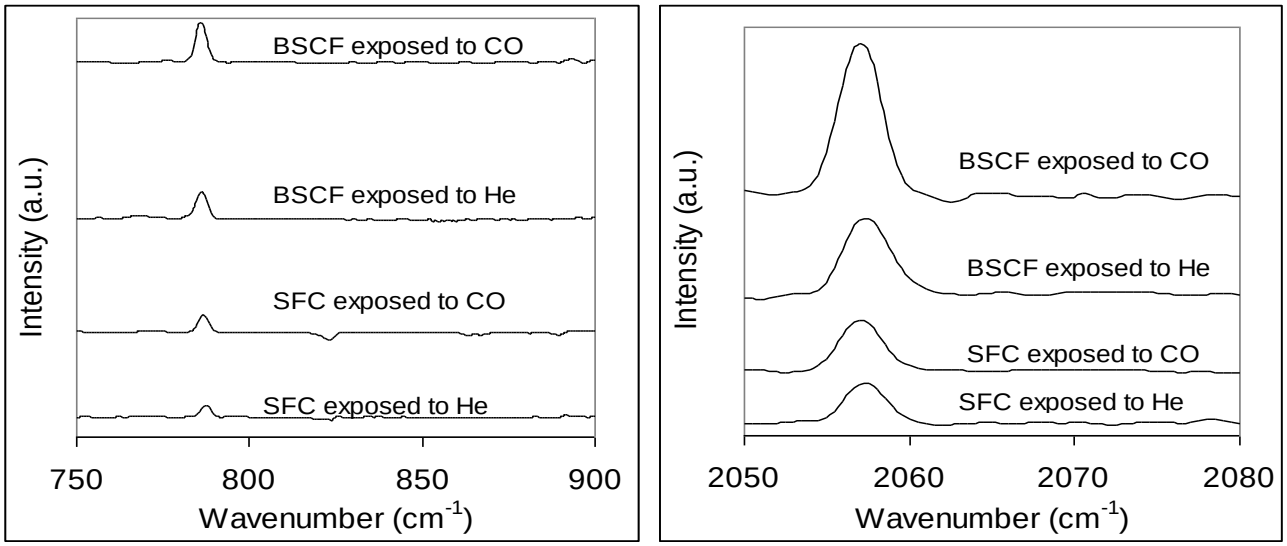

Figure 5.9. The Raman spectra of crushed SFC and BSCF at room temperature in flowing CO.

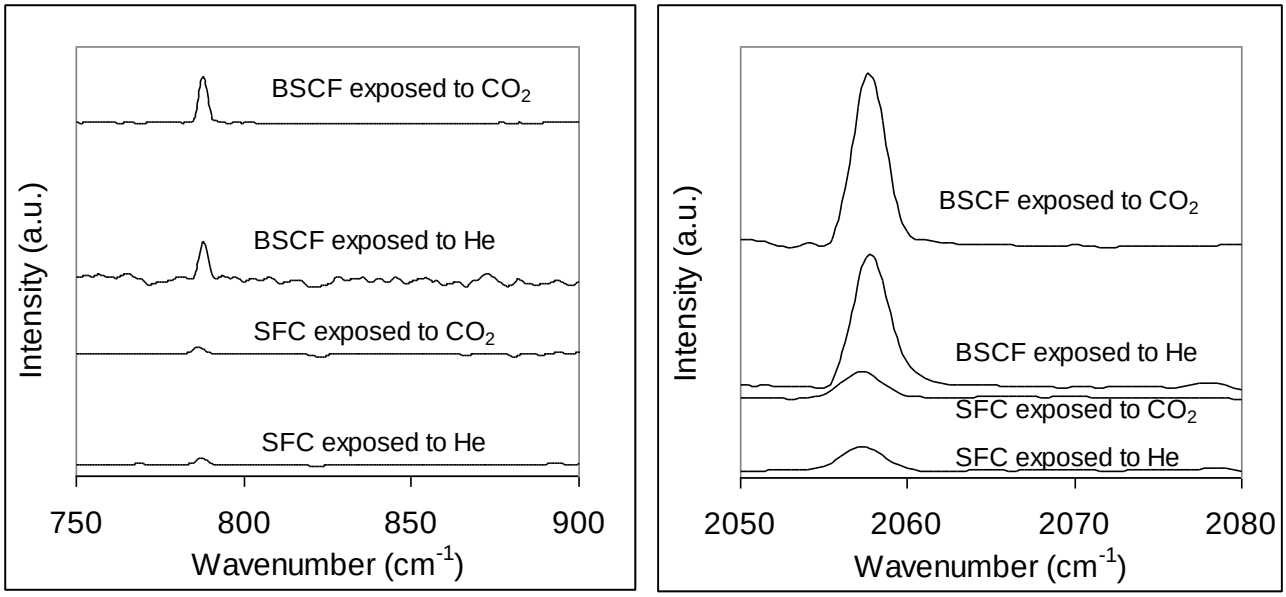

Figure 5.10. The Raman spectra of crushed SFC and BSCF at room temperature in flowing CO_2.

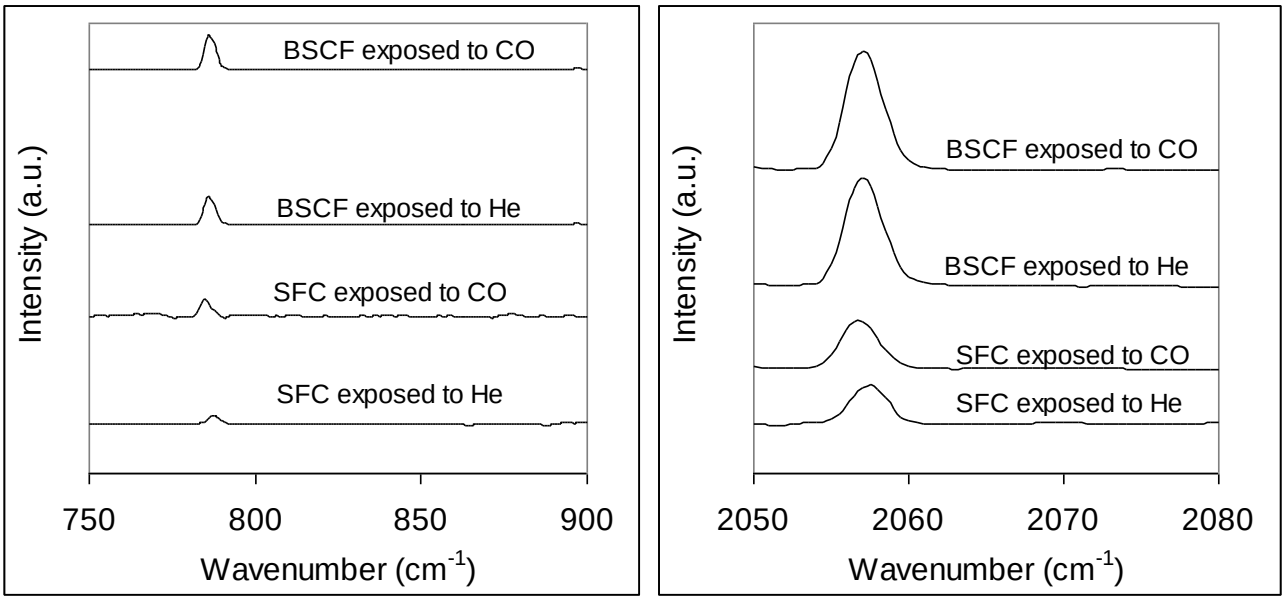

Figure 5.11. The Raman spectra of crushed SFC and BSCF at 400°C in flowing CO.

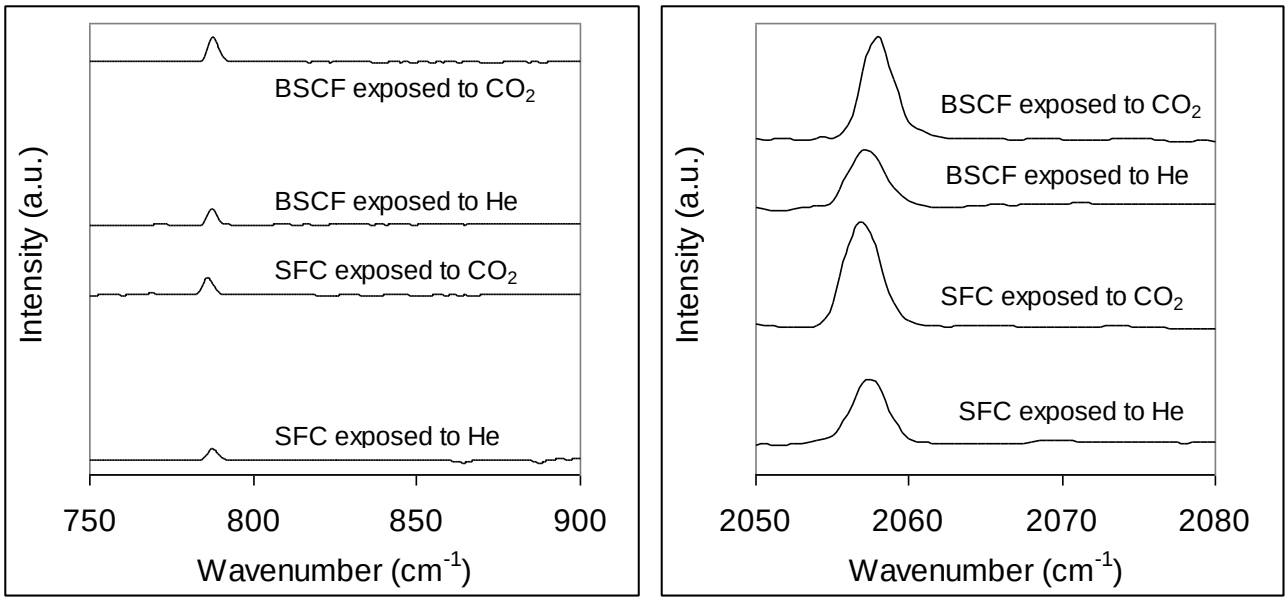

Figure 5.12. The Raman spectra of crushed SFC and BSCF at 400°C in flowing CO_2.

5.3.3. Reaction Studies in Plug Flow Reactor

In order to determine the role of the ceramic material in the conversion of methane, samples were heated to 800°C in Ar and then exposed to pulses of methane while the effluent was monitored using the mass spectrometer. Four samples were studied: 1) a crushed SFC membrane, 2) a crushed BSCF membrane, 3) a physical mixture of the SFC and $Pt/CeZrO_2$ catalyst with mass ratio = 1, and 4) a physical mixture of the BSCF and $Pt/CeZrO_2$ catalyst with mass ratio = 1. These samples were chosen so that the effect of each individual component on the methane conversion and the possible synergistic effect of the combination of membrane and catalyst could be explored.

According to Figure 5.13, the methane conversion for the both SFC and BSCF were less than 5% for all of the pulses which is similar to what was observed for methane conversion for SFC membranes in the absence of a catalyst [4]. In contrast to the low methane conversion for the SFC and BSCF alone, the methane conversion on the physical mixtures of $Pt/CeZrO_2$ and ceramic materials was maintained at a high level for approximately 17 pulses. It is not unexpected that the methane conversion would quickly decrease, as the only species being fed into the reactor is methane and, in the absence of an oxygen source, deactivation of the catalyst would be expected to rapidly occur. It is interesting to note that the methane conversions for the physical mixtures of BSCF and SFC with the catalyst are the same for the first 17 pulses. The conversion of methane begins to decline when the oxygen in the ceramic material is depleted. However, a quicker drop in conversion was observed for BSCF, indicating that BSCF is a better oxygen supplier and loses its lattice oxygen easier and faster than SFC when no oxygen is available in the feed to replenish the oxygen in the ceramic material. CO production is observed to be significantly lower for BSCF compared to SFC, which could be due to more CO conversion to CO_2 on BSCF. This result is consistent with Figure 5.5 and shows that oxygen consumption is significantly higher in the test with BSCF and for this reason oxygen is depleted faster, resulting in a rapid decline in methane conversion.

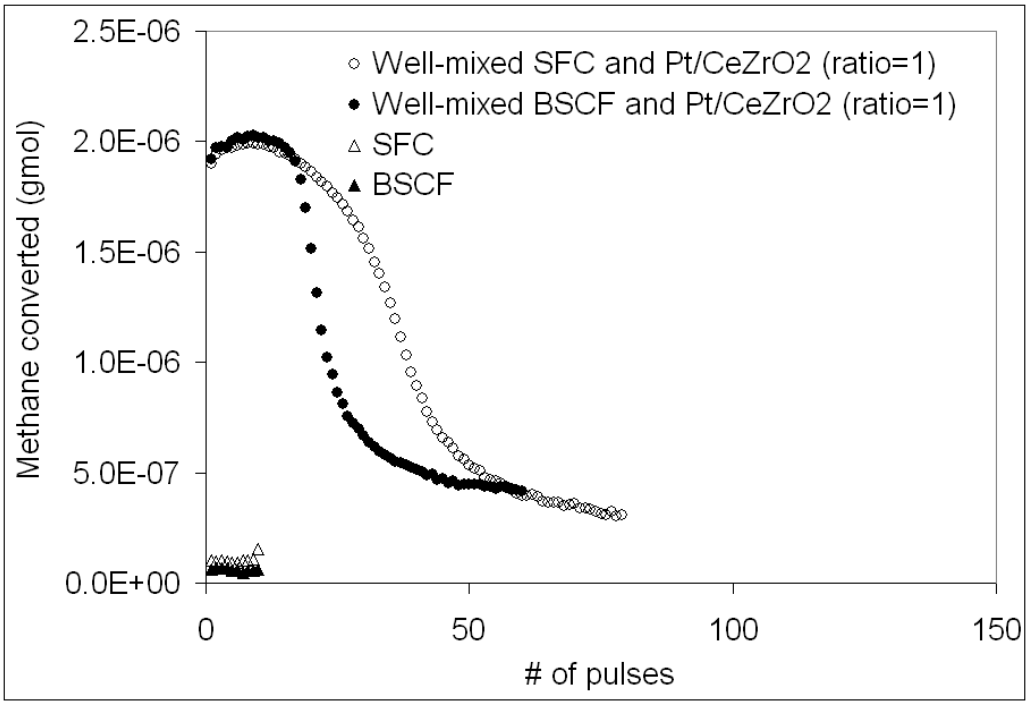

Figure 5.13. Methane conversion profiles for four samples during pulses of methane at 800°C and atmospheric pressure in a plug flow reactor. The four samples are: 1) crushed SFC, 2) crushed BSCF, 3) physical mixture of SFC and $Pt/CeZrO_2$ catalyst (mass ratio = 1), and 4) physical mixture of BSCF and $Pt/CeZrO_2$ catalyst (mass ratio = 1).

For a better comparison to the membrane reactor system, the above experiments were repeated with exposure to pulses containing a 1:1 mixture of CH_4 and CO_2. Figure 5.14 shows the methane conversion profiles for the physical mixtures with CO_2 in the pulses. It is clear that the presence of CO_2 increases the methane conversion and the ability of the catalyst to maintain high conversion for longer periods of time. The CO_2 provides an oxygen source to replenish the oxygen in the catalyst support and ceramic membrane lattice, which assists in preventing carbon deposition. The results in Figure 5.14 again demonstrate that oxygen in BSCF depletes easier and quicker than that in SFC.

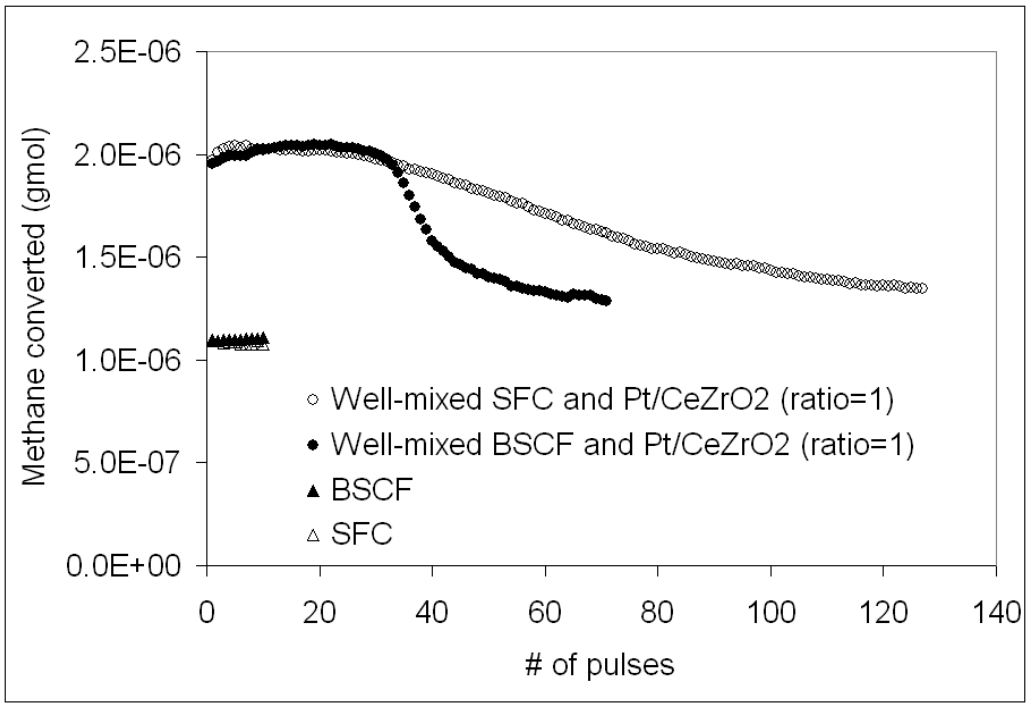

Figure 5.14. Methane conversion profiles for four samples during pulses of CH_4 and CO_2 (1:1 ratio) at 800°C and atmospheric pressure in a plug flow reactor. The four samples are: 1) crushed SFC, 2) crushed BSCF, 3) physical mixture of SFC and $Pt/CeZrO_2$ catalyst (mass ratio = 1), and 4) physical mixture of BSCF and $Pt/CeZrO_2$ catalyst (mass ratio = 1).

5.3.4. CO_2 Reforming of Methane in Membrane Reactor

The previously described pulse and TPD studies in sections 5.3.1 and 5.3.2 have shown that when SFC and BSCF are exposed to H_2 and CO gases, H_2O and CO_2 formation occur. Also, BSCF has a higher interaction with O_2, H_2, and CO gases compared to SFC, resulting in higher H_2O and CO_2 production. Thus, under reaction conditions and in the presence of a catalyst, hydrogen produced from methane decomposition is expected to result in significant water formation on the BSCF membrane. In addition, both the CO and CO_2 can interact with the membrane surface forming carbonates. The increased water production with the BSCF membranes

could lead to more steam reforming in the reactor, effectively increasing the methane conversion. In addition, higher amounts of stream reforming would lead to higher H_2:CO ratios in the reactor effluent due to the 3:1 ratio of H_2:CO for steam reforming compared to the 1:1 H_2:CO ratio expected for CO_2 reforming.

These hypotheses were tested by investigating the CO_2 reforming of CH_4 at 800°C over Pt/ZrO_2 and Pt/$CeZrO_2$ catalysts on dense BSCF and SFC membranes. To understand the role of the membrane, the reactions were also carried out using the catalysts placed on top of a stainless steel blank coated with an inert BN_3 paint. In the tests with the inert blank, the reaction was not assisted by oxygen since there is no oxygen flux with the stainless steel blank. Figures 5.15 and 5.16 show the methane conversion profile and H_2/CO ratio for the experiments described above. For all tests, CH_4 conversion and H_2/CO ratio decrease as time proceeds. As is expected, the H_2/CO ratio of Pt/$CeZrO_2$ is higher than that of Pt/ZrO_2 both with and without the ceramic membranes due to the ability of the Ce promoted support to participate in the reaction [14]. Both catalysts show higher H_2/CO ratio in the presence of ceramic membranes than in the presence of stainless steel blank, indicating the beneficial effects of oxygen from ceramic membrane on the reaction. More importantly, the methane conversion and the H_2:CO ratio are both higher on the BSCF membrane than on low-oxygen-flux SFC membrane, while the CO_2 conversion is less on BSCF.

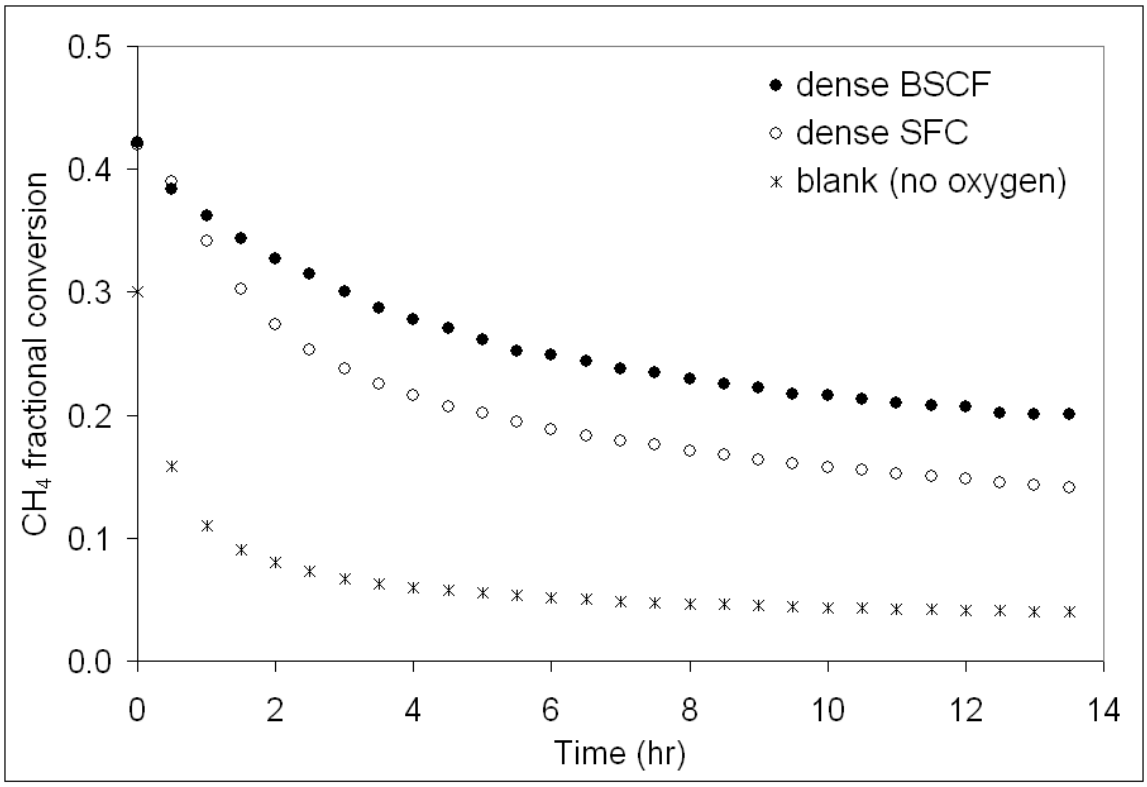

Figure 5.15. Methane conversion during CO_2 reforming of methane (1:1 ratio) at 800°C and atmospheric pressure in a membrane reactor over Pt/ZrO_2 catalyst. Feed composition is: 40% CH_4, 40% CO_2, and 20% argon; space velocity is 150 $l/hr/g_{catalyst}$.

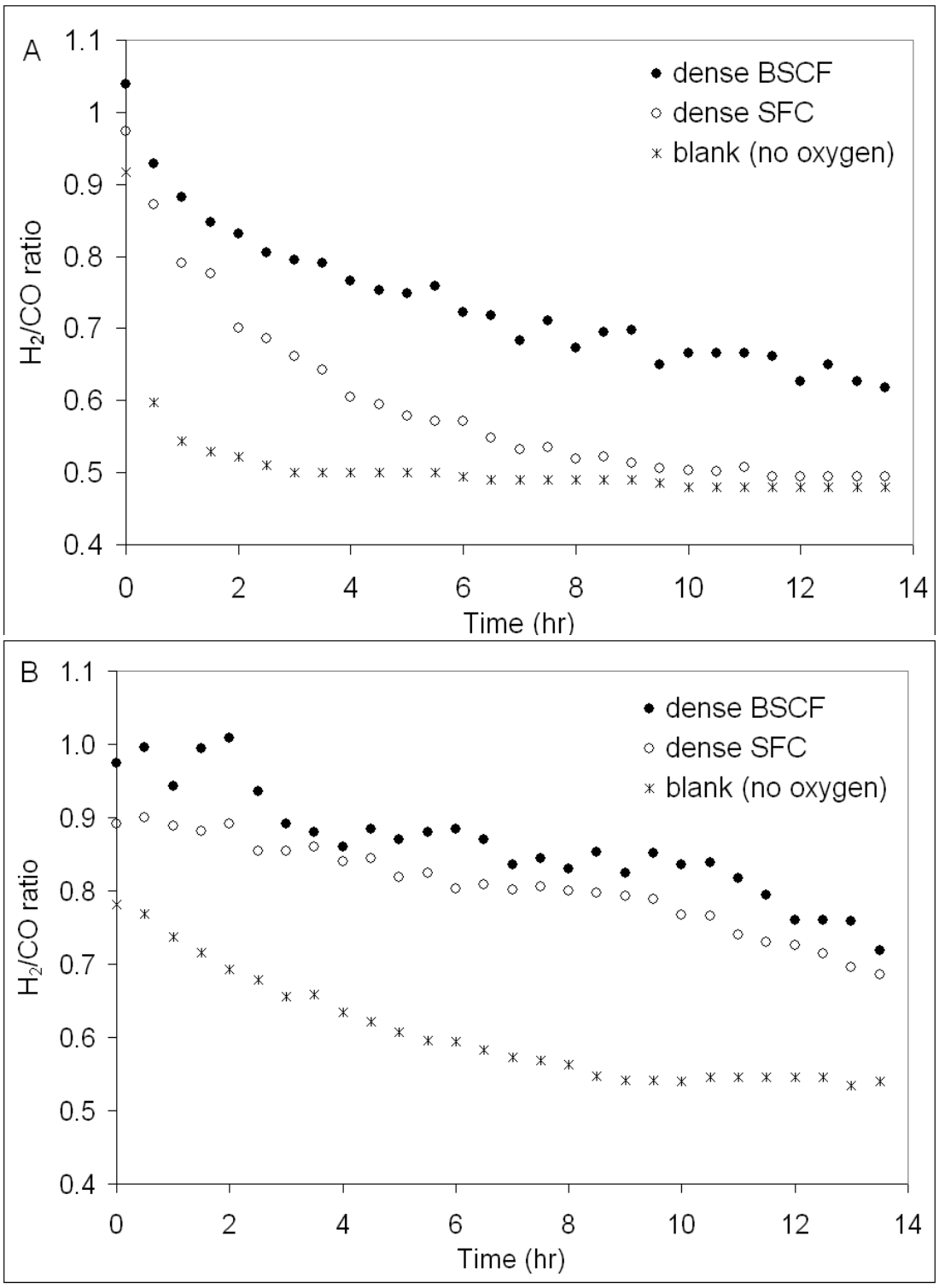

Figure 5.16. H_2:CO ratios during CO_2 reforming of methane (1:1 ratio) at 800°C and atmospheric pressure in a membrane reactor over: A) Pt/ZrO_2 catalyst and B) $Pt/CeZrO_2$ catalyst. Feed composition is: 40% CH_4, 40% CO_2, and 20% argon; space velocity is 150 l/hr/$g_{catalyst}$.

The high H_2:CO ratio and low CO_2 conversion on BSCF can be due to increased steam reforming and more CO conversion to CO_2 on the BSCF membrane compared to the SFC membrane. Figure 5.17 shows the water production and CO_2 conversion over Pt/$CeZrO_2$ catalyst. Relative water production is high on the BSCF membrane with the Pt/$CeZrO_2$ catalyst but not with the Pt/ZrO_2 catalyst. The low CO_2 conversion and high water production eliminate the possibility of significant reverse water gas shift reaction with the BSCF membrane and the Pt/$CeZrO_2$ catalyst. Combustion is a possible co-reaction with CO_2 reforming on the Pt/$CeZrO_2$ catalyst. Previous studies [15] have suggested that combustion occurs via oxygen diffusion from the membrane to the gas phase, or oxygen spillover directly to the catalyst. Based on the studies in this work, diffusion of molecular oxygen from the membrane surface to the gas phase under reaction conditions seems unlikely. Oxygen spillover from highly reducible supports to metal particles has been shown for many reactions. However, the spillover usually occurs when the metal particle is in intimate contact with the support. In this case, the catalyst is loosely dispersed on the membrane surface, and the spillover would have to occur from the membrane surface to the metal particle via the catalyst support. Thus, while oxygen spillover from the membrane surface to the catalyst is then possible, it would be more probable if the catalyst were directly supported on the membrane surface. It should be noted that the products of combustion, water and CO_2, are the same products that are formed from hydrogen and CO oxidation on the membrane surface.

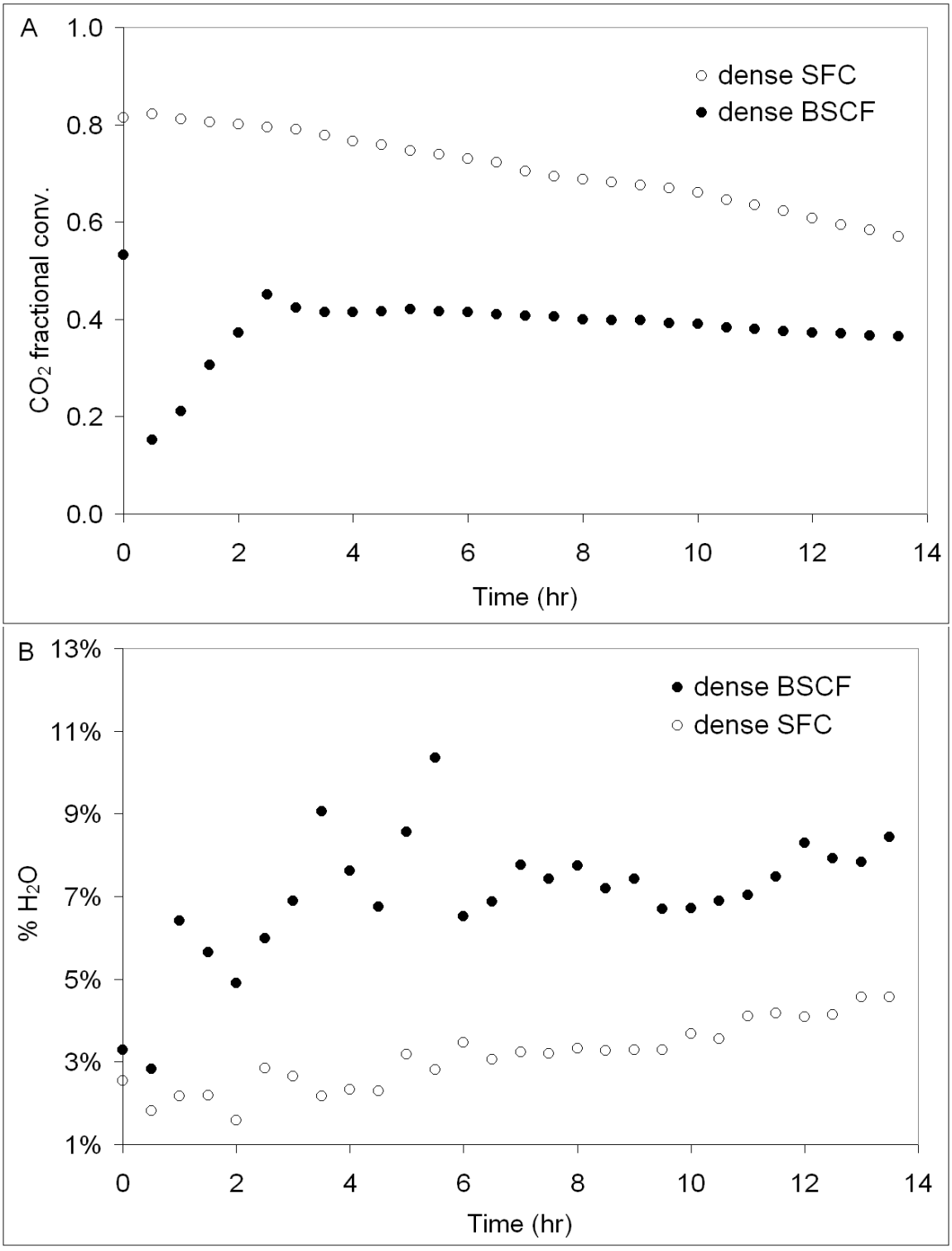

Figure 5.17. CO_2 conversion (A) and water production (B) during CO_2 reforming of methane (1:1 ratio) at 800°C and atmospheric pressure in a membrane reactor over $Pt/CeZrO_2$ catalyst. Feed composition is: 40% CH_4, 40% CO_2, and 20% argon; space velocity is 150 l/hr/$g_{catalyst}$.

Based on the data from the studies in this work, the most likely explanation for the high H_2:CO ratio, increased CH_4 conversion, and decreased CO_2 conversion observed is the interaction of oxygen species on the membrane surface with H_2 leading to the formation of water. The water can then participate in the reaction via steam reforming. Similarly, for Pt/ZrO_2 catalyst on BSCF, a combination of CO_2 reforming and steam reforming seems most likely. These results are similar to the results obtained previously where asymmetric BSCF showed higher methane conversion and H_2:CO ratio but lower CO_2 conversion than dense SFC for CO_2 reforming of CH_4 [16].

Based on the reaction tests and the surface studies performed, a network of possible reactions can occur. CO_2 dissociation to CO and CH_4 decomposition to H_2 are two initial steps of the reaction mechanism when CH_4 and CO_2 are fed into reactor simultaneously. H_2 and CO are both reducing agents, which can reduce the ceramic membrane and produce H_2O and CO_2 (according to Figures 5.4 and 5.5). Water can react with CH_4 and produce more CO and H_2 (steam reforming). Water can also participate in a reaction with CO to produce H_2 and CO_2 (water gas shift). Furthermore, for high oxygen flux membranes, and with intimate contact of the membrane and catalyst, it may be possible that some combustion occurs. Thus, based on the type of catalyst and ceramic membrane used, the extent of each reaction in the above system would vary, resulting in slightly different CH_4 and CO_2 conversions and H_2:CO ratios.

5.4. Conclusions

Unlike SFC, BSCF exhibited significantly higher O_2 release at low temperatures. This indicates that BSCF could be a promising material for low temperature oxygen-assisted reactions. BSCF showed higher O_2, H_2, and CO adsorption than SFC. Carbonates were detected on both BSCF and SFC during CO and CO_2 exposure.

The results of CO_2 reforming of CH_4 on dense BSCF and SFC membranes over Pt/ZrO_2 and $Pt/CeZrO_2$ catalysts clearly demonstrated higher methane conversion and H_2:CO ratio on BSCF compared to SFC at 800°C. The ability of BSCF to adsorb more H_2 and CO than SFC at 800°C could lead to higher water formation and CO_2 production on this ceramic membrane during CO_2 reforming of methane. The increased formation of H_2O and CO_2 and simultaneous occurrence of steam and CO_2 reforming of CH_4, lead to higher methane conversions and H_2:CO ratio.

5.5. References

[1] Q. Jiang, S. Faraji, D. A. Slade, K. J. Nordheden, and S. M. Stagg-Williams, "Performance analysis of mixed-conducting ceramic membranes for membrane reactor applications," presented at AIChE Annual Meeting, Salt Lake City, 2007.

[2] H. Dong, Z. P. Shao, G. X. Xiong, J. H. Tong, S. S. Sheng, and W. S. Yang, "Investigation on POM reaction in a new perovskite membrane reactor," *Catalysis Today*, vol. 67, pp. 3-13, 2001.

[3] J. Caro, H. H. Wang, C. Tablet, A. Kleinert, A. Feldhoff, T. Schiestel, M. Kilgus, P. Kolsch, and S. Werth, "Evaluation of perovskites in hollow fibre and disk geometry in catalytic membrane reactors and in oxygen separators," *Catalysis Today*, vol. 118, pp. 128-135, 2006.

[4] D. A. Slade, A. M. Duncan, K. J. Nordheden, and S. M. Stagg-Williams, "Mixed-conducting oxygen permeable ceramic membranes for the carbon dioxide reforming of methane," *Green Chemistry*, vol. 9, pp. 577-581, 2007.

[5] V. Galvita, L. K. Rihko-Struckmann, and K. Sundmacher, "The CO Adsorption on a Fe_2O_3-$Ce_{0.5}Zr_{0.5}O_2$ Catalyst Studied by TPD, Isotope Exchange and FTIR Spectroscopy," *Journal of Molecular Catalysis A: Chemical*, vol. 283, pp. 43-51, 2008.

[6] I. Kaus and K. Wiik, "Stability of $SrFeO_3$-Based Materials in H_2O/CO_2-Containing Atmospheres at High Temperatures and Pressures," *J. Am. Ceram. Soc.*, vol. 90, pp. 2226-2230, 2007.

[7] W. Zhou, R. Ran, and Z. P. Shao, "Progress in understanding and development of $Ba_{0.5}Sr_{0.5}Co_{0.8}Fe_{0.2}O_{3-\delta}$-based cathodes for intermediate-temperature solid-oxide fuel cells: A review," *Journal of Power Sources*, vol. 192, pp. 231-246, 2009.

[8] A. Y. Yan, L. Bin, Y. L. Dong, Z. J. Tian, D. Z. Wang, and M. J. Cheng, "A temperature programmed desorption investigation on the interaction of $Ba_{0.5}Sr_{0.5}Co_{0.8}Fe_{0.2}O_{3-\delta}$ perovskite oxides with CO_2 in the absence and presence of H_2O and O_2," *Applied Catalysis B-Environmental*, vol. 80, pp. 24-31, 2008.

[9] Z. Yang, A. S. Harvey, and L. J. Gauckler, "Influence of CO_2 on $Ba_{0.5}Sr_{0.5}Co_{0.8}Fe_{0.2}O_{3-\delta}$ at elevated temperatures," *Scripta Materialia*, vol. 61, pp. 1083-1086, 2009.

[10] S. Faraji, K. J. Nordheden, and S. M. Stagg-Williams, "The Interaction Between $SrFeCo_{0.5}O_{(x)}$ Ceramic Membranes and $Pt/CeZrO_2$ During Syngas Production from Methane," *Catalysis Letters*, vol. 131, pp. 114-121, 2009.

[11] C. Li, Y. Sakata, T. Arai, K. Domen, K. Maruya, and T. Onishi, "Carbon-Monoxide and Carbon-Dioxide Adsorption on Cerium Oxide Studied by Fourier-Transform Infrared-Spectroscopy .1. Formation of Carbonate Species on Dehydroxylated CeO_2 at Room-Temperature," *Journal of the Chemical Society-Faraday Transactions I*, vol. 85, pp. 929-943, 1989.

[12] L. S. F. Feio, C. E. Hori, S. Damyanova, F. B. Noronha, W. H. Cassinelli, C. M. P. Marques, and J. M. C. Bueno, "The effect of ceria content on the properties of $Pd/CeO_2/Al_2O_3$ catalysts for steam reforming of methane," *Applied Catalysis A : General*, vol. 316, pp. 107-116, 2007.

[13] A. Davydov, *Molecular Spectroscopy of Oxide Catalyst Surfaces*. Chichester: John Wiley & Sons Ltd., 2003.

[14] R. Radhakrishnan, R. R. Willigan, Z. Dardas, and T. H. Vanderspurt, "Water gas shift activity and kinetics of Pt/Re catalysts supported on ceria-zirconia oxides," *Applied Catalysis B-Environmental*, vol. 66, pp. 23-28, 2006.

[15] M. Ikeguchi, T. Mimura, Y. Sekine, E. Kikuchi, and M. Matsukata, "Reaction and oxygen permeation studies in $Sm_{0.4}Ba_{0.6}Fe_{0.8}Co_{0.2}O_{3-\delta}$ membrane reactor for partial oxidation of methane to syngas," *Applied Catalysis A : General*, vol. 290, pp. 212-220, 2005.

[16] D. A. Slade, Q. Jiang, K. J. Nordheden, and S. M. Stagg-Williams, "A Comparison of Mixed-conducting Oxygen-permeable Membranes for CO_2 Reforming," *Catalysis Today*, vol. 148, pp. 290-297, 2009.

Chapter 6: Developing New Bimetallic Catalysts for CO_2 Reforming of CH_4

6.1. Introduction

As stated in Chapter 2, the utilization of CO_2 for the reforming of CH_4 has attracted significant attention in recent decades due to its advantages over steam reforming of CH_4. The major barrier preventing commercialization of this reaction is the inability to find a catalyst with both high activity and stability [1].

Previous studies have shown that supported noble metals are suitable catalysts for CO_2 reforming of CH_4 and the order of reactivity over these catalysts is: Ru > Rh > Ni > Pt > Pd [2]. Nickel-based catalysts have been investigated because of their low cost and widespread use in industry, but they deactivate easily [3, 4]. A previous study of $Ni/CeZrO_2$ has shown lower activity than Ni/Al_2O_3 catalyst during steam reforming of CH_4 at 900°C [5]. For autothermal reforming of CH_4 at 800°C, conversion on $Ni/CeZrO_2$ was reported to be more than Ni/Al_2O_3 [6]. Although Pt is expensive, Pt-based catalysts have shown to be very active and stable for the dry reforming reaction [7-9]. With these in mind, new catalysts need to be developed to fulfill the industrial requirements for this reaction. In this chapter, new Pt-based and Ni-based bimetallic catalysts have been developed for the dry reforming reaction of methane. Specific emphasis has been placed on studying the effects of the addition of Pt as a promoter on catalytic performance of two different Ni-based catalysts.

6.2. Experimental

All pulse and TPR studies were performed in a PFR, which was described in Chapter 3. Detailed information about catalysts preparation methods, Raman, and TPR techniques can also be found in Chapter 3.

6.3. Results and Discussion

6.3.1. CH_4 Pulses over Pt-Ni/$CeZrO_2$ and Pt-Ni/Al_2O_3 Catalysts

In order to determine the catalytic activity of Ni/$CeZrO_2$, Pt-Ni/$CeZrO_2$, and Pt-Ni/Al_2O_3 catalysts, three experiments were performed in which the new catalysts were exposed to pulses containing CH_4 at 800°C in a plug flow reactor. Hydrogen, CO, CO_2, and H_2O were observed as reaction products in mass spectrometer. Figure

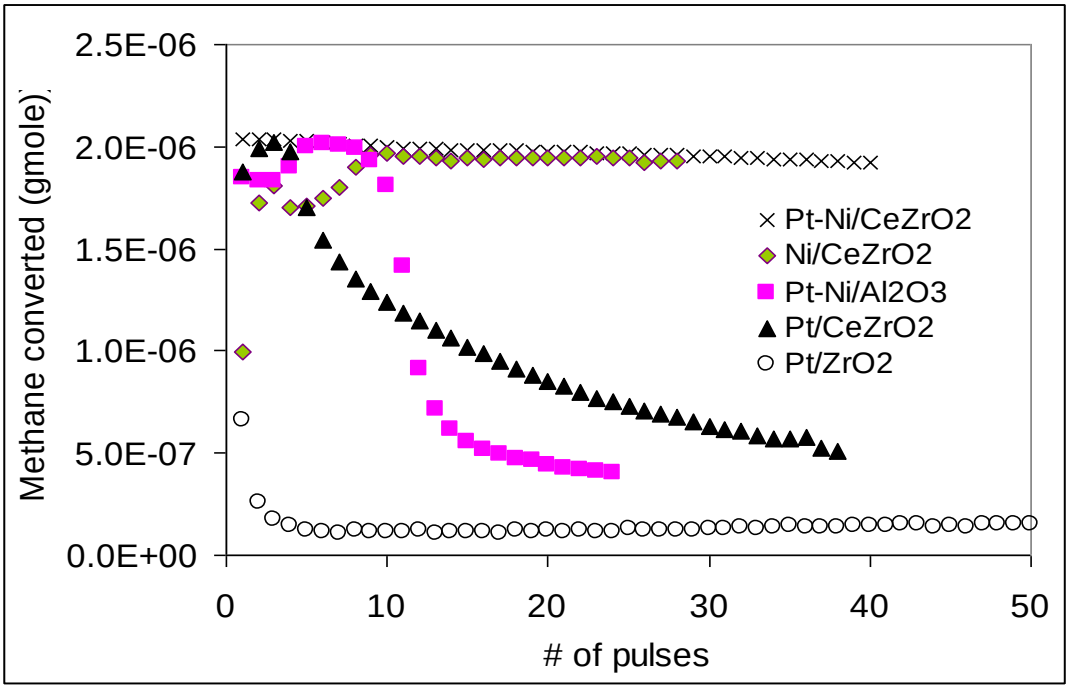

Figure 6.1. Methane conversion profiles for pulses of methane in PFR at 800°C.

6.1 shows the methane conversion profiles for these new catalysts compared to $Pt/CeZrO_2$ and Pt/ZrO_2 catalysts, which had been previously studied in Chapter 4.

As mentioned previously in Chapter 4, the Pt/ZrO_2 catalyst has a low activity and deactivates quickly compared to $Pt/CeZrO_2$ catalyst. The $Pt\text{-}Ni/CeZrO_2$ catalyst shows a very high activity with a very small deactivation rate. Its activity is higher than $Pt/CeZrO_2$ and Pt/ZrO_2 catalysts throughout the test. The initial methane conversions for $Pt\text{-}Ni/Al_2O_3$ catalyst are high and close to conversions for $Pt\text{-}Ni/CeZrO_2$ catalyst, but the $Pt\text{-}Ni/Al_2O_3$ conversion starts to decline quickly after 8 pulses and continues to decline with each subsequent pulse of methane. The color of $Pt\text{-}Ni/Al_2O_3$ catalyst after reaction was observed to be black and this observation suggests that the deactivation is probably due to carbon deposition. Compared to the $Pt\text{-}Ni/Al_2O_3$, which shows a rapid deactivation after 8 pulses, the $Pt/CeZrO_2$ exhibits gradual deactivation after 4 pulses of methane. These results suggest that in the absence of any oxygen source, $Pt\text{-}Ni/Al_2O_3$ catalyst tends to deactivate faster than $Pt\text{-}Ni/CeZrO_2$ catalyst because Al_2O_3 support is not a good oxygen provider in comparison to the $CeZrO_2$ support, which is well known for its high oxygen release and storage capability [10].

The $Ni/CeZrO_2$ catalyst initially shows a low activity, but activity starts to increase over time and after 10 pulses of methane, the activity of $Ni/CeZrO_2$ catalyst is almost equal to that of $Pt\text{-}Ni/CeZrO_2$ catalyst. This induction period in methane conversion could be due to the time required for Ni particles to be completely reduced. There is no induction period in the methane conversion profile of Pt-

$Ni/CeZrO_2$ catalyst because it is believed that Pt can increase the reducibility of the Ni-based catalyst [11]. These results suggest that $Pt\text{-}Ni/CeZrO_2$ catalyst is a promising candidate for catalyzing H_2 production from CH_4 decomposition at 800°C.

6.3.2. TPR for $Pt\text{-}Ni/CeZrO_2$ and $Pt\text{-}Ni/Al_2O_3$ Catalysts

The reducibility of catalysts was studied by performing TPR for each catalyst. TPR can also provide detailed information about the interaction between Pt and Ni in bimetallic catalysts. Catalysts were heated in flowing hydrogen (5% in argon) in a PFR while the effluent was monitored using a mass spectrometer. In all cases, considerable amounts of hydrogen consumption and water production were observed during the TPR. Figure 6.2 shows TPR profile for each catalyst. The data clearly demonstrate the consequence of the addition of Pt atoms to Ni on the two different catalyst supports. Table 6.1 summarizes the calculated amounts of H_2 consumption for each catalyst.

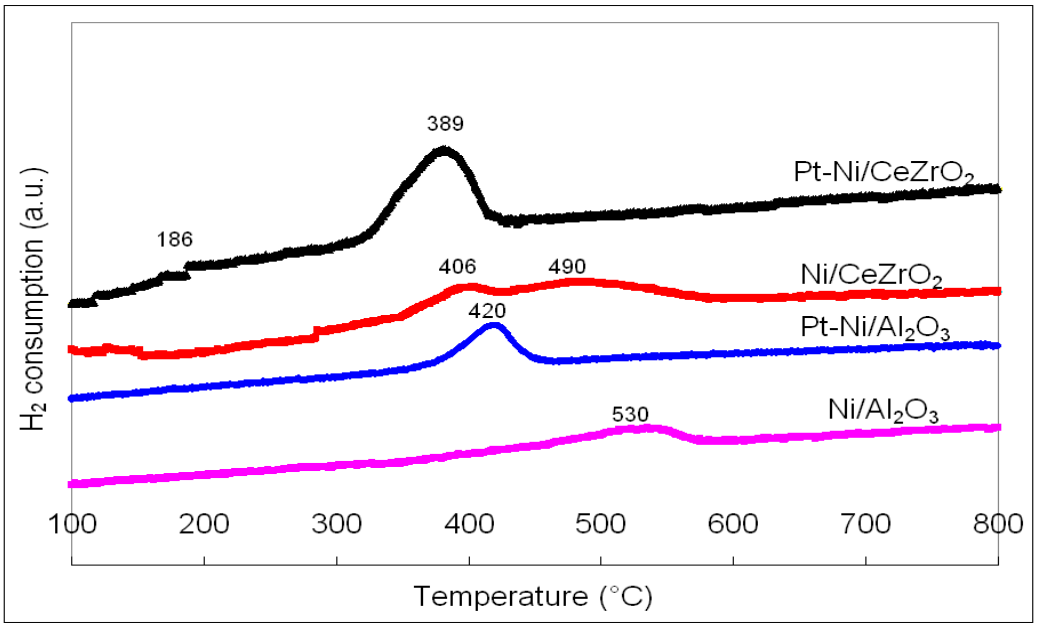

Figure 6.2. TPR profiles for monometallic and bimetallic catalysts in flowing H_2.

Table 6.1. The results of TPR for monometallic and bimetallic catalysts.

Catalyst	Area underneath the TPR peak	Moles of H_2 consumed[1]
Pt-Ni/$CeZrO_2$	1.72×10^{-7}	1.52×10^{-5}
Ni/$CeZrO_2$	1.416×10^{-7}	1.25×10^{-5}
Pt-Ni/Al_2O_3	7.95×10^{-8}	7×10^{-6}
Ni/Al_2O_3	7×10^{-8}	6.19×10^{-6}

Note 1: The calculated moles of H_2 are less than the amounts of H_2 should be consumed based on the nominal metal loadings. It is more likely that the real metal loadings are less than the nominal loadings.

Ni/Al_2O_3 and Pt-Ni/Al_2O_3 catalysts show medium temperature hydrogen consumption peaks at 530°C and 420°C respectively. So, the reduction peak is shifted to lower temperatures with the added Pt. According to the literature, the hydrogen consumption peak for Pt/Al_2O_3 monometallic catalyst should appear at low temperatures (around 104°C) [12]. Since only one hydrogen consumption peak is observed for the bimetallic Pt-Ni/Al_2O_3 and no Pt reduction peak is observed at very low temperatures, there might be an alloy formation (an alloy of Pt and Ni) for the bimetallic Pt-Ni/Al_2O_3. According to Table 6.1, the total amount of H_2 consumed for Pt-Ni/Al_2O_3 during the TPR is higher than that for Ni/Al_2O_3 (7×10^{-6} moles for Pt-Ni versus 6.19×10^{-6} moles for Ni) due to higher metal loading or likelihood of alloy formation in the bimetallic catalyst.

For the Ni/$CeZrO_2$ catalyst, two broad hydrogen consumption peaks are observed at 406°C and 490°C, in agreement with the literature [13]. The Pt-Ni/$CeZrO_2$ catalyst shows a low temperature peak at 186°C, which is more likely due to reduction of Pt, and a medium temperature peak at 389°C, which is more likely due to reduction of Ni atoms. The peak at 186°C is very small because of the low

concentration of Pt (only 0.2 wt %). These results suggest two things: first, the addition of platinum to Ni decreases the reduction temperature of the bimetallic catalyst; and second, it is less likely that there is an alloy formation in the bimetallic Pt-Ni/$CeZrO_2$. The total amount of H_2 consumed for Pt-Ni/$CeZrO_2$ during the TPR is higher than that for Ni/$CeZrO_2$ (1.52×10^{-5} moles for bimetallic versus 1.25×10^{-5} moles for monometallic). The higher amount of H_2 consumption in the bimetallic catalyst could be due to higher metal loading in the catalyst.

6.3.3. Temperature Programmed Reaction in Flowing CH_4 and CO_2

Catalysts were heated in flowing CH_4 and CO_2 (CH_4:CO_2 = 1) while mass spectrometer signals were recording. Figure 6.3 shows the results of theses studies. In all cases, no catalytic activity was observed at very low temperatures. As the temperature increased to higher than 400°C, catalysts started to show activity and significant amounts of hydrogen, CO, CO_2, and H_2O production were observed. Table 6.2 lists the minimum temperature for each catalyst at which H_2 is generated during the dry reforming of methane.

Since catalysts were not reduced prior to these tests, auto-reduction of each catalyst occurs during the reactions [14]. Pt-Ni/$CeZrO_2$ starts to show activity at about 440°C, while Ni/$CeZrO_2$ shows no activity before 587°C. Similarly, Pt-Ni/Al_2O_3 catalyst is activated for reforming reaction at much lower temperatures (475 °C) than Ni/Al_2O_3 catalyst (575 °C). According to Figure 6.3, Pt-Ni/$CeZrO_2$ is the only suitable catalyst for the dry reforming reaction in the 440-475°C

temperature range. However, both steam reforming and dry reforming of methane are not thermodynamically favorable at temperatures lower than 600°C because standard Gibbs free energy of reaction becomes positive at these temperatures [1, 15]. The results suggest that the addition of a small amount of Pt to Ni promotes the reduction of Ni atoms and creates a bimetallic catalyst, which is more active at lower operating temperatures for H_2 production. These results are consistent with previous studies, which have shown that Pt can increase the reducibility of Ni-based catalyst [11, 15].

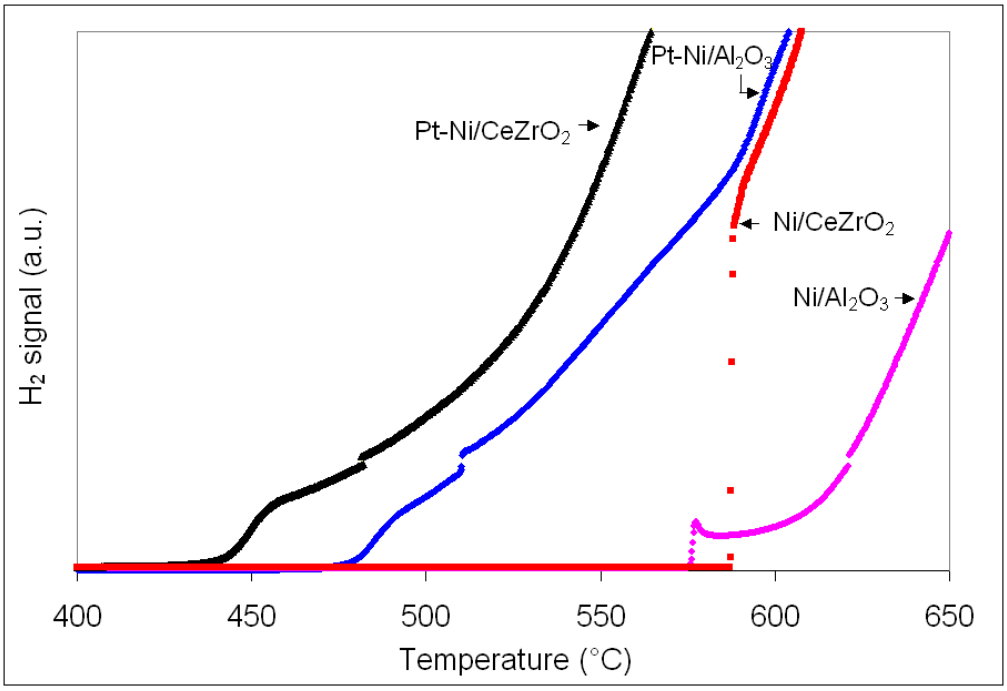

Figure 6.3. H_2 signals for monometallic and bimetallic catalysts in flowing CH_4+CO_2 (CH_4:CO_2 = 1).

Table 6.2. The minimum temperature for H_2 production for each catalyst during dry reforming of methane (CH_4:CO_2 = 1).

Catalyst	**Minimum temperature (°C)**
Pt-Ni/$CeZrO_2$	440
Ni/$CeZrO_2$	587
Pt-Ni/Al_2O_3	475
Ni/Al_2O_3	575

6.3.4. Raman Spectroscopy Study of Pt-Ni/Al_2O_3 Catalyst

In order to determine the interaction between Pt and Ni in Pt-Ni/Al_2O_3 bimetallic catalyst, Raman studies of both Ni/Al_2O_3 and Pt-Ni/Al_2O_3 catalysts were performed after exposure to CO_2 at room temperature. The results are shown in Figure 6.4.

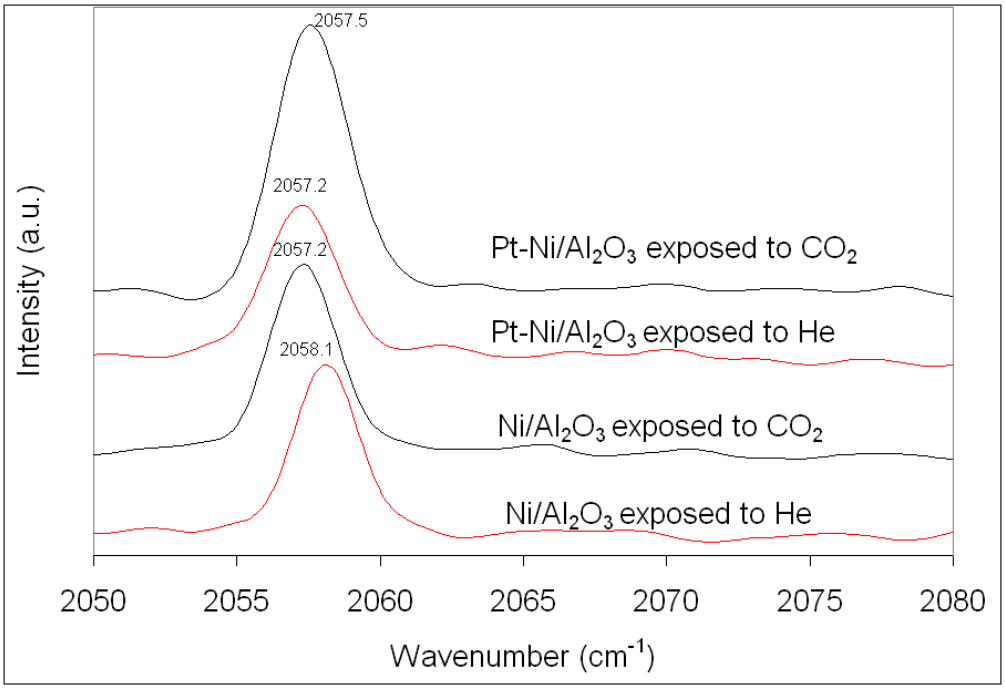

Figure 6.4. The Raman spectra of catalysts at room temperature.

The Raman spectra of Ni/Al_2O_3 and Pt-Ni/Al_2O_3 at room temperature in flowing helium are similar; however, the peaks in the spectra of Pt-Ni/Al_2O_3 are slightly shifted to lower wavenumbers. These changes are believed to be due to the presence of Pt in the Pt-Ni/Al_2O_3 sample. The band previously assigned to linear CO bonded to the surface [16, 17] was detected at 2058.1 and 2057.2 cm^{-1} for Ni/Al_2O_3 and Pt-Ni/Al_2O_3 respectively when samples were scanned in helium. The Raman

spectra of the samples after a 30-minute exposure to CO_2 at room temperature (Figure 6.4) showed adsorption of this chemical on the surfaces of Ni/Al_2O_3 and Pt-Ni/Al_2O_3. When CO_2 passes over the sample, dissociation of CO_2 occurs, which results in CO production. Then, this CO can adsorb linearly to the metals on the surface of sample and cause an increase in the intensity of the band at 2057.2 cm^{-1} for Ni/Al_2O_3 and 2057.5 cm^{-1} for Pt-Ni/Al_2O_3. Interestingly, the amount of CO_2 adsorption on bimetallic catalyst is higher than that on monometallic catalyst (by calculating the relative intensity of the linear CO peak). Previously, it had been shown by other researchers that Rh-Ni/Al_2O_3 adsorbs more CO_2 than monometallic Ni/Al_2O_3 [18] ; so, our results are in agreement with the published data for the bimetallic Rh-Ni/Al_2O_3 catalyst.

Since the peak at 2057.5 cm^{-1} for Pt-Ni/Al_2O_3, shows no shoulder at lower wavenumbers, it is more likely that Pt and Ni form an alloy. Observation of alloy formation for bimetallic Pt-Ni catalyst has been reported previously in the literature [17, 19]. However, in order to confirm the existence of an alloy in bimetallic catalyst, more studies need to be performed using TEM and also IR spectroscopy.

6.4. Conclusions

Pt-$Ni/CeZrO_2$ catalyst exhibits promising performance for hydrogen production during pulses of methane at 800°C. Platinum enhances the reducibility of Ni/Al_2O_3 and $Ni/CeZrO_2$ catalysts and makes them better catalysts for H_2 production at moderate temperatures. TPR and Raman studies indicate an alloy formation in Pt-

Ni/Al_2O_3 catalyst. Further work is required to study the interaction between Pt and Ni in the bimetallic Pt-$Ni/CeZrO_2$ and Pt-Ni/Al_2O_3 catalysts.

6.5. References

[1] M. S. Fan, A. Z. Abdullah, and S. Bhatia, "Catalytic Technology for Carbon Dioxide Reforming of Methane to Synthesis Gas," *Chemcatchem*, vol. 1, pp. 192-208, 2009.

[2] P. Gronchi, D. Fumagalli, R. DelRosso, and P. Centola, "Carbon deposition in methane reforming with carbon dioxide - Dry reforming," *Journal of Thermal Analysis and Calorimetry*, vol. 47, pp. 227-234, 1996.

[3] S. Therdthianwong, C. Siangchin, and A. Therdthianwong, "Improvement of coke resistance of Ni/Al_2O_3 catalyst in CH_4/CO_2 reforming by ZrO_2 addition," *Fuel Processing Technology*, vol. 89, pp. 160-168, 2008.

[4] J. Sehested, "Four challenges for nickel steam-reforming catalysts," *Catalysis Today*, vol. 111, pp. 103-110, 2006.

[5] N. Laosiripojana and S. Assabumrungrat, "Methane steam reforming over $Ni/Ce-ZrO_2$ catalyst: Influences of $Ce-ZrO_2$ support on reactivity, resistance toward carbon formation, and intrinsic reaction kinetics," *Applied Catalysis A-General*, vol. 290, pp. 200-211, 2005.

[6] J. C. Escritori, S. C. Dantas, R. R. Soares, and C. E. Hori, "Methane autothermal reforming on nickel-ceria-zirconia based catalysts," *Catalysis Communications*, vol. 10, pp. 1090-1094, 2009.

[7] S. Ozkara-Aydinoglu, E. Ozensoy, and A. E. Aksoylu, "The effect of impregnation strategy on methane dry reforming activity of Ce promoted Pt/ZrO_2," *International Journal of Hydrogen Energy*, vol. 34, pp. 9711-9722, 2009.

[8] M. Garcia-Dieguez, I. S. Pieta, M. C. Herrera, M. A. Larrubia, I. Malpartida, and L. J. Alemany, "Transient study of the dry reforming of methane over Pt supported on different gamma-Al_2O_3," *Catalysis Today*, vol. 149, pp. 380-387, 2010.

[9] S. Damyanova, B. Pawelec, K. Arishtirova, M. V. M. Huerta, and J. L. G. Fierro, "The effect of CeO_2 on the surface and catalytic properties of Pt/CeO_2-ZrO_2 catalysts for methane dry reforming," *Applied Catalysis B-Environmental*, vol. 89, pp. 149-159, 2009.

[10] W. Wei, S. M. Stagg-Williams, F. B. Noronha, L. V. Mattos, and F. B. Passos, "Partial oxidation and combined reforming of methane on Ce-promoted catalysts," *Catalysis Today*, vol. 98, pp. 553-563, 2004.

[11] K. Tomishige, S. Kanazawa, M. Sato, K. Ikushima, and K. Kunimori, "Catalyst design of Pt-modified Ni/Al_2O_3 catalyst with flat temperature profile

in methane reforming with CO_2 and O_2," *Catalysis Letters*, vol. 84, pp. 69-74, 2002.
[12] F. Pompeo, N. N. Nichio, M. Souza, D. V. Cesar, O. A. Ferretti, and M. Schmal, "Study of Ni and Pt catalysts supported on α-Al_2O_3 and ZrO_2 applied in methane reforming with CO_2," *Applied Catalysis A : General*, vol. 316, pp. 175-183, 2007.
[13] S. C. Dantas, J. C. Escritori, R. R. Soares, and C. E. Hori, "Effect of different promoters on Ni/$CeZrO_2$ catalyst for autothermal reforming and partial oxidation of methane," *Chemical Engineering Journal*, vol. 156, pp. 380-387.
[14] J. A. C. Dias and J. M. Assaf, "Autoreduction of promoted Ni/γ-Al_2O_3 during autothermal reforming of methane," *Journal of Power Sources*, vol. 139, pp. 176-181, 2005.
[15] R. R. Davda, J. W. Shabaker, G. W. Huber, R. D. Cortright, and J. A. Dumesic, "A review of catalytic issues and process conditions for renewable hydrogen and alkanes by aqueous-phase reforming of oxygenated hydrocarbons over supported metal catalysts," *Applied Catalysis B-Environmental*, vol. 56, pp. 171-186, 2005.
[16] B. Pawelec, S. Damyanova, K. Arishtirova, J. L. G. Fierro, and L. Petrov, "Structural and surface features of PtNi catalysts for reforming of methane with CO_2," *Applied Catalysis A-General*, vol. 323, pp. 188-201, 2007.
[17] A. Davydov, *Molecular Spectroscopy of Oxide Catalyst Surfaces*. Chichester: John Wiley & Sons Ltd., 2003.
[18] B. T. Li, S. Kado, Y. Mukainakano, T. Miyazawa, T. Miyao, S. Naito, K. Okumura, K. Kunimori, and K. Tomishige, "Surface modification of Ni catalysts with trace Pt for oxidative steam reforming of methane," *Journal of Catalysis*, vol. 245, pp. 144-155, 2007.
[19] Z. Y. Hou and T. Yashima, "Small amounts of Rh-promoted Ni catalysts for methane reforming with CO_2," *Catalysis Letters*, vol. 89, pp. 193-197, 2003.
[20] G. W. Huber, J. W. Shabaker, S. T. Evans, and J. A. Dumesic, "Aqueous-phase reforming of ethylene glycol over supported Pt and Pd bimetallic catalysts," *Applied Catalysis B-Environmental*, vol. 62, pp. 226-235, 2006.

Chapter 7: The Influence of Different Factors on Catalytic Syngas Production from Methane Using BSCF Ceramic Membranes

7.1. Introduction

As discussed in Chapter 5, BSCF is a promising material for hydrogen production via dry reforming of methane. It was shown in Chapter 5 that both the methane conversion and H_2:CO ratio are higher on dense BSCF than dense SFC membranes at 800°C.

The dry reforming reaction of methane on a dense BSCF membrane can be influenced by several factors such as: pH at which membrane is prepared, membrane thickness, CH_4:CO_2 feed ratio, type of catalyst, and reaction temperature. Since our goal is the improvement of the reaction on dense BSCF membranes to commercialize hydrogen production, it is important to know the effects of each of these factors on reaction. In this chapter, how these parameters can influence the reaction on dense BSCF membranes is discussed.

7.2. Experimental

All reaction studies were performed in a membrane reactor, which was described in Chapter 3 (see Figure 3.3). Detailed information about catalysts and membrane preparation methods can also be found in Chapter 3.

7.3. Results and Discussion

7.3.1. The Effect of pH

Although BSCF membranes have been studied for different reaction tests, the effect of pH (i.e. the pH of the precursor solution during membrane preparation) on hydrogen production reaction is still unknown. Most research groups have prepared BSCF at pH = 6 [1, 2], but they have not provided any reason behind this pH choice. For this reason, it is important to study the possible effects of pH on the membrane oxygen flux and methane conversion during dry reforming of methane.

Three BSCF membranes were prepared at three different pH values and then three reaction tests were performed on these BSCF membranes over Pt/ZrO_2 catalyst at 800°C. Figure 7.1 shows the methane conversion profiles for this study. As can be seen, pH has no significant effect on the methane conversion. A previous study in our research group has shown that altering pH had no effect on BSCF membrane oxygen flux in an air:Ar gradient [3]. Figure 7.2 shows the effect of pH on membrane oxygen flux during dry reforming reaction of methane. As can be observed, varying pH does not affect membrane oxygen flux significantly during the reaction. Since membrane oxygen flux, membrane composition, and membrane structure are not affected by altering pH according to the previous study in our group; it is logical that reaction would not be affected by pH either.

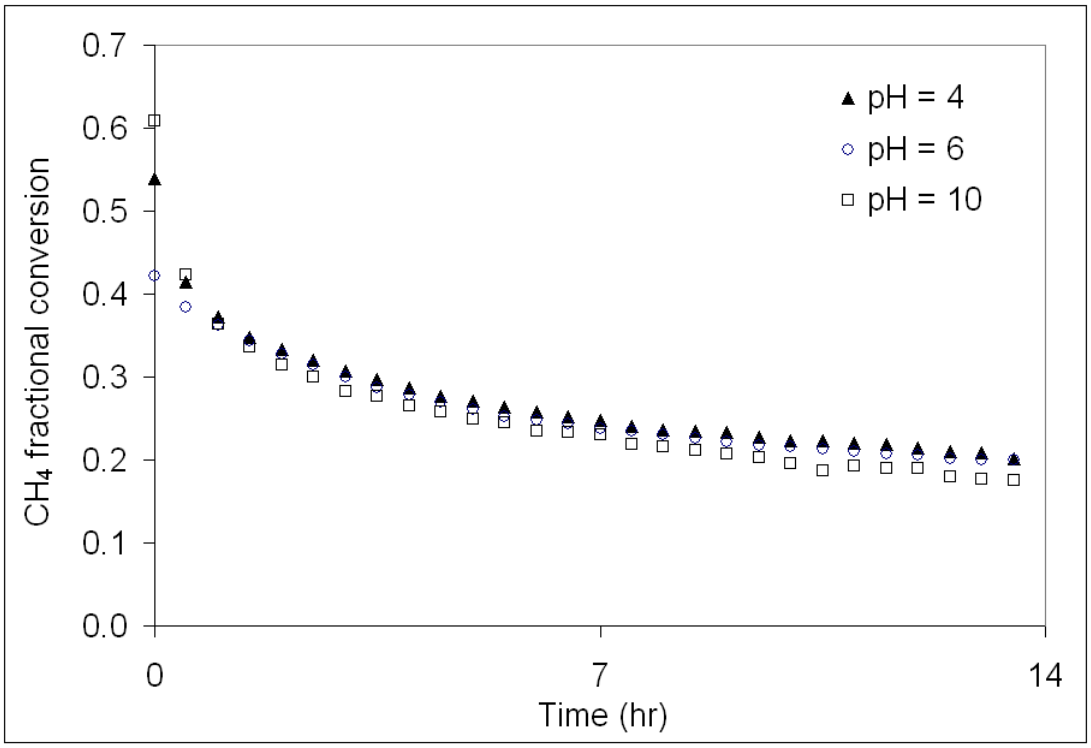

Figure 7.1. CH_4 conversion during CO_2 reforming of methane on dense BSCF prepared at different pH values at 800°C and atmospheric pressure over Pt/ZrO_2 catalyst (space velocity is 150 $l/hr/g_{catalyst}$).

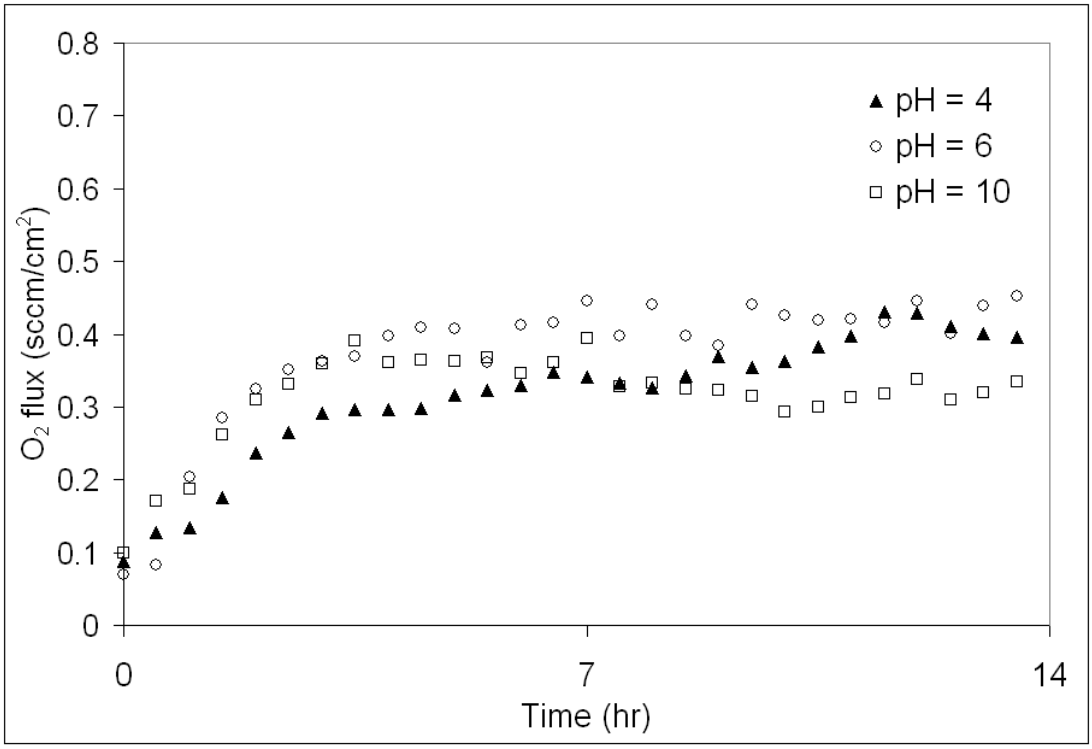

Figure 7.2. Membrane O_2 fluxes during CO_2 reforming of methane on dense BSCF prepared at different pH values at 800°C and atmospheric pressure over Pt/ZrO_2 catalyst (space velocity is 150 $l/hr/g_{catalyst}$).

7.3.2. The Effect of Membrane Thickness

It has been shown that membrane thickness has an impact on membrane oxygen flux [4, 5]. Mathematically speaking, membrane oxygen flux is inversely proportional to membrane thickness. When thickness decreases, a low mass transfer resistance is available for oxygen ions; and, therefore, more oxygen ions are transferred through membrane, resulting in a higher oxygen flux [4, 5]. Thus, the thinner the membrane, the higher the oxygen flux; however, for dense membranes, there is a limitation in decreasing thickness because mechanical stability of the dense membrane decreases with a decrease in thickness. For bilayer BSCF and SFC membranes, this problem has been solved by placing a very thin layer of dense BSCF or SFC (almost 200-400 micron) on a porous substrate [3, 6-8].

In order to understand the advantages of using thin membranes for dry reforming reaction, two reaction tests were performed over Pt/ZrO_2 catalyst at 800°C on two BSCF membranes prepared with different thickness (2.2 mm and 2.6 mm). Figures 7.3 and 7.4 show the CH_4 conversion and H_2:CO ratio for these two dense membranes. As it can be seen from Figure 7.4, the thinner BSCF membrane shows higher H_2:CO ratio than the thicker one. However, the benefit of using the thin BSCF membrane is not observed in Figure 7.3 until after about 2 or 3 hours of reaction. The results of membrane oxygen flux under reaction conditions are shown in Figure 7.5. Compared with the thicker membrane, the thinner membrane starts to release more oxygen after about 3 hours of reaction. This delay time observation is consistent with the delay time observed in the methane conversion profile (Figure 7.3).

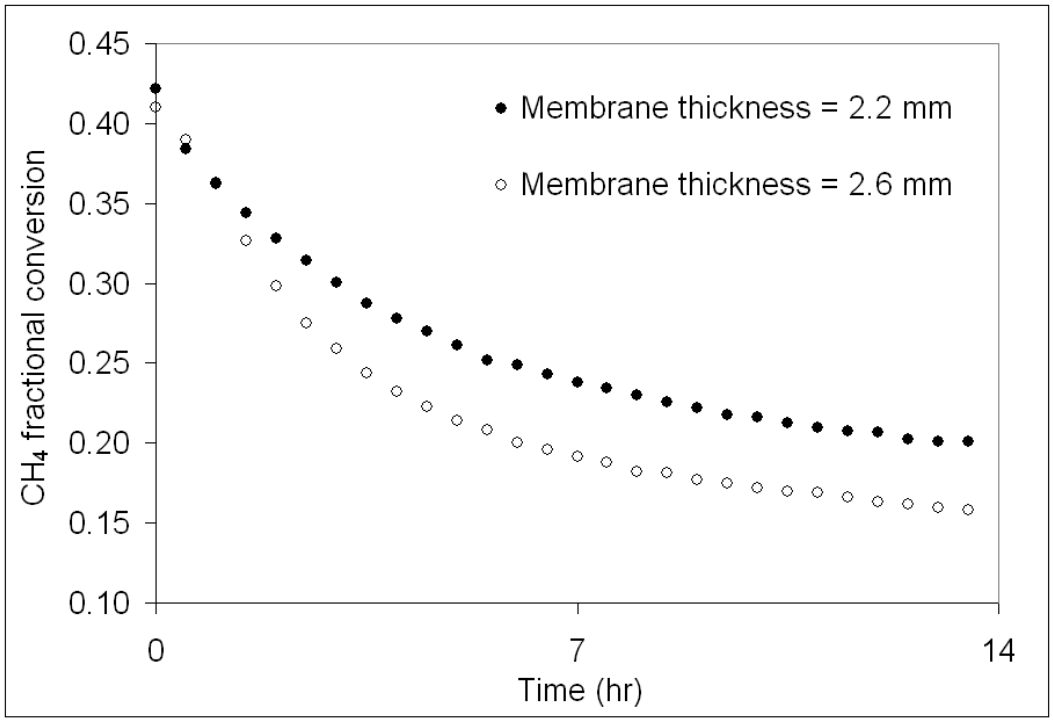

Figure 7.3. CH_4 conversion during CO_2 reforming of methane on dense BSCF with different thickness at 800°C and atmospheric pressure over Pt/ZrO_2 catalyst (space velocity is 150 $l/hr/g_{catalyst}$).

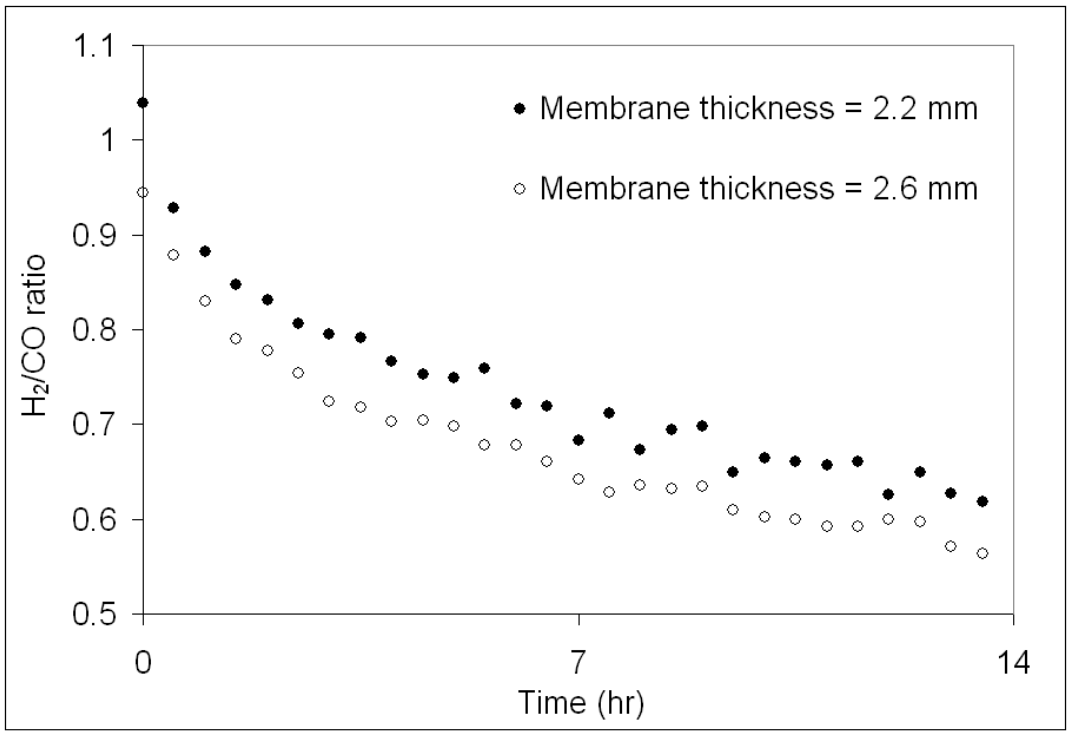

Figure 7.4. H_2/CO ratio during CO_2 reforming of methane on dense BSCF with different thickness at 800°C and atmospheric pressure over Pt/ZrO_2 catalyst (space velocity is 150 $l/hr/g_{catalyst}$).

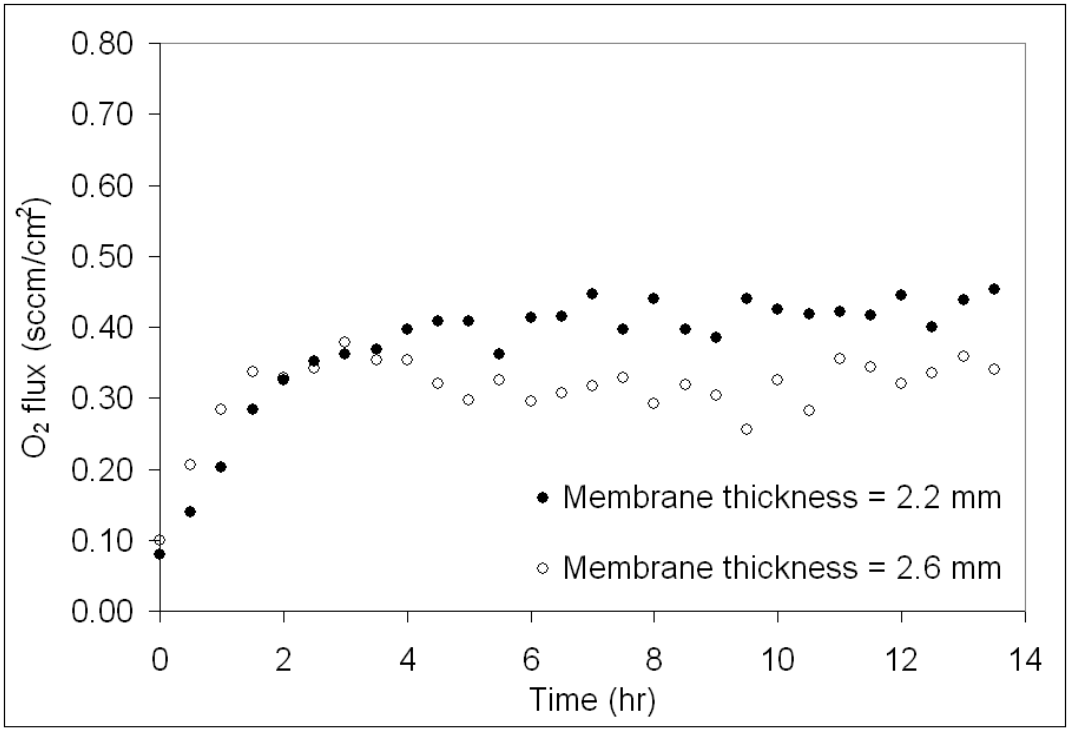

Figure 7.5. Membrane O_2 fluxes during CO_2 reforming of methane on dense BSCF with different thickness at 800°C and atmospheric pressure over Pt/ZrO_2 catalyst (space velocity is 150 l/hr/$g_{catalyst}$).

A previous study in our research group has shown that membrane oxygen flux under an air:Ar gradient increases with a decrease in the thickness of dense BSCF membranes [8]. While it is still unknown what specifically causes the delay time in oxygen flux observed in Figure 7.5, it is clear that the membrane thickness affects the reaction. The results of this study, which is consistent with the previous study in our group, show that a thinner membrane can provide more oxygen for reaction, leading to a higher methane conversion and H_2:CO ratio.

After understanding the effects of pH and thickness on the reaction, these factors will be fixed for the rest of our studies. A pH = 6 and thickness = 2.2 mm were chosen for studying the effect of other parameters like CH_4:CO_2 feed ratio, catalyst type, and reaction temperature.

7.3.3. The Effect of CH_4:CO_2 Feed Ratio

The concentration of CH_4 and CO_2 in the feed can significantly change the reaction conversion, product distribution, and the overall reaction scheme. Thus, it is important to understand the effects of various feed CH_4:CO_2 ratios on the reaction and membrane. The Pt/ZrO_2 catalyst was chosen for this part of the study because it has been studied previously for CO_2 reforming in conventional quartz tube PFR reactors [9] and has been shown to have low activity and to deactivate quickly. These attributes allow any improvement to be seen more readily because the catalyst is certain to operate well below equilibrium for all tests and to deactivate quickly.

Reaction tests were conducted on Pt/ZrO_2 catalyst, which was loosely packed on a dense BSCF membrane, at 800°C with three molar CH_4:CO_2 ratios (0.5, 1, and 2). Figure 7.6 shows the methane conversion profiles for different CH_4:CO_2 ratios at 800°C. For all tests, CH_4 conversion decreases as time proceeds because of catalyst deactivation over time. However, the extent of deactivation is smaller when CH_4:CO_2 ratio is equal to 0.5 and this shows the beneficial effect of CO_2 for removing carbon from catalyst surface via CO_2 dissociation. The methane conversion for the test with CH_4:CO_2 = 0.5 remains significantly greater throughout the test period than for the other tests. The methane conversion profile for the test with CH_4:CO_2 = 2 shows a rapid decline within the first 7 hours of reaction. This rapid decline in CH_4 conversion can be ascribed to the low amount of CO_2 and thus, high amount of catalyst deactivation. Our data agree with other studies which have shown that methane conversion increases with decreasing CH_4:CO_2 ratio [10, 11].

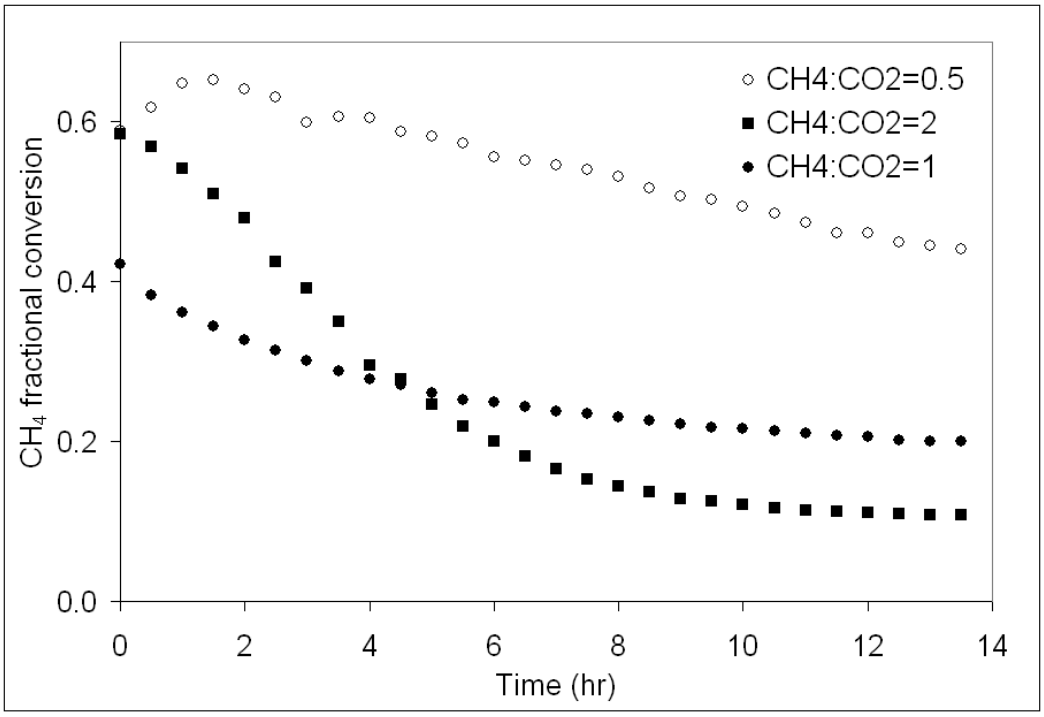

Figure 7.6. CH_4 conversion during CO_2 reforming of methane with different CH_4:CO_2 ratios at 800°C and atmospheric pressure on a dense BSCF over Pt/ZrO_2 catalyst (space velocity is 150 l/hr/$g_{catalyst}$).

Figures 7.7, 7.8, and 7.9 show the membrane oxygen flux, H_2/CO ratios, and CO_2 conversion profiles respectively for the tests with various CH_4:CO_2 ratios at 800°C. According to Figure 7.7, for the first six hours of reaction, membrane oxygen flux under reaction conditions is significantly higher when CH_4 to CO_2 ratio is 2 due to having a highly reductive environment under reaction conditions. As the amount of CO_2 increases in the feed, the reaction environment becomes less reducing and thus the driving force for releasing oxygen from the membrane decreases. During the first seven hours of the reaction, oxygen flux for the test with CH_4:CO_2 = 2 drops dramatically and after this period of time the oxygen fluxes for all three tests become almost equal. Since for the same time period, methane conversions for the tests with CH_4:CO_2 = 1 and 0.5 are still high (Figure 7.6), it is less likely that catalyst deactivation causes the drop in oxygen flux. According to Figures 7.8 and 7.9, when

CH_4:CO_2 = 2, the highest H_2/CO ratios and the lowest CO_2 conversions are observed. This high H_2:CO and low CO_2 conversion are due to higher amount of CH_4 in feed which results in more H_2 production via methane decomposition. The low CO_2 conversion could be due to more CO conversion to CO_2 by removing oxygen from the BSCF surface. A comparison between Figure 7.7 and Figure 7.9 when CH_4:CO_2 = 2 shows that CO_2 conversion has an increasing trend during the first 7 hours of reaction, whereas oxygen flux shows a decreasing trend over this period. This comparison confirms that CO receives oxygen from the membrane to produce CO_2. Since oxygen flux decreases in a less reducing environment, the high CO_2 production in this test impacts negatively on oxygen flux and the flux starts to drop. Eventually, the high concentration of CO_2 might cause membrane surface destruction and membrane oxygen flux decreases significantly [3].

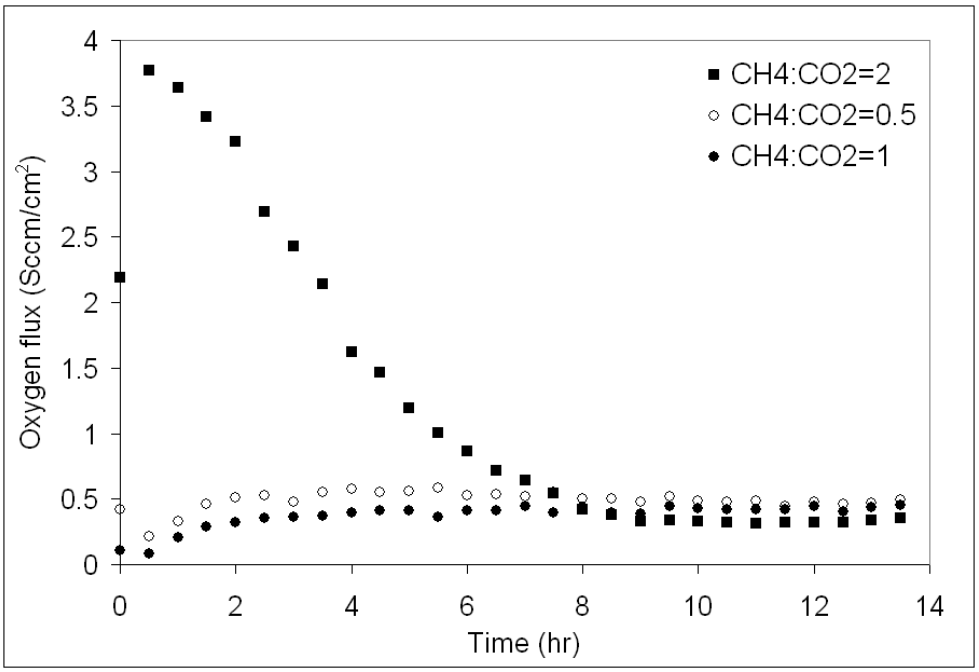

Figure 7.7. Membrane oxygen flux during CO_2 reforming of methane with different CH_4:CO_2 ratios at 800°C and atmospheric pressure on a dense BSCF over Pt/ZrO_2 catalyst (space velocity is 150 l/hr/$g_{catalyst}$).

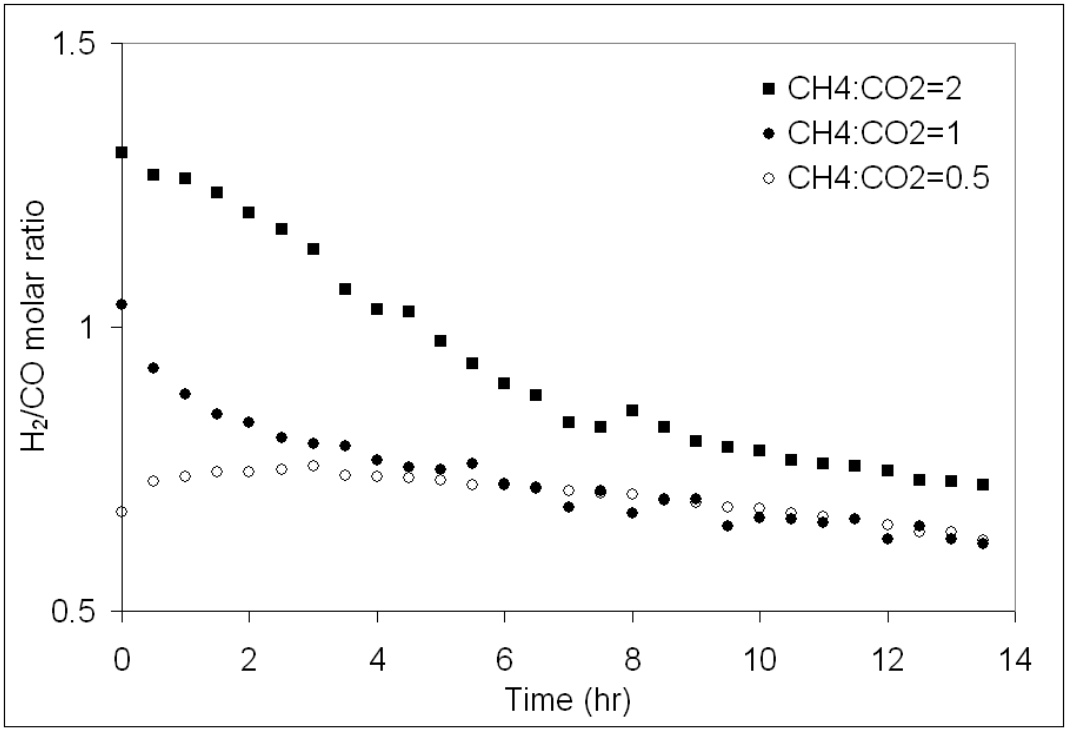

Figure 7.8. H_2:CO ratios during CO_2 reforming of methane with different CH_4:CO_2 ratios at 800°C and atmospheric pressure on a dense BSCF over Pt/ZrO_2 catalyst (space velocity is 150 l/hr/$g_{catalyst}$).

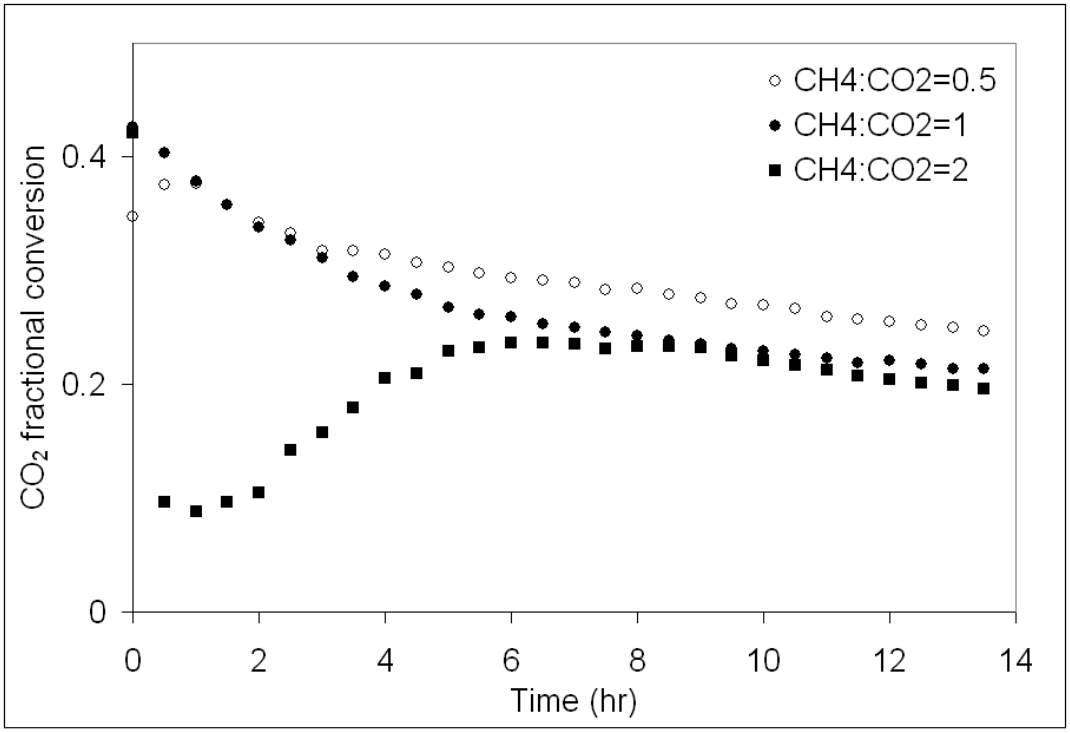

Figure 7.9. CO_2 conversion during CO_2 reforming of methane with different CH_4:CO_2 ratios at 800°C and atmospheric pressure on a dense BSCF over Pt/ZrO_2 catalyst (space velocity is 150 l/hr/$g_{catalyst}$).

The relative amount of water production within 9 hours of reaction is higher with a CH_4:CO_2 = 2 compared to other tests (Figure 7.10). The low CO_2 conversion and high water production eliminate the possibility of significant reverse water gas shift for this ratio. The following reactions appear to happen simultaneously when the ratio of CH_4:CO_2 is equal to 2:

Water production:	$H_2 + 0.5\ O_2 \longrightarrow H_2O$	(1)
Carbon dioxide production:	$CO + 0.5\ O_2 \longrightarrow CO_2$	(2)
Dry reforming of methane:	$CH_4 + CO_2 \longrightarrow 2CO + 2H_2$	(3)
Steam reforming of methane:	$CH_4 + H_2O \longrightarrow CO + 3H_2$	(4)

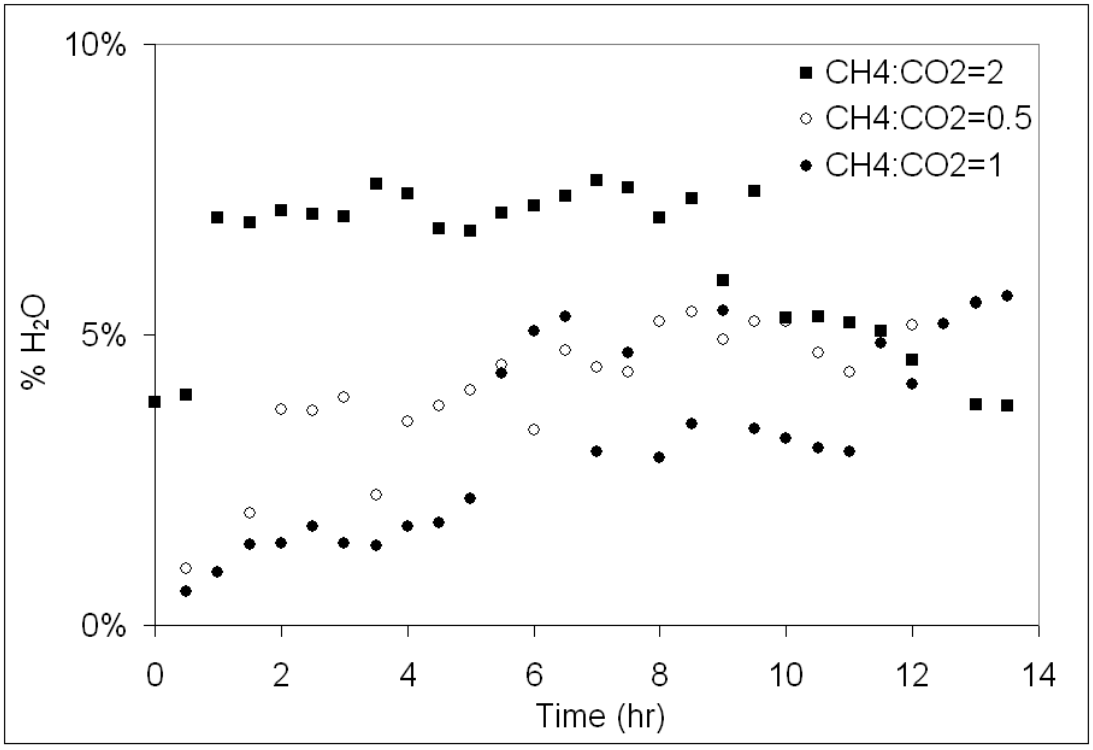

Figure 7.10. H_2O production during CO_2 reforming of methane with different CH_4:CO_2 ratios at 800°C and atmospheric pressure on a dense BSCF over Pt/ZrO_2 catalyst (space velocity is 150 l/hr/$g_{catalyst}$).

Hydrogen and carbon are the primary products of methane decomposition on the catalyst surface. Because the BSCF membrane releases a large amount of oxygen during reaction with a CH_4:CO_2 ratio of 2, hydrogen can take oxygen from BSCF surface to produce significant amounts of water. Carbon monoxide, which is produced by reactions 3 and 4, can be converted to CO_2 by taking oxygen from BSCF, resulting in low CO_2 conversion and a high H_2/CO ratio. The CO_2 and water production are driving forces for reactions 3 and 4 to occur more readily, resulting in more H_2 and CO production. Membrane surface destruction might occur due to the CO_2 production and this might lead to a rapid decrease in the oxygen flux profile. It is believed that CO_2 prevents catalyst deactivation during dry reforming of methane [12]. With this ratio, the amount of CO_2 is less than the amount of methane in the feed, so catalyst deactivation rate is higher compared to the other ratios.

When the CH_4:CO_2 ratio is 0.5, the amount of BSCF oxygen flux is low (Figure 7.7); therefore, less H_2O is produced via reaction 1. So, steam reforming is less likely to happen due to low amount of water produced during the reaction. A decrease in the steam reforming reaction (reaction 4) would result in a lower H_2/CO ratio. Another possible reason for a lower H_2/CO ratio is that less CO conversion to CO_2 occurs when the CH_4:CO_2 ratio is lower. As mentioned before, the high level of CO_2 in the feed creates a low driving force for the membrane to release oxygen. The lower amount of oxygen, which is required for CO conversion to CO_2, causes a decrease in CO_2 formation from CO and hence increases the CO concentration,

leading to a low H_2/CO ratio. The excess amount of CO_2 in the feed prevents catalyst deactivation and a higher methane conversion is achieved through reaction 3.

According to the data, the CH_4:CO_2 feed ratio is a very important factor for the CO_2 reforming of methane. This ratio can change the reaction scenario drastically and thus needs to be chosen carefully. In a membrane reactor, various CH_4:CO_2 ratios can change the reaction pathway by increasing or decreasing membrane oxygen flux and it would be worthwhile to optimize this ratio.

Natural gas, which contains both CH_4 and CO_2, is the most commonly used feedstock for hydrogen production. The investigation on the effect of the CH_4:CO_2 feed ratio on conversion and product distribution could be important when natural gas or other CO_2 containing hydrocarbon feedstock is used for hydrogen production. The variation of CH_4:CO_2 in natural gas from one reservoir to another could impact the conversion and product distribution. The size of the reformer and other equipment in the plant might be affected by changing this ratio. So, the results of this study can help in designing hydrogen production plants, which are more cost effective and less sensitive to a change in the natural gas composition.

7.3.4. The Effect of Catalyst Selection on the CO_2 Reforming Reaction at 800°C

One of the most important parts of a membrane reactor is the catalyst, as it is responsible for the majority of hydrocarbon conversion to syngas. A suitable catalyst for the reforming reaction of methane must be able to facilitate C-H bond cleavage and also remove deposited carbon (resulting from C-H bond breakage) from the

catalyst surface or prevent coke formation. Thus, it is important to study the effect of catalysts for dry reforming of methane on the dense BSCF membrane.

As mentioned in Chapter 6, Ni-based and Pt-based catalysts have been investigated for dry reforming of methane and there is a trade-off between cost and activity for these two types of catalysts. The catalyst support itself can affect the products distribution and therefore is an important consideration when optimizing the reaction conditions. It has been suggested that the support material plays an important role in preventing catalyst deactivation and facilitating methane conversion to syngas. The most commonly used support material for hydrogen production from methane is Al_2O_3 [13, 14] because it possesses a high surface area, is abundant and inexpensive. Other support materials such as ZrO_2 and $CeZrO_2$ have also been used in the literature [15, 16]. These supports are known to be thermally stable and less susceptible to carbon deposition because of their oxygen storage and release capacity [17]. Compared with ZrO_2, $CeZrO_2$ is more resistant to carbon deposition because of the reducibility of cerium to convert from Ce^{4+} to Ce^{3+} [18].

To understand the effect of the catalyst on the reaction, six Pt-based and Ni-based catalysts were studied in this chapter: Pt/ZrO_2, $Pt/CeZrO_2$, $Ni/CeZrO_2$, $Pt-Ni/CeZrO_2$, Ni/Al_2O_3, and $Pt-Ni/Al_2O_3$. These catalysts were chosen to compare the performance of commercial Ni/Al_2O_3 catalyst with that of Pt-based catalysts and to decide which catalyst performs better for hydrogen production at 800°C. The ultimate goal is to find a catalyst that has a very good activity and selectivity for dry reforming of methane at this temperature.

The inherent activities of the catalysts for the CO_2 reforming reaction at 800°C were assessed by conducting the reaction tests without using any oxygen-permeable ceramic membrane in the membrane reactor. In these tests, catalysts were spread on top of a piece of a disk-shaped stainless steel (blank membrane); therefore, the reaction was not assisted by oxygen, as there is no oxygen flux for the blank membrane. Figures 7.11 and 7.12 show the methane conversion and H_2/CO ratio profiles for the experiments with the different catalysts using a blank membrane. Except for Ni/Al_2O_3 and Pt-Ni/Al_2O_3, the CH_4 conversion and H_2/CO ratio decrease as time proceeds for the other catalysts because of catalyst deactivation. As can be seen from Figures 7.11 and 7.12, Pt/ZrO_2 catalyst shows a low activity for hydrogen production at 800°C. Pt/$CeZrO_2$ shows a higher activity than Pt/ZrO_2 catalyst and this difference is due to the beneficial effect of having Ce in the support as a promoter. These results are consistent with what was previously seen in PFR during methane pulse studies (Figure 4.4).

Compared to Pt/$CeZrO_2$ catalyst, Ni/$CeZrO_2$ performs much better for hydrogen production at 800°C and this could be due to the high amount of Ni loading in this catalyst (Ni loading 15% vs. Pt loading 0.4 %). The initial activity of Ni/$CeZrO_2$ is similar to Pt-Ni/$CeZrO_2$ bimetallic catalyst; however, the differences between the activities of these two catalysts become more considerable as the reaction time proceeds. The amount of methane conversion decrease for Pt-Ni/$CeZrO_2$ is less than Ni/$CeZrO_2$ after 14 hours on stream, indicating that the addition of a small amount of Pt to Ni/$CeZrO_2$ might decrease the catalyst

deactivation. Two previous studies have reported that the promotion of Ni catalyst with a small amount of Pt and Rh can decrease the coke formation during CO_2 reforming of methane [13, 19]. The decrease in carbon deposition is ascribed to the improvement of Ni dispersion by the addition of the noble metal [13, 19]. It is also believed that the noble metal promotes the CO_2 dissociation and the oxygen produced from this decomposition can assist carbon removal from the catalyst surface [13].

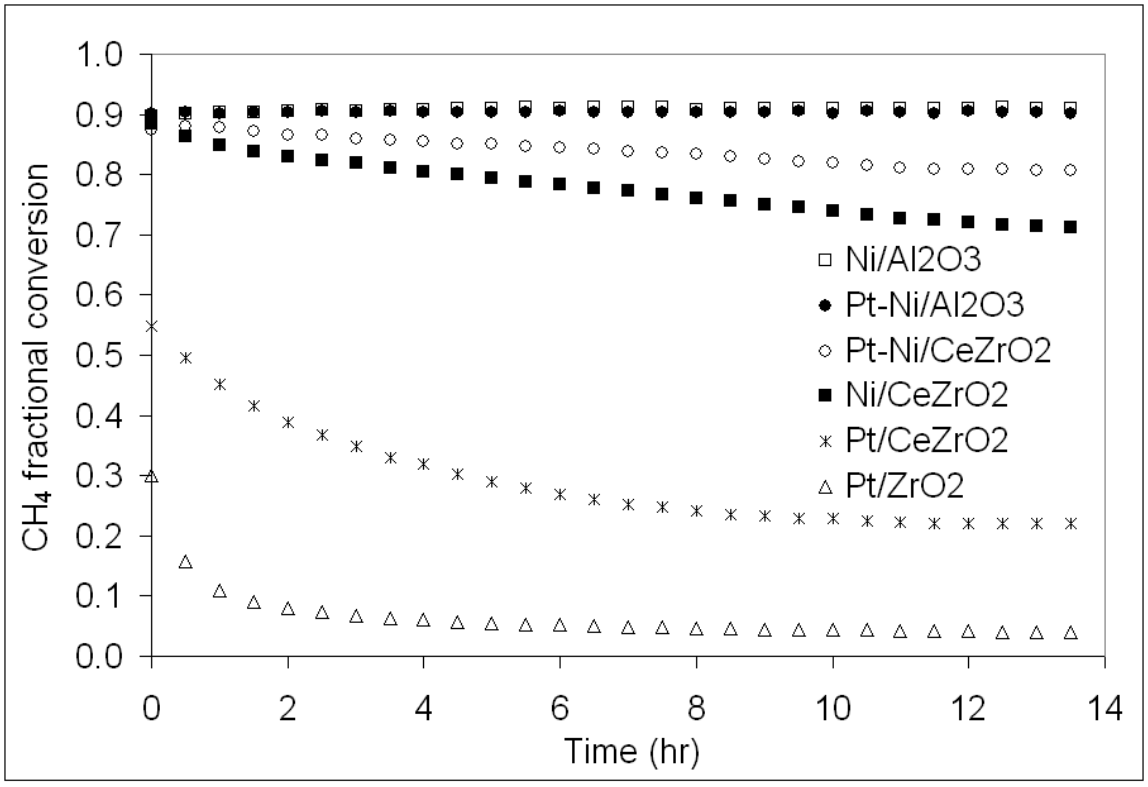

Figure 7.11. CH_4 conversion profiles for different catalysts at 800°C and atmospheric pressure in a membrane reactor on a piece of stainless steel. Feed composition: 40% CH_4, 40% CO_2, and 20% Ar; space velocity: 150 l/hr/$g_{catalyst}$.

The Ni/Al_2O_3 shows a high methane conversion (~90%) as well as a high H_2/CO ratio (~0.95) at 800°C and its activity is higher than $Ni/CeZrO_2$ and Pt-$Ni/CeZrO_2$ catalysts probably due to its higher surface area [20]. More importantly, this catalyst maintains high activity over the 14-hour reaction period, so the addition of Pt to Ni/Al_2O_3 might not change the activity of this catalyst significantly. These hypotheses were tested by investigating CH_4 conversion over Pt-Ni/Al_2O_3 catalyst and no difference was observed between the performance of Ni/Al_2O_3 catalyst and that of Pt-Ni/Al_2O_3 catalyst.

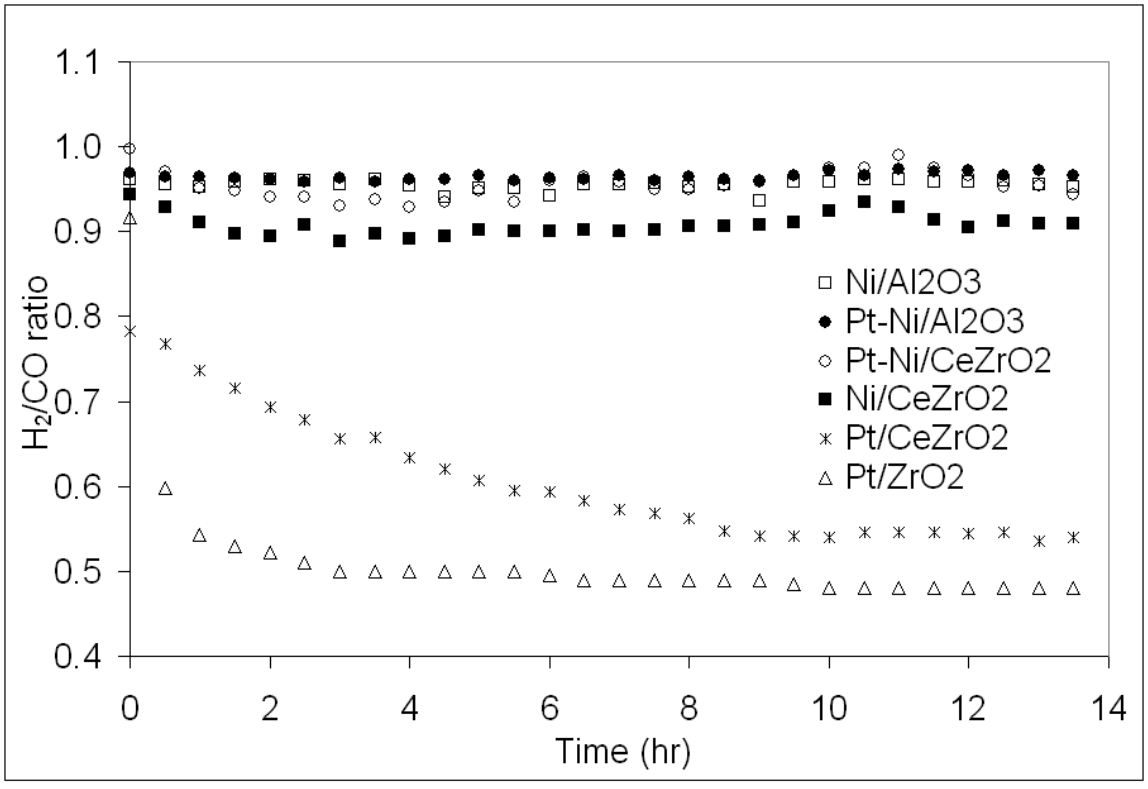

Figure 7.12. H_2/CO ratios for different catalysts at 800°C and atmospheric pressure in a membrane reactor on a piece of stainless steel. Feed composition is: 40% CH_4, 40% CO_2, and 20% Ar; space velocity is 150 l/hr/$g_{catalyst}$.

The CO_2 conversion of each catalyst was calculated and the results were compared in Figure 7.13. The results show a similar trend to what was described before. Again, both Ni/Al_2O_3 and $Pt\text{-}Ni/Al_2O_3$ catalysts show the highest CO_2 conversions.

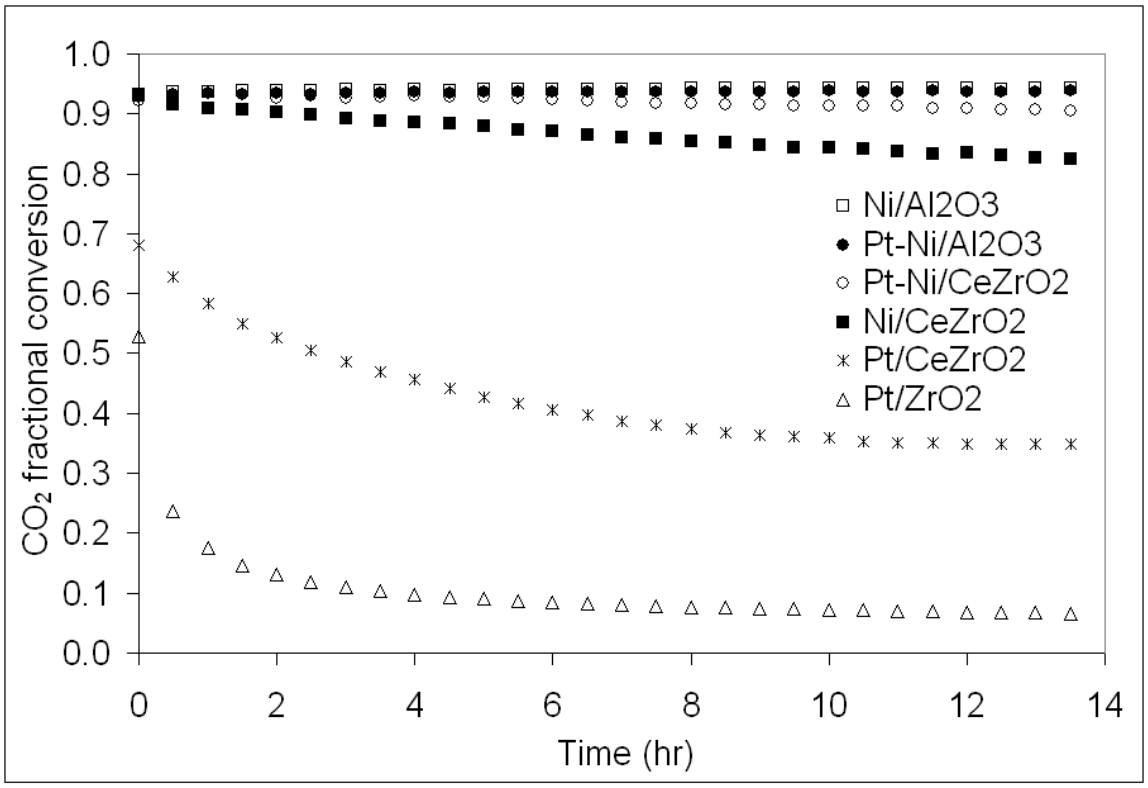

Figure 7.13. CO_2 conversion for different catalysts at 800°C and atmospheric pressure in a membrane reactor on a piece of stainless steel. Feed composition: 40% CH_4, 40% CO_2, and 20% Ar; space velocity: 150 $l/hr/g_{catalyst}$.

In order to understand the effect of BSCF on reaction, the reaction tests were performed on dense BSCF membranes. Figures 7.14 and 7.15 show the methane conversion profiles and H_2/CO ratios respectively for these experiments. According to Tables 7.1 and 7.2, all catalysts show higher CH_4 conversion and H_2/CO ratio in the presence of BSCF ceramic membrane than in the presence of the stainless steel blank at 800°C and this indicates the beneficial effects of distributed oxygen from the ceramic membrane on the reaction. As shown in Figures 7.11, 7.12, and 7.13, CH_4 conversion, H_2/CO ratio, and CO_2 conversion for the Pt-Ni/Al_2O_3 catalyst were almost equal to those for the Ni/Al_2O_3 catalyst. For this reason, the activity of Ni/Al_2O_3 catalyst was not tested on the BSCF membrane.

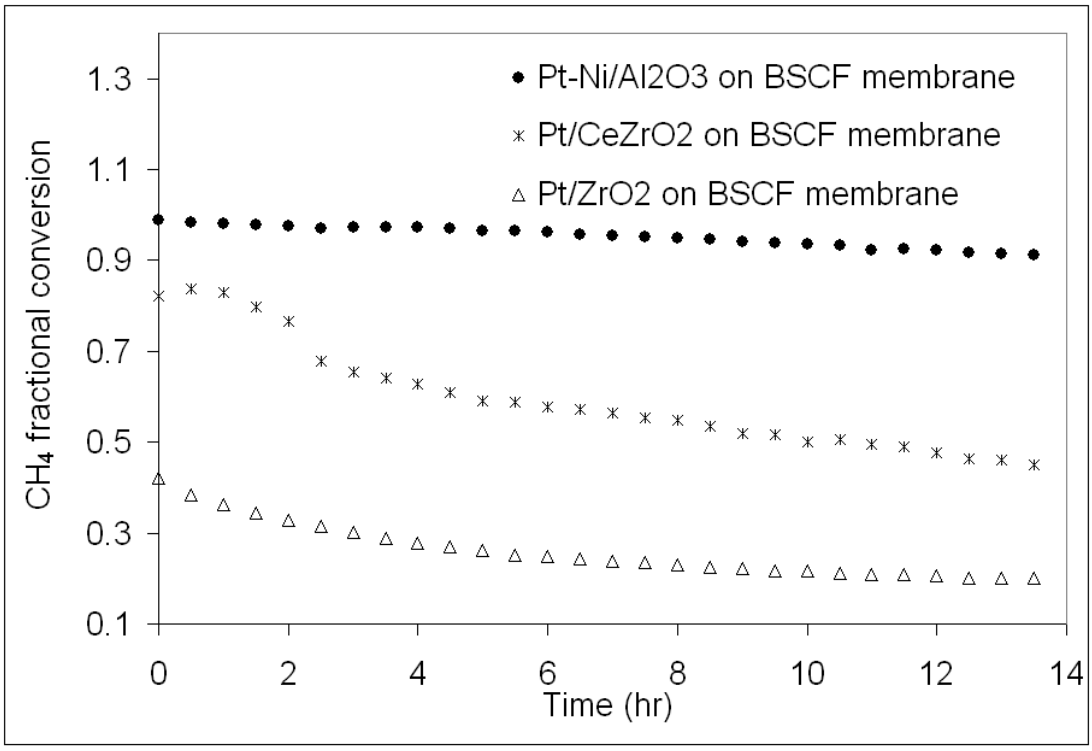

Figure 7.14. CH_4 conversion profiles for different catalysts at 800°C and atmospheric pressure on a dense BSCF membrane. Feed composition is: 40% CH_4, 40% CO_2, and 20% Ar; space velocity: 150 l/hr/$g_{catalyst}$.

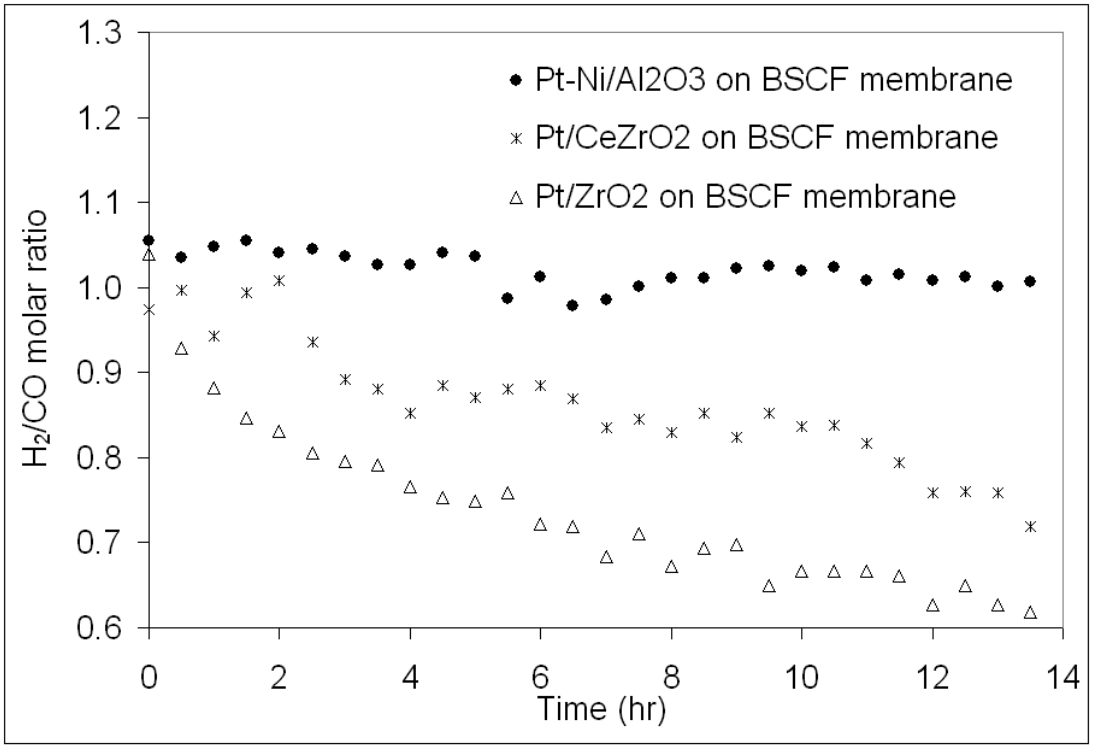

Figure 7.15. H_2/CO ratios for different catalysts at 800°C and atmospheric pressure on a dense BSCF membrane. Feed composition: 40% CH_4, 40% CO_2, and 20% argon; space velocity: 150 l/hr/$g_{catalyst}$.

Table 7.1. H_2/CO ratios during CO_2 reforming of methane over different catalysts at 800°C.

Catalyst	**H_2/CO ratio on S.S. blank**		**H_2/CO ratio on dense BSCF membrane**	
	Initial	Final	Initial	Final
Pt-Ni/Al_2O_3	0.97	0.96	1.06	1.01
Pt/$CeZrO_2$	0.78	0.54	0.97	0.72
Pt/ZrO_2	0.91	0.48	1	0.6

Table 7.2. CH_4 conversion during CO_2 reforming of methane over different catalysts at 800°C.

Catalyst	**CH_4 conversion on S.S. blank**		**CH_4 conversion on dense BSCF membrane**	
	Initial	Final	Initial	Final
Pt-Ni/Al_2O_3	0.9	0.9	0.99	0.91
Pt/$CeZrO_2$	0.55	0.22	0.82	0.45
Pt/ZrO_2	0.3	0.04	0.42	0.2

Figure 7.16 shows the CO_2 conversion profile for the tests on BSCF. Except for the initial CO_2 conversion, Pt-Ni/Al_2O_3 catalyst shows higher CO_2 conversion than Pt/ZrO_2 and Pt/$CeZrO_2$ catalysts, which is to be expected due to the high methane conversion and (close to 100%) and high H_2/CO ratio (close to 1) observed before. It seems that dry reforming reaction of methane on Pt-Ni/Al_2O_3 catalyst is close to equilibrium on the BSCF membrane. It is worth mentioning that for Pt/$CeZrO_2$ catalyst, it is possible that reverse water gas shift occurs during the first 2 hours of reaction. During this period of time, CH_4 conversion and H_2 production are high, resulting in more CO_2 conversion to CO via reverse water gas shift reaction.

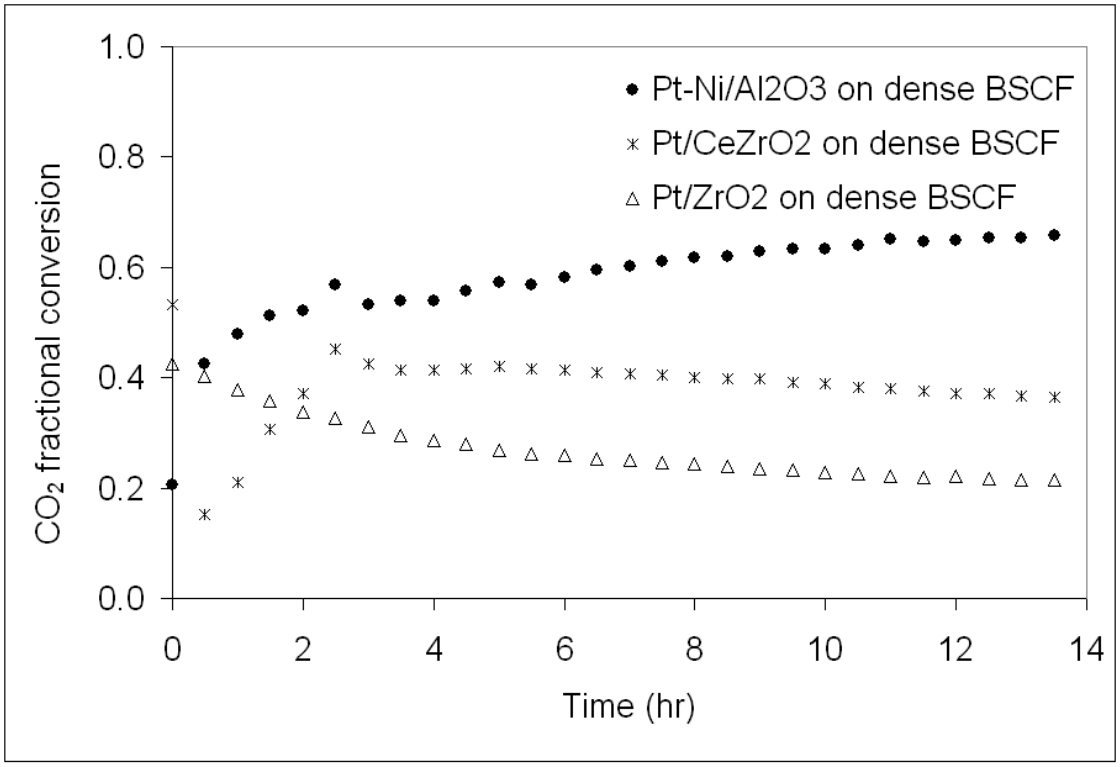

Figure 7.16. CO_2 conversion for different catalysts at 800°C and atmospheric pressure on a dense BSCF membrane. Feed composition is: 40% CH_4, 40% CO_2, and 20% argon; space velocity is 150 l/hr/$g_{catalyst}$.

Membrane oxygen flux was calculated for each test by an oxygen atom material balance. Figure 7.17 demonstrates the change in O_2 flux for each catalyst with reaction time. As can be seen, the catalyst type affects membrane oxygen flux significantly. The Pt-Ni/Al_2O_3 catalyst, which is a good catalyst for H_2 production through CO_2 reforming reaction, creates a highly reduced environment by producing a significant amount of hydrogen during the reaction. This leads to a decrease in oxygen partial pressure in reaction chamber and thus, creates a higher driving force for oxygen transfer through BSCF membrane. This phenomenon results in observing a very high oxygen flux during the test with Pt-Ni/Al_2O_3 catalyst compared to other

catalysts. The average oxygen fluxes on Pt-Ni/Al_2O_3 and Pt/$CeZrO_2$ catalysts increase 7-fold and 3-fold from those fluxes in an air:Ar gradient (when no reaction occurs). These results are in agreement with what have been published before in the literature [21, 22]. Pt/ZrO_2 catalyst, which is not a suitable catalyst for H_2 production through CO_2 reforming reaction, is not able to produce a significant amount of hydrogen to facilitate the oxygen transport through BSCF membrane; thus, oxygen flux with Pt/ZrO_2 test is very low and close to oxygen flux in an air:argon gradient.

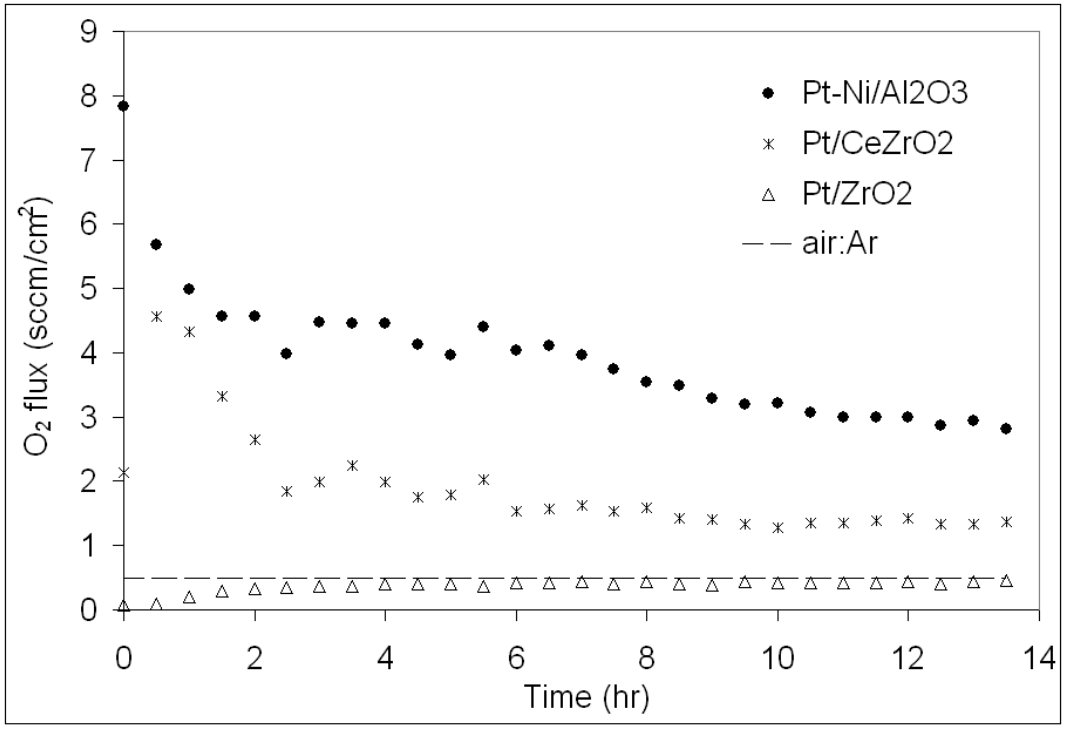

Figure 7.17. Membrane O_2 flux during reaction over different catalysts at 800°C and atmospheric pressure in a membrane reactor. Feed composition is: 40% CH_4, 40% CO_2, and 20% argon; space velocity is 150 l/hr/$g_{catalyst}$.

From Chapter 5, it is known that hydrogen from methane decomposition reacts with oxygen from the membrane to produce water. So, water production should be higher on Pt-Ni/Al_2O_3 catalyst compared to other catalysts due to the higher amount of oxygen flux observed on this catalyst. The average percentage of water production is higher on Pt-Ni/Al_2O_3 catalyst than other catalysts (8% for Pt-Ni/Al_2O_3 catalyst, 7% for Pt/$CeZrO_2$ catalyst, and 3% for Pt/ZrO_2). These results suggest that more steam reforming might occur on Pt-Ni/Al_2O_3 catalyst than other catalysts in the presence of the BSCF membrane.

Although the methane conversion profile of Pt-Ni/Al_2O_3 catalyst does not show a severe deactivation over time, the flux shown in Figure 7.17 does not stay stable throughout the test and tends to drop significantly. So, the decreasing trend in oxygen flux profile is less likely to be due to catalyst deactivation. A similar drop in oxygen flux profile is observed for Pt/$CeZrO_2$ catalysts in Figure 7.17. It is believed that the perovskite ceramic membrane surface is destroyed during the hydrogen production reaction [23, 24]. This destruction could be due to the reduction of Co and Fe ions under severely reduced reaction environment [23] or the presence of $SrCO_3$ and $BaCO_3$ carbonates [24]. In an attempt to study the destructive effects of reaction on our BSCF membrane surface, Raman images of the membrane surface were taken before and after reaction at 800°C. Figure 7.18 compares the surface of BSCF membrane after reaction with that of fresh membrane (before reaction).

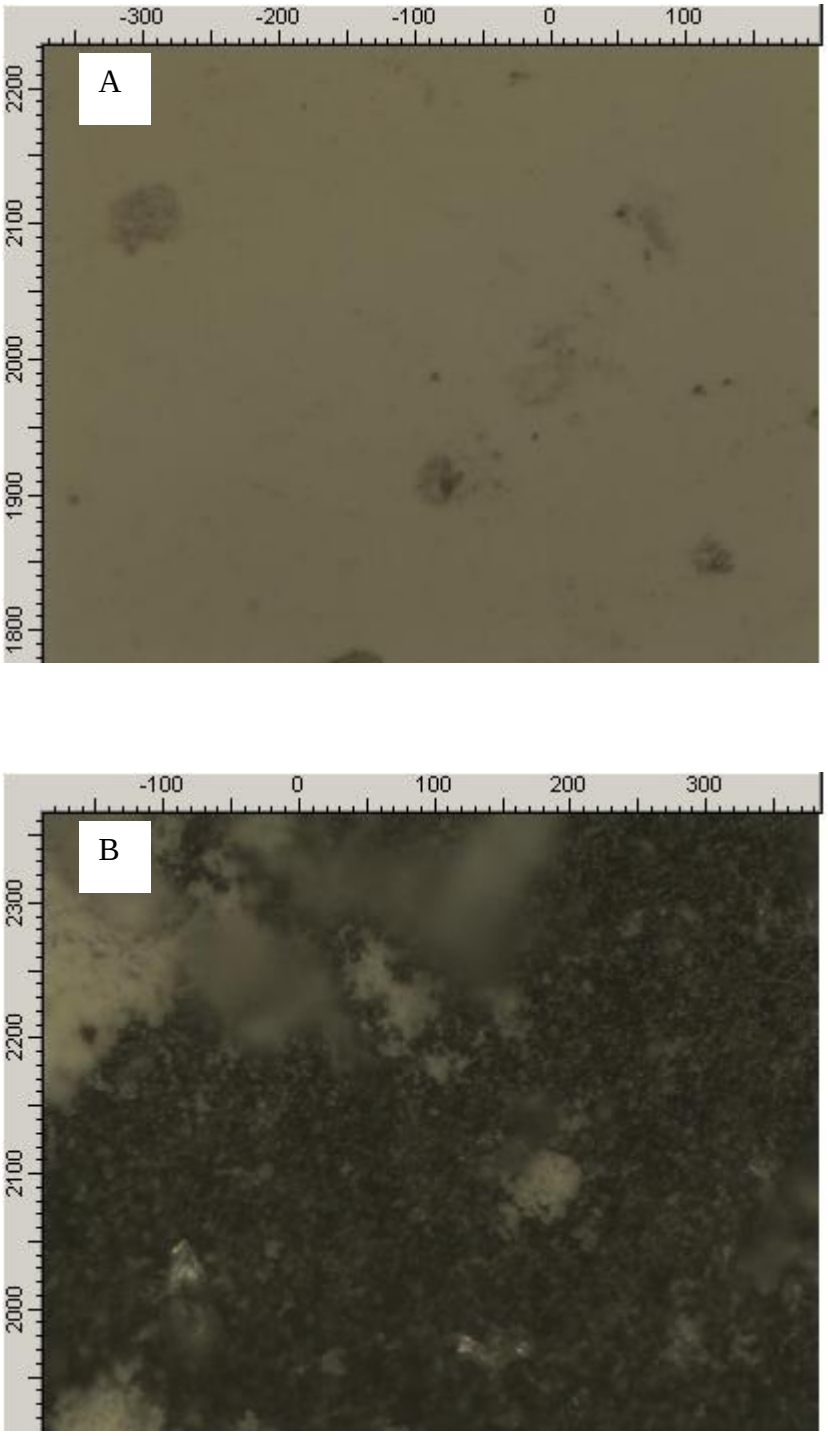

Figure 7.18. Raman images of BSCF reaction-side surface: A) before reaction, B) after 14-hr dry reforming reaction at 800°C.

According to Figure 7.18A, the surface of BSCF membrane before using for hydrogen production reaction is completely smooth. Figure 7.18B shows the BSCF surface after being used in the reaction. The white spots seen on the surface of membrane in Figure 7.18B are catalyst particles. The dark area in Figure 7.18B is the surface of membrane and it can be seen that the membrane surface is eroded after reaction. These results are in agreement with the literature data. The results of previous SEM and EDAX study in our research group showed carbonate formation on the surface of membrane after the reaction and the previous results are in agreement with this study [3].

7.3.5. The Effect of Reaction Temperature

Low and medium temperature reactions for syngas production are of interest, specifically in fuel cells, because of their low heating costs [25]. To gain a better understanding of the effects of operating temperature on H_2 production during CO_2 reforming of CH_4, reaction studies were performed at temperatures of 600°C and 700°C. The results of these studies were compared with the data at 800°C to see the effects of temperature on catalyst activity and eventually to find the activation energy of the reaction.

7.3.5.1. The Effect of Pt Addition to Ni-based Catalyst on Blank

According to our results in Chapter 6, Pt can change the reduction temperature of Ni catalyst to lower temperatures in a PFR. To find out the effects of Pt addition to

Ni catalyst under real reaction conditions, Pt promoted Ni/Al_2O_3 and $Ni/CeZrO_2$ catalysts were investigated for dry reforming of methane in a membrane reactor on a piece of stainless steel (i.e. no oxygen is available for reaction).

Figures 7.19 and 7.20 present CH_4 conversions and H_2/CO ratios over the catalysts as a function of reaction temperature on a piece of stainless steel during dry reforming of methane. According to Figures 7.19 and 7.20, both CH_4 conversions and H_2/CO ratios show a decreasing trend with decreasing temperature, which is to be expected due to the endothermic nature of the reforming reaction. Pt-Ni/Al_2O_3 and Ni/Al_2O_3 catalysts show similar methane conversions and H_2/CO ratios at 800°C as well as 700°C; however, there is a large difference between the performance of Pt-Ni/Al_2O_3 catalyst and that of Ni/Al_2O_3 catalyst at 600°C. At this temperature, the Ni/Al_2O_3 catalyst shows no activity for H_2 production and only a small amount of CO is produced during the reaction. This observation is consistent with the temperature programmed reaction data in a mixture of CH_4 and CO_2 for Ni/Al_2O_3 catalyst, which were discussed in Chapter 6. According to Figure 6.3, Ni/Al_2O_3 catalyst in a PFR starts to produce H_2 at 575°C, but initial H_2 production is very small and the H_2 signal in mass spectrometer does not increase significantly until 600°C; after which, a large amount of H_2 is produced. This delay in H_2 production over Ni/Al_2O_3 catalyst in the PFR could be due to the time required for Ni particles to be completely reduced. In addition, according to Figure 6.3, Pt-Ni/Al_2O_3 catalyst is active at 600°C in the PFR and these results are in agreement with Figures 7.19 and 7.20.

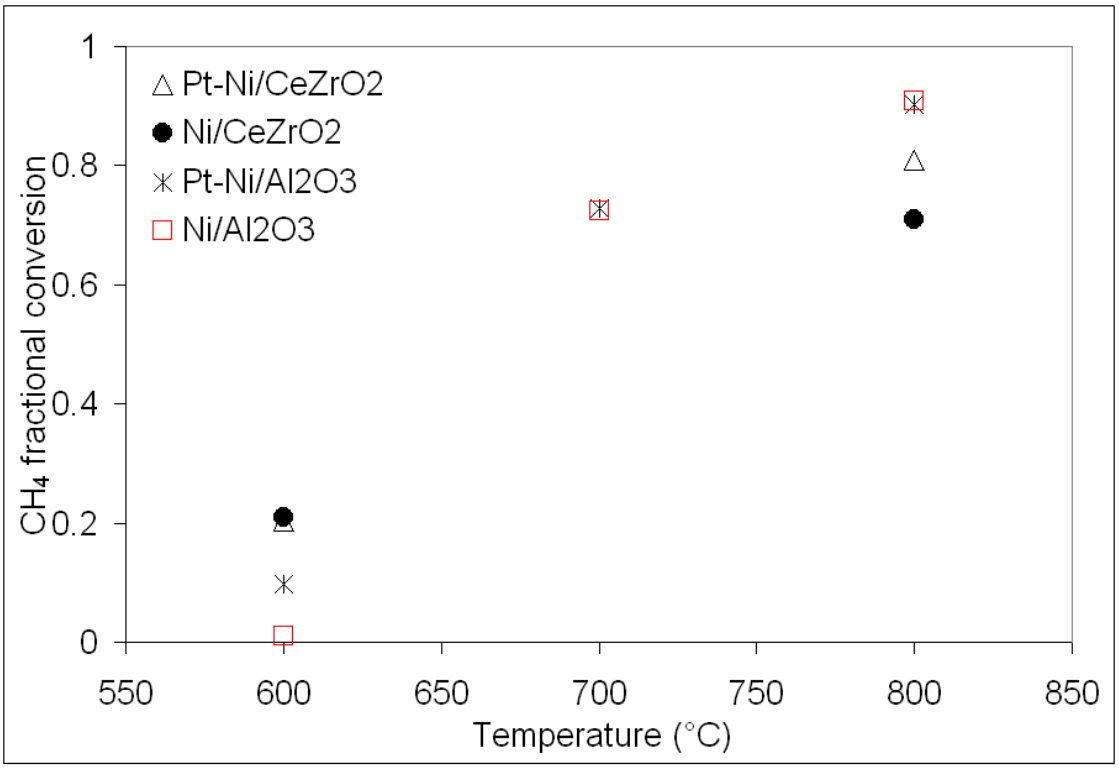

Figure 7.19. Temperature dependent CH_4 conversions for different catalysts after 14-hr reaction at atmospheric pressure on a piece of stainless steel. Feed composition: 40% CH_4, 40% CO_2, and 20% Ar.

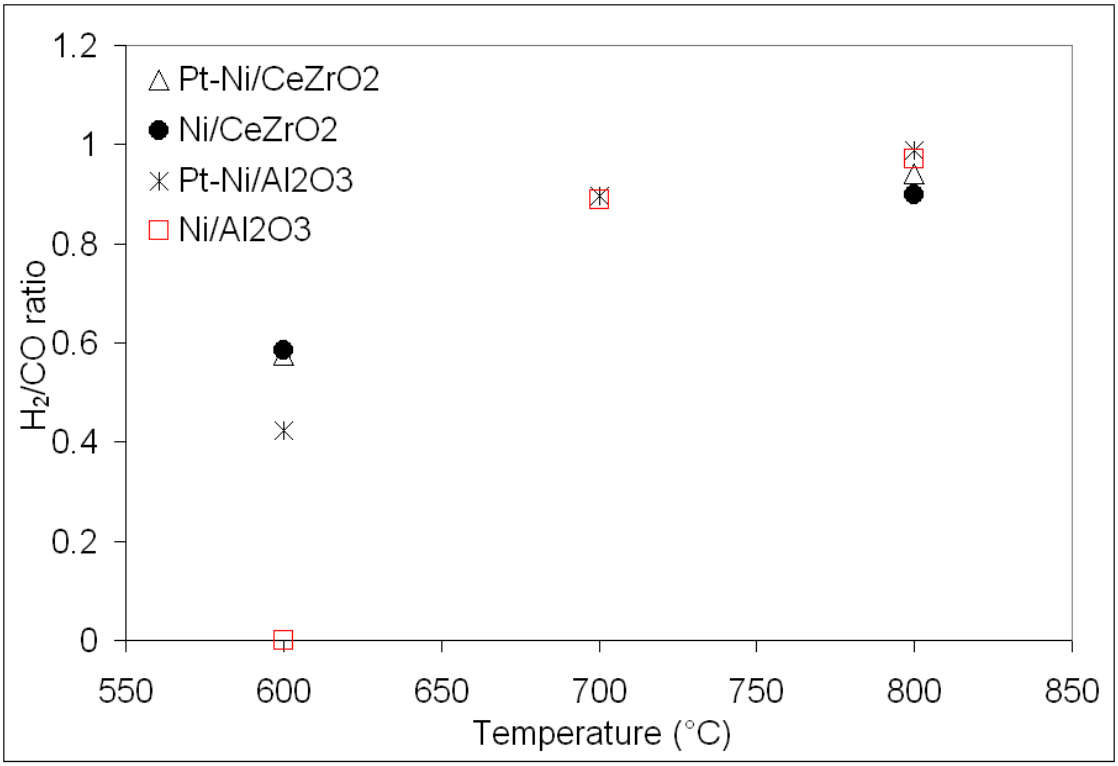

Figure 7.20. Temperature dependent H_2/CO ratio for different catalysts after 14-hr reaction at atmospheric pressure on a piece of stainless steel. Feed composition: 40% CH_4, 40% CO_2, and 20% Ar.

$Ni/CeZrO_2$ and $Pt\text{-}Ni/CeZrO_2$ catalysts were tested for dry reforming reaction only at 600 and 800°C and the results were compared with those of $Pt\text{-}Ni/Al_2O_3$ and Ni/Al_2O_3 catalysts. Although the activity of $Ni/CeZrO_2$ is similar to $Pt\text{-}Ni/CeZrO_2$ at 600°C according to Figures 7.19 and 7.20, they are different at 800°C after 14 hours of reaction. According to Figure 7.11 in section 7.3.4, the deactivation rate for the conversion profile of $Ni/CeZrO_2$ is higher than $Pt\text{-}Ni/CeZrO_2$ at 800°C and these differences might be because of beneficial effects of Pt on carbon removal during reaction. The reason why no difference is observed between the conversion profiles of $Ni/CeZrO_2$ and $Pt\text{-}Ni/CeZrO_2$ at 600°C is still unknown, but one speculation is that carbon deposition at 600°C might be more severe than at 800°C and the CO_2 cleaning mechanism might not be effective at 600°C. According to the observations reported in the literature, carbon deposition occurs more at low temperature because carbon removal by CO_2 ($C+CO_2 \leftrightarrow 2\ CO$) is more effective at high temperatures (the equilibrium constant of this reaction decreases with a decrese in temperature) [12]. More importantly, at 600°C, $Pt\text{-}Ni/CeZrO_2$ shows higher CH_4 conversions and H_2/CO ratios than $Pt\text{-}Ni/Al_2O_3$ catalyst and this is in agreement with Figure 6.3.

Figure 7.21 shows the CO_2 concentration at 600°C compared to 800°C. For both catalysts the CO_2 concentration at 600°C is significantly higher than 800°C. Also, the average water production at 600°C is higher than 800°C (e.g. for $Pt\text{-}Ni/CeZrO_2$: 3% at 600°C vs. 2% at 800°C). It is well known that reverse water-gas shift is thermodynamically favorable at low temperatures [26]. The high concentration of H_2O and CO_2 indicates that more reverse water-gas shift reaction

could occur at low temperatures and more H_2 is converted to CO through this reaction, resulting in lower H_2/CO ratios at 600°C.

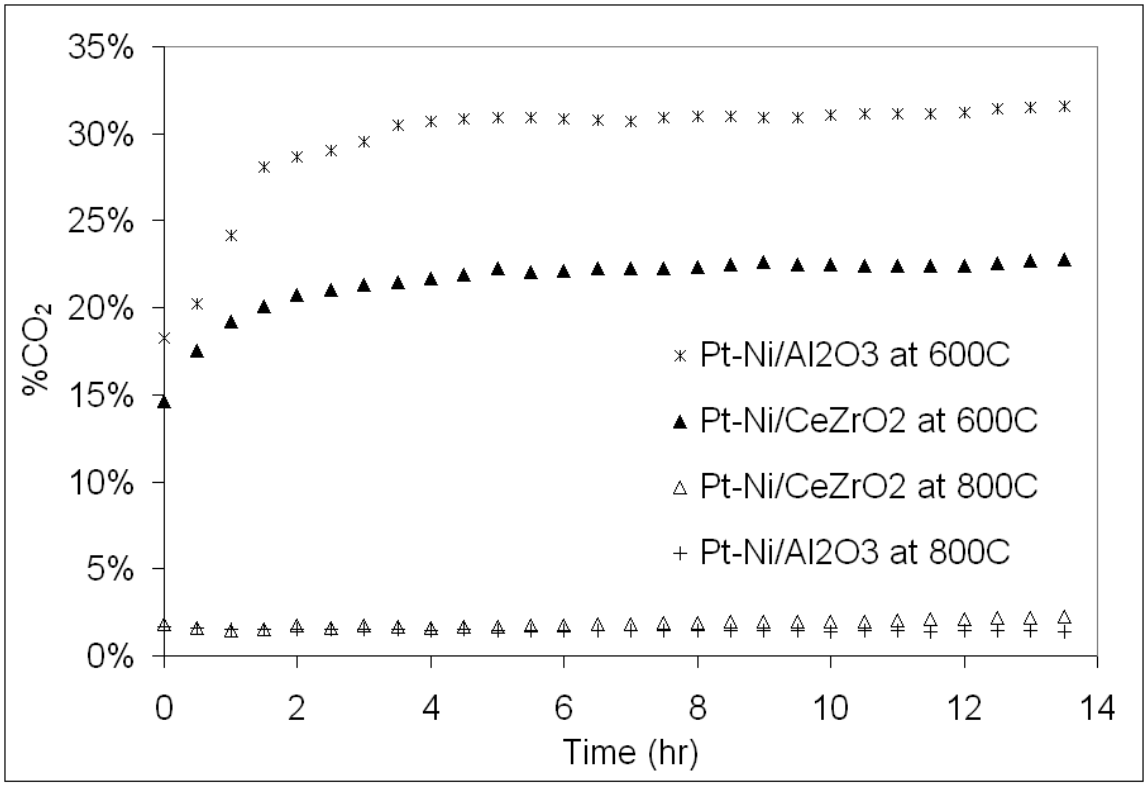

Figure 7.21. CO_2 concentration for different catalysts at atmospheric pressure on a piece of stainless steel. Feed composition: 40% CH_4, 40% CO_2, and 20% Ar; space velocity is 150 l/hr/$g_{catalyst}$.

At 600°C, the average water production for Pt-Ni/$CeZrO_2$ is 0.1% less than Pt-Ni/Al_2O_3. According to Figure 7.21, a higher concentration of carbon dioxide is observed for Pt-Ni/Al_2O_3. The higher water production together with the high CO_2 available inside the reactor could result in slightly more reverse water gas shift on the Pt-Ni/Al_2O_3 catalyst, which results in less H_2/CO ratios for this catalyst compared to Pt-Ni/$CeZrO_2$ catalyst. In addition, oxygen release capability of the $CeZrO_2$ support

could be one of other reasons for the superior performance of Pt-Ni/$CeZrO_2$ compared with Pt-Ni/Al_2O_3 at this temperature. Further work is required to study the interaction between Pt and Ni in the bimetallic Pt-Ni/$CeZrO_2$ and Pt-Ni/Al_2O_3 catalysts at different temperatures.

7.3.5.2. The Effects of BSCF on Reaction at Different Temperatures

In section 7.3.5.1, it was found that in the temperature range of 600-800°C, supported bimetallic Pt-Ni reveals either similar or higher performance to the supported monometallic Ni catalyst. So, only bimetallic catalysts will be studied on BSCF membranes hereafter.

As discussed in Chapter 5 and also in section 7.3.4, oxygen from dense BSCF can enhance the dry reforming reaction at 800°C. Little work has been devoted to syngas generation from methane during medium temperature CO_2 reforming. In order to explore the effects of temperature on reaction in the presence of BSCF, the four catalysts (Pt-Ni/$CeZrO_2$, Pt/$CeZrO_2$, Pt/ZrO_2, and Pt-Ni/Al_2O_3) were tested for dry reforming reaction in the presence and absence of a BSCF membrane over the temperature range from 600°C to 800°C. The aim of this study is to compare the activities of bimetallic Pt-Ni/Al_2O_3 and Pt-Ni/$CeZrO_2$ with those of Pt/$CeZrO_2$ and Pt/ZrO_2 catalysts, which were studied previously in Chapters 4 and 5.

First, the performance of the catalysts was investigated on a piece of stainless steel (blank). Figures 7.22 and 7.23 show the CH_4 conversions and H_2/CO ratios respectively over the catalysts as a function of temperature on a piece of stainless steel during dry reforming of methane. Again, the activity of catalysts drops as

temperature decreases, resulting in lower conversions and H_2/CO ratios at lower temperatures. The Pt/ZrO_2 shows almost no activity at 600°C and decreasing the temperature to 500°C does not change the activity. The Pt-Ni/Al_2O_3 shows higher CH_4 conversions and H_2/CO ratios than Pt/$CeZrO_2$ and Pt/ZrO_2 catalysts, so at the temperatures ranging from to 600°C to 800°C, the order of activity is: Pt-Ni/Al_2O_3> Pt/$CeZrO_2$> Pt/ZrO_2. These results are expected due to higher metal loading on Pt-Ni/Al_2O_3 compared to Pt/$CeZrO_2$ and Pt/ZrO_2 catalysts. The differences between conversions of bimetallic Pt-Ni/Al_2O_3 and Pt-Ni/$CeZrO_2$ were discussed in detail in section 7.3.5.1.

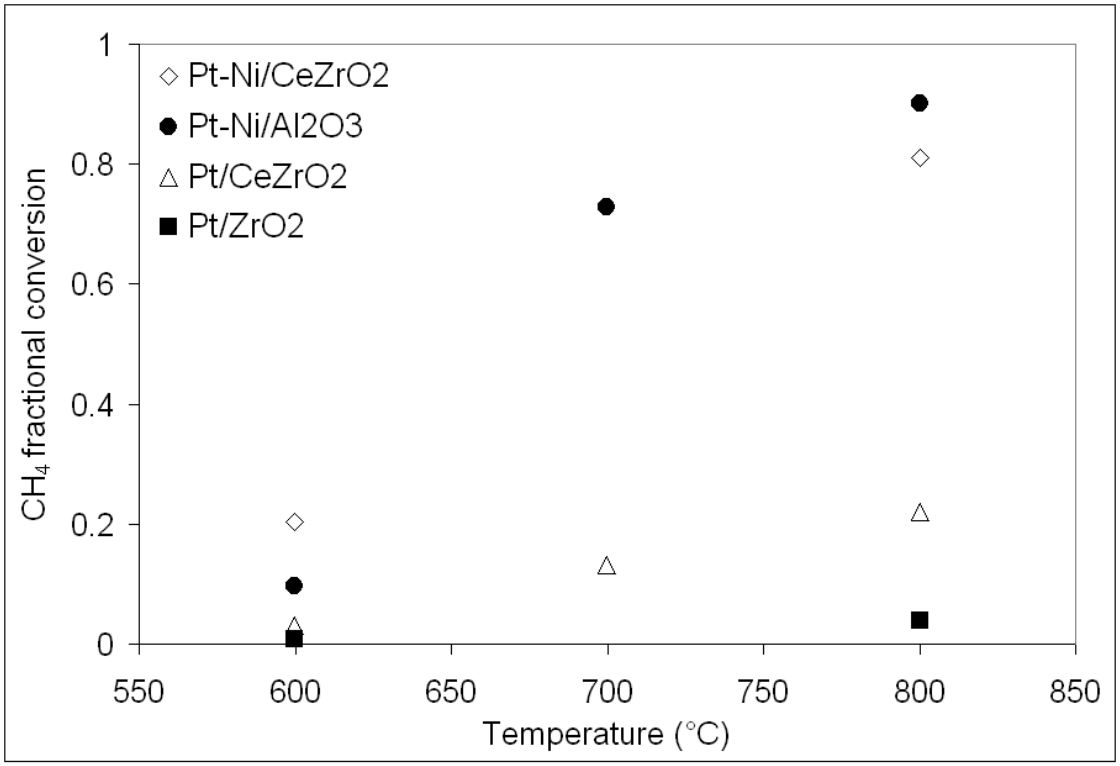

Figure 7.22. Temperature dependent CH_4 conversions for different catalysts after 14-hr reaction at atmospheric pressure on a piece of stainless steel. Feed composition: 40% CH_4, 40% CO_2, and 20% Ar; space velocity: 150 l/hr/$g_{catalyst}$.

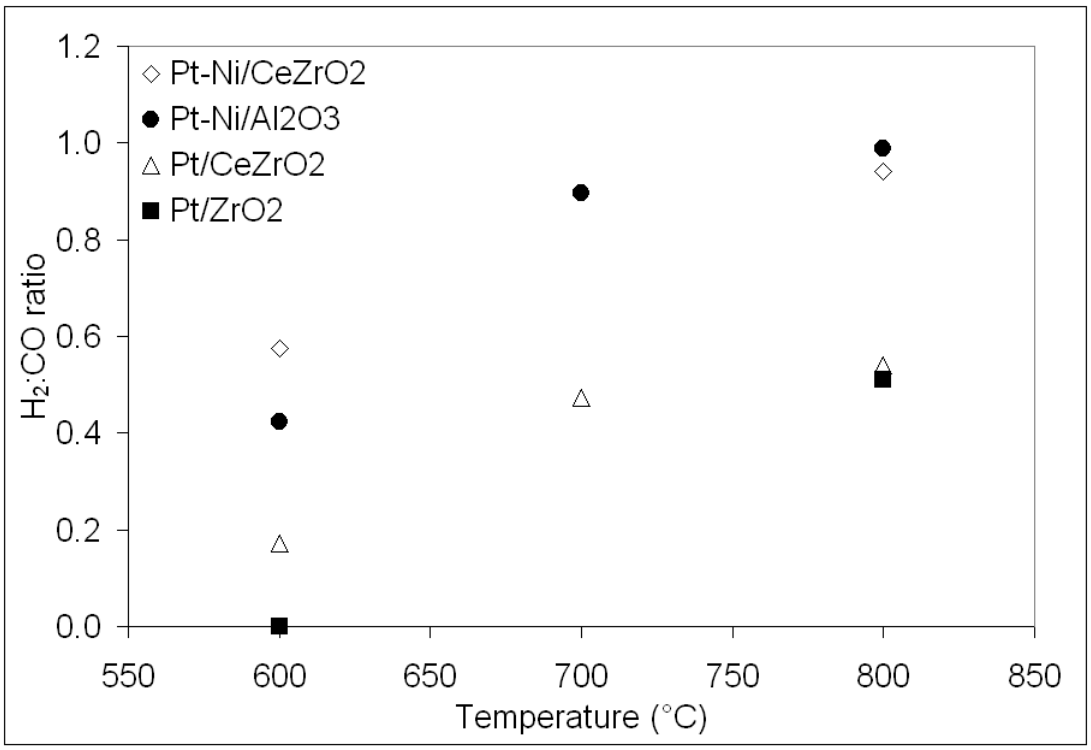

Figure 7.23. Temperature dependent H_2/CO ratio for different catalysts after 14-hr reaction at atmospheric pressure on a piece of stainless steel. Feed composition: 40% CH_4, 40% CO_2, and 20% Ar; space velocity: 150 l/hr/$g_{catalyst}$.

CO_2 conversions, H_2 selectivity, and CO selectivity are shown in Figures 7.24, 7.25, and 7.26 respectively. Again, the selectivity drops as temperature decreases and the order of selectivity is: Pt-Ni/Al_2O_3> Pt/$CeZrO_2$> Pt/ZrO_2. Although Pt-Ni/$CeZrO_2$ shows lower CH_4 conversion, CO_2 conversion, H_2 and CO selectivity, and H_2/CO ratio than Pt-Ni/Al_2O_3 at 800°C (probably due to its lower surface area [20]), its activity is higher than Pt-Ni/Al_2O_3 at 600°C. The possible reasons for these differences were discussed in section 7.3.5.1. These results, suggest that Pt-Ni/$CeZrO_2$ might be a promising catalyst for H_2 production during CO_2 reforming of CH_4 at medium and low temperatures.

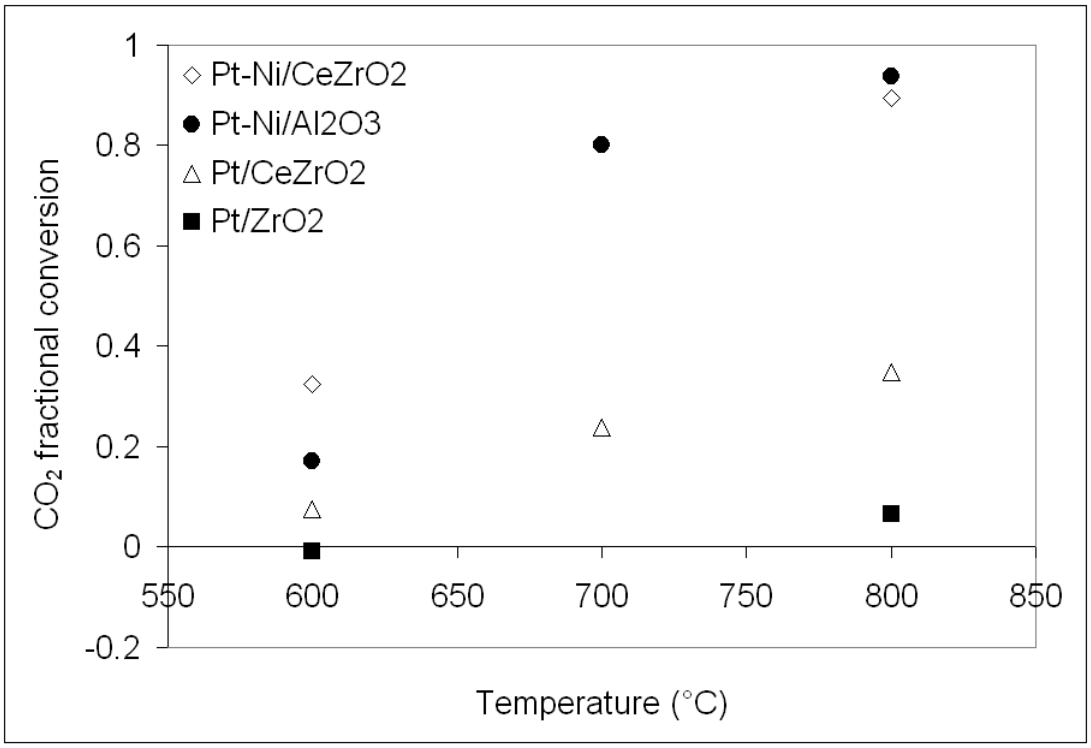

Figure 7.24. Temperature dependent CO_2 conversion for different catalysts after 14 hr at atmospheric pressure on a piece of stainless steel. Feed composition: 40% CH_4, 40% CO_2, and 20% Ar; space velocity: 150 l/hr/$g_{catalyst}$.

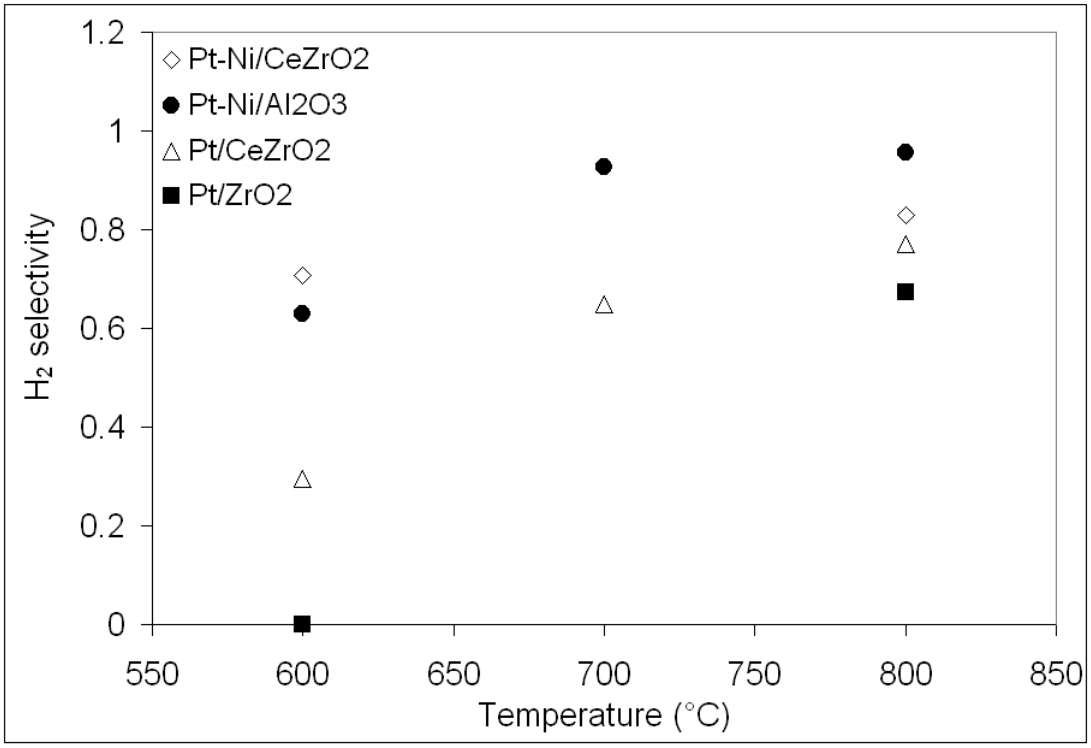

Figure 7.25. Temperature dependent H_2 selectivity for different catalysts after 14 hr at atmospheric pressure on a piece of stainless steel. Feed composition: 40% CH_4, 40% CO_2, and 20% Ar; space velocity: 150 l/hr/$g_{catalyst}$.

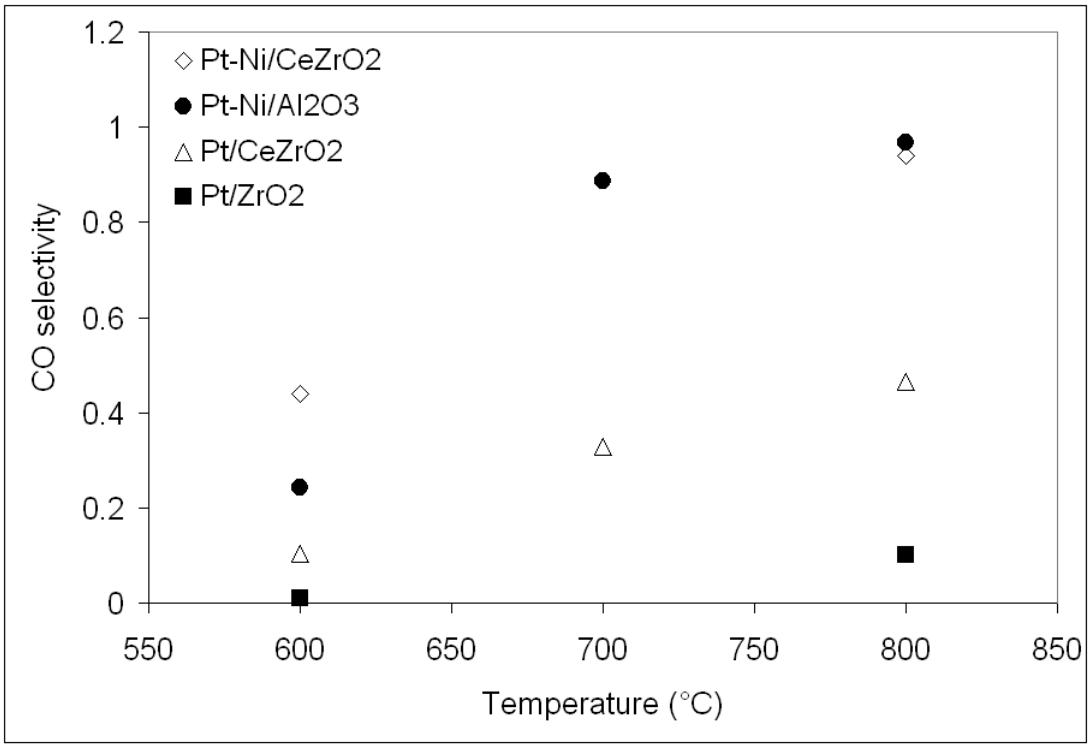

Figure 7.26. Temperature dependent CO selectivity for different catalysts after 14 hr at atmospheric pressure on a piece of stainless steel. Feed composition: 40% CH_4, 40% CO_2, and 20% Ar; space velocity: 150 $l/hr/g_{catalyst}$.

After understanding how the activities of each catalyst changes versus temperature on a piece of stainless steel, it is important to determine the effects of the BSCF membrane on the reaction. To understand the role of the BSCF membrane, the reactions were also carried out using the catalysts placed on top of a dense disk-shaped BSCF membrane at temperatures ranging from 600°C to 800°C.

The beneficial effects of BSCF on reaction at 800°C were previously shown in Table 7.1 and 7.2. At 600°C, each catalyst shows higher CH_4 conversion and H_2/CO ratio in the presence of ceramic membranes than in the presence of the stainless steel blank, indicating the beneficial effects of oxygen from the ceramic

membrane on the reaction. Table 7.3 shows the effects of BSCF on the reaction at 600°C. It was shown in Chapter 5 that both H_2 and CO have interactions with the BSCF membrane to produce water and CO_2. The high H_2:CO ratio on tests with BSCF can be due to increased steam reforming on the BSCF membrane compared to the tests on stainless-steel [27].

Table 7.3. CH_4 conversion during CO_2 reforming of methane over different catalysts at 600°C.

Catalyst	**CH_4 conversion on S.S. blank**		**CH_4 conversion on dense BSCF membrane**	
	Initial	Final	Initial	Final
Pt-Ni/$CeZrO_2$	0.44	0.2	0.46	0.2
Pt-Ni/Al_2O_3	0.33	0.097	0.4	0.13
Pt/$CeZrO_2$	0.084	0.032	0.13	0.08
Pt/ZrO_2	0.023	0.007	0.07	0.007

CH_4 conversion, H_2/CO ratio, and CO selectivity are shown respectively in Figures 7.27, 7.28, and 7.29. Similar to what was observed for blank tests, the order of activity in the presence of BSCF at each temperature is: Pt-Ni/Al_2O_3> Pt/$CeZrO_2$> Pt/ZrO_2.

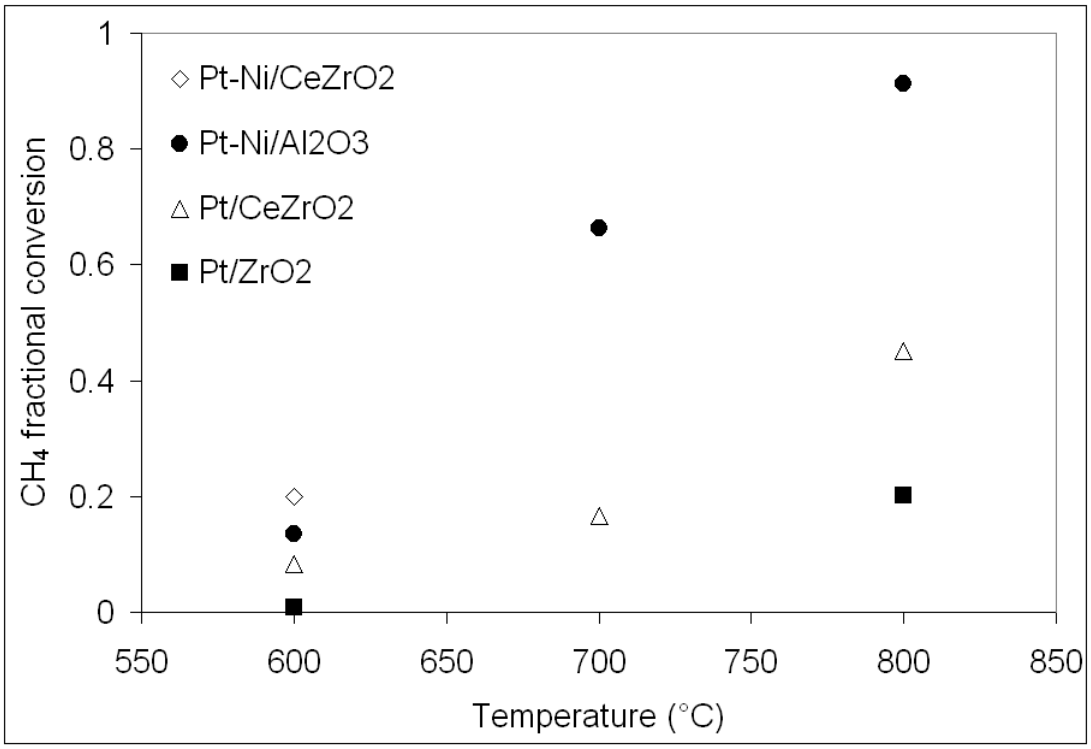

Figure 7.27. Temperature dependent CH_4 conversions for different catalysts after 14-hr reaction at atmospheric pressure on a dense BSCF. Feed composition: 40% CH_4, 40% CO_2, and 20% Ar.

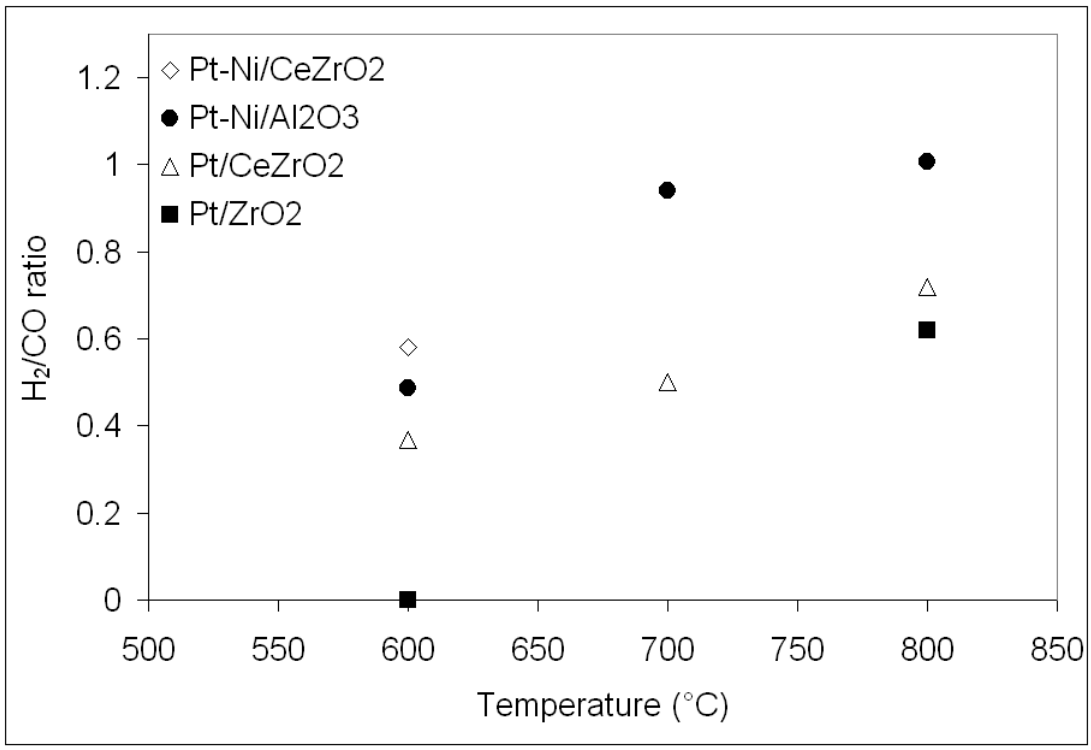

Figure 7.28. Temperature dependent H_2/CO ratio for different catalysts after 14-hr reaction at atmospheric pressure on a dense BSCF. Feed composition: 40% CH_4, 40% CO_2, and 20% Ar; space velocity: 150 l/hr/$g_{catalyst}$.

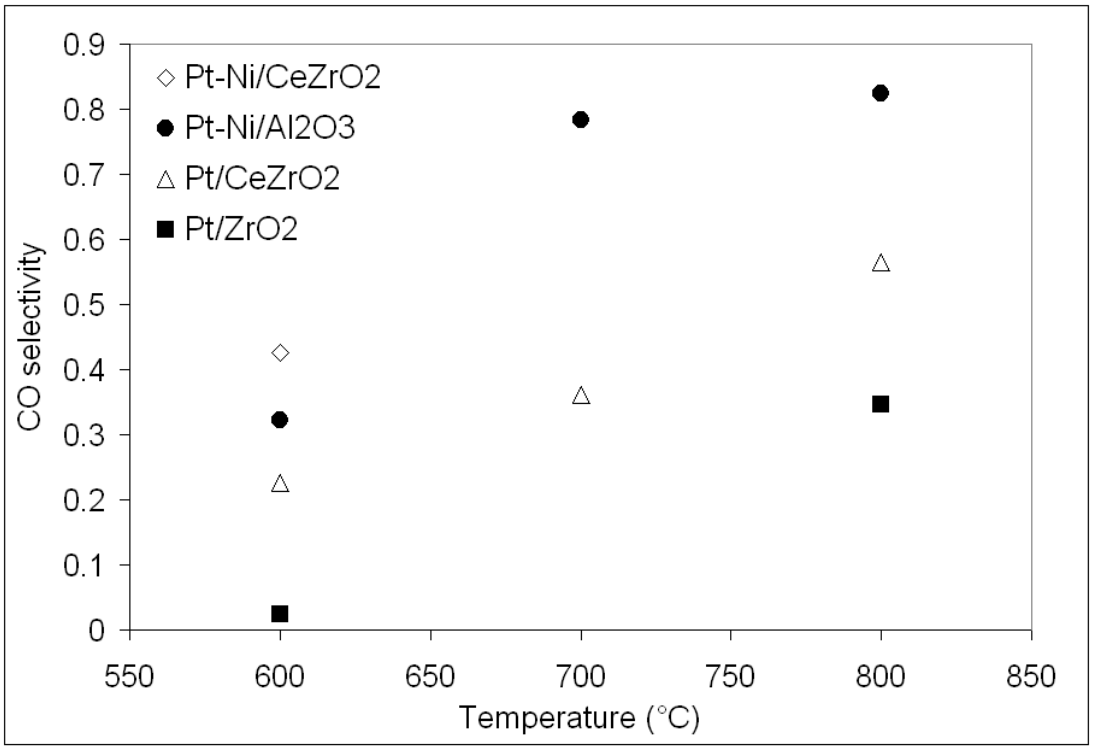

Figure 7.29. Temperature dependent CO selectivity for different catalysts after 14-hr reaction at atmospheric pressure on a dense BSCF. Feed composition: 40% CH_4, 40% CO_2, and 20% Ar; space velocity: 150 $l/hr/g_{catalyst}$.

At 600°C and in the presence of BSCF, CH_4 conversion, H_2/CO ratio, and CO selectivity for Pt-Ni/$CeZrO_2$ are higher than those for Pt-Ni/Al_2O_3 and these results are similar to the results on stainless steel blank. Figures 7.30 and 7.31 show the CO_2 conversion and H_2 selectivity respectively. Unlike the blank tests, BSCF tests show lower CO_2 conversion and H_2 selectivity for Pt-Ni/$CeZrO_2$ compared to Pt-Ni/Al_2O_3 at 600°C. Low CO_2 conversion could be due to more CO conversion to CO_2 and low H_2 selectivity might be because of more water production. Figure 7.32 confirms that water production is higher on Pt-Ni/$CeZrO_2$ compared to Pt-Ni/Al_2O_3 at 600°C on BSCF, resulting in more steam reforming on Pt-Ni/$CeZrO_2$ test.

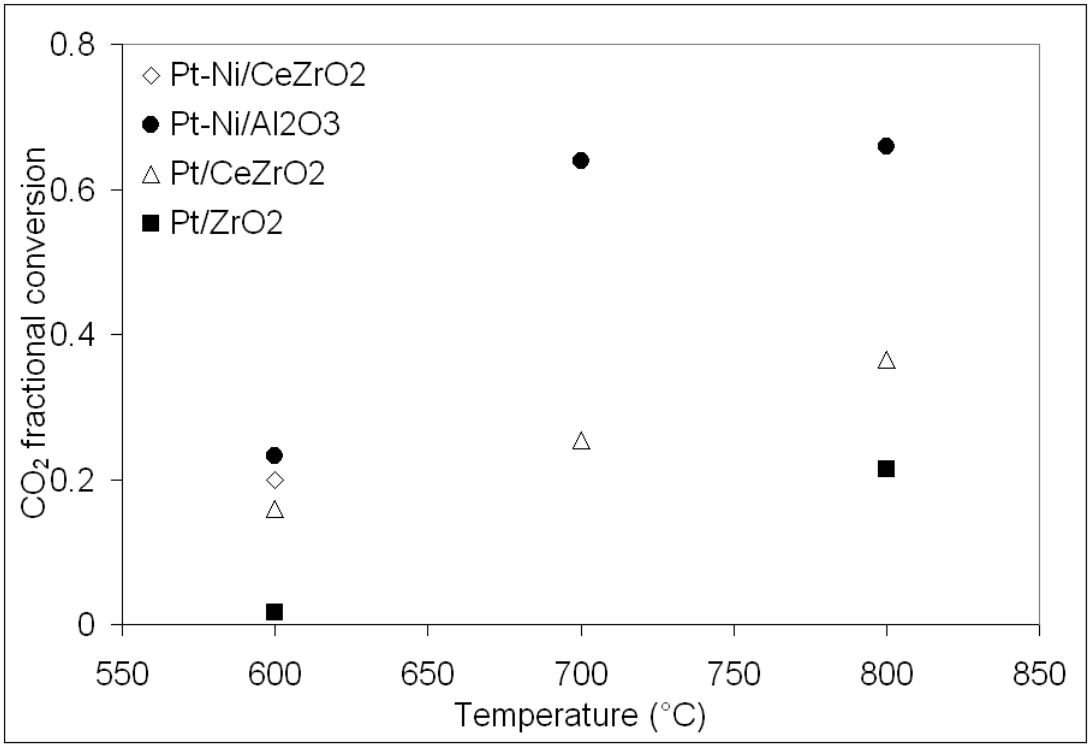

Figure 7.30. Temperature dependent CO_2 conversion for different catalysts after 14 -hr reaction at atmospheric pressure on a dense BSCF. Feed composition: 40% CH_4, 40% CO_2, and 20% Ar.

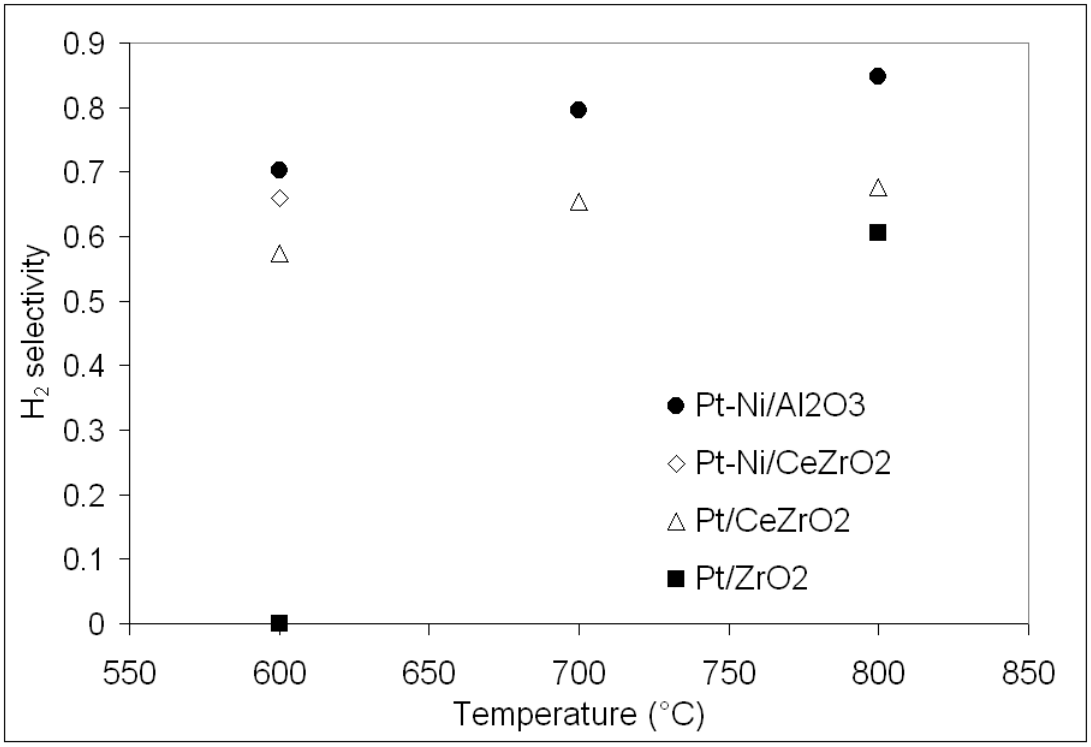

Figure 7.31. Temperature dependent H_2 selectivity for different catalysts after 14-hr reaction at atmospheric pressure on a dense BSCF. Feed composition: 40% CH_4, 40% CO_2, and 20% Ar; space velocity: 150 l/hr/$g_{catalyst}$.

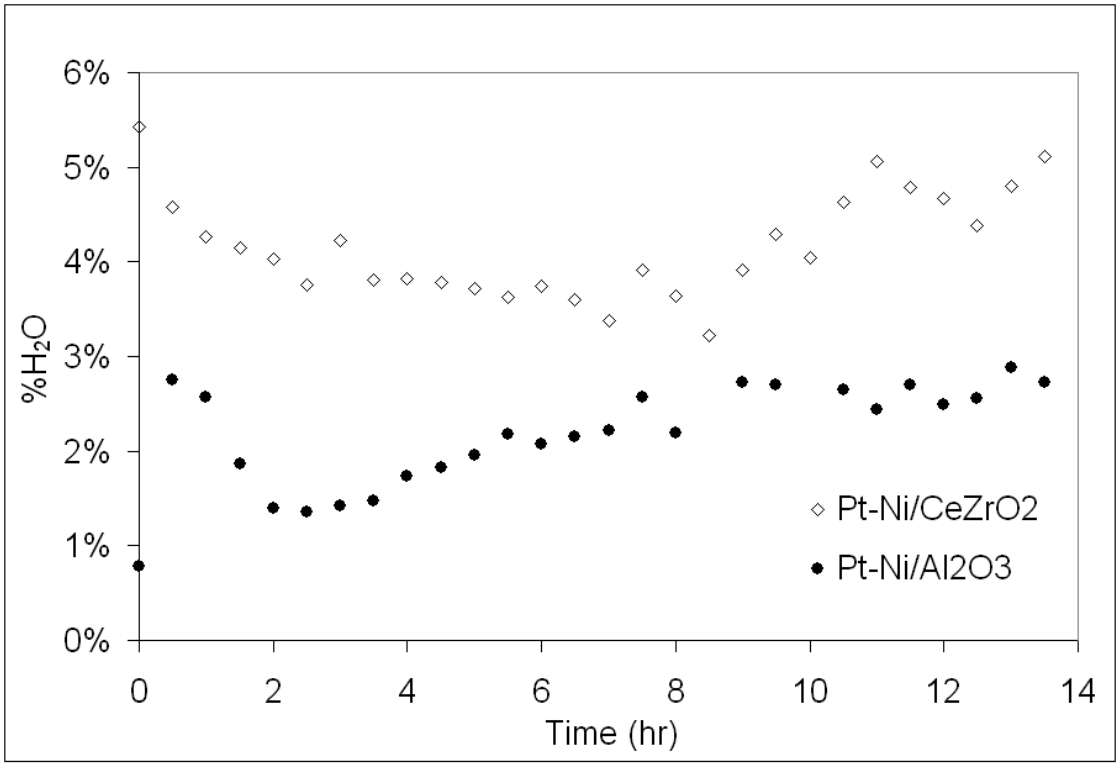

Figure 7.32. Water production for different catalysts at 600°C and atmospheric pressure on a dense BSCF. Feed composition: 40% CH_4, 40% CO_2, and 20% Ar; space velocity: 150 l/hr/$g_{catalyst}$.

Although H_2 production reaction at 600°C requires less heat than the reaction at 800°C, there are two main difficulties for H_2 production at 600°C on BSCF: low catalyst activity and low membrane oxygen flux. According to the literature, BSCF oxygen flux under reaction conditions decreases with a decrease in temperature [24, 28]. The oxygen flux of our BSCF membrane was calculated during the reaction on Pt-Ni/Al_2O_3 at 600°C, 700°C, and 800°C and the results, which are in agreement with literature, are shown in Figure 7.33. As can be seen, O_2 fluxes at 600°C are close to zero and this small amount of oxygen cannot assist carbon removal, resulting in a severe catalyst deactivation at 600°C. A higher oxygen flux membrane, like an

asymmetric BSCF membrane, might be a better option for H_2 production at 600°C or even lower temperatures.

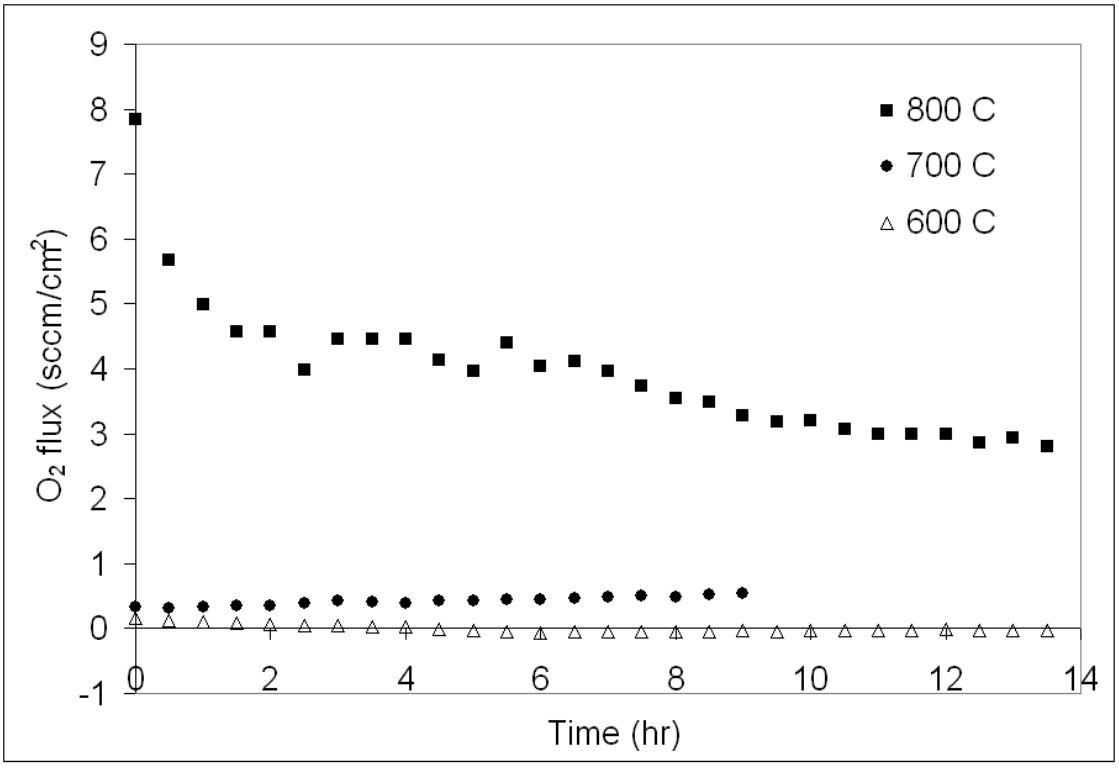

Figure 7.33. Membrane O_2 fluxes during reaction over Pt-Ni/Al_2O_3 at atmospheric pressure on a dense BSCF. Feed composition is: 40% CH_4, 40% CO_2, and 20% argon; space velocity is 150 l/hr/$g_{catalyst}$.

7.3.5.3. Reaction Activation Energy ($E_{act.}$) for CO_2 Reforming of Methane

To study the effect of the membrane on the apparent activation energy for the dry reforming reaction of methane, activation energies for the reactions with and without BSCF membranes were calculated based on the Arrhenius theory. Figures 7.34 shows the Arrhenius plots for Pt/$CeZrO_2$ and Pt-Ni/Al_2O_3 catalysts at temperatures ranging from 600°C to 800°C. The results for these two different types

of catalyst are also tabulated in Table 7.4. This table shows that the activation energy depends on the presence of the membrane as well as the catalyst type. The activation energy is lower when the membrane is employed.

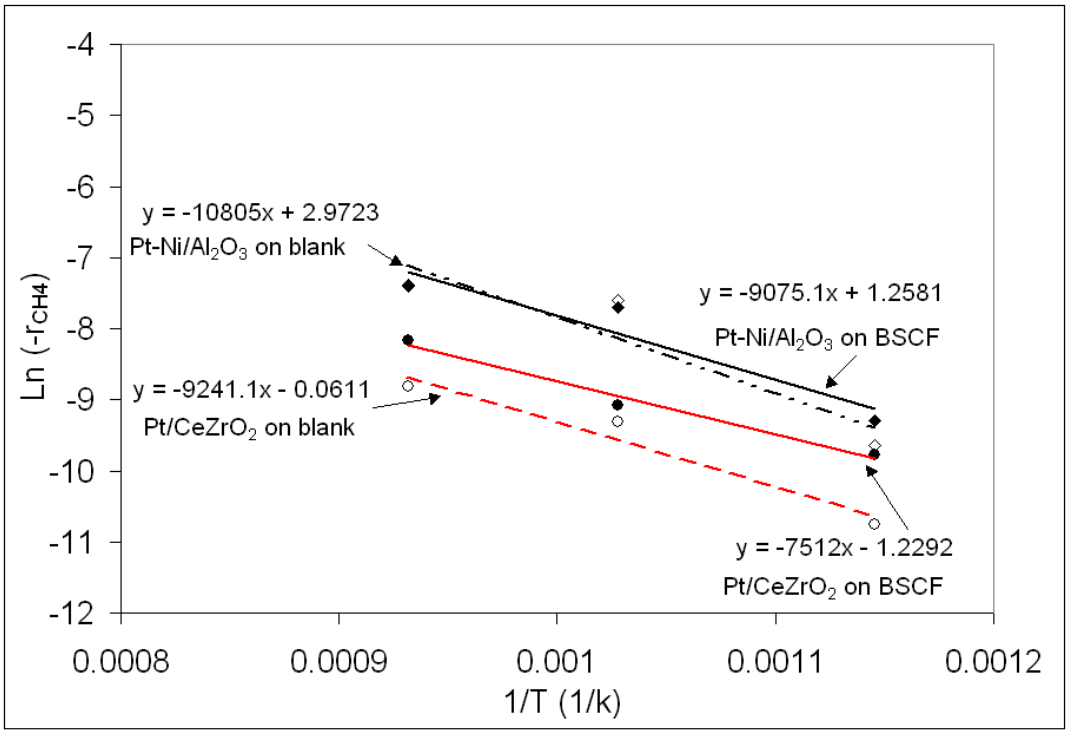

Figure 7.34. Arrhenius plots for $Pt/CeZrO_2$ and $Pt\text{-}Ni/Al_2O_3$ catalysts at atmospheric pressure in a membrane reactor with/without BSCF membrane. Feed composition: 40% CH_4, 40% CO_2, and 20% Ar; space velocity: 150 l/hr/$g_{catalyst}$.

Table 7.4. Apparent activation energies during CO_2 reforming of methane over $Pt/CeZrO_2$ and $Pt\text{-}Ni/Al_2O_3$ catalysts at the 600-800°C temperature range.

Catalyst	**$E_{act.}$ on blank (no oxygen) (kJ/mol)**	**$E_{act.}$ on dense BSCF membrane (kJ/mol)**
$Pt\text{-}Ni/Al_2O_3$	89.83 ± 35	75.45 ± 24
$Pt/CeZrO_2$	76.83 ± 16	62.45 ± 8

It was previously reported that activation energies during the dry reforming of methane are typically in the range of 33-100 kJ/mol [12]. The activation energy calculated in this study for Pt-Ni/Al_2O_3 catalyst without a membrane (89.83 kJ/mol) is in agreement with data published for CO_2 reforming of methane over Ni/La/Al_2O_3 at 700-900°C (90 kJ/mol) [29] . The data previously reported for Ni/Al_2O_3 catalyst (26.7 wt% Ni) for the same reaction is 76 kJ/mol [11], which is also close to our results. For the Pt/$CeZrO_2$ catalyst, the calculated value of the apparent activation energy in the absence of a membrane (76.83 kJ/mol) is comparable with activation energy on Pt/ZrO_2 catalyst during CO_2 reforming of methane over 550-750°C temperature range (83 kJ/mol) [30].

Based on the differences observed in the activation energies of the two tests for each catalyst (with BSCF and without BSCF), it is believed that lattice oxygen from the membrane has a large impact on the activation energy by changing the reaction pathway. It was shown in other studies that the activation energy for dry reforming of methane is higher than that for steam reforming of methane [30]. The difference between activation energies of the dry reforming reaction and the steam reforming reaction was reported to be 8 kJ/mol in the previous study, while the differences observed between the tests with BSCF and without BSCF in our studies is approximately 14 kJ/mol. This inconsistency could be due to different catalysts used in our studies compared to the previous study. Additionally, we know from Chapters 4 and 5 that water production is higher when the membrane is present compared to the tests without the membrane. Thus, the lower activation energies observed in tests

with BSCF in Table 7.4 could be due to higher amount of steam reforming occurring inside reactor when the membrane is present.

7.4. Conclusions

The main conclusions of this chapter can be summarized as follows:

1. Catalyst type, reaction temperature, feed concentration, and membrane thickness can influence the dry reforming reaction on BSCF membranes:
    - Although Pt-Ni/Al_2O_3 catalyst shows high methane conversion in the presence of the BSCF membrane at 800°C, the activity of this catalyst is low at 600°C. Pt-Ni/$CeZrO_2$ bimetallic catalyst demonstrates superior performance compared to Pt-Ni/Al_2O_3 catalyst at 600°C due to more steam reforming occurring on this catalyst. Medium temperature hydrogen production using BSCF needs to be explored further in order to obtain a higher conversion and H_2/CO ratio.
    - The CH_4:CO_2 feed ratio significantly affects the hydrogen production over the BSCF membrane. Altering the CH_4:CO_2 ratio has a direct impact on the oxygen flux, which in turn can influence the reaction pathway.
    - The BSCF membrane with lower thickness demonstrates a higher methane conversion and H_2:CO ratio than the BSCF membrane with the higher thickness because membrane oxygen flux is inversely proportional to thickness.

2. Membrane preparation pH has no significant effect on the reaction.
3. The BSCF membrane can reduce the apparent activation energy of the CO_2 reforming reaction by changing the reaction pathway to include more steam reforming.

7.5. References

[1] J. H. Tong, W. S. Yang, H. Suda, and K. Haraya, "Initiation of oxygen permeation and POM reaction in different mixed conducting ceramic membrane reactors," *Catalysis Today*, vol. 118, pp. 144-150, 2006.

[2] Z. P. Shao, W. S. Yang, Y. Cong, H. Dong, J. H. Tong, and G. X. Xiong, "Investigation of the permeation behavior and stability of a $Ba_{0.5}Sr_{0.5}Co_{0.8}Fe_{0.2}O_{3-\delta}$ oxygen membrane," *Journal of Membrane Science*, vol. 172, pp. 177-188, 2000.

[3] Q. Jiang, K. J. Nordheden, and S. M. Stagg-Williams, " $Ba_{0.5}Sr_{0.5}Co_{0.8}Fe_{0.2}O_x$ Asymmetric Oxygen-permeable Ceramic Membrane for CO_2 Reforming and Partial Oxidation of Methane " presented at ACS National Meeting, San Francisco, CA, March 2010.

[4] Z. H. Chen, R. Ran, Z. P. Shao, H. Yu, J. C. D. da Costa, and S. M. Liu, "Further performance improvement of $Ba_{0.5}Sr_{0.5}Co_{0.8}Fe_{0.2}O_{3-\delta}$ perovskite membranes for air separation," *Ceramics International*, vol. 35, pp. 2455-2461, 2009.

[5] W. K. Hong and G. M. Choi, "Oxygen permeation of BSCF membrane with varying thickness and surface coating," *Journal of Membrane Science*, vol. 346, pp. 353-360.

[6] M. Ikeguchi, Y. Uchida, Y. Sekine, E. Kikuchi, and M. Matsukata, "Solid state synthesis of $SrFeCo_{0.5}O_x$ asymmetric membranes for oxygen separation," *Journal of Chemical Engineering of Japan*, vol. 38, pp. 502-508, 2005.

[7] D. A. Slade, Q. Jiang, K. J. Nordheden, and S. M. Stagg-Williams, "A Comparison of Mixed-conducting Oxygen-permeable Membranes for CO_2 Reforming," *Catalysis Today*, vol. 148, pp. 290-297, 2009.

[8] Q. Jiang, S. Faraji, K. J. Nordheden, and S. M. Stagg-Williams, "Application of $Ba_{0.5}Sr_{0.5}Co_{0.8}Fe_{0.2}O_x$ Asymmetric Oxygen-permeable Membranes for Hydrocarbon Conversion Reactions," presented at North American Meeting, San Francisco, CA, June 2009.

[9] F. B. Noronha, E. C. Fendley, R. R. Soares, W. E. Alvarez, and D. E. Resasco, "Correlation between catalytic activity and support reducibility in the CO_2

reforming of methane over $Pt/Ce_xZr_{1-x}O_2$ catalysts," *Chemical Engineering Journal*, vol. 82, pp. 21-31, 2001.
[10] S. B. Wang, G. Q. M. Lu, and G. J. Millar, "Carbon dioxide reforming of methane to produce synthesis gas over metal-supported catalysts: State of the art," *Energy & Fuels*, vol. 10, pp. 896-904, 1996.
[11] A. Takano, T. Tagawa, and S. Goto, "Carbon-Dioxide Reforming of Methane on Supported Nickel-Catalysts," *Journal of Chemical Engineering of Japan*, vol. 27, pp. 727-731, 1994.
[12] M. C. J. Bradford and M. A. Vannice, "CO_2 reforming of CH_4," *Catalysis Reviews-Science and Engineering*, vol. 41, pp. 1-42, 1999.
[13] Z. Y. Hou and T. Yashima, "Small amounts of Rh-promoted Ni catalysts for methane reforming with CO_2," *Catalysis Letters*, vol. 89, pp. 193-197, 2003.
[14] B. C. Enger, R. Lodeng, and A. Holmen, "Evaluation of reactor and catalyst performance in methane partial oxidation over modified nickel catalysts," *Applied Catalysis A-General*, vol. 364, pp. 15-26, 2009.
[15] S. Damyanova, B. Pawelec, K. Arishtirova, M. V. M. Huerta, and J. L. G. Fierro, "The effect of CeO_2 on the surface and catalytic properties of Pt/CeO_2-ZrO_2 catalysts for methane dry reforming," *Applied Catalysis B-Environmental*, vol. 89, pp. 149-159, 2009.
[16] S. M. Stagg-Williams, F. B. Noronha, G. Fendley, and D. E. Resasco, "CO_2 reforming of CH_4 over Pt/ZrO_2 catalysts promoted with La and Ce oxides," *Journal of Catalysis*, vol. 194, pp. 240-249, 2000.
[17] S. Ozkara-Aydinoglu, E. Ozensoy, and A. E. Aksoylu, "The effect of impregnation strategy on methane dry reforming activity of Ce promoted Pt/ZrO_2," *International Journal of Hydrogen Energy*, vol. 34, pp. 9711-9722, 2009.
[18] A. Lamacz, A. Krzton, A. Musi, and P. Da Costa, "Reforming of Model Gasification Tar Compounds," *Catalysis Letters*, vol. 128, pp. 40-48, 2009.
[19] B. Pawelec, S. Damyanova, K. Arishtirova, J. L. G. Fierro, and L. Petrov, "Structural and surface features of PtNi catalysts for reforming of methane with CO_2," *Applied Catalysis A-General*, vol. 323, pp. 188-201, 2007.
[20] N. Laosiripojana and S. Assabumrungrat, "Methane steam reforming over $Ni/Ce\text{-}ZrO_2$ catalyst: Influences of $Ce\text{-}ZrO_2$ support on reactivity, resistance toward carbon formation, and intrinsic reaction kinetics," *Applied Catalysis A-General*, vol. 290, pp. 200-211, 2005.
[21] H. H. Wang, Y. Cong, and W. S. Yang, "Investigation on the partial oxidation of methane to syngas in a tubular $Ba_{0.5}Sr_{0.5}Co_{0.8}Fe_{0.2}O_{3-\delta}$ membrane reactor," *Catalysis Today*, vol. 82, pp. 157-166, 2003.
[22] M. Ikeguchi, T. Mimura, Y. Sekine, E. Kikuchi, and M. Matsukata, "Reaction and oxygen permeation studies in $Sm_{0.4}Ba_{0.6}Fe_{0.8}Co_{0.2}O_{3-\delta}$ membrane reactor for partial oxidation of methane to syngas," *Applied Catalysis A-General*, vol. 290, pp. 212-220, 2005.
[23] C.-Y. Tsai, A. G. Dixon, Y. H. Ma, W. R. Moser, and M. R. Pascucci, "Dense perovskite $La_{1-x}A'_xFe_{1-y}Co_yO_{3-\delta}$ (A' = Ba, Sr, Ca) membrane synthesis,

applications, and characterization," *J Amer Ceram Soc*, vol. 81, pp. 1437-1444, 1998.

[24] W. Zhu, W. Han, G. Xiong, and W. Yang, "Mixed Reforming of Simulated Gasoline to Hydrogen in a BSCFO Membrane Reactor," *Catalysis Today*, vol. 118, pp. 39-43, 2006.

[25] Y. Z. Chen, P. Cui, G. X. Xiong, and H. Y. Xu, "Novel nickel-based catalyst for low temperature hydrogen production from methane steam reforming in membrane reformer," *Asia-Pacific Journal of Chemical Engineering*, vol. 5, pp. 93-100.

[26] E. D. Park, D. Lee, and H. C. Lee, "Recent progress in selective CO removal in a H_2-rich stream," *Catalysis Today*, vol. 139, pp. 280-290, 2009.

[27] M. Ikeguchi, T. Mimura, Y. Sekine, E. Kikuchi, and M. Matsukata, "Reaction and oxygen permeation studies in $Sm_{0.4}Ba_{0.6}Fe_{0.8}Co_{0.2}O_{3-\delta}$ membrane reactor for partial oxidation of methane to syngas," *Applied Catalysis A : General*, vol. 290, pp. 212-220, 2005.

[28] W. Zhu, W. Han, G. Xiong, and W. Yang, "Mixed Reforming of Heptane to Syngas in the $Ba_{0.5}Sr_{0.5}Co_{0.8}Fe_{0.2}O_{3-\delta}$ Membrane Reactor," *Catalysis Today*, vol. 104, pp. 149-153, 2005.

[29] U. Olsbye, T. Wurzel, and L. Mleczko, "Kinetics and reaction engineering studies of dry reforming of methane over a $Ni/La/Al_2O_3$ catalyst," *Industrial & Engineering Chemistry Research*, vol. 36, pp. 5180-5188, 1997.

[30] J. M. Wei and E. Iglesia, "Mechanism and site requirements for activation and chemical conversion of methane on supported Pt clusters and turnover rate comparisons among noble metals," *Journal of Physical Chemistry B*, vol. 108, pp. 4094-4103, 2004.

Chapter 8: Conclusions and Recommendations

8.1. Conclusions

Mixed ionic-electronic conductors (MIEC) are 100% selective to oxygen and they have the ability to conduct both electrons and ions. The investigation of these MIEC membranes has gained significant attention recently because of their different applications in fuel processors, oxygen sensors, and oxygen generation systems. However, low membrane oxygen flux, high membrane fabrication costs, and high temperatures required for operation are among the disadvantages of this technology. Some modifications are necessary to overcome these barriers.

Our research was directed towards the investigation and fabrication of two different kinds of MIEC ceramic membranes: $SrFeCo_{0.5}O_x$ (SFC) and $Ba_{0.5}Sr_{0.5}Co_{0.8}Fe_{0.2}O_x$ (BSCF). In this dissertation, SFC and BSCF oxygen-permeable ceramic membranes were explored as alternative oxygen sources for carbon dioxide reforming of methane to syngas ($CO+H_2$). Our goal was to gain a fundamental understanding of the role of the membrane, the role of the catalyst, and their interactions for syngas production enhancement. The ultimate goal was to improve this process towards commercialization of these membranes in medical, environmental, and energy applications.

The interaction between the $Pt/CeZrO_2$ catalyst and the SFC membrane during hydrogen production from methane was investigated by pulse studies in a PFR and it was shown that there is a synergistic relationship between this catalyst and the membrane. When a physical mixture of $Pt/CeZrO_2$ catalyst and powdered SFC

membrane material was exposed to H_2 and CO, significantly higher amounts of water and CO_2 were produced compared to the catalyst and SFC alone. This increased formation of H_2O and CO_2 and subsequent occurrence of steam and carbon dioxide reforming of methane under reaction conditions will lead to higher methane conversions. The degree of SFC and catalyst interaction is important and a higher degree of interaction is required for maximum benefit. Specifically, the products of the reaction are maximized with intimate contact between the membrane and the catalyst. Although oxygen is not continually supplied in a PFR, and it is significantly different from the membrane reactor, the results of the pulse studies in the PFR have demonstrated that pulse studies can provide valuable information about the interaction between the catalyst and membrane under reaction conditions. A Raman spectroscopy study of physical mixtures of a $Pt/CeZrO_2$ catalyst and crushed SFC membrane material demonstrated significantly higher CO and CO_2 adsorption than the catalyst and SFC alone for temperatures ranging from room temperature to 600°C.

In an attempt to study the role of the membrane material in the enhancement of methane conversion to syngas, CO_2 reforming reaction of CH_4 in membrane reactor on the dense BSCF and dense SFC membranes were investigated and compared. Higher methane conversion and H_2:CO ratio on BSCF were observed compared to SFC at 800°C. The ability of BSCF to adsorb more H_2 and CO than SFC at 800°C could lead to higher water formation and CO_2 production on this ceramic membrane during CO_2 reforming of methane. The increased formation of H_2O and

CO_2 and simultaneous occurrence of steam and CO_2 reforming of CH_4, lead to higher methane conversion and H_2:CO ratio on BSCF. Also, BSCF showed higher O_2 release at moderate temperatures than SFC. This indicates that not only is BSCF a better material than SFC at 800°C, but also it could be a better material than SFC for low and medium temperature oxygen-assisted hydrogen production reactions.

Thermodynamically, hydrogen production via reforming reaction is more favorable at high temperatures. In order to enhance dry reforming of methane on BSCF at low and medium temperatures, four Pt and Ni containing catalysts were developed and investigated. It was shown that platinum enhances the reducibility of Ni/Al_2O_3 and $Ni/CeZrO_2$ catalysts and makes them active for H_2 production at moderate temperatures. Also, TPR and Raman studies showed that it is likely that there is an alloy formation in the $Pt\text{-}Ni/Al_2O_3$ catalyst.

To improve the catalytic hydrogen production reaction on BSCF, it is important to know the controlling factors affecting the reaction. The effects of various parameters on syngas production over a dense BSCF membrane were investigated: catalyst type, reaction temperature, membrane thickness, membrane preparation pH, and feed concentration. Although the $Pt\text{-}Ni/Al_2O_3$ catalyst showed high methane conversion in the presence of the BSCF membrane at 800°C, the activity of this catalyst was low at 600°C. $Pt\text{-}Ni/CeZrO_2$ bimetallic catalyst demonstrated superior performance compared to $Pt\text{-}Ni/Al_2O_3$ catalyst at 600°C. The BSCF membrane can reduce the apparent activation energy of CO_2 reforming reaction by changing the reaction pathway. The thinner BSCF membrane demonstrated a higher methane

conversion and H_2:CO ratio than the thicker BSCF membrane because membrane oxygen flux is inversely proportional to thickness. Varying the pH of the precursor solution during membrane preparation had no significant effect on the oxygen flux or the reaction. The CH_4:CO_2 feed ratio significantly affected the hydrogen production over the BSCF membrane. Altering the CH_4:CO_2 ratio had a direct impact on the oxygen flux, which in turn influenced the reaction pathway. These studies suggest that Pt-Ni/$CeZrO_2$ catalyst might be suitable for low-temperature hydrocarbon conversion reactions over low-thickness BSCF ceramic membranes.

Generally speaking, the results of this dissertation are very interesting and encouraging to do further research in the area of hydrogen production using ceramic membranes. Further work in this field could open a new door for us and it would help our society to meet its energy demand.

8.2. Recommendations

8.2.1. Low and Medium-temperature H_2 Production Reaction

As it mentioned previously, little work has been devoted to the development of a process to produce syngas from methane during medium temperature CO_2 reforming. So, more investigations on low and medium temperature H_2 production will provide valuable insight into the advantages and disadvantages of the reforming reaction at temperatures lower than 800°C.

8.2.1.1. Using Asymmetric BSCF Membranes

In consideration of the existing reaction problems at 600°C, which include low rate of hydrogen production and carbon deposition, the reaction at 600°C or lower temperature needs to be improved. According to Chapter 7, the amount of membrane oxygen flux at 600°C is smaller than 800°C and this might be one of the reasons for carbon deposition at 600°C. Higher amounts of oxygen from the ceramic membrane could help to remove deposited carbon from the catalyst surface at 600°C. Thus, it would be a good idea to concentrate on using ceramic membranes with higher oxygen flux such as asymmetric BSCF for reactions at 600°C and lower. This asymmetric membrane has been fabricated successfully in Dr. Susan Stagg-Williams' group and it has been shown that this membrane performs better than dense SFC and dense BSCF membranes during dry reforming of methane because of its higher oxygen flux [1]. Therefore, it is more likely that using this membrane would enhance the reaction at moderate temperatures and reduce the carbon deposition.

8.2.1.2. Catalyst Improvement

As discussed in Chapter 7, Pt-Ni/Al_2O_3 and Pt-Ni/$CeZrO_2$ catalysts are susceptible to carbon deposition at 600°C. For this reason, new catalysts with low deactivation rates at medium temperatures need to be developed for H_2 production during dry reforming of methane. The Al_2O_3 support is known to have higher surface area and higher metal dispersion than the $CeZrO_2$ support, which is well known for its high oxygen storage/release capacity resulting in higher thermal stability [2]. By

combining these two supports, we can benefit from the advantages of both supports simultaneously. A Pt/$CeZrO_2$-Al_2O_3 catalyst has been previously studied for partial oxidation of methane and it has shown a very good activity and stability for hydrogen production [2]. With this in mind, Pt-Ni/$CeZrO_2$-Al_2O_3 could be a good choice to be tested on the BSCF membrane at 600°C due to its higher surface area and higher metal dispersion compared with Pt-Ni/$CeZrO_2$ catalyst. The problem of carbon deposition might be resolved using this proposed catalyst at 600°C.

8.2.1.3. Renewable Resources for H_2 Production

Methods which are currently used for syngas production are based on non-renewable hydrocarbon feedstocks like methane [3, 4]. Technologies based on renewable resources for syngas production are seen as feasible options for the future [5, 6]. Among these technologies, the production of syngas from glycerin has received significant interest during the past few years [6]. Recently, several groups have investigated hydrogen production from waste glycerol on different supported metal catalysts [7-9]. However, the catalysts, which have been studied so far, suffer from low activity and product selectivity. Using ceramic membranes might be a good way to improve the catalyst performance in this reaction. It is recommended that dense or asymmetric BSCF membranes be tested for hydrogen production from both pure and waste glycerol.

Ethanol is another renewable feedstock used for hydrogen production according to the literature [10, 11]. A previous study has suggested that the presence

of oxygen can prevent formation of carbon during steam reforming of ethanol [12]. So oxygen from ceramic membranes might improve the catalyst activity during hydrogen production from ethanol by suppressing carbon deposition. It is recommended to explore the use of dense or asymmetric BSCF membranes for hydrogen production from ethanol.

8.2.2. The Interaction between Pt and Ni in Bimetallic Pt-Ni catalysts

As was discussed in Chapters 6 and 7, understanding the interactions between Pt and Ni in bimetallic Pt-Ni/Al_2O_3 and Pt-Ni/$CeZrO_2$ catalysts could lead to improving these two catalysts or developing new bimetallic catalysts for the dry reforming reaction of methane. With this in mind, it is recommended to conduct a comprehensive study on the role of the metals and their interactions at each temperature. BET, TEM, EXAFS, and IR are among the useful techniques that might shed some light on how the Pt and Ni interact.

8.3. References

[1] D. A. Slade, Q. Jiang, K. J. Nordheden, and S. M. Stagg-Williams, "A Comparison of Mixed-conducting Oxygen-permeable Membranes for CO_2 Reforming," *Catalysis Today*, vol. 148, pp. 290-297, 2009.

[2] F. A. Silva, D. S. Martinez, J. A. C. Ruiz, L. V. Mattos, C. E. Hori, and F. B. Noronha, "The effect of the use of cerium-doped alumina on the performance of Pt/CeO_2/Al_2O_3, and Pt/$CeZrO_2$/Al_2O_3 catalysts on the partial oxidation of methane," *Applied Catalysis A-General*, vol. 335, pp. 145-152, 2008.

[3] J. R. Frade, V. V. Kharton, A. Yaremchenko , and E. Naumovich, "Methane to syngas conversion Part 1: Equilibrium conditions and stability requirements of membrane materials," *Jnl of Power Sources*, vol. 130, pp. 77-84, 2004.

[4] A. P. E. York, T. Xiao, and M. L. H. Green, "Brief Overview of the Partial Oxidation of Methane to Syngas," *Topics in Catalysis*, vol. 22, pp. 345-358, 2003.

[5] S. Adhikari, S. D. Fernando, and A. Haryanto, "Glycerin steam reforming for hydrogen production," *Transactions of the Asabe*, vol. 50, pp. 591-595, 2007.

[6] C. Rossi, C. G. Alonso, O. A. C. Antunes, R. Guirardello, and L. Cardozo, "Thermodynamic analysis of steam reforming of ethanol and glycerine for hydrogen production," *International Journal of Hydrogen Energy*, vol. 34, pp. 323-332, 2009.

[7] A. Iriondo, V. L. Barrio, J. F. Cambra, P. L. Arias, M. B. Guemez, R. M. Navarro, M. C. Sanchez-Sanchez, and J. L. G. Fierro, "Hydrogen production from glycerol over nickel catalysts supported on Al_2O_3 modified by Mg, Zr, Ce or La," *Topics in Catalysis*, vol. 49, pp. 46-58, 2008.

[8] B. L. Dou, G. L. Rickett, V. Dupont, P. T. Williams, H. S. Chen, Y. L. Ding, and M. Ghadiri, "Steam reforming of crude glycerol with in situ CO_2 sorption," *Bioresource Technology*, vol. 101, pp. 2436-2442.

[9] A. Iulianelli, T. Longo, S. Liguori, and A. Basile, "Production of hydrogen via glycerol steam reforming in a Pd-Ag membrane reactor over Co-Al_2O_3 catalyst," *Asia-Pacific Journal of Chemical Engineering*, vol. 5, pp. 138-145.

[10] J. Sun, Y. G. Wang, J. G. Li, G. L. Xiao, L. G. Zhang, H. Li, Y. L. Cheng, C. W. Sun, Z. X. Cheng, Z. C. Dong, and L. Q. Chen, "H_2 production from stable ethanol steam reforming over catalyst of NiO based on flowerlike CeO_2 microspheres," *International Journal of Hydrogen Energy*, vol. 35, pp. 3087-3091.

[11] S. M. de Lima, I. O. da Cruz, G. Jacobs, B. H. Davis, L. V. Mattos, and F. B. Noronha, "Steam reforming, partial oxidation, and oxidative steam reforming of ethanol over Pt/$CeZrO_2$ catalyst," *Journal of Catalysis*, vol. 257, pp. 356-368, 2008.

[12] S. M. de Lima, A. M. da Silva, L. O. O. da Costa, J. M. Assaf, G. Jacobs, B. H. Davis, L. V. Mattos, and F. B. Noronha, "Evaluation of the performance of Ni/La_2O_3 catalyst prepared from $LaNiO_3$ perovskite-type oxides for the production of hydrogen through steam reforming and oxidative steam reforming of ethanol," *Applied Catalysis A-General*, vol. 377, pp. 181-190.

Appendix A: Raman Spectroscopy Study of CO and CO_2 Adsorption on $Pt/CeZrO_2$ Compared to Pt/ZrO_2 Catalyst

Although this appendix is not related to hydrogen production, it provides some information about $Pt/CeZrO_2$ and Pt/ZrO_2 catalysts that might be helpful for using these catalysts in the process of hydrogen production.

A.1. Introduction

The catalytic performance of platinum has received significant attention over the past few decades. A Pt catalyst supported on $CeZrO_2$ is known for its high oxygen release and storage capability [1, 2] because of the reducibility of cerium to convert from Ce^{4+} to Ce^{3+} in the presence of reducing agents like H_2 and CO [3]. Since this catalyst has shown high stability at high temperatures, it has been employed for syngas ($CO+H_2$) production from different hydrocarbons [4-6]. Another application of this catalyst would be selective oxidation of CO to CO_2 in fuel cells where CO removal is highly desired [7]. In these fuel cells, the CO level must be less than 50 ppm [7]. Additionally, $Pt/CeZrO_2$ behaves as a three-way catalyst for lowering automotive emissions [8]. Furthermore, the conversion of carbon monoxide to hydrogen in the presence of water (water gas shift reaction) can be performed on $Pt/CeZrO_2$ catalyst [9].

The mechanism of CO oxidation to CO_2 on different catalysts has been investigated by different research groups for many years. According to these studies, carbonate species are intermediate surface complexes even at low temperature [10-

12]. It is clear that the large amount of information about the role of these reaction intermediates can be obtained by means of IR and Raman spectroscopy. However, no detailed studies have been reported on the Raman spectroscopy of $Pt/CeZrO_2$ and Pt/ZrO_2 catalysts in the presence of CO and CO_2.

We have shown previously in Chapters 4 and 5 that the conversion of methane to hydrogen is higher in the presence of $Pt/CeZrO_2$ catalyst than Pt/ZrO_2 catalyst [14]. Moreover, the previous diffuse reflectance infrared fourier transform spectroscopy (DRIFTS) studies about CO and CO_2 adsorption on the reduced Ce promoted Pt/ZrO_2 have suggested that the presence of Ce affects the adsorption and desorption of CO and CO_2 on the catalyst surface [13]. The aim of this study is to compare the reactivity of $Pt/CeZrO_2$ with that of Pt/ZrO_2 catalyst for converting CO to CO_2 focusing on the surface species formed at different temperatures. In this appendix, we compare Raman spectra of $Pt/CeZrO_2$ with that of Pt/ZrO_2 catalyst in He, O_2, CO, and CO_2 atmosphere. The role of Ce on CO and CO_2 adsorption on the catalyst surface via carbonate species is also investigated at different temperatures.

A.2. Experimental

All information about catalyst preparation methods, Raman spectroscopy, TPO, TPD, and TPR can be found in Chapter 3.

A.3. Results and Discussion

A.3.1. Catalytic Activity of $Pt/CeZrO_2$ and Pt/ZrO_2 for CO Oxidation Reaction

The unreduced catalyst samples were heated to 200°C in argon and then were exposed to a mixture of hydrogen and CO pulses (30:1 H_2:CO molar ratio) at 200°C while monitoring the effluent using a mass spectrometer. The consumption of oxygen and the appearance of carbon dioxide clearly demonstrated that Pt/ZrO_2 and $Pt/CeZrO_2$ samples have the ability to catalyze CO oxidation in the presence of excess hydrogen at 200 °C. However, the amount of CO_2 production on $Pt/CeZrO_2$ catalyst was 1.5 times higher than that on Pt/ZrO_2 catalyst. This result suggests that $Pt/CeZrO_2$ might be a good catalyst for preferential oxidation of CO at low temperature. Since it has been suggested that carbonate species are intermediates formed during CO oxidation to CO_2 [10-12], it is likely that the $Pt/CeZrO_2$ catalyst is better able to produce these species than the Pt/ZrO_2 catalyst due to the reducibility of Ce. To verify this hypothesis, a spectroscopic analysis of these catalysts needs to be performed.

A.3.2. Raman Spectroscopy of $Pt/CeZrO_2$ and Pt/ZrO_2 at Room Temperature

In order to determine the role of the surface species on the catalysts during the conversion of CO to CO_2, samples were scanned by a Raman spectroscope in different flowing gases (He, CO, CO_2, O_2, and H_2) at room temperature. Figure A.1 compares the Raman spectra of $Pt/CeZrO_2$ with Pt/ZrO_2 catalyst (both untreated) at room temperature in an inert atmosphere (He, 30 ml/min). The band assignments are

provided in table A.1. For $Pt/CeZrO_2$, the peaks between 120 and 500 cm^{-1} are characteristic of CeO_2 structure and as is expected, they are not observed for the Pt/ZrO_2 catalyst. These peaks have also been observed for bare $CeZrO_2$ support. Also, the band at 643 cm^{-1} for $Pt/CeZrO_2$ catalyst is attributed to tetragonal ZrO_2 which is consistent with our XRD data. Bands related to the surface contaminants are formed in the 800-2600 cm^{-1} region due to the exposure of catalysts to room air, which contains CO and CO_2. These contaminants confirm the adsorption of CO and CO_2 on the catalyst surface at room temperature. Unlike $Pt/CeZrO_2$ catalyst, Pt/ZrO_2 showed fewer carbonate species and no adsorbed CO_2 on its surface. The amount of CO linearly bonded to Pt (the band at 2057 cm^{-1}) is higher for Pt/ZrO_2 than $Pt/CeZrO_2$, which could be because of a slightly higher amount of Pt loading for Pt/ZrO_2.

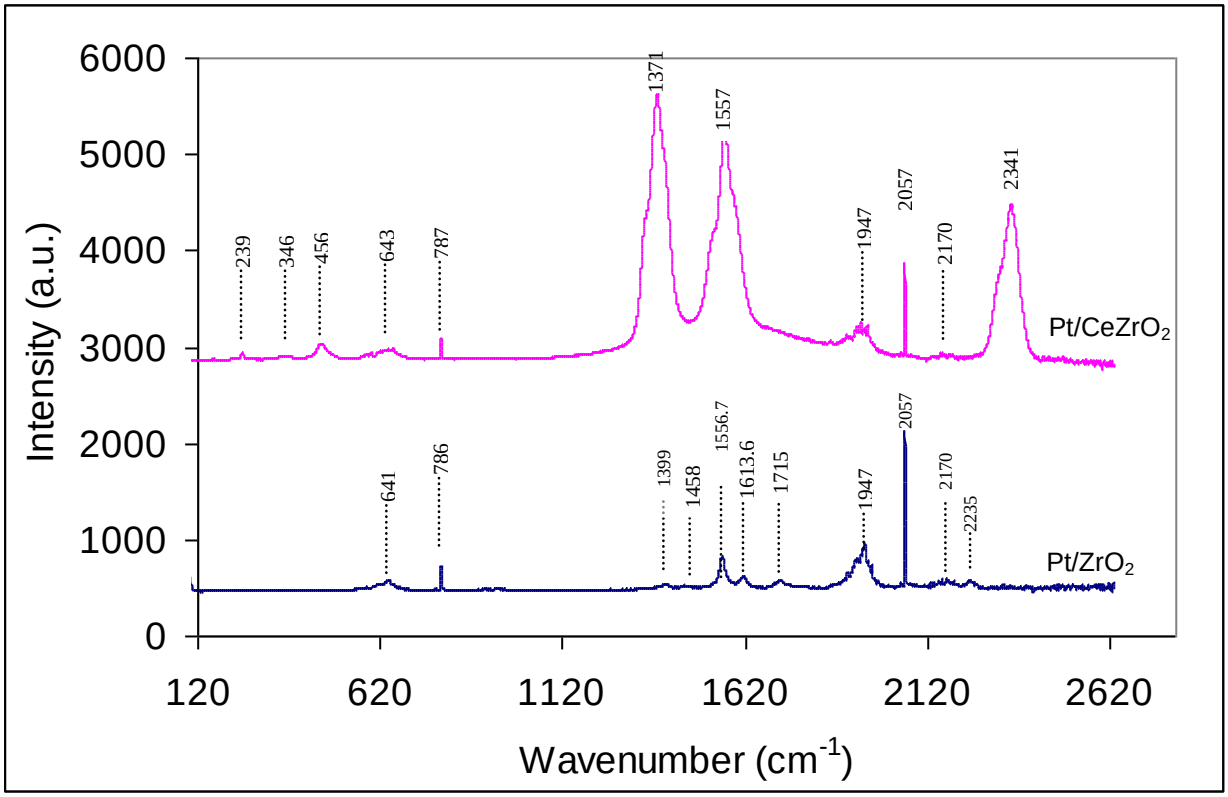

Figure A.1. The Raman spectra of $Pt/CeZrO_2$ and Pt/ZrO_2 catalysts at room temperature in an inert atmosphere (He).

Table A.1. The Raman band assignments.

Sample	Wavenumber (cm^{-1})	Assignment	Reference
$Pt/CeZrO_2$	239	CeO_2	[14-16]
	346	CeO_2	[14]
	456	CeO_2	[14-19]
	643	tetragonal ZrO_2	[17]
	787	carbonate (on Ce)	[10, 20]
	1371	unidentate carbonate (on Ce)	[20-22]
	1557	bidentate carbonate (on Ce)	[10, 20-22]
	1947	bridging carbonyl on Pt	[10, 23]
	2057	CO linearly bonded to Pt	[23, 24]
	2170	CO linearly adsorbed on Ce^{4+}	[20, 22, 25]
	2341	CO_2 (adsorbed on Ce)	[10]
Pt/ZrO_2	641	tetragonal ZrO_2	[17]
	786	Carbonate on Zr	[10, 20]
	1399	Carbonate on Zr	[26, 27]
	1458	Carbonate on Zr	[26, 27]
	1556.7	Carbonate on Zr	[26, 27]
	1613.6	Carbonate on Zr	[26, 27]
	1715	Carbonate on Zr	[26, 27]
	1947	bridging carbonyl on Pt	[10, 23]
	2057	CO linearly bonded to Pt	[23, 24]
	2170	CO adsorbed on Zr^{4+}	[11, 27]
	2235	CO adsorbed on Zr^{4+}	[11]

The spectra of samples after exposure to CO and CO_2 at room temperature were studied (data not shown). Although the surfaces of untreated catalysts are covered with contaminants, these catalysts still can adsorb CO and CO_2 at room temperature. With exposure to CO and CO_2, the intensities of the carbonate bands at 1371 and 1557 cm^{-1} and also the CO_2 band at 2341cm^{-1} increased for $Pt/CeZrO_2$ catalyst. This shows that CO reduces the $CeZrO_2$ support by producing carbonates, which subsequently decompose to CO_2 on the surface and leads to an increase in the intensity of the CO_2 peak. When $Pt/CeZrO_2$ catalyst is exposed to molecules of CO_2, these molecules can either directly stick to the support, or oxidize the support through the production of carbonate species. CO_2 exposure causes an increase in the amount of carbonates (at 1399, 1458, 1556.7, 1613.6, and 1715 cm^{-1}) for Pt/ZrO_2 catalyst while CO has the tendency to adsorb on this catalyst at wavenumbers: 1947, 2057, and 2170 cm^{-1}. The results of CO and CO_2 adsorption studies suggest that CO has the capability to form more carbonates on $Pt/CeZrO_2$ than on Pt/ZrO_2, resulting in a higher amount of CO_2 production on $Pt/CeZrO_2$. It is possible that the difference in the amount of carbonates can be ascribed to the differences in the ability of each support to provide oxygen and facilitate the carbonate formation. It should be noted that no significant changes in the Raman spectra of samples were observed when the catalysts were flushed in helium after CO and CO_2 exposure, indicating that CO and CO_2 are not weakly adsorbed to the catalyst surface.

The samples were also scanned in flowing oxygen at room temperature. The intensities of bands at 785 and 2057 cm^{-1} decreased (not significantly) and this

showed that oxygen could remove only a small amount of contaminants at room temperature.

The spectroscopy of reduced catalysts (reduced at 400°C), which was performed at room temperature in flowing helium, showed that significant amounts of almost all types of contaminants were removed. It is likely that the majority of surface contaminants are converted to formate species at 400°C.

A.3.3. Raman Spectroscopy of $Pt/CeZrO_2$ and Pt/ZrO_2 at Elevated Temperature

High temperature Raman spectra of the catalysts at 200°C, 400°C, and 600°C were studied in order to understand the interaction between the catalyst surface and different adsorbates at these temperatures. The results are shown in Figures A.2, A.3, and A.4.

To investigate the surface contaminants desorption, Raman spectroscopy was performed while the samples were heating in flowing helium. The spectroscopy at 200°C showed a significant decrease in the intensity of the carbonate bands at 1371 and 1557 cm^{-1} and also the band at 2341 cm^{-1} for $Pt/CeZrO_2$. However, this temperature increase did not change the intensity of the other peaks significantly, indicating that desorption of these surface contaminants cannot occur at temperatures below 200°C. The decrease in the intensity of bands at 200°C for Pt/ZrO_2 occurs at wavenumbers 1556.7, 786, 1947, and 2057 cm^{-1}. Increasing the temperature to 400°C resulted in a subsequent decrease in the intensity of the above-mentioned peaks. At this temperature, the weak bands at 1399, 1458, 1613.6, 1715, and 2235 cm^{-1} for the

Pt/ZrO_2 sample completely vanished. When the temperature was increased to 600°C, the spectra for $Pt/CeZrO_2$ sample showed the complete disappearance of the CO_2 band at 2341cm^{-1}. At 600°C, small amounts of carbonates are observed on the surface of both samples and the residual amount of carbonate species for $Pt/CeZrO_2$ is still more than that for Pt/ZrO_2. To remove all contaminants, temperatures higher than 600°C are required.

The ratio of the intensity of unidentate to bidentate carbonate peaks was calculated for $Pt/CeZrO_2$ at each temperature during the removal of species in helium and the results showed that this ratio increased as a consequence of temperature increase. The rise in unidentate : bidentate ratio can be attributed to higher thermal stability of unidentate carbonate compared to bidentate, in good agreement with what was demonstrated before for CeO_2 in the literature [21].

The spectra recorded during CO and CO_2 exposure at 400°C are shown in Figure A.2. According to the data, CO_2 adsorption on both catalysts results in carbonate formation at 787, 1371 and 1557 cm^{-1} for $Pt/CeZrO_2$ and 786, 1556.7 and 1613.6 cm^{-1} for Pt/ZrO_2. For $Pt/CeZrO_2$, CO_2 adsorption also results in more carbonyls, linear CO bonded to the surface, and CO_2 at 1947, 2057, and 2341cm^{-1}. The influence of CO adsorption on $Pt/CeZrO_2$ is similar to CO_2 adsorption on this catalyst. CO adsorption on Pt/ZrO_2 changes only the intensity of the bands at 1947, 2057, and 2170 cm^{-1}.

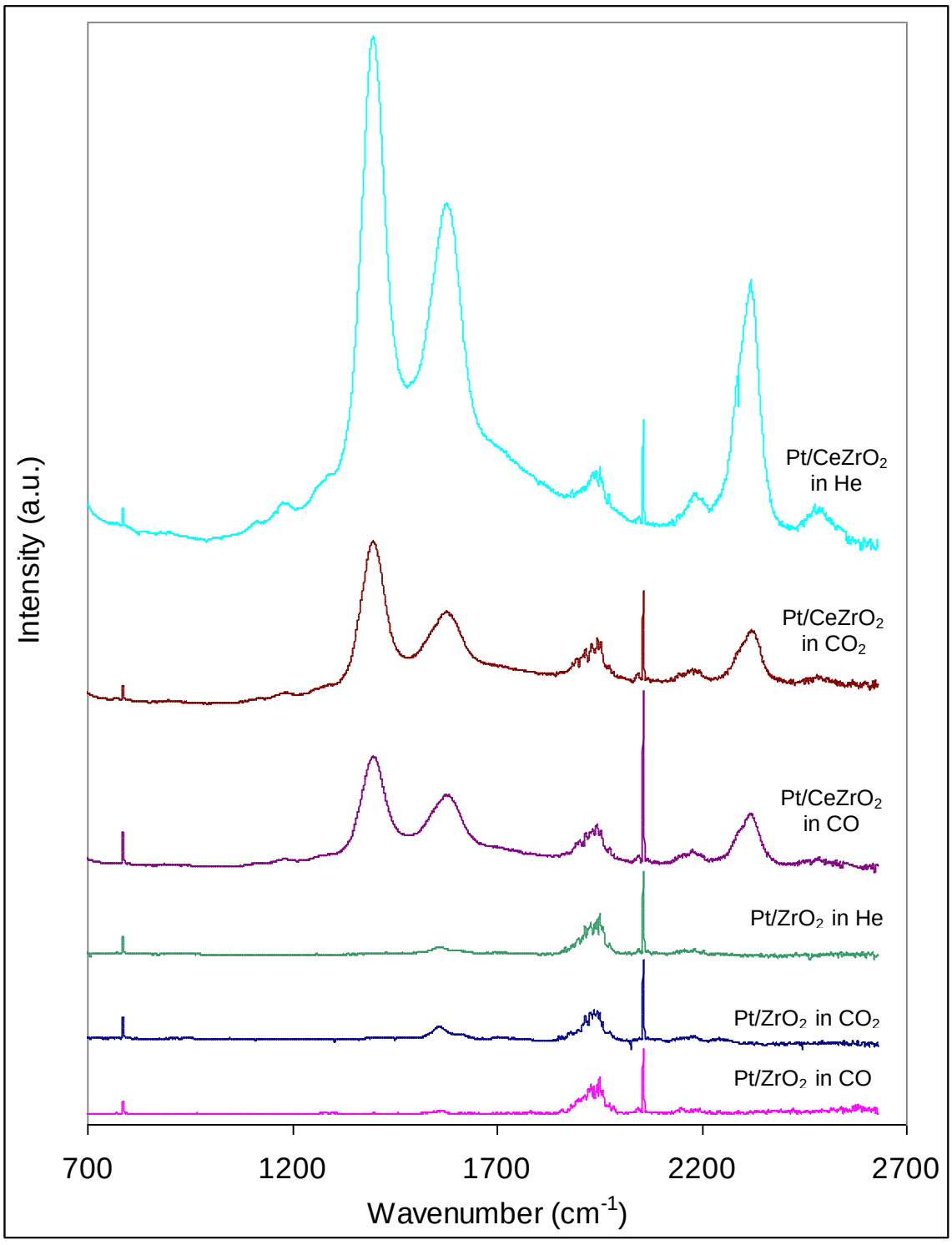

Figure A.2. The Raman spectra of $Pt/CeZrO_2$ and Pt/ZrO_2 catalysts at 400°C in flowing He, CO, and CO_2.

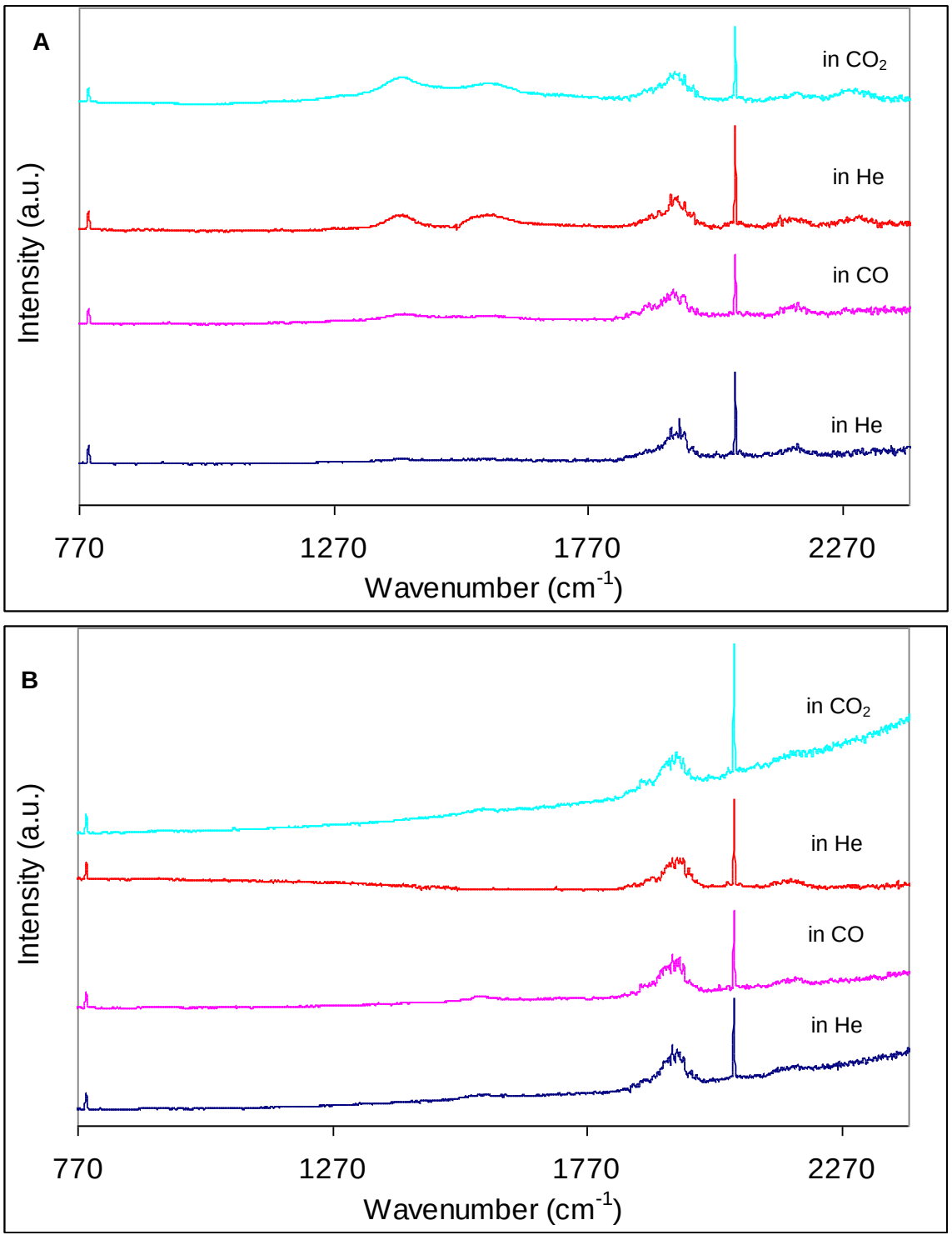

Figure A.3. The Raman spectra for A) $Pt/CeZrO_2$ and B) Pt/ZrO_2 during exposure to He, CO, and CO_2 at 600°C.

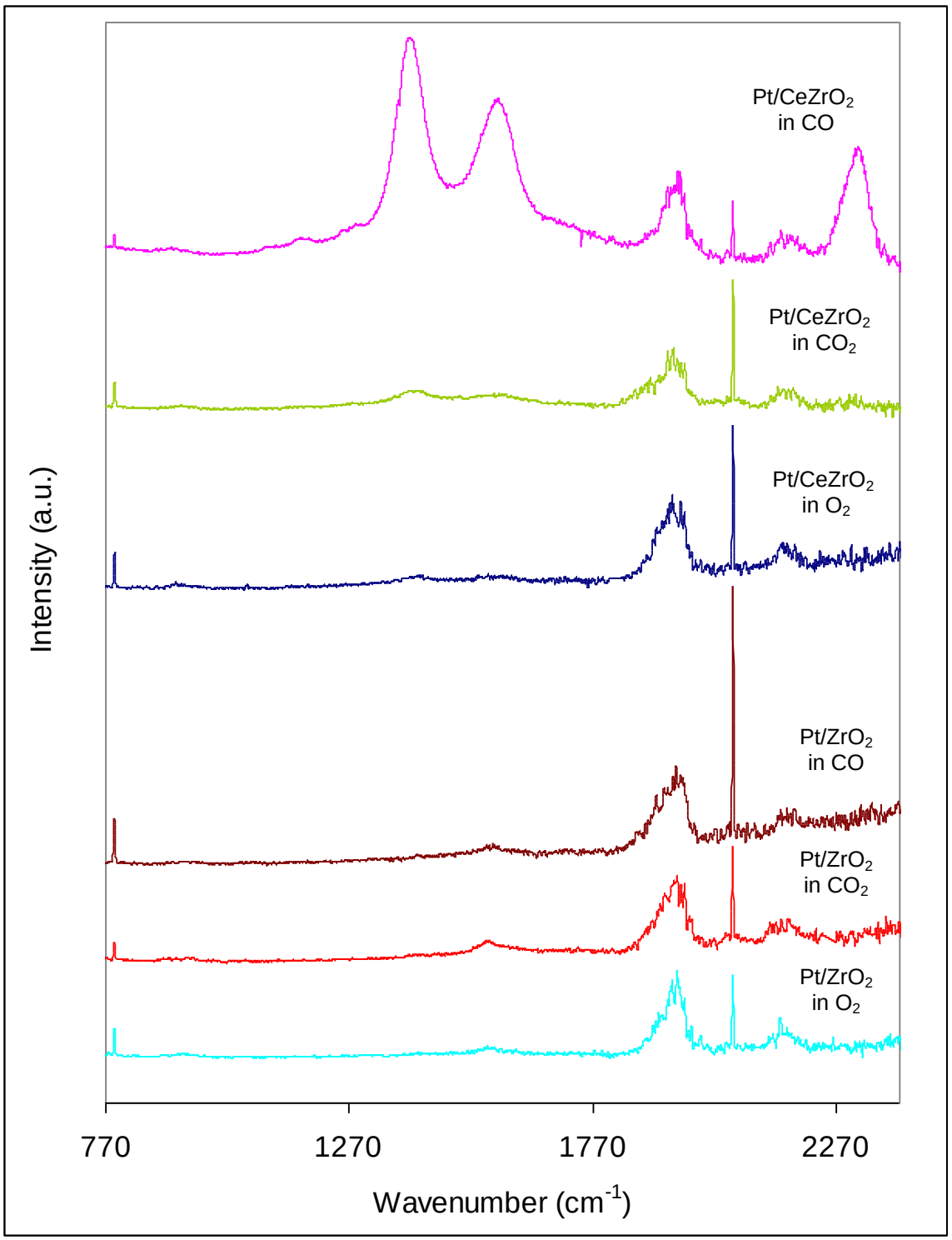

Figure A.4. The Raman spectra of $Pt/CeZrO_2$ and Pt/ZrO_2 catalyst at 600°C in flowing CO and CO_2 after O_2 pretreatment.

Figure A.3 shows the spectra taken during CO and CO_2 exposure at 600°C. During CO and CO_2 introduction to the surface, carbonate bands at 1371 and 1557 cm^{-1} and also the CO_2 band at 2341cm^{-1} grow on $Pt/CeZrO_2$. CO introduction does not change the spectra of Pt/ZrO_2 but CO_2 introduction can result in a small amount of carbonate formation at 1556.7 cm^{-1}.

Both samples were heated in flowing oxygen (20 cc/min) to 600°C and then held at this temperature. Raman spectroscopy of the samples at 600°C (Figure A.4) showed similar spectra for both catalysts because the bands attributed to carbonates in the range of 1300-1800 cm^{-1} were vanished. These results indicate that the most stable contaminants in the presence of O_2 are the bands at 787, 1947, 2057, and 2170 cm^{-1} at this temperature. Figure A.4 also shows the results of CO and CO_2 exposure after oxygen pretreatment at 600°C. As can be seen in this figure, when CO and CO_2 pass over the $Pt/CeZrO_2$ the carbonates and CO_2 peaks reappear. Although CO_2 exposure after oxygen pretreatment leads to carbonate formation at 1556.7 cm^{-1} on Pt/ZrO_2, there is no significant difference between the spectra of this catalyst before and after CO exposure. These results, which are similar to what was obtained before in Figure A.3, show that the adsorption of CO in form of carbonate on $Pt/CeZrO_2$ is higher than that on Pt/ZrO_2 at 600°C and this makes $Pt/CeZrO_2$ a good candidate for catalyzing CO oxidation at this temperature.

It should be noted that no significant changes in the Raman spectra of samples were observed when the catalysts were flushed in helium after CO and CO_2 exposure. This indicates that CO and CO_2 were not weakly adsorbed to the catalyst surface.

A.3.4. Surface Treatment

In order to specify the desorption temperature of the contaminant species in the presence of different gases, catalyst surface treatment was studied. Surface contaminant removal can be accomplished by thermal treatment (TPD) or oxidation of contaminants (TPO) or hydrogenation of these species (TPR). These methods are discussed hereinafter.

A.3.4.1. TPD

Thermal stability of surface contaminants of the catalysts was studied by performing TPD. Each sample was heated to 800°C in argon (15 cc/min). The effluent was then monitored using a mass spectrometer. Figure A.5 shows the CO_2 desorption profiles for the samples. According to the data, significant amount of CO_2 was formed for both catalysts while no CO desorption was observed. TPD data of untreated $Pt/CeZrO_2$ catalyst shows that surface contaminants are stable up to a temperature of 200°C in flowing argon. Increasing the temperature leads to decomposition of these species to form carbon dioxide by taking oxygen from the catalyst support lattice. Unlike the Ce-promoted catalyst, Pt/ZrO_2 showed a higher onset temperature of CO_2 release (225°C) because of the lower oxygen release capability of ZrO_2. The onset temperature of CO_2 release for both samples is almost consistent with Raman spectra at 200°C, which shows that species start being removed from the surface at this temperature. The amount of CO_2 release for the

$Pt/CeZrO_2$ catalyst was higher than that for Pt/ZrO_2 suggesting the existence of a higher amount of surface contaminants on this catalyst.

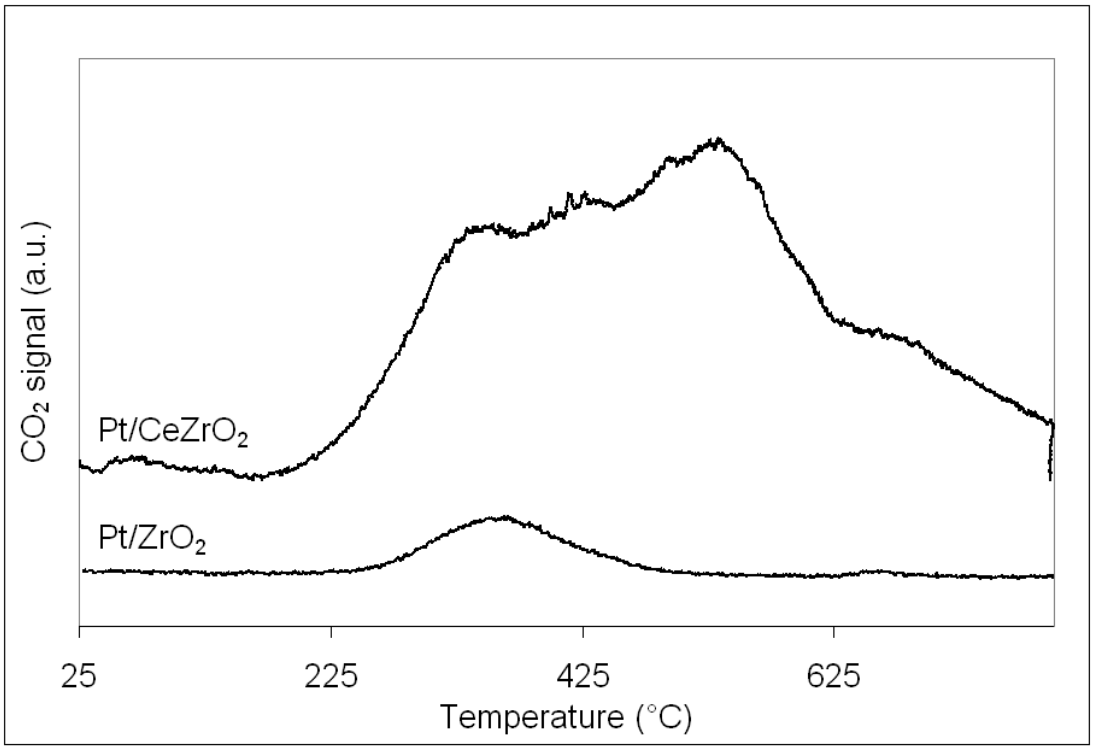

Figure A.5. CO_2 desorption profiles during temperature programmed desorption for $Pt/CeZrO_2$ and Pt/ZrO_2 catalysts.

According to Figure A.5, four peaks were observed for the $Pt/CeZrO_2$ catalyst during TPD. Each peak shows the region in which a group of surface contaminants are thermally removed. The 200-380°C is the region in which the surface contaminants with weakest chemical bonding to the catalyst surface are removed. According to the previously described Raman data, these species are mostly bidentate and unidentate carbonates as well as adsorbed CO_2, with a higher removal of bidentate carbonate than unidentate. The second and third region, which is located

between 380 and 625°C, is a complete removal region for CO_2. Also, the carbonates continue desorbing in this region. The last region (625-800°C) shows the temperature range required for the removal of bridging carbonyls on Pt, CO linearly bonded to Pt or Ce, and the residual amount of carbonates. Thus, the order of thermal resistance of contaminant species for $Pt/CeZrO_2$ catalyst is: adsorbed CO_2 < bidentate carbonates < unidentate carbonate < carbonyls and CO linearly bonded to surface (Pt or Ce). These results, which show unidentate carbonates are more thermally stable than bidentate carbonates, are consistent with the previous study for cerium oxide [21]. Similarly, for Pt/ZrO_2, carbonates are the most sensitive species to temperature increase and some of the carbonate species totally disappear at 400°C.

The TPD of CO and CO_2 were performed on both catalyst samples. Each sample was exposed to a continuous flow of CO and CO_2 at room temperature for 30 minutes and then heated to 800°C in argon (15 cc/min). The effluent was monitored using a mass spectrometer. Figures A.6 and A.7 show the CO_2 desorption profile for the studied samples after exposure to CO and CO_2. In both cases, a significant amount of CO_2 was formed while no CO desorption was observed. Since the only source of oxygen in the reactor is from the catalyst support, it is believed that CO and CO_2 adsorb to the surface and then form CO_2 by reducing or oxidizing the support. After CO admission, the onset temperature of the CO_2 desorption profile decreases for each sample (150°C and 200°C for $Pt/CeZrO_2$ and Pt/ZrO_2 catalyst, respectively). This decline can be ascribed to the fact that CO adsorbs in the form of species which have a lower desorption temperature. For both samples, the onset temperature of the

CO_2 desorption profile after CO_2 exposure changes to 250°C. For each catalyst, the area underneath the TPD curve after CO exposure was higher than that after CO_2 exposure, indicating higher CO adsorption than CO_2 adsorption at room temperature. Furthermore, the area of TPD profile after CO and CO_2 exposure was larger than the area of the TPD curve shown in Figure A.5 for each sample. This result, which is consistent with the results of our Raman spectroscopy, shows that CO and CO_2 exposure at room temperature leads to adsorption of these chemicals on the surface of untreated catalyst.

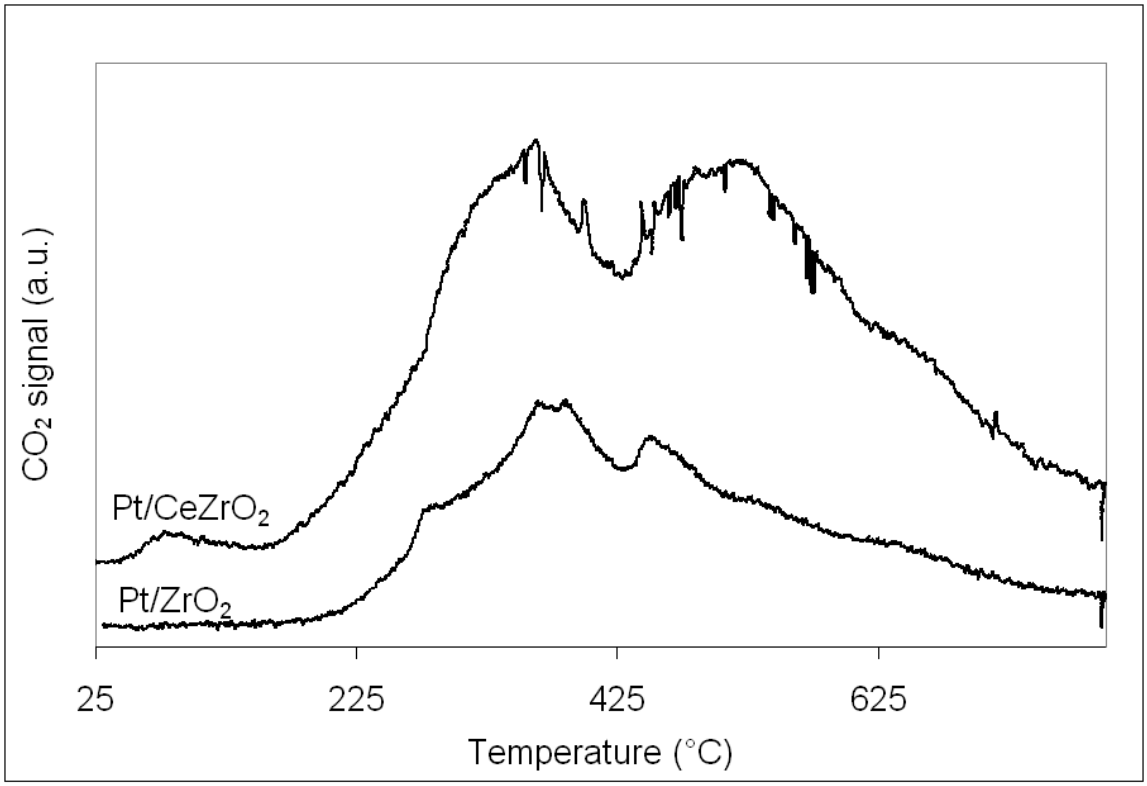

Figure A.6. CO_2 desorption profiles during temperature programmed desorption of CO after exposure to a continuous flow of CO at room temperature.

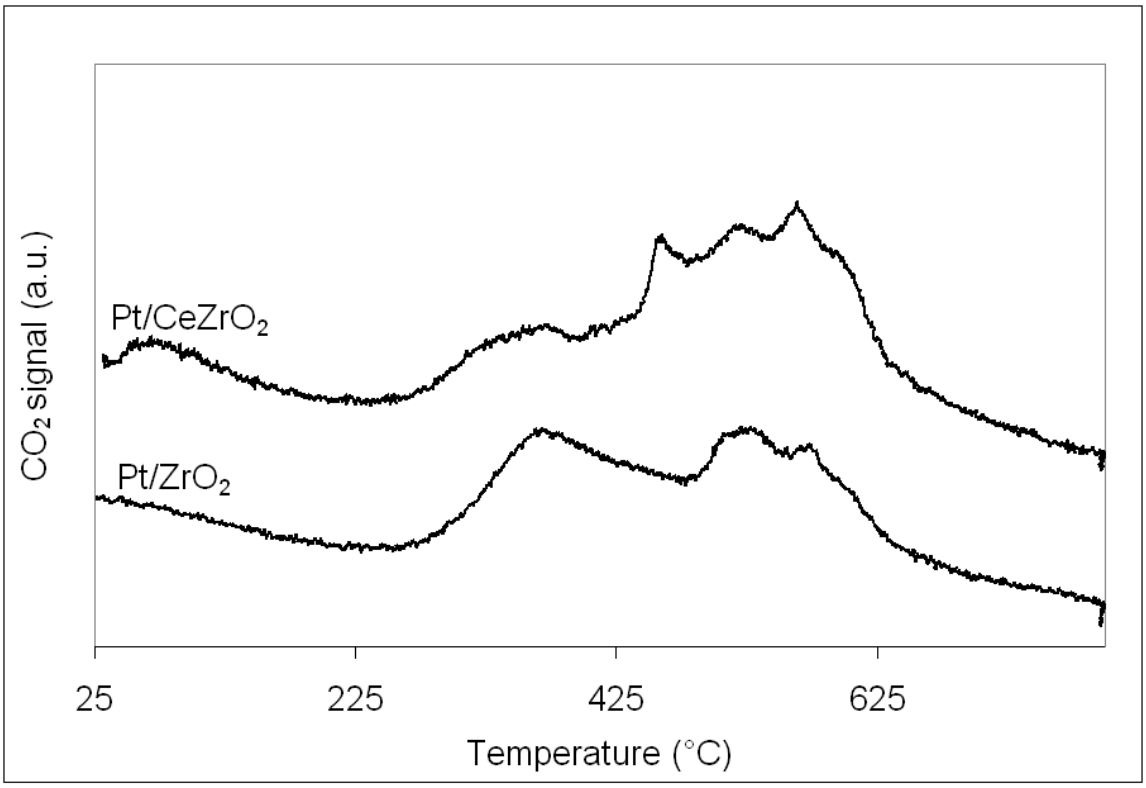

Figure A.7. CO_2 desorption profiles during temperature programmed desorption of CO after exposure to a continuous flow of CO_2 at room temperature.

A.3.4.2. TPO

TPO experiments were performed to determine the amount of CO_2 formation for each catalyst during oxygen exposure. Each sample was heated to 800°C in a 5% O_2/He mixture (15 cc/min) and then the effluent gases were analyzed using a mass spectrometer. Figure A.8 shows the CO_2 desorption profiles for the samples. According to Figure A.8, the total amount of CO_2 desorption for the Pt/$CeZrO_2$ catalyst was again greater than that for Pt/ZrO_2. This suggests that the Pt/$CeZrO_2$ catalyst adsorbs more contaminants than Pt/ZrO_2 when exposed to air due to its higher oxygen donation capacity. Interestingly, the amount of CO_2 formed for each catalyst during TPO was greater than that during TPD. This could be due to the fact

that the only source of oxygen for contaminants decomposition during TPD is from the support and without an oxygen source in the gas phase to replenish the oxygen in support; the support lattice oxygen is quickly depleted. Thus, some of surface contaminants remain on the surface during TPD and this leads to higher CO_2 desorption during TPO. Since a sufficient amount of oxygen is available for CO_2 formation in this experiment, the onset of CO_2 desorption shifts to lower temperatures (175°C for $Pt/CeZrO_2$ and 225°C for Pt/ZrO_2) compared to TPD.

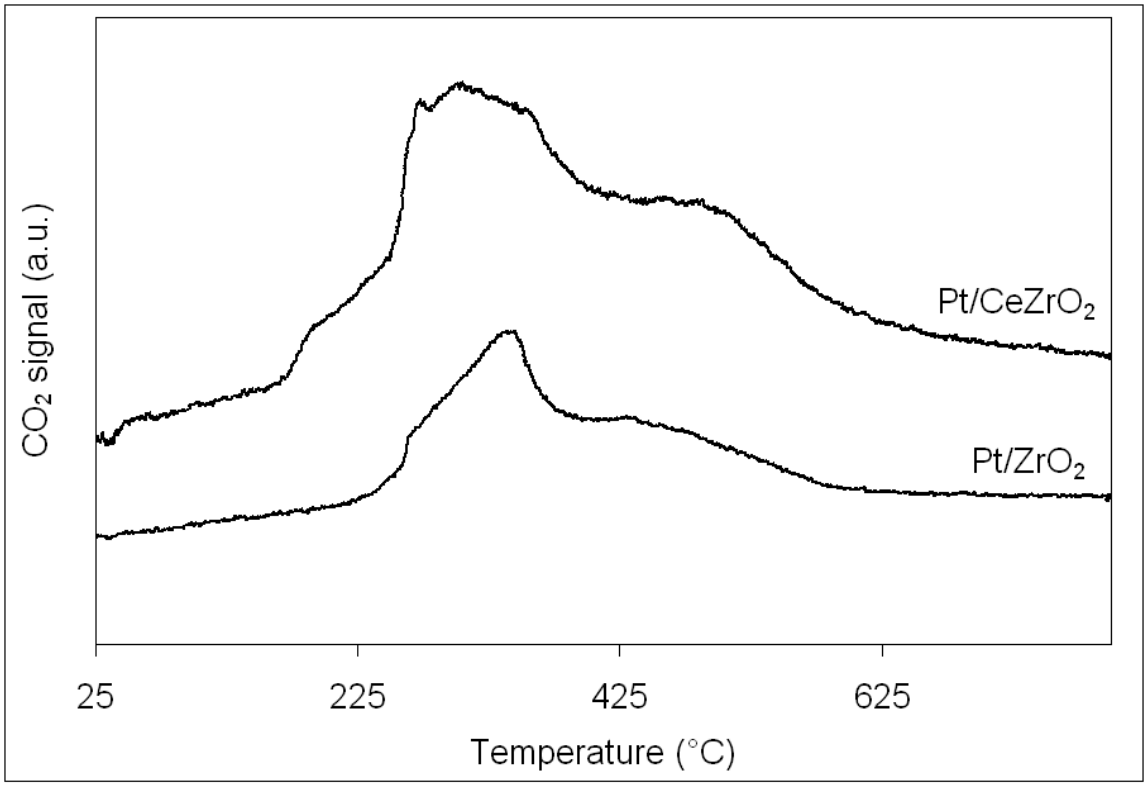

Figure A.8. CO_2 desorption profiles during temperature programmed oxidation for $Pt/CeZrO_2$ and Pt/ZrO_2 catalysts.

A.3.4.3. TPR

Heating the $Pt/CeZrO_2$ sample in flowing hydrogen (5% H_2 in He, 15 cc/min) to 800°C showed only a small peak of CO_2 between 500°C and 600°C. A similar experiment was performed for Pt/ZrO_2 and no CO_2 peak was observed. It is believed that the majority of surface contaminants are converted to formate species, which cannot be detected in our mass spectrometer.

A.4. Conclusions

The results of carbon monoxide and carbon dioxide adsorption studies on Pt/ZrO_2 and $Pt/CeZrO_2$ catalysts clearly demonstrated more carbonates with higher thermal stability on $Pt/CeZrO_2$ than on Pt/ZrO_2 at temperatures ranging from room temperature to 600°C. The $Pt/CeZrO_2$ catalyst demonstrated more CO_2 production than Pt/ZrO_2 during TPD, TPO, and TPR studies suggesting the beneficial effects of Ce in the support. The ability of $Pt/CeZrO_2$ catalyst to adsorb more CO than Pt/ZrO_2 in the form of carbonates could lead to higher CO conversion on this catalyst during preferential oxidation of CO to CO_2.

A.5. References

[1] C. E. Hori, K. Y. S. Ng, A. Brenner, K. M. Rahmoeller, and D. Belton, "The effects of aging temperature and aging time on the oxygen storage capacity of Pt-Rh/$CeZrO_2$ catalysts," *Brazilian Journal of Chemical Engineering*, vol. 18, pp. 23-33, 2001.

[2] M. W. Zhao, M. Q. Shen, and J. Wang, "Effect of surface area and bulk structure on oxygen storage capacity of $Ce_{0.67}Zr_{0.33}O_2$," *Journal of Catalysis*, vol. 248, pp. 258-267, 2007.

[3] F. B. Noronha, E. C. Fendley, R. R. Soares, W. E. Alvarez, and D. E. Resasco, "Correlation between catalytic activity and support reducibility in the CO_2 reforming of methane over $Pt/Ce_xZr_{1-x}O_2$ catalysts," *Chemical Engineering Journal*, vol. 82, pp. 21-31, 2001.

[4] S. M. de Lima, A. M. Silva, I. O. da Cruz, G. Jacobs, B. H. Davis, L. V. Mattos, and F. B. Noronha, "H_2 production through steam reforming of ethanol over Pt/ZrO_2, Pt/CeO_2 and $Pt/CeZrO_2$ catalysts," *Catalysis Today*, vol. 138, pp. 162-168, 2008.

[5] J. A. C. Ruiz, F. B. Passos, J. M. C. Bueno, E. F. Souza-Aguiar, L. V. Mattos, and F. B. Noronha, "Syngas production by autothermal reforming of methane on supported platinum catalysts," *Applied Catalysis A-General*, vol. 334, pp. 259-267, 2008.

[6] W. Wei, S. M. Stagg-Williams, F. B. Noronha, L. V. Mattos, and F. B. Passos, "Partial oxidation and combined reforming of methane on Ce-promoted catalysts," *Catalysis Today*, vol. 98, pp. 553-563, 2004.

[7] F. Marino, C. Descorme, and D. Duprez, "Noble metal catalysts for the preferential oxidation of carbon monoxide in the presence of hydrogen (PROX)," *Applied Catalysis B-Environmental*, vol. 54, pp. 59-66, 2004.

[8] J. R. Gonzalez-Velasco, M. A. Gutierrez-Ortiz, J. L. Marc, J. A. Botas, M. P. Gonzalez-Marcos, and G. Blanchard, "TWC behaviour of platinum supported on high and low surface area cerium/zirconium mixed oxides," *Topics in Catalysis*, vol. 16, pp. 101-106, 2001.

[9] S. Lim, J. Bae, and K. Kim, "Study of activity and effectiveness factor of noble metal catalysts for water-gas shift reaction," *International Journal of Hydrogen Energy*, vol. 34, pp. 870-876, 2009.

[10] F. C. Meunier, D. Tibiletti, A. Goguet, D. Reid, and R. Burch, "On the reactivity of carbonate species on a Pt/CeO_2 catalyst under various reaction atmospheres: Application of the isotopic exchange technique," *Applied Catalysis A-General*, vol. 289, pp. 104-112, 2005.

[11] A. Davydov, *Molecular Spectroscopy of Oxide Catalyst Surfaces*. Chichester: John Wiley & Sons Ltd., 2003.

[12] S. Hilaire, X. Wang, T. Luo, R. J. Gorte, and J. Wagner, "A comparative study of water-gas-shift reaction over ceria supported metallic catalysts," *Applied Catalysis A-General*, vol. 215, pp. 271-278, 2001.

[13] J. J. Daniels, A. R. Arther, B. L. Lee, and S. M. Stagg-Williams, "Infrared spectroscopy study of CO and CO_2 on Ce- and La-promoted Pt/ZrO_2 catalysts," *Catalysis Letters*, vol. 103, pp. 169-177, 2005.

[14] V. V. Pushkarev, V. I. Kovalchuk, and J. L. d'Itri, "Probing defect sites on the CeO_2 surface with dioxygen," *Journal of Physical Chemistry B*, vol. 108, pp. 5341-5348, 2004.

[15] A. Martinez-Arias, D. Gamarra, M. Fernandez-Garcia, X. Q. Wang, J. C. Hanson, and J. A. Rodriguez, "Comparative study on redox properties of nanosized CeO_2 and CuO/CeO_2 under CO/O_2," *Journal of Catalysis*, vol. 240, pp. 1-7, 2006.

[16] J. Guzman, S. Carrettin, and A. Corma, "Spectroscopic evidence for the supply of reactive oxygen during CO oxidation catalyzed by gold supported on nanocrystalline CeO_2," *Journal of the American Chemical Society*, vol. 127, pp. 3286-3287, 2005.

[17] G. Aguila, F. Gracia, and P. Araya, "CuO and CeO_2 catalysts supported on Al_2O_3, ZrO_2, and SiO_2 in the oxidation of CO at low temperature," *Applied Catalysis A-General*, vol. 343, pp. 16-24, 2008.

[18] M. Manzoli, G. Avgouropoulos, T. Tabakova, J. Papavasiliou, T. Ioannides, and F. Boccuzzi, "Preferential CO oxidation in H_2-rich gas mixtures over Au/doped ceria catalysts," *Catalysis Today*, vol. 138, pp. 239-243, 2008.

[19] C. Li, Y. Z. Song, Y. X. Chen, Q. Xin, X. W. Han, and W. Z. Li, "Spectroscopic studies of oxygen spillover on Pt/CeO_2 catalyst," *Spillover and Migration of Surface Species on Catalysts*, vol. 112, pp. 439-446, 1997.

[20] C. Li, Y. Sakata, T. Arai, K. Domen, K. Maruya, and T. Onishi, "Carbon-Monoxide and Carbon-Dioxide Adsorption on Cerium Oxide Studied by Fourier-Transform Infrared-Spectroscopy .1. Formation of Carbonate Species on Dehydroxylated CeO_2 at Room-Temperature," *Journal of the Chemical Society-Faraday Transactions I*, vol. 85, pp. 929-943, 1989.

[21] V. Galvita, L. K. Rihko-Struckmann, and K. Sundmacher, "The CO adsorption on a Fe_2O_3-$Ce_{0.5}Zr_{0.5}O_2$ catalyst studied by TPD, isotope exchange and FTIR spectroscopy," *Journal of Molecular Catalysis A-Chemical*, vol. 283, pp. 43-51, 2008.

[22] A. Holmgren, B. Andersson, and D. Duprez, "Interactions of CO with Pt/ceria catalysts," *Applied Catalysis B-Environmental*, vol. 22, pp. 215-230, 1999.

[23] L. S. F. Feio, C. E. Hori, S. Damyanova, F. B. Noronha, W. H. Cassinelli, C. M. P. Marques, and J. M. C. Bueno, "The effect of ceria content on the properties of $Pd/CeO_2/Al_2O_3$ catalysts for steam reforming of methane," *Applied Catalysis A : General*, vol. 316, pp. 107-116, 2007.

[24] S. M. de Lima, I. O. da Cruz, G. Jacobs, B. H. Davis, L. V. Mattos, and F. B. Noronha, "Steam reforming, partial oxidation, and oxidative steam reforming of ethanol over $Pt/CeZrO_2$ catalyst," *Journal of Catalysis*, vol. 257, pp. 356-368, 2008.

[25] N. G. Willis and J. Guzman, "Influence of the support during homocoupling of phenylboronic acid catalyzed by supported gold," *Applied Catalysis A-General*, vol. 339, pp. 68-75, 2008.

[26] J. M. Pigos, C. J. Brooks, G. Jacobs, and B. H. Davis, "Low temperature water-gas shift: The effect of alkali doping on the C-H bond of formate over Pt/ZrO_2 catalysts," *Applied Catalysis A-General*, vol. 328, pp. 14-26, 2007.

[27] E. Guglielminotti, "Infrared Study of Syngas Adsorption on Zirconia," *Langmuir*, vol. 6, pp. 1455-1460, 1990.

Appendix B: Calculation of Conversion and Selectivity

For reaction studies in both the PFR and the membrane reactor, the conversion of CH_4 and CO_2 and selectivity of H_2 and CO were calculated using the following equations:

CH_4 conversion: $$X_{CH4} = \frac{F_{CH4,in} - F_{CH4,out}}{F_{CH4,in}}$$

CO_2 conversion: $$X_{CO2} = \frac{F_{CO2,in} - F_{CO2,out}}{F_{CO2,in}}$$

H_2 selectivity: $$S_{H2} = \frac{F_{H2,out}}{F_{H2,out} + F_{H2O,out}}$$

CO selectivity: $$S_{CO} = \frac{F_{CO,out}}{F_{CO,out} + F_{CO2,out}}$$

where F is the molar flow rate.

Appendix C: Uncertainty Analysis for CH_4 Conversion

The CH_4 conversion uncertainty was calculated for one of the experiments on dense BSCF membrane. Figure C.1 shows the error bars for this experiment. As can be seen, the error bars were very small. For this reason, the error bars were not shown for other experiments conducted in this research project.

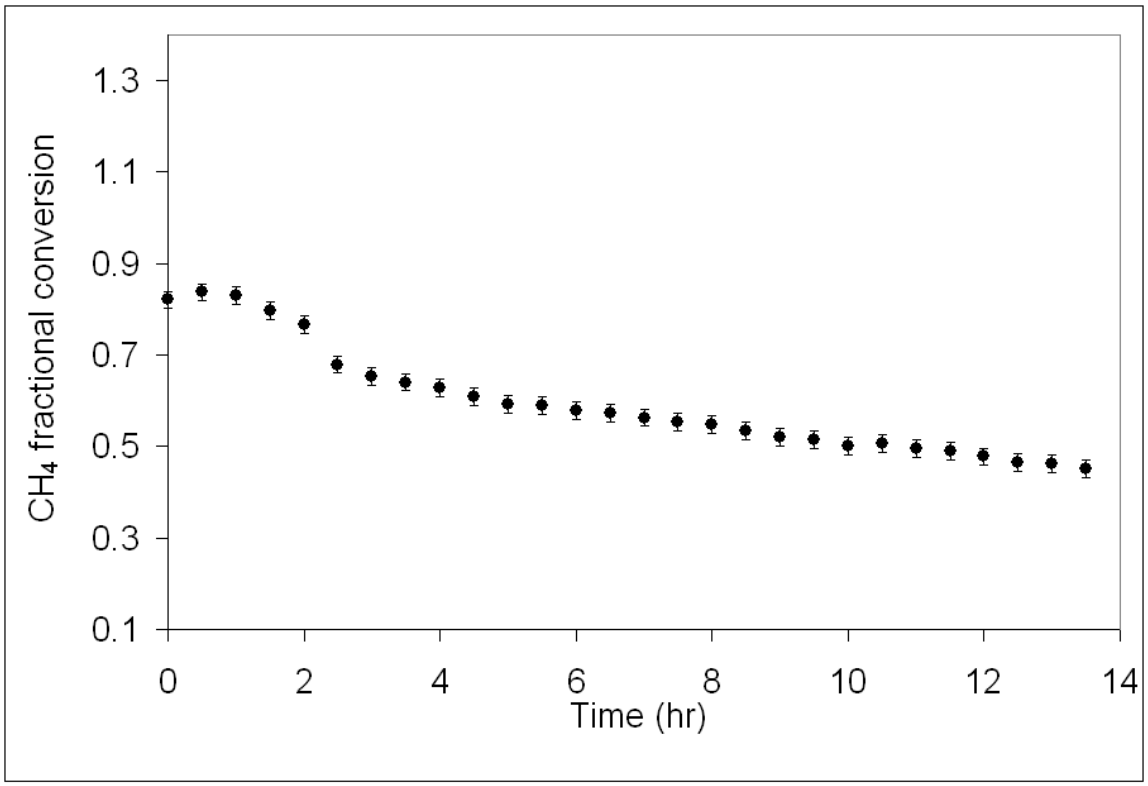

Figure C.1. Uncertainty analysis for CH_4 conversion profile on dense BSCF during CO_2 reforming of methane over $Pt/CeZrO_2$ catalyst at 800°C.